REVERSE-CYCLIC SHEAR IN REINFORCED CONCRETE ELEMENTS

by

MARC CLAUDE GERIN

BASc., The University of Waterloo, 1989

A THESIS SUBMITTED IN PARTIAL FULFILMENT OF
THE REQUIREMENTS FOR THE DEGREE OF

DOCTOR OF PHILOSOPHY

in

THE FACULTY OF GRADUATE STUDIES

(Department of Civil Engineering)

We accept this thesis as conforming
to the required standard

THE UNIVERSITY OF BRITISH COLUMBIA

July 2003

In presenting this thesis in partial fulfilment of the requirements for an advanced degree at the University of British Columbia, I agree that the Library shall make it freely available for reference and study. I further agree that permission for extensive copying of this thesis for scholarly purposes may be granted by the head of my department or by his or her representatives. It is understood that copying or publication of this thesis for financial gain shall not be allowed without my written permission.

Department of CIVIL ENGINEERING

The University of British Columbia
Vancouver, Canada

Date August 12, 2003

DE-6 (2/88)

Abstract

Previously there were no simple, rational models for reinforced concrete elements subjected to seismic (reverse-cyclic) shear. Efforts to modify existing monotonic shear models resulted in complex formulations that use empirical rules to capture the complexities of the reverse-cyclic response as the fundamental mechanisms governing seismic shear in reinforced concrete were poorly understood.

A primary objective of this thesis was to identify the fundamental mechanisms of seismic shear. A detailed study of experimental data from membrane elements subjected to reverse-cyclic shear identified the governing relationships between various stress and strain components. To capture these relationships in a rational model, deformations at the cracks need to be considered separately from deformations of concrete between cracks. This leads to a qualitative and quantitative understanding of the fundamental mechanisms: yielding in shear corresponds to yielding of the weak reinforcement; plastic strain in reinforcement determines the degree of pinching of the hysteresis loops; principal stress and principal strain angles deviate significantly during load reversal; apparent compression softening of concrete is a function of shear slip along cracks which increases significantly after yielding of reinforcement.

In the model, shear slip along cracks is assumed to be a consequence of strain compatibility between reinforcement and concrete between cracks as they equilibrate the applied stresses. This allows the model to be formulated entirely in terms of average stresses and strains, avoiding the complexity of modelling local effects at cracks.

The fundamental principles used in the proposed model provide a general framework which can be used to develop simplified models for analysis and design. As an example, a bi-linear envelope model and a reverse-cyclic model are presented. The yield point and failure point define the bi-linear envelope to the reverse-cyclic response. Together, the envelope model and the reverse-cyclic model can predict the complete cyclic shear response of reinforced concrete in a simple way.

Contents

Contents: Tables

Contents: Figures

Acknowledgements

Many thanks to Barbara for being there and to Tristan for bringing so much joy.

Many thanks to Dr. Adebar for his insightful questioning and his many suggestions.

Thanks also to Dr. Collins for providing raw experimental data from the reverse-cyclic membrane element tests conducted at the University of Toronto.

1

Introduction

1.1 SEISMIC SHEAR IN REINFORCED CONCRETE

An important objective of seismic design is to avoid brittle failures which can lead to collapse of a structure. This can be achieved by ensuring that individual members and connections respond to seismic (reverse-cyclic) loads in a ductile manner. The mechanisms involved in the flexural response of reinforced concrete are well understood and can be used to guide the flexural design. The same cannot be said for the seismic shear response. Many failures of reinforced concrete structures during recent earthquakes were the result of seismic shear (Fig. 1.1). The problem facing designers is how to avoid brittle shear failures, or conversely, how to ensure a ductile seismic shear response.

In the design of new concrete structures it is possible to protect certain elements against seismic shear failure by ensuring that the flexural capacity is less than the shear capacity. Such a capacity design approach is commonly used, for example, in the design of beams of ductile frames, and in the design of slender walls. Since an elastic shear response is often assured, a simple conservative model for shear strength is sufficient.

There are elements of concrete structures which cannot be protected from shear failure by simply using a capacity design approach. The low height of a squat wall, for example, means it may not be possible to develop flexural yielding prior to yielding of the shear reinforcement. In this case, the maximum shear force will be a function of the shear stiffness of

each element. For such structures, a more sophisticated model is needed for the seismic shear response of reinforced concrete.

Many existing concrete structures were designed prior to the development of current seismic shear design procedures and are therefore deficient according to current building codes. In the evaluation of such structures, the conservative seismic shear design rules may suggest an expensive retrofit is required, while a more sophisticated analysis may indicate that a retrofit is unnecessary, or that a simpler retrofit is adequate. Such an analysis requires a comprehensive understanding of the response of reinforced concrete subjected to seismic shear.

Although rational models for the monotonic shear response of reinforced concrete have been in existence for over a decade, they are not directly applicable to reverse-cyclic shear. Cyclic shear models currently available are predominantly empirical: either simple envelope-type models which relate shear strength to ductility demand, or rule-based models that mimic the observations from specific tests. These models have limited application in the seismic assessment of existing structures where the characteristics of the elements can vary widely.

The research for this thesis began by examining the results from a series of experiments on reinforced concrete beam elements subjected to reverse cyclic shear (Roux 1998). Due to the applied bending moments on these elements, the stresses and deformations varied greatly over each element: the inclination of diagonal cracks varied along the element, the crack deformations varied along the length of each crack, and the shear stress distribution was not uniform. Reversing of the load further complicated the distribution of stresses and deformations in the element. It was decided that a fundamental understanding of the mechanisms involved in the seismic shear response of reinforced concrete had to begin with simpler elements that did not have the complicating influence of bending deformations.

A review of research on membrane elements – reinforced concrete panels with uniform stresses and strains – revealed that the fundamental mechanisms of the reverse cyclic shear response were poorly understood. Principal characteristics of the response, such as pinching of hysteresis loops and degradation of shear stiffness, were being modelled by complex empirical formulations. A good understanding of the fundamentals of seismic shear was not

yet available in even the simplest elements. Thus it was decided to focus this research on identifying the fundamental mechanisms of the reverse-cyclic shear response by conducting a detailed examination of data from membrane elements subjected to reverse-cyclic shear; and by developing a rational model that not only captured the important characteristics of the observed response, but also helped to explain them.

1.2 MEMBRANE ELEMENTS

Membrane elements are elements with only in-plane stresses applied to the boundaries and where stresses and strains are assumed to be uniform over the area of the element. They can represent small regions of larger structures. For example, for each of the small elements identified on the concrete structures shown in Fig. 1.2, it is reasonable to assume that the stresses and strains within the element are approximately uniform. The uniform membrane stresses applied to such elements can be described by two normal stress components parallel to the two sides of the element (σ_x and σ_y) and the membrane shear stress (v_{xy}). Typically, membrane elements are reinforced in two orthogonal directions. The deformations of the membrane element can be described by the two normal strain components (ε_x, ε_y), and the shear strain (γ_{xy}).

Collins (1979) first developed the concept of studying reinforced concrete membrane elements in order to define the fundamental relationship between applied shear stress and the resulting shear deformation. For this purpose, Collins, together with his colleagues, developed the Panel Element Tester (Vecchio and Collins 1982), Fig. 1.3, and the Shell Element Tester (Kirschner and Collins 1986), Fig. 1.4. Following the success of this approach, similar testers were constructed in Japan (Ohmori et al. 1987), and the United States (Hsu, Belarbi, and Pang 1991). Based on the results of their membrane element tests, Vecchio and Collins (1982) developed the Modified Compression Field Theory for reinforced concrete subjected to monotonic shear.

1.3 MONOTONIC SHEAR IN MEMBRANE ELEMENTS

The response to monotonic shear is simpler than the response to reverse-cyclic shear and has been studied more extensively. Current reverse-cyclic models use many of the same

fundamental assumptions as used in the monotonic models. Thus some of the important background to the monotonic shear response of reinforced concrete is briefly reviewed here.

Design for shear has traditionally been based on a truss analogy, with the transverse and longitudinal reinforcement modelled as tension ties and the concrete modelled as compression "struts" inclined at 45°. Because the 45° truss analogy does not always reflect actual behaviour – often, the cracks are inclined at less than 45° – it tends to underestimate the shear strength. To compensate, an empirical adjustment, called concrete contribution, is made. The result is the $V_s + V_c$ approach which is the basis for the design method still prevalent in North American codes. Because of the empirical nature of the V_c adjustment, numerous different adjustments are used depending on the level of axial loads, prestress, and so forth. Collins et al. (1996) wrote that this approach has led to there being 43 equations for shear in the 1995 ACI Building Code.

One branch of shear research has aimed to develop better truss models with different strut angles, the addition of concrete in tension normal to the struts and other effects. Such models are applied directly to beams and columns, not membrane elements, and therefore are not discussed here. A complete discussion of these is given in the ASCE/ACI Committee 445 State-of-the-art report (1998).

In 1974, Mitchell and Collins developed the Compression Field Theory (CFT) for reinforced concrete beams subjected to torsion (Mitchell and Collins 1974), and in 1978, Collins applied the CFT to reinforced concrete beams subjected to shear (Collins 1978). Similar to Wagner's tension field theory for thin steel plates (it assumes that after buckling the steel resists no compression and that shear is carried by a field of diagonal tension), the Compression Field Theory assumes that after cracking the concrete resists no tension and that shear is carried by a field of diagonal compression. The concrete compression stress field was assumed to rotate freely to whatever inclination simultaneously satisfied equilibrium (the compression stress field in concrete is equilibrated by tension stresses in the reinforcement), strain compatibility (between concrete and reinforcement), and the assumed stress-strain relationships for cracked concrete and reinforcement. The CFT was formulated in terms of average stresses and average strains in order to avoid dealing with

local variations (larger deformations at the cracks and smaller deformations away from the cracks).

In order to develop stress-strain relationships for diagonally cracked concrete subjected to shear, Vecchio and Collins (1982) conducted a large series of membrane element tests. These tests indicated that concrete tensile stresses can be significant even after cracking. The assumptions of the CFT were combined with the new stress-strain relationships for cracked concrete (including concrete tensile stresses) and the result was called the Modified Compression Field Theory (Vecchio and Collins 1986). This theory is probably the most widely referenced rational model for shear in reinforced concrete and forms the basis of many other models. The method has been implemented in a number of North American codes as a general method to replace the 45° truss analogy.

1.3.1 The Modified Compression Field Theory

The Modified Compression Field Theory (MCFT) is summarized in Fig. 1.5 (Collins and Mitchell 1991).The underlying premise is that reinforced concrete can be modelled by the superposition of reinforcement and cracked concrete. It is assumed that cracked concrete can be treated as a new material defined in terms of relationships between average stresses and average strains. The reinforcement and the cracked concrete are linked by assuming the following equilibrium and strain compatibility requirements:

Equilibrium in terms of average stresses: In each reinforcement direction, the average normal stress in the reinforcement and the average normal stress in the concrete sum to the applied normal stress. Dowel action in the reinforcing bars is assumed negligible such that only the concrete resists the applied shear stress.

Compatibility conditions in terms of average strains: It is assumed that average strains (measured over a base length that includes a number of cracks) satisfy the compatibility requirements (transformation equations). Also, it is assumed that average strains of the cracked concrete are equal to average strains of the reinforcement (i.e., on average, the two are perfectly bonded).

Some other important assumptions of the MCFT are:

Rotating crack angle: the cracks are assumed to rotate freely, remaining perpendicular to the principal average tension stress.

Principal angles coincide: for cracked concrete, the principal average stress is assumed to coincide with the principal average strain.

Average stress-strain relationships for cracked concrete: it is assumed that a relationship can be defined which relates the average principal concrete compression stress and the average principal compression strain. This relationship is typically assumed to be similar in form to that of plain concrete, but softer (larger strains) and weaker (lower peak compressive stress). The softening and weakening is assumed to be a function of the principal tension strain occurring transverse to the principal compression. A separate relationship is used to relate the average principal concrete tension stress and the average principal tension strain.

Crack check: While the CFT was formulated entirely in terms of average stress and average strain, the MCFT includes a check on the local stresses at a crack. The crack check has two purposes. Firstly, the concrete is assumed to have zero tension locally at a crack, and thus the local stresses in the reinforcement will be higher than on average. The crack check verifies the ability of the reinforcement to resist the higher local stresses. The crack check is also used to apply a limit on the local shear stress as a function of the crack width.

1.3.2 Other Monotonic Models

Other models have been proposed for the monotonic shear response of reinforced concrete. These models share many features of the MCFT such as the fundamental equilibrium and strain compatibility assumptions and the modelling of cracked concrete as a new material.

They differ primarily in the constitutive relationships for the materials. For reasons of brevity, only the main differences are summarized below.

Using the University of Houston panel element tester, Belarbi and Hsu formulated different constitutive relationships for cracked concrete in compression, for cracked concrete in tension, and for the reinforcement (Belarbi and Hsu 1994; Belarbi and Hsu 1995). Whereas the MCFT relationships were derived from elements subjected to shear with the reinforcement at 45° to the principal stress directions, the relationships used in the Rotating Angle - Softened Truss Model or RA-STM (Pang and Hsu 1995) were derived from elements subjected to tension-compression loading parallel to the reinforcement. The principal difference between the RA-STM and the MCFT is the way concrete tension stresses and reinforcement stresses are applied (Hsu and Zhang 1996). In the RA-STM, the average yield stress of the reinforcement depends on the average concrete tension stress, which ensures that the local tension stress in the reinforcement at a crack does not exceed the yield strength of the bare bar. This approach was first proposed by Stevens et al. (1987).

Pang and Hsu also formulated a model with a fixed crack orientation, the Fixed Angle - Softened Truss Model (Pang and Hsu 1996), which has become the Softened Membrane Model or SMM (Hsu and Zhu 2002). Because of the fixed crack orientation, the SMM requires an additional link between stresses and strains: unlike rotating crack models where the average shear at the crack orientation is zero, with fixed cracks at other than the principal orientation there is shear stress at the crack interface. The SMM adds a relationship between the average shear stress and the average shear strain. Otherwise, it is similar to the RA-STM (Pang and Hsu 1995).

In their Cracked Membrane Model, Kaufmann and Marti (1998) used a more fundamental approach for modelling the tension stresses transferred from the reinforcement to the concrete. Instead of using an empirical relationship directly for the principal tension stress, as in the MCFT and the other models mentioned above, the concrete tension stiffening is determined from an assumed bond stress vs slip relationship applied in each of the reinforcement directions. Deformations at the cracks are also considered more explicitly and are used as the basis for defining average stresses. The general formulation of the model

assumes the cracks are at a fixed orientation; however, a simplified solution procedure assumes rotating cracks.

In his theory for membrane elements, Zararis (1986) explicitly considers shear stress in the reinforcement. Strain compatibility and equilibrium equations are formulated locally at the cracks. Zararis has focussed in particular on the failure mechanisms: yielding of the reinforcement, crushing of the concrete, and concrete shear failures due to excessive shear deformation at the cracks (Zararis 1988, 1996).

Recently, Vecchio (2000) proposed the Disturbed Stress Field Model (DSFM) which makes two fundamental assumptions that differ from the MCFT. First, the assumption that the principal stress angle coincides with the principal strain angle is modified to include a "lag" or fixed difference between the two angles. Secondly, the strain compatibility requirements are re-formulated whereby shear slip along the cracks is considered explicitly instead of included in the overall average deformations of cracked concrete. Consequently, a new stress-strain relationship for the cracked concrete in compression is formulated where the average principal compression strain excludes strain due to shear slip along the cracks. Walraven's (1981) relationship is used to define shear strain due to slip along the cracks.

1.3.3 Cracked concrete as a new material

A common aspect of all the monotonic shear models is the representation of cracked concrete as a single, homogeneous material which is assumed independent of the reinforcement. The representation of cracked concrete has evolved over time. In the CFT, it was a relationship in the principal compression direction only. With the MCFT, the principal tension direction was added and it was called a new material. Hsu has added Poisson effects and a shear stress-strain relationship making it a fully defined homogeneous material.

Defining cracked concrete has been difficult. The parabola, widely used to model the loading branch for plain concrete, serves as the base curve up to the peak compression stress (modelling of the descending branch varies between models). A softening coefficient is then applied to the peak stress, and in some cases to the strain at peak stress. In the last 20 years there has been a tremendous effort aimed at defining this softening coefficient and

many variations have been proposed. Although most are a function of the principal tensile strain – some are a function of tensile stress and some are fixed coefficients – there is little consensus; almost every experimental test series has yielded a different softening coefficient. Vecchio and Collins (1993) and Duthinh (1999) reviewed a number of the functions use to define compression softening of cracked concrete.

In reality, cracked concrete is not independent of the reinforcement. This partly explains why different tests give different results. Hsu's Poisson's ratios for cracked concrete (Zhu and Hsu 2002) are a function of the reinforcement and therefore link the concrete response to the reinforcement.

The definition of cracked concrete as a homogenous isotropic material also implies that the stress and strain angles coincide. This is a fundamental assumption of the MCFT (Vecchio and Collins 1986), and is a requirement in Hsu's models: the stress-strain relationship for shear is taken from elasticity theory for homogeneous isotropic materials which requires coincident principal angles (Zhu, Hsu, and Lee 2001).

Assuming that cracked concrete behaves as a homogenous isotropic material leads to reasonable predictions of the response to monotonic shear, but as discussed in this thesis, it is not appropriate for modelling the response to reverse cyclic shear.

1.3.4 Local shear stress at the cracks

Most monotonic shear models include a representation of local shear stress at the crack interface. As noted above, the MCFT includes a crack check to determine local stresses. Fixed crack models generally include the shear stress and shear strain (shear slip) at the crack interface in the solution. For example, Kaufmann and Marti (1998) and Vecchio (2000) use Walraven's (1981) relationship for the slip on a crack as a function of the shear stress and the crack width.

Proponents of fixed crack models view modelling local effects as an opportunity to include mechanisms such as aggregate interlock and dowel action. However, the problem is they are complicated and locally highly variable mechanisms. To be manageable, a local model can only approximate or average local effects. There is also disagreement over which mechanisms are involved: aggregate interlock, dowel action, damage on cracks and tension

splitting have been proposed in various combinations. Typically, deformations at the cracks are modelled by slip and normal displacements as a function of stresses; average strains are obtained by dividing displacements by an estimated crack spacing. To obtain local reinforcement strains, a length of reinforcement, the de-bonded length, must be assumed. The net result is a collection of mostly empirical relationships countering the gains made conceptually.

A model based entirely on average stresses and strains, such as the CFT (Collins 1978), avoids the problem of capturing local effects.

1.4 REVERSE-CYCLIC SHEAR IN MEMBRANE ELEMENTS

Until recently, efforts towards formulating a rational model for membrane elements subjected to reverse-cyclic shear have focussed on extending the principles of the Modified Compression Field Theory (Vecchio and Collins 1986) to the cyclic case. For example, Stevens et al. (1987) used the same equilibrium and strain compatibility requirements as the MCFT. They also applied the concept of cracked concrete as a single material; this required formulating a reverse-cyclic stress-strain relationship for cracked-concrete. Similarly, Mansour, Hsu and Lee (2000) have applied the monotonic Softened Membrane Model (Hsu and Zhu 2002) to the cyclic case by formulating a reverse-cyclic cracked concrete function. Vecchio (1999) proposed a different approach for defining cracked concrete where plastic strains are used to account for reverse-cyclic effects. Similar to monotonic models, current models for reverse-cyclic shear treat cracked concrete as a single material.

The stress-strain relationship needed to capture reverse-cyclic effects in cracked-concrete is very complex. The experimental data indicates a region where the minimum principal strain is tensile while the minimum principal concrete stress is compressive. To capture this effect, the concrete compression and tension relationships are combined into a single stress-strain function. This function includes a transition zone which, unlike typical materials, relates tensile strains to compressive stresses.

To model this behaviour, Stevens et al (1987) combined a compression and a tension backbone curve with a series of empirically derived transition curves. This required 16 different equations defined by a number of empirical coefficients and applied through a

number of rules. Ohmori et al. (1987) similarly defined a cyclic cracked concrete stress-strain function by a series of empirically fitted equations. Hsu and Mansour (2000) formulated a reverse-cyclic cracked concrete function using 11 empirically fitted equations. The complicated and empirical nature of these cracked concrete functions indicates this approach is more empirical than fundamental and general.

A common failing of reverse-cyclic models based on the cracked concrete approach is the lack of rational explanations for the complex behaviour observed experimentally. The models are able to mimic the observed behaviour of a particular series of tests by using a suitably complex formulation for the cracked concrete, however, this hides the underlying mechanisms behind an empirical representation. For example, pinching of the hysteresis loops, the most prominent characteristic of the reverse-cyclic shear response, has been attributed to different phenomena: Stevens et al. (1987) attribute the pinching to bond slip; Mansour and Hsu (2000) suggest the orientation of the reinforcement is responsible; Paulay and Priestley (1992), in a comment pertaining to seismic shear in beams, relate the pinching to opening and closing of shear cracks in conjunction with plastic strains in the reinforcement. Although existing models capture the pinching, they provide no insight into the underlying mechanisms.

The assumption that the principal concrete stresses coincide with the principal strains hampers the application of monotonic models to the reverse-cyclic case; Stevens et al. (1987) found the principal angles are clearly not equal during the load reversal. To compensate, they assumed that only the increments of stress and strain occur at the same orientation. In his recent model, presented for the monotonic case, Vecchio (Vecchio 2000) introduced a constant difference between the two angles. Mansour, Hsu and Lee (2000) do not directly address the issue. Ideally, the two angles should be allowed to rotate independently during the reversal, as needed to maintain equilibrium and strain compatibility.

In a recent model by Rose et al (2002), stresses and strains at the cracks are modelled explicitly instead of combined with the concrete. The model assumes a fixed orientation for the cracks and includes relationships for sliding, opening and closing (contact) at the cracks. The model for the concrete applies only to the concrete between the cracks. Equilibrium is defined both in terms of average stresses in the concrete and in terms of local stresses at the

cracks. Local strains in the reinforcement at a crack are based on an effective de-bonding length. Similar to fixed-crack monotonic models, the gains in conceptual detail are offset by the empirical nature of the relationships used to describe local conditions at the cracks. Due to the complexity of these relationships and of the overall model, sophisticated non-linear equation solving techniques are required ("including the arclength method, quadratic back-tracking line search and subincrementation").

Separating the strains at the cracks from the strains in the concrete between the cracks appears to be the right approach for modelling reverse-cyclic shear. However, as noted earlier, this should be done in terms of average strains (and average stresses) to avoid the complexity and empiricism associated with modelling local effects at the cracks.

1.5 THESIS OBJECTIVES

The first objective of this thesis is to identify the fundamental mechanisms governing the response of reinforced concrete membrane elements to reverse-cyclic shear. This includes determining what controls the pinching of the hysteresis loops, what defines the cracked section shear stiffness and what causes it to degrade. The conditions which determine whether failure will be brittle or ductile, and at what maximum strain, should also be identified. The role of the concrete, the role of the reinforcement and the interaction between the two need to be better understood.

The second objective of the research is to develop a rational model to predict the complete load-deformation response of these elements. The model should combine strain compatibility, equilibrium and constitutive relationships to capture the complex response through the interaction of simple and fundamental components. It should be simple, transparent, general, and should reflect the fundamental mechanisms.

The third objective is to demonstrate how the rational model can lead to simplified models suitable for the analysis and design of structures. These models should allow designers to determine, in a simple way, what is an appropriate cracked section shear stiffness. They should indicate whether yielding constitutes failure or if there is some ductility in the response and, if so, how much. They should enable designers to include the shear response in the dynamic or static non-linear analysis of structures.

Together, these objectives form a new framework for modelling reverse-cyclic shear in a rational and simple way.

1.6 METHODOLOGY AND THESIS ORGANIZATION

Existing rational models for monotonic shear and for reverse-cyclic shear were developed by formulating a model or theory, then performing experiments to define certain components, calibrate coefficients and verify the resulting model. This approach has been successful for modelling monotonic shear, but so far not for reverse-cyclic shear. Therefore, for this thesis it was decided to reverse the process and start with a broad examination of experimental data.

The raw experimental data from a series of membrane element tests was obtained from the University of Toronto. The experiments had been conducted, and the data previously examined, to determine average stress-strain relationships for cracked concrete within the framework of the Modified Compression Field Theory. For this thesis, the same experimental data was used to identify all three components of a rational model (strain compatibility, equilibrium, and constitutive relationships). The observed relationships between the various strain components were used to develop new strain compatibility assumptions more appropriate for reverse-cyclic shear. The relationships between the various stress components were used to confirm existing equilibrium requirements. The relationships between the various stress and strain components were used to develop new constitutive relationships.

The shear response of reinforced concrete is the end result of complex interactions between the reinforcement and the concrete. To investigate these interactions, a large number of plots were generated, arbitrarily combining stress and strain components at different orientations (in the reinforcement directions, in the principal directions, and at +45° and −45° to the reinforcement). From these plots, significant relationships emerged: certain components are clearly dominant and certain pairs of components are closely related. These relationships, presented in Chapter 2, guide the development of the rational model presented in Chapter 3, and the constitutive relationships presented in Chapter 4. In Chapter 3, the knowledge gained by the development of the model helps to identify the fundamental

mechanisms and explain the relationships observed in the experimental data. Model predictions are compared to the experimental data in Chapter 5.

A simplified version of the proposed model is developed in Chapter 6. The proposed model is used to formulate equations for the shear at yielding and at failure. These are then simplified by introducing approximations based on an understanding of the fundamental mechanisms. The resulting simplified model is applied to the experimental data, demonstrating its easy application to analysis and design of reinforced concrete elements.

Conclusions are gathered in Chapter 7.

2

Understanding the seismic shear response: Review of experimental data

This chapter presents the important experimentally observed relationships which led to the development of the proposed model and which are significant for explaining the mechanics of reinforced concrete subjected to reverse cyclic shear.

2.1 TEST SPECIMENS AND LOADING

To study the response of membrane elements subjected to shear, Collins, together with his colleagues, developed the Panel Element Tester (Vecchio and Collins, 1982). Figure 2.1 shows a schematic of the tester. The specimens for this tester are 890mm square by 70 mm thick. The tester applies uniform loads via shear keys around the perimeter of the specimens. Each shear key is connected to hydraulic jacks by two orthogonal links. By varying the intensity and the direction of the load in each link, any combination of shear and tension or compression can be applied to the specimens. For example, applying tension in one link and compression of equal magnitude in the other link results in pure shear on the edges.

To test larger specimens, Collins and his colleagues designed the Shell Element Tester (Kirschner and Collins 1986), shown schematically in Fig. 2.2. In addition to in-plane forces, the Shell Element Tester has the capability to apply shear transverse to the

specimens for the study of shell elements. The specimens for this tester are 1524 mm square by 285 mm thick. In the Shell Element Tester, the reinforcement is welded directly to the shear keys. By varying the direction and magnitude of the stresses on each face of the specimen, different combinations of shear and axial tension or compression can be applied. For example, pure shear loading (with respect to the reinforcement axes) is generated by applying normal forces of equal magnitude but opposite direction to orthogonal faces of the specimen.

The membrane element specimens are typically reinforced in two orthogonal directions with the element axes aligned with the reinforcement (Fig. 2.3). General convention is to label the stronger reinforcement direction the x axis and the weaker reinforcement direction the y axis. With reference to beams, these would be the longitudinal and transverse reinforcement directions respectively. Membrane elements are subjected to in-plane loading which is typically represented by normal stress in the x and y directions, n_x and n_y, and shear stress, v_{xy}. The resulting in-plane deformations or strains are typically described by normal strains in the x and y directions, ε_x and ε_y, and shear strain γ_{xy}.

For this thesis, seven specimens were selected from three different research projects conducted at the University of Toronto. Three specimens, SE8, SE9 and SE10, were tested in reverse-cyclic shear by Stevens et al. (1987), using the University of Toronto Shell Element Tester (Kirschner and Collins 1986). One specimen, PP1, which has section properties similar to SE8, was tested in monotonic shear by Meyboom (1987) using the Shell Element Tester. Including this specimen in the study enables comparisons between the reverse-cyclic case and the simpler monotonic case. Three smaller specimens, PDV1, PDV2 and PDV3, were tested by Villani (1995) in monotonic shear, reverse-cyclic shear, and positive-only cyclic shear respectively. They were tested on the University of Toronto Panel Element Tester (Vecchio and Collins 1982). All these specimens were instrumented with displacement transducers (LVDTs) which provided a continuous measurement of deformations.

The characteristics of each specimen and of the applied loading are summarized in Tables 2.1 and 2.2. Specimens SE8, SE9, SE10, and PP1 were 1524 mm square by 285 mm thick and reinforced with 10M and 20M bars arranged in two layers. The PDV specimens

were 890 mm square by 70 mm thick and reinforced with two layers of 6 mm bars. All the specimens were reinforced in two orthogonal directions with the x direction parallel to the larger quantity of reinforcement and the y direction parallel to the smaller quantity of reinforcement.

The SE specimens were instrumented with 6 LVDTs per face while specimen PP1 had 8 LVDTs per face. The PDV specimens were instrumented with 3 LVDTs per face. The LVDTs were installed in the x and y directions and on the diagonals (±45°).

All the tests were stress controlled: for each cycle, the load was increased until the desired applied shear stress was reached. For the reverse-cyclic shear tests, the load was

Table 2.1 1524 mm x 1524 mm x 285 mm specimens

Parameter	SE8	SE9	SE10	PP1
shear load	reverse-cyclic	reverse-cyclic	reverse-cyclic	monotonic
axial load	$N_x = N_y = 0$	$N_x = N_y = 0$	$N_x = N_y = -{}^1/_3\lvert V_{xy}\rvert$	$N_x = N_y = 0$
Concrete				
f_c' (MPa)	37.0	44.2	34.0	27 .0
ε_c'	0.0026	0.00265	0.0022	0.00217
E_c (MPa) [1]	28770	31450	27580	24580
f_t (MPa) [2]	2.0	2.2	1.9	1.7
Reinforcement				
x direction	20M @ 72 mm,ea. face	20M @ 72 mm,ea. face	20M @ 72 mm,ea. face	20M @ 108 mm,ea. face
ρ_x	0.0294	0.0294	0.0294	0.0195
y direction	10M @ 72 mm,ea. face	20M @ 72 mm,ea. face	10M @ 72 mm,ea. face	10M @ 108 mm,ea. face
ρ_y	0.0098	0.0294	0.0098	0.0065
$\rho_x : \rho_y$	3:1	1:1	3:1	3:1
f_{yx}, f_{yy} (MPa)	492, 479	422, 422	422, 479	480, 480

[1] estimated as $E_c = 4730\sqrt{f_c'}$, as suggested in Collins and Mitchell (1991)

[2] estimated as $f_t = 0.33\sqrt{f_c'}$, as suggested in Collins and Mitchell (1991)

gradually increased to a target level, reduced to zero, increased in the opposite direction to another target level, then unloaded back to zero to complete one full cycle. Typically, a number of cycles were performed at a stress level below yielding of the reinforcement; these are the elastic cycles. The load was then cycled at a level causing yielding of the weak reinforcement (y-direction reinforcement). These yield cycles were continued until the element failed. For the monotonic shear tests, the load was gradually increased until the specimen failed.

Table 2.2 890 mm x 890 mm x 70 mm specimens

Parameter	PDV1	PDV2	PDV3
shear load	monotonic	reverse-cyclic	cyclic
axial load	$N_x = N_y = -0.4\|V_{xy}\|$	$N_x = N_y = -0.4\|V_{xy}\|$	$N_x = N_y = -0.4\|V_{xy}\|$
Concrete			
f_c' (MPa)	26.8	23.7	34.1
ε_c'	0.00162	0.00163	0.00169
E_c (MPa) [1]	24480	23030	27620
f_t (MPa) [2]	1.7	1.6	1.9
Reinforcement			
x direction ρ_x	6 mm⌀@ 45 mm, ea. face 0.0182	6 mm⌀ @ 45 mm, ea. face 0.0182	6 mm⌀ @ 45 mm, ea. face 0.0182
y direction ρ_y	6 mm⌀ @ 89 mm, ea. face 0.0091	6 mm⌀ @ 89mm, ea. face 0.0091	6 mm⌀ @ 89 mm, ea. face 0.0091
$\rho_x : \rho_y$	2:1	2:1	2:1
f_{yx}, f_{yy} (MPa)	282 / 282	282 / 282	282 / 282

[1] estimated as $E_c = 4730\sqrt{f_c'}$, as suggested in Collins and Mitchell (1991)

[2] estimated as $f_t = 0.33\sqrt{f_c'}$, as suggested in Collins and Mitchell (1991)

The stress controlled approach means that post-peak data is not reliable since it is subject to the rate of application of the loading and the rate at which the loading is removed once failure occurs, i.e., the failures were not controlled events.

2.2 EXPERIMENTAL DATA

2.2.1 Measured Experimental Data: Average Strains and Applied Stresses

Average Strains

The LVDTs measure deformations as a change in length of the specimen in the x and y directions and at $+45°$ and $-45°$ with respect to the x axis (defined clockwise positive). Strains are obtained by dividing the measured change in length by the original gauge length. Therefore, the experimentally measured strains are average strains, representing average deformations. Since each LVDT spans a number of cracks, the deformations at any single crack are not measured, instead the cracks are assumed to be uniformly smeared over the element.

An important assumption associated with membrane elements is that the average strain components satisfy the compatibility equations (Vecchio and Collins 1982). Thus the average strains in the four directions can be combined into an average strain state. For the SE specimens, the strains were averaged by the author following the method described in Appendix A.1. For the PDV specimens and PP1, the reported data was already averaged.

Applied Stresses

In both the Shell Element Tester and the Panel Element Tester, the applied loading is measured using pressure transducers installed on the hydraulic lines which supply the loading jacks. The measured hydraulic pressures are converted to applied stresses, n_x, n_y, and v_{xy} which are reported for each test

2.2.2 Derived Experimental Data: Reinforcement and Concrete Stresses and Strains

Stresses and strains in the concrete and in the reinforcement are not directly measured, instead they are derived from the applied stresses and the measured average strains by using some rational assumptions.

Reinforcement Stress and Strain

The average strain in the reinforcement is assumed equal to the total average strain (Vecchio and Collins 1982), i.e.,

$$\begin{aligned} \varepsilon_{sx} &= \varepsilon_x \\ \varepsilon_{sy} &= \varepsilon_y \end{aligned} \tag{2.1}$$

where ε_{sx} and ε_{sy} are the average strains in the reinforcement and ε_x and ε_y are the measured total strains. This is a reasonable assumption considering that the reinforcing bars remain bonded to the concrete midway between cracks and thus average deformations are the same.

To define the reinforcement stresses, Vecchio and Collins (1982) used a simple bi-linear, elastic-plastic stress-strain relationship defined by the yield stress (f_y) and the steel modulus (E_s). This model is used here; it is termed the bare-bar model since the stress-strain relationship is obtained from tension tests on plain reinforcing bars:

$$\begin{aligned} \sigma_{sx} &= E_s \cdot \varepsilon_{sx} \leq f_{yx} \\ \sigma_{sy} &= E_s \cdot \varepsilon_{sy} \leq f_{yy} \end{aligned} \tag{2.2}$$

Reinforcement stresses unload linearly at a slope of E_s.

Reinforcement stress-strain functions that include the influence of the concrete have been proposed (Stevens, Uzumeri, and Collins 1987; Hsu and Zhang 1996; Kaufmann and Marti 1998). Although they are considered conceptually more detailed, these functions are more complex and less general than the bare bar model. By comparison, the bare bar model is simple and transparent, important attributes when trying to understand the experimental data. Ultimately it is the sum of the reinforcement and concrete stresses which is important, the details of the individual stress-strain models are secondary and somewhat arbitrary.

The point at which yielding occurs in the reinforcement is an important parameter of the shear response. In terms of average strains and stresses, yielding occurs gradually. In contrast, the bare bar model (Eq. 2.2) has a distinct yield point at the yield stress (f_y). The yield point for the quantitative analysis is the last data point before the reinforcement stress σ_s equals or exceeds the yield stress. Because this criteria may not be appropriate for all cases, a qualitative or graphical yield point is also considered (see Appendix B.4). Using both measures of yielding is preferable to making arbitrary adjustments for each specimen.

Concrete Stress

Concrete stresses are obtained through the equilibrium requirement:

force in the concrete + force in the reinforcement = total applied force

For membrane elements, it is typical to assume all the applied shear stress is resisted by the concrete (Vecchio and Collins 1982; Stevens, Uzumeri, and Collins 1987; Pang and Hsu 1995; Kaufmann and Marti 1998). The equilibrium equations are then

$$\begin{aligned} V_{cxy} &= V_{xy} \\ N_{cx} + N_{sx} &= N_x \\ N_{cy} + N_{sy} &= N_y \end{aligned} \tag{2.3}$$

where V_{xy} is the applied shear force, N_x and N_y are the applied normal forces in the x and y reinforcement directions, and the subscripts c and s refer to the concrete and reinforcement components respectively.

Converting forces to stresses, Eq. 2.3 becomes

$$\begin{aligned} v_{cxy} A_c &= v_{xy} A_t \\ \sigma_{cx} A_c + \sigma_{sx} A_s &= n_x A_t \\ \sigma_{cy} A_c + \sigma_{sy} A_s &= n_y A_t \end{aligned} \tag{2.4}$$

where A_t is the total loaded area and is equal to the sum of the concrete area A_c and the steel area A_s. For typical quantities of reinforcement, it is reasonable to assume the concrete area is equal to the total area, i.e., $A_c = A_t$. Then, dividing each term by the total area A_t and

substituting the reinforcement ratio ρ for A_s/A_t, the equilibrium equations can be expressed as stresses:

$$\begin{aligned} v_{cxy} &= v_{xy} \\ \sigma_{cx} + \rho_x \cdot \sigma_{sx} &= n_x \\ \sigma_{cy} + \rho_y \cdot \sigma_{sy} &= n_y \end{aligned} \tag{2.5}$$

where the $\rho\sigma_s$ terms (the reinforcement force divided by the total area) represent an effective stress which can be added to the concrete stress.

Re-arranging Eq. 2.5, the complete concrete stress state, defined by σ_{cx}, σ_{cy}, v_{cxy}, is obtained by subtracting the reinforcement stresses from the total stresses. The principal concrete tension stress σ_{c1} and the principal concrete compression stress σ_{c2} are then obtained from the standard transformation equations:

$$\begin{aligned} \sigma_{c1} &= \frac{\sigma_{cx} + \sigma_{cy}}{2} + \frac{1}{2}\sqrt{(\sigma_{cy} - \sigma_{cx})^2 + (2v_{cxy})^2} \\ \sigma_{c2} &= \frac{\sigma_{cx} + \sigma_{cy}}{2} - \frac{1}{2}\sqrt{(\sigma_{cy} - \sigma_{cx})^2 + (2v_{cxy})^2} \end{aligned} \tag{2.6}$$

The orientation of the principal concrete stresses is calculated from:

$$\theta_{c\sigma} = \begin{cases} \frac{1}{2}\tan^{-1}\left(\frac{2v_{cxy}}{\sigma_{cy} - \sigma_{cx}}\right); \sigma_{cy} \neq \sigma_{cx} \\ 45^\circ \cdot \frac{v_{cxy}}{|v_{cxy}|}; \sigma_{cy} = \sigma_{cx} \end{cases} \tag{2.7}$$

where $\theta_{c\sigma}$ is the principal concrete stress angle, defined clockwise positive from the x axis to the principal compression (2) axis.

Influence of the reinforcement model on the concrete stresses

The influence of the reinforcement model, specifically the yield stress, on the calculated concrete stresses is examined in Table 2.3. Reducing the yield stress reduces the maximum

stress in the reinforcement and through the equilibrium equations reduces compression stresses in the concrete at first yielding. The principal angle is essentially unaffected.

The principal concrete tension σ_{c1} is the component most affected by the change in reinforcement yield stress. This stress component is also considerably smaller than the others. These two factors make the concrete tension stress less reliable as well as less significant than the other stress components.

Table 2.3 Influence of reinforcement model: specimen SE8

stress component	value at first yielding of the y reinforcement		relative change: ratio B / A
	A: with $1.0f_{yy}$ (MPa or deg.)	B: with $0.8f_{yy}$ (MPa or deg.)	
v_{cxy}	5.64	5.07	0.90
σ_{cx}	-6.80	-5.80	0.85
σ_{cy}	-4.56	-3.71	0.81
σ_{c2}	-11.43	-9.93	0.87
σ_{c1}	0.06	0.42	6.48
θ_{σ}	39.4	39.2	0.99

2.2.3 Minor Residual Stresses and Strains

During elastic cycles, small residual stresses and strains typically remain at the point of zero applied shear stress. These are believed to be caused by the cracks not closing completely due to some mis-alignment or some damage of the crack surfaces. The result is small tensile strains and stresses in the reinforcement and corresponding compressive stresses in the concrete. These residuals are considered negligible.

2.3 SHEAR RESPONSE: SHEAR STRESS VS SHEAR STRAIN

2.3.1 Response to monotonic shear loading: specimen PP1

The response of specimen PP1 to the application of monotonic shear is shown in Fig. 2.4. Initially the concrete was uncracked and the applied shear was resisted primarily by the

gross concrete section. The uncracked response is linear with a shear stiffness G_{gross} of approximately 12,000 MPa. The first visible cracks occurred at a shear stress of 1.6 MPa which corresponds to a principal tension in the concrete of approximately 1.6 MPa. The cracks formed at roughly 45° to the x axis, i.e., normal to the principal applied tension. During the cracking stage, when more cracks formed and cracks widened, the reinforcement started carrying more of the load. At a shear stress of 3.9 MPa, the stress in the y reinforcement reached yield (480 MPa). At this point the shear strain started to increase more rapidly. Prior to yielding, the tangent shear stiffness was approximately 600 MPa (5% of gross), after yielding it reduced to 80 MPa (less than 1% of gross). The element shear strength started to degrade after reaching a peak shear stress of 4.95 MPa.

2.3.2 Response to reverse–cyclic shear loading: specimen SE8

The response of specimen SE8 to reverse-cyclic shear is shown in Fig. 2.5. The initial uncracked linear response, with $G_{gross} \approx$ 12,000 MPa, is followed by a cracking stage with reduced shear stiffness. In the positive direction, the first cracks occurred at a shear stress of +2.0 MPa and formed at +45° to the x axis; in the negative direction they occurred at −2.1 MPa and formed at −45° to the x axis. Cracking in the second direction appears unaffected by cracking in the first direction. When the load was cycled between ±4.5 MPa, the element displayed a linear elastic response with a shear stiffness of approximately 1,200 MPa or one tenth the gross section stiffness. For the next group of cycles, the peak shear stress was increased to ±5.6 MPa. Around ±5.4 MPa the stress in the y reinforcement reached yield (479 MPa). At the same time, the shear stiffness started to reduce as the shear strains increased more rapidly. After six complete yielding cycles, the element failed before reaching the target stress level.

Each loading segment displays a linear response when the shear stress is between about 2.0 and 5.0 MPa. The tangent stiffness of these segments decreases from one yielding cycle to the next. The stiffness during unloading, however, remains relatively constant and similar to the stiffness during the elastic cycles. The yielding cycles display the pinching of the loops which is characteristic of reverse-cyclic shear.

A single yield cycle is examined more closely in Fig. 2.6. The cycle can be divided into four stages:

Unloading. Unloading from a peak shear stress of +5.8 MPa, the response is approximately linear. At the end of the unloading stage (point A), there is some residual shear strain even though the shear stress is zero.

Reversal. As the shear stress is applied in the negative direction, the shear strain reverses from a positive value to a negative value. Relatively little shear stress is required to bring the shear strain to zero (point B); the tangent stiffness is approximately 400 MPa. From there, the tangent stiffness increases gradually until it reaches 1100 MPa at a shear stress of 2.4 MPa (point C).

Elastic Loading. Point C marks the beginning of the elastic loading stage during which the shear strain increases linearly with the shear stress.

Yielding. When the stress in the y reinforcement reaches yield (at a shear stress of −5.26 MPa), the shear strain increases rapidly as the shear stress increases to the maximum value of −5.68 MPa.

The same four stages are repeated in the second half of the cycle, when the shear stress is reversed from the peak negative to the peak positive value.

2.3.3 Comparison of Monotonic and Reverse–Cyclic Shear Response

Figure 2.7 compares the reverse-cyclic response of SE8 to the monotonic response of PP1. For these well reinforced elements the shear strength is governed by the yield strength of the weak reinforcement ($A_{sy}f_{yy}$). Since specimens SE8 and PP1 have the same dimensions and

the same reinforcement yield strength, the difference between the two is a function of the reinforcement ratios:

$$\frac{\rho_{y,SE8}}{\rho_{y,PP1}} = \frac{0.0098}{0.0065} = 1.5 \tag{2.8}$$

In Fig. 2.7, the shear stress for PP1 is scaled by 1.5. The shear strains are not scaled since the yield strain of the y-reinforcement is the same for both specimens. Before cracking, and during initial crack formation, the response is governed by the concrete tensile strength. For this part of the comparison the 1.5 scaling factor is likely too high given that the actual tension strengths (determined from concrete cylinder splitting tests) are very similar: f_{sp} = 3.4 MPa for SE8 and 3.5 MPa for PP1.

Figure 2.7 supports the notion that the monotonic response is the envelope to the reverse-cyclic response, with one caveat: in the monotonic case, the shear stress continues to increase after yielding while in the reverse-cyclic case, yielding occurs at a constant shear stress for each cycle resulting in no significant post-yield stress increase.

2.3.4 Shear Response: Other specimens

The shear response for the remaining specimens is shown in Figs. 2.8 to 2.10. They all display the same uncracked, cracking and yielding stages as PP1 and SE8. The cyclic specimens include linear-elastic cycles and yielding cycles where plastic shear strains accumulate. Details of the responses are summarized in Tables 2.4 and 2.5. Shear stiffness values are compared separately in the next section.

SE9 and SE10 (Figs. 2.8, 2.9) include elastic cycles at three different stress levels during the cracking stage. At each level, the shear stiffness reduces noticeably between the first and the second cycle, then remains relatively constant for the subsequent cycles.

The PDV specimens are shown in Fig. 2.10 (plotted at the same scale as the others). The response of PDV1 (Fig. 2.10a) is similar to PP1. For PDV2 (Fig. 2.10b), most of the cycling occurs in the cracking stage. For these cycles, the re-loading curve goes through the last point in the previous cycle in the same direction. PDV3 (Fig. 2.10c) is cycled in positive shear only and all but one cycle occurs before yielding. Cycling in the cracking stage results

in some accumulation of residual shear strains, although at less than 1 mε these residuals are very small compared to the residual strains of the other specimens.

Table 2.4 Summary of shear responses, large specimens

	SE8	SE9	SE10	PP1
shear stress at first cracking	1.88	2.34	3.04	1.65
principal concrete tension at first cracking	2.07	2.18	2.08	1.55
shear stress at first yielding a) at yielding of *y* reinforcement b) at shear yielding (graphical)*	 5.71 5.80	 -9.45 9.55	 -7.70 8.20	 4.05 4.40
shear strain at first yielding a) at yielding of *y* reinforcement b) at shear yielding (graphical)*	 0.0048 0.0045	 0.0073 0.006	 -0.0056 0.0059	 0.0045 0.0052
peak shear stress	5.79 -5.79	9.59 -9.56	8.11 -8.20	4.95
shear strain at failure	0.0115	-0.0085	-0.0076	0.0114

* see Appendix B.4 for graphical determination of shear yielding; only positive shear stress considered

Table 2.5 Summary of shear responses, small specimens

	PDV1	PDV2	PDV3
shear stress at first cracking	3.62	3.71	4.63
principal concrete tension at first cracking	2.12	2.20	2.71
shear stress at first yielding a) at yielding of *y* reinforcement b) at shear yielding (graphical)*	 6.16 6.40	 5.90 5.90	 6.70 7.00
shear strain at first yielding a) at yielding of *y* reinforcement b) at shear yielding (graphical)*	 0.0031 0.0035	 0.0037 0.0035	 0.0030 0.0035
peak shear stress	6.43	6.35 -5.88	7.21
shear strain at peak shear stress	0.0047	0.0057	0.0047

* see Appendix B.4 for graphical determination of shear yielding; only positive shear stress considered

2.3.5 Shear stiffness

The shear modulus for an elastic isotropic material is

$$G = \frac{E}{2(1+\nu)} \tag{2.9}$$

where E is the modulus of elasticity and ν is the Poisson's ratio (Popov 1968). For concrete, ν is commonly assumed equal to 0.2 and the uncracked or gross section shear stiffness G_{gross} is approximately $0.4E_c$.

Once the concrete has cracked, the shear stiffness is a function of both the concrete and the reinforcement. Assuming that cracking has stabilized before the element yields, the cracked section shear stiffness G_{cr} can be defined as the secant stiffness to the yield point. The gross section shear stiffness and the cracked section shear stiffness are compared in Table 2.6. The graphical yield point was used to determine the cracked section stiffness.

Table 2.6 Experimental Values of Shear Stiffness

Specimen	Uncracked Stiffness		Cracked Section Stiffness	
	G_{gross} (MPa)	$\frac{G_{gross}}{0.4E_c^*}$	G_{cr} (MPa)	G_{cr}/G_{gross}
PP1	12,000	1.22	850	0.07
SE8	12,000	1.04	1290	0.11
SE9	14,000	1.11	1590	0.11
SE10	14,000	1.27	1390	0.10
PDV1	11,500	1.17	1830	0.16
PDV2	10,700	1.16	1690	0.16
PDV3	18,700	1.69	2000	0.11

* see tables 2.1 and 2.2 for values of E_c

2.4 BEHAVIOUR OF STRAIN COMPONENTS

To better understand the shear response, the individual components of stress and strain are examined, starting with the measured strains. Figure 2.11 shows the strain components for

an elastic cycle and a yield cycle of SE8. The components of particular interest are the strains in the reinforcement directions (ε_x, ε_y), the minimum principal strain (ε_2) which reflects compression in the concrete, and the shear strain (γ_{xy}) which is the end product. Examining the relationships between these components provides information on the mechanics of the shear response.

In Fig. 2.11, the strain data is plotted against the cumulative shear stress. Using a cumulative value for the horizontal axis results in an expansion of the cycles. Cumulative shear stress is calculated as the sum of the absolute value of each increment:

$$v^{n}_{xy,cumulative} = \sum_{i=1}^{n} \left| v^{i}_{xy} - v^{i-1}_{xy} \right| \tag{2.10}$$

where the superscripts indicate the ith data point and the nth cumulative value. Cumulative shear strain is similarly used in some plots.

During the elastic cycle (Fig. 2.11a), all the strains vary linearly with loading and unloading of the shear stress. Correspondingly, the principal strain angle is essentially constant. The small residual strains and non-linear behaviour which occur around zero shear stress are attributed to cracks not closing completely and possibly some slip between the concrete and the reinforcement as the load is reversed.

At the beginning of the yield cycle (Fig. 2.11b), the shear stress is zero but ε_y is non-zero due to the accumulation of plastic strains during the previous yield cycles. As the shear stress is increased, ε_x and ε_y increase linearly, similar to the elastic cycle. Meanwhile, ε_2 is briefly positive (tensile) before becoming increasingly negative (compressive). Above a shear stress of about 2 MPa, all the strain components vary linearly. At a shear stress of about 5.5 MPa, the y reinforcement starts to yield. Simultaneously, γ_{xy} starts increasing more rapidly. In contrast, ε_x continues to increase linearly. After the peak, ε_x and ε_y reduce linearly until zero shear stress; ε_2 and γ_{xy} reduce linearly until close to zero shear stress. At zero shear stress, the residual ε_y is greater than at the start of the cycle by an amount approximately equal to the yielding segment.

2.5 ROLE OF WEAK REINFORCEMENT IN SHEAR RESPONSE

The weak reinforcement is defined as the reinforcement that yields first. Typically this is the y-direction reinforcement which was defined as the direction with the smaller quantity of reinforcement (Sec. 2.1).

2.5.1 Element Yielding vs Reinforcement Yielding

In Figs. 2.4 to 2.10 and 2.11b, the element appears to yield in shear, i.e., the shear strain increases rapidly for only a small increase in shear stress, when the weak reinforcement yields. This behaviour is further confirmed in the following sections where other interactions are examined.

2.5.2 Accumulation of Weak Reinforcement Plastic Strain

The accumulation of plastic strains in the weak reinforcement is seen in Fig 2.12. For each yield cycle, the y reinforcement has a linear-elastic strain component which is recovered during unloading and a plastic component which is not recovered. By contrast, the x reinforcement remains linear-elastic throughout the test. Loading and unloading slopes are equal and remain constant for all cycles. The slopes for the x and y reinforcement are different due to the different quantities of reinforcement. The accumulation of plastic strains is cumulative from one shear stress direction to the other, i.e., the residual strain increases with each half-cycle.

Specimens SE9 (Fig. 2.13a) and SE10 (Fig. 2.13b) display the same characteristics as SE8. As expected with equal reinforcement in both directions, SE9 has much less yielding and accumulation of plastic strains than SE8 and the loading and unloading slopes for the x and y reinforcement are equal. Specimen SE10 shows some recovery of the plastic strain at the end of unloading and at the beginning of loading in the other direction. This is likely due to the bi-axial compression which is applied to specimen SE10. The gap between peaks of subsequent cycles, seen for all three SE specimens, indicates that plastic strains in the weak reinforcement are cumulative from one direction of shear to the other.

The PDV specimens are not examined since yielding occurs only in the last, or next to last cycle.

2.5.3 Elastic and Plastic Reinforcement Strains

The assumed stress-strain relationship for the reinforcement (Eq. 2.2) has a linear-elastic component and a plastic component. By applying Eq. 2.2 at each increment of the reinforcement strain ε_y, the elastic and plastic components can be identified. They are shown in Fig. 2.14 for SE8, SE9 and SE10.

The estimated plastic strain appears too low for the first few yield cycles, likely the result of ignoring initial residual strains and using f_y as the yield stress. Assuming the plastic strains are fully cumulative results in a faster accumulation of plastic strain compared to the experimental data. Overall, the bare bar model seems to capture the accumulation of plastic strains in the reinforcement.

2.5.4 Linear Relationship Between Shear Strain and Weak Reinforcement Strain

For the monotonic case (PP1), Fig. 2.15 shows an approximately bi-linear relationship between the shear strain (γ_{xy}) and the weak reinforcement strain (ε_y). Before yielding of the y reinforcement, the slope is 1.8 mε/mε; after yielding it reduces to 1.2 mε/mε. The relationship remains essentially linear until the peak shear stress is reached at a shear strain of 12 mε. Figure 2.16 shows similar behaviour for PDV1 and PDV3. For PDV3, the relationship is also linear during the unloading and re-loading segments. That the shear strain varies linearly with the weak reinforcement strain, before and after yielding, points to a direct link between the two.

Figure 2.17 shows the interaction between the shear strain and the weak reinforcement strain for the reverse-cyclic case (SE8). Two distinct zones are apparent on the plot; the strain reversal zone between lines X-X and Y-Y, and the loading-unloading zone on either side of the reversal zone. Lines X-X and Y-Y connect the points corresponding to zero shear stress thus they represent the residual strains at the end of unloading. Note that the reference lines are symmetrical about the zero shear strain axis. The single cycle from Fig. 2.6 is highlighted and the three reference points corresponding to zero shear stress (A), zero shear

strain (B) and stiffening of the response (C) are shown. This plot provides a lot of information about the mechanics of the shear response and deserves to be examined in detail.

The loading/unloading zone shows consistency between cycles: each loading-unloading segment appears unaffected by the number of previous cycles or by the increasing residual strains. The slopes are constant from cycle to cycle. The segments from the reference line to the yield point have a constant length from cycle to cycle. Outside of the reversal zone, the shear strain is directly related to the weak reinforcement strain and this relationship is independent of previous cycles. This is related primarily to the elastic strain in the reinforcement.

In the reversal zone, the shear strain goes from one reference line to the other as the shear stress is increased from zero to approximately 2 MPa. Even though the magnitude of the shear strain reversal increases from cycle to cycle, the increase in reinforcement strain is relatively constant around 0.65 mε. As implied by the straight reference lines, the residual shear strain is proportional to the residual strain in the reinforcement which is the plastic strain component.

Outside of the reversal zone, the response converges to the monotonic response (Fig. 2.18). In terms of the two strains ε_y and γ_{xy}, the monotonic case is clearly the envelope to the reverse-cyclic case.

Figure 2.19 shows the shear strain as a function of the reinforcement strain for SE9 and SE10. Specimen SE9 mostly shows a linear relationship between γ_{xy} and ε_y during elastic cycles. Specimen SE10 includes more yielding cycles and displays the same characteristics as SE8. The three PDV specimens are compared in Fig. 2.20. The comparison mainly indicates the relationship between the shear strain and the reinforcement strain is independent of the load history.

Since the strong reinforcement does not yield, its relationship with the shear strain is similar to the linear elastic cycles shown for the weak reinforcement. The strong reinforcement will have little influence on the behaviour during the reversal since it does not contribute to the residual strains.

In the loading, yielding and unloading stages of the shear response, the shear strain is directly related to the weak reinforcement strain. In the strain reversal stage (the pinching of

the loops), the shear strain is related primarily to the plastic component of the weak reinforcement strain. In Chapter 3, the rational model is used to provide an explanation of this behaviour.

2.6 DEFORMATIONS AT THE CRACKS: STRAINS AT ±45°

In the monotonic tests reviewed here, the application of positive shear stress causes cracks to form at +45° (clockwise positive from the x axis) and in the reverse-cyclic tests, the reversing shear stress causes cracks to form at ±45°, therefore, the experimental strains at ±45° are representative of the deformations at the cracks. The ε_{+45} and ε_{-45} strain components are defined parallel to the +45° and the −45° cracks respectively. For the reverse-cyclic specimens, the cracks are orthogonal thus the strains parallel to one set of cracks are also normal to the other set of cracks.

Figure 2.21 shows the strains at ±45° for the monotonic case (PP1) as a function of the shear strain. The strain normal to the cracks (ε_{-45}) increases linearly with increasing shear strain, i.e., the cracks open proportionally to the shear strain (or vice versa). This linear relationship is unaffected by yielding of the y reinforcement. Meanwhile, the strain parallel to the cracks is negative, reflecting compression in the concrete.

The strains at ±45° for the reverse-cyclic case (SE8) are plotted against the shear strain in Fig. 2.22(a). Consider the strain component ε_{+45}: for increasing positive shear strain it is parallel to the opening cracks and for increasing negative shear strain it is normal to the opening cracks. Lines X-X and Y-Y join the points of zero shear stress and delimit the reversal zone. On the positive shear strain side of the reversal zone, ε_{+45} becomes negative which reflects increasing compression in the concrete between the cracks. On the negative shear strain side of the reversal zone, ε_{+45} reflects the opening of the cracks as the load is increased. As the load is removed the cracks do not close completely, as indicated by the residual strains at zero shear stress. Note the linear relationship with the shear strain remains constant before and after yielding of the reinforcement, for loading and unloading segments, and from cycle to cycle. The reversal zone grows with each subsequent yield cycle as the residual ε_{+45} strain increases linearly with the residual shear strain.

Plotting the ±45° strains as a function of the shear stress (Fig. 2.22b) provides a different perspective on the behaviour of the cracks. During the elastic cycles, the 45° strains behave linear elastically, i.e., the cracks open and close almost completely. During the yield cycles, the strains normal to the opening cracks increase linearly at first, then more quickly as yielding occurs. Unloading occurs at the same slope as loading and ends with an increased residual strain. There is a gap between the peaks of subsequent cycles, similar to the accumulation of plastic strains in the reinforcement.

The details of the reversal are more clearly seen by considering a single yield cycle (Fig. 2.23). Unloading from the maximum positive shear stress to the point of zero shear stress (point A), there is a residual ε_{-45} of 1.8 mε: the positive-shear cracks have not fully closed. In the other direction, ε_{+45} is essentially zero, i.e., the negative-shear cracks are closed and the compression in the concrete has been removed. Increasing the shear stress in the negative direction causes the shear strain to reduce to zero (point B). It also causes ε_{-45} to reduce and ε_{+45} to increase: the positive-shear cracks close while the negative cracks open. At point B the two strains are equal at 0.9 mε. The sum of the two 45° strains is constant from point A to point B. With increasing shear stress, ε_{-45} decreases at a reducing rate while ε_{+45} increases linearly with respect to the shear strain: the positive-shear cracks close with increasing resistance while the negative-shear cracks open proportionally to the shear strain. At a shear stress of −2.4 MPa (point C), ε_{-45} is zero; the positive-shear cracks are considered fully closed.

The reverse-cyclic case is compared to the monotonic case in Fig. 2.24. In terms of strains, the monotonic case is a very good envelope to the reverse-cyclic case.

Specimen SE9 is shown in Fig. 2.25 as an example of the reverse-cyclic case with little accumulation of plastic strain in the reinforcement. In this case, the cracks open and close in a linear-elastic manner for most of the test.

2.7 LINEAR RELATIONSHIP BETWEEN STRESS COMPONENTS

Figure 2.26 compares the measured strains, the concrete stresses and the principal angles for the monotonic case (PP1). After the element has fully cracked, at a shear stress of about 2 MPa, the concrete stresses vary approximately linearly (Fig. 2.26b). This results in an

approximately constant principal stress angle (Fig. 2.26c). After the y reinforcement yields, the reinforcement stress σ_{sy} is limited to the yield stress f_{yy} . Through the equilibrium requirement (Eq. 2.5), the concrete stress in the y direction is limited to $-\rho_y f_{yy}$. Meanwhile, the concrete stress in the x direction σ_{cx} and in the principal compression stress (σ_{c2}) continue to decrease (increasing compression). Correspondingly, the principal concrete stress angle rotates towards the x axis as more load is transferred to the x reinforcement.

The relationship between stress components for the reverse-cyclic case (SE8) is examined by following the transformation of reinforcement strains to principal concrete stresses. The reinforcement strains ε_{sx} and ε_{sy} are plotted in Fig. 2.27(a). The figure shows a constant linear relationship between the two reinforcement strains for loading and unloading segments and from cycle to cycle.

The reinforcement stresses σ_{sx} and σ_{sy} (Fig. 2.27b) are obtained by applying the reinforcement stress-strain model (Eq. 2.2). The relationships between the reinforcement stresses and with the shear stress are linear and constant until yielding of the y reinforcement. During yielding, the y reinforcement stress is limited to the yield stress (479 MPa).

The concrete stresses in the reinforcement directions, σ_{cx}, σ_{cy} (Fig. 2.28a), are derived from the reinforcement stresses by applying the equilibrium equations (Eq. 2.5); they vary linearly with the shear stress.

The principal concrete stresses, σ_{c1} and σ_{c2} (Fig. 2.28b), are obtained from the concrete stress components σ_{cx}, σ_{cy}, and v_{xy} using Eq. 2.6. After initial cracking, the principal compression σ_{c2} varies linearly with the shear stress v_{xy}. The slope is constant for loading and unloading segments and from cycle to cycle. The principal tension σ_{c1} reduces significantly during the initial cracking stage. During the elastic cycles, it varies with the shear stress but much less than the principal compression. During the yield cycles, it is essentially independent of the shear stress.

After initial cracking, the stresses in the concrete and the reinforcement vary with the shear stress in a stable linear-elastic manner. This is characteristic of the response during loading up to yielding of the weak reinforcement and during unloading from the peak shear stress back to zero.

2.8 CONCRETE STRESS AND STRAIN ANGLES

Figure 2.29(a) plots the principal concrete stress angle (the stress angle) and the principal strain angle (the strain angle) for the monotonic case (PP1). Before cracking, the stress angle is 45° as expected with pure shear loading. As cracks form, the stress angle drops to about 40° and the stress and strain angles are approximately equal. The stress angle then remains approximately constant until the *y* reinforcement yields, at a shear strain of 4.5 mε. At yielding, the difference between the angles is about 5 degrees. After yielding, both angles reduce approximately in parallel. For the monotonic case, the principal angles are relatively close during the whole response.

The principal angles for the reverse-cyclic case (SE8) are shown in Fig. 2.29(b). The cycles are expanded by using cumulative shear strain along the horizontal axis. Looking at only the peak of each cycle, the behaviour of the angles is similar to the monotonic case. On the positive side, the stress angle starts at 45°, reduces to 40° during cracking, then remains constant until yielding occurs. After yielding, both the stress and the strain angles reduce approximately in parallel: the difference between the two is 5° after the first yield cycle and 8° at the end of the test. As Fig. 2.30 indicates, the monotonic angles form an envelope to the reverse-cyclic angles.

During the load reversal, the strain angle lags the stress angle by up to 35°. This is shown in Fig. 2.31(a) for the selected single cycle. At zero shear stress (point A), the principal stress angle is zero while the principal strain angle is 25°. At zero shear strain (point B), the principal stress angle is -35° while the principal strain angle is zero. At the point where the shear response stiffens (point C), the difference between the angles has reduced to 8°. For the rest of the loading stage, including yielding, the difference between the angles remains approximately constant. During the reversal, the principal concrete stress angle deviates significantly from the principal strain angle.

Figure 2.31(b) indicates the principal concrete stress angle is essentially constant for most of the cycle. This is consistent with the linear-elastic relationship observed between concrete stress components in the previous section.

The principal angles for specimens SE9 and SE10 are shown in Fig. 2.32. For SE9 (Fig. 2.32a), the behaviour is similar to the elastic cycles of SE8. The principal stress angle above 45° indicates principal compression oriented closer to the y reinforcement than to the x reinforcement due to some experimental non-uniformity. Specimen SE10 (Fig. 2.32b) includes elastic and yield cycles similar to SE8. Both these specimens show a large difference between the stress and strain angles during the reversal.

2.9 CONCRETE IN COMPRESSION

In formulating the MCFT, Vecchio and Collins (1986) established cracked-concrete as a new material for which there exists a relationship relating average stresses to average strains. Since the MCFT assumes the principal concrete stress angle coincides with the principal strain angle, the stress-strain relationship for cracked concrete relates the principal concrete compression stress σ_{c2} to the principal average strain ε_2. Vecchio and Collins (1986) found that in an element subjected to shear, the response of cracked concrete is similar to plain concrete but softer and weaker. In Fig. 2.33(a), the experimental data for PP1 is compared to the parabolic relationship often used to represent the loading response of plain concrete (Park and Paulay 1975):

$$\sigma_{c2} = f_c' \left[\frac{2\varepsilon_{c2}}{\varepsilon_c'} - \left(\frac{\varepsilon_{c2}}{\varepsilon_c'} \right)^2 \right] \tag{2.11}$$

where the maximum compression strength f_c' and the corresponding strain ε_c' are determined from a standard concrete cylinder compression test.

Note that characterizing the concrete response using the minimum principal concrete stress (σ_{c2}) and the principal compression strain (ε_2) is appropriate for monotonic shear where the principal concrete stress angle is close to the principal strain angle. However, for reverse-cyclic shear it is only appropriate at peak shear stress values and not during the reversal. Nonetheless, for simplicity and consistency with other studies, σ_{c2} and ε_2 are used here to examine the concrete compression response.

As Fig. 2.33(a) indicates, there is relatively little softening before yielding of the y reinforcement. Collins made a similar observation in formulating the Compression Field

Theory (Collins 1978). When formulating the MCFT, to maintain the simplicity of the model, the cracked concrete stress-strain relationship was assumed independent of the reinforcement. That assumption is not made here. Specimens PP1 and SE8 (Fig. 2.33) indicate that the majority of the softening occurs after the y reinforcement yields.

cyclic softening

Specimens SE9 and SE10 show increased softening of the concrete response due to cycling before yielding of the reinforcement (Fig. 2.34). The first cycle at each new stress level results in additional softening while subsequent cycles at the same stress level appear essentially stable.

"Bulge" in the concrete response

At low stress values, the concrete response for reverse-cyclic specimens includes a region where the minimum principal strain is tensile while the minimum principal concrete stress is compressive – this is seen as a "bulge" in the response. The bulge appears in the response of SE8, SE9 and SE10 (Figs 2.33 and 2.34) but does not appear in the response of PDV3 (Fig. 2.35) which was cycled only in positive shear, indicating this phenomena is particular to reverse-cyclic shear.

The bulge in the reverse-cyclic response is examined more closely in Fig. 2.36 using the single cycle for SE8. At the point of zero shear stress (point A) there is some residual compressive strain and compressive stress – these are attributed to the cracks not closing completely. As shear stress is applied in the negative direction, ε_2 becomes tensile while σ_{c2} increases slightly in compression. The principal strain reaches a maximum at the point of zero shear strain (point B). As the compression stress continues to increase, the principal strain decreases and returns to the negative (compressive) side. From there the response gradually stiffens until, at point C, it reaches a relatively constant slope for the rest of the loading stage. As the reference points indicate, the bulge coincides with the load reversal.

2.10 IMPORTANT CHARACTERISTICS OF THE REVERSE-CYCLIC SHEAR RESPONSE

Experimental data from membrane elements subjected to reverse-cyclic shear was examined in detail in this Chapter. Some important relationships between stress and strain components were identified and are summarized below:

- The shear strain is closely related to the weak reinforcement strain; the relationship is essentially linear,
- Plastic strains in the weak reinforcement are cumulative from one direction of shear to the other,
- The shear strain during the reversal stage is related to the plastic strain in the reinforcement,
- Strains normal to the opening cracks vary linearly with the shear strain,
- The relationship between concrete stress components is linear during the loading (before yielding) and unloading stages,
- The principal concrete stress angle and the principal average strain angle are close at the peak of each cycle but they deviate significantly during the load reversal,
- The concrete compression response softens significantly when the weak reinforcement yields,
- The concrete compression response has a region of compressive stress associated with tensile strain.

A rational model must account for these relationships in order to fully represent the mechanics of the reverse-cyclic shear response of membrane elements. The model presented in Chapter 3 achieves this with a simple, transparent formulation.

3

Rational Model for Reverse-Cyclic Shear

A rational model has been developed for membrane elements subjected to reverse-cyclic shear, based on the analysis and interpretation of the experimental data. It combines strain compatibility, equilibrium and constitutive relationships to predict the complete load-deformation response based on fundamental mechanics.

Much of this Chapter details the new strain compatibility requirements required to model the reverse-cyclic response. These include defining the strains at the cracks and in the concrete between the cracks. New constitutive relationships were also required in conjunction with the new strain compatibility relationships; these are introduced here and defined in more detail in Chapter 4.

The proposed model is shown to not only capture the experimental behaviour observed in Chapter 2, but to provide rational explanations for it.

3.1 SEPARATING CONCRETE AND CRACK DEFORMATIONS

As described in Chapter 1, the cracked concrete approach prevalent in current models is based on the assumptions that the principal angles are equal and that the response of cracked concrete can be defined independently of the reinforcement. However, the review of the experimental data in Chapter 2 has shown that during the reversal stage, deformations at the cracks are closely linked to the reinforcement and the principal angles deviate considerably.

With reverse-cyclic shear, the presence of cracks in two directions results in a complex behaviour that is difficult to model with a single cracked concrete material approach. The proposed solution is to separate the deformations at the cracks from the deformations in the concrete between the cracks. In the proposed model this is done on an average strain basis. The cracks are assumed to have a fixed orientation and their effect is averaged uniformly over the element. Separating the cracks from the concrete provides the necessary framework for modelling all aspects of the reverse-cyclic response in a rational manner.

Figure 3.1 shows how considering the cracks separately captures the complex response during the load reversal. It follows the strains in specimen SE8 through a load reversal, using the single cycle and three reference points from Chapter 2. At point (A) the element has been unloaded and the shear stress is zero. As the x reinforcement has not previously yielded, all of the x-direction strain is assumed to be elastic and has fully recovered except for a small residual. The elastic strains in the y reinforcement have also recovered, however, significant accumulated plastic strains remain. The normal strain parallel to the open cracks (ε_{+45}) is very small, on par with the residual strains. These three normal strain components define the complete biaxial strain state, which is summarized by the Mohr's circle shown in Figure 3.1(a). At this point the shear strain is positive and the minimum principal strain is compressive. The sketch of the deformed membrane element illustrates that the cracks from the previous load cycle remain open at this point.

As shear stress is applied in the new direction of loading, the shear strain reduces. At point (B), the element is at the point of zero shear strain. Due to the applied shear stress, there are diagonal compression stresses in the concrete and associated tensile stresses in the reinforcement. The diagonal compression stresses in the concrete cause the previous direction cracks to close. The complete biaxial strain state is defined by the x-direction elastic strain, y-direction elastic and plastic strains, and the strain normal to the closing cracks (ε_{-45}). The opening of the current direction cracks (ε_{+45}) is assumed to be a consequence of the other three strain components. This strain state is shown in the Mohr's circle in Figure 3.1(b). At this point, the two sets of cracks are open an equal amount. Note that the minimum principal strain is tensile.

Once sufficient shear stress has been applied (point C), the previous direction cracks close completely due to the high diagonal compression stress in the concrete. At this point, the x-direction and y-direction strains have increased significantly due to additional elastic strains. From this point, the behaviour is similar to a membrane element under monotonic loading, i.e., with cracks in one direction.

The explanation of the reversal stage can be applied conceptually to the relationship between the shear strain and the weak reinforcement strain observed in Fig. 2.17. Consider a concrete element which is fully cracked and where the pieces between the cracks are held in place by the reinforcement. At the end of unloading, plastic strain in the y reinforcement prevents the cracks from closing completely, resulting in a residual shear strain. The plastic strain in the reinforcement represents "looseness" in the element. As the shear stress is applied in the new direction, the principal compression causes the open cracks to close. Given that the plastic strain in the reinforcement is essentially fixed, the cracks in the new direction are forced to open; the element pivots about the plastic strain in the reinforcement with little resistance. Once the cracks in the previous direction have closed and the "looseness" has been taken up by the cracks in the new direction, the shear strain increases linearly with the reinforcement strain. This simple conceptual model is consistent with the observed relationship between the shear strain and the reinforcement strain, in particular the plastic strain in the reinforcement.

As a further indication of the primary importance of the relationship between the weak reinforcement and the shear strain, Fig. 3.2 illustrates how the shear strain can be uniquely defined by a given combination of elastic and plastic reinforcement strains, if the "elastic" and "plastic" slopes were known. For example, in the figure a y-reinforcement plastic strain of 4.25 mε corresponds to a residual or plastic shear strain of 3 mε. Then a y-reinforcement elastic strain of 1.25 mε corresponds to an additional shear strain of 2.5 mε for a total shear strain of 5.5 mε. The figure is intended only to illustrate the close relationship between the shear strain and the reinforcement strain.

3.2 STRAIN COMPATIBILITY REQUIREMENT

The strain compatibility requirement for the proposed model is:

deformations in the concrete + deformations at the cracks = total deformations

Like the total deformations, the concrete and crack components of deformation are assumed averaged over the element, i.e., they are defined as average strains. For example, given an initial length l and a total change in length Δl, the average strain components are

$$\begin{aligned} \varepsilon_t &= \frac{\Delta l}{l} \\ &= \frac{\Delta l_c + \Delta l_k}{l} \\ &= \varepsilon_c + \varepsilon_k \end{aligned} \tag{3.1}$$

where Δl_c and ε_c are the change in length and average strain associated with the concrete, and Δl_k and ε_k are the change in length and average strain associated with the cracks. To represent average conditions, the deformations should be measured over a gauge length (l) that includes a number of cracks.

This approach is reasonable for elements with well distributed reinforcement and having a number of cracks over the measurement length. For example, SE8 had reinforcement evenly spaced at 72 mm and an average crack spacing of 50 mm, both much less than the gauge length of 1200 mm.

In terms of average strains, the proposed compatibility requirement is:

$$\begin{aligned} \varepsilon_{cx} + \varepsilon_{kx} &= \varepsilon_x \\ \varepsilon_{cy} + \varepsilon_{ky} &= \varepsilon_y \\ \gamma_{cxy} + \gamma_{kxy} &= \gamma_{xy} \end{aligned} \tag{3.2}$$

where ε_{cx}, ε_{cy}, γ_{cxy} define the average strains due to deformations in the concrete between the cracks (the concrete strains), ε_{kx}, ε_{ky}, γ_{kxy} define the average strains due to deformations at the cracks (the crack strains), and ε_x, ε_y, γ_{xy} define the total average strains. Similar to existing models, the average strains in the reinforcement are assumed equal to the total average strains:

$$\begin{aligned} \varepsilon_{sx} &= \varepsilon_x \\ \varepsilon_{sy} &= \varepsilon_y \end{aligned} \tag{3.3}$$

3.3 DEFINING CRACK AND CONCRETE STRAINS: CRACKS IN ONE DIRECTION

The crack and concrete strains are first defined for the case of cracks in only one direction. This occurs with monotonic loading and with reverse-cyclic loading after the cracks in one of the two directions have closed. It is convenient to define reference axes relative to the orientation of the cracks (see Fig. 3.3a):

n axis is normal to the crack orientation

p axis is parallel to the crack orientation

θ_k (the crack angle) is the angle clockwise positive from the x axis to the p axis

3.3.1 Components of Deformation

The concrete between the cracks is treated as a homogeneous material. Consequently, there are three independent components of strain: e.g., two normal strain components and shear strain. With reference to the crack directions, the concrete strains are defined by ε_{cn}, ε_{cp}, and γ_{cnp} (Fig. 3.3b).

Deformations at the cracks are typically represented by two independent components: opening normal to the cracks (Fig. 3.3c) and shear slip parallel to the cracks (Fig. 3.3d) (Adebar 1989; Kaufmann and Marti 1998). Represented as average strains, these deformations correspond to the normal strain normal to the crack orientation, ε_{kn}, and the shear strain with respect to the crack orientation, γ_{knp}. To complete the definition of the crack strains, the normal strain parallel to the crack orientation, ε_{kp}, is assumed to be zero.

3.3.2 Separating Total Strains into Crack and Concrete Components

Separating experimental strains into their crack and concrete components illustrates how the crack and concrete strains are defined. In Section 3.5, the process is reversed and estimated crack and concrete strain components are combined to predict total strains. The experimental data consists of the total strains (ε_x, ε_y, γ_{xy}), the applied stresses (n_x, n_y, v_{xy}), and the crack angle θ_k. The latter is assumed perpendicular to the orientation of the maximum principal applied stress when it reaches the concrete cracking strength.

The process of separating the total strains into components is based on the strain compatibility equations (Eq. 3.2) which can be expressed in the crack directions:

$$\begin{aligned} \varepsilon_{cn} + \varepsilon_{kn} &= \varepsilon_n \\ \varepsilon_{cp} + \varepsilon_{kp} &= \varepsilon_p \\ \gamma_{cnp} + \gamma_{knp} &= \gamma_{np} \end{aligned} \tag{3.4}$$

First, the concrete strains are obtained from the following three assumptions:

1. *After cracking, the concrete strain normal to the cracks is zero:*

$$\varepsilon_{cn} = 0 \tag{3.5}$$

The strains normal to the cracks are assumed to be predominantly due to the opening of the cracks. This is reasonable since the concrete strains are limited to the concrete cracking strain (about 0.065 mε for 40 MPa concrete) whereas the crack strains can become quite large, especially after yielding of the reinforcement (up to 10 mε or 150 times greater for SE8, for example). Consequently, the concrete strain normal to the cracks can be neglected. This assumption is reviewed in Section 3.3.4.

2. *The concrete strain parallel to the cracks equals the total strain parallel to the cracks:*

$$\varepsilon_{cp} = \varepsilon_p \tag{3.6}$$

This assumption follows from the definition of the crack strain components where the crack strain parallel to the cracks is zero; $\varepsilon_{kp} = 0$.

3. *The concrete principal strain angle coincides with the concrete principal stress angle:*

$$\theta_{c\varepsilon} = \theta_{c\sigma} \tag{3.7}$$

This assumption is consistent with treating the concrete between the cracks as a homogeneous isotropic material.

Equations 3.5 to 3.7 define the complete concrete strain state. The concrete shear strain relative to the crack directions is:

$$\gamma_{cnp} = (\varepsilon_{cn} - \varepsilon_{cp}) \tan(2\theta_{c\varepsilon} - 2\theta_k) \tag{3.8}$$

Second, the total strains (ε_x, ε_y, γ_{xy}) are converted to the crack axes using the standard transformation equations:

$$\begin{aligned} \varepsilon_n &= \frac{1}{2}[\varepsilon_x + \varepsilon_y + (\varepsilon_x - \varepsilon_y)\cos 2\theta_k + \gamma_{xy} \sin 2\theta_k] \\ \varepsilon_p &= \frac{1}{2}[\varepsilon_x + \varepsilon_y - (\varepsilon_x - \varepsilon_y)\cos 2\theta_k - \gamma_{xy} \sin 2\theta_k] \\ \gamma_{np} &= (\varepsilon_x - \varepsilon_y)\sin 2\theta_k - \gamma_{xy} \cos 2\theta_k \end{aligned} \tag{3.9}$$

Third, re-arranging the compatibility equations (Eq. 3.4) yields the crack strains:

$$\varepsilon_{kn} = \varepsilon_n \tag{3.10}$$

$$\varepsilon_{kp} = 0 \tag{3.11}$$

$$\gamma_{knp} = \gamma_{np} - \gamma_{cnp} \tag{3.12}$$

As an example, Table 3.1 lists the concrete strains and the crack strains for two points from the response of PP1. The first point is taken from the elastic loading stage, the second point from after yielding of the weak reinforcement (see inset, Fig. 3.4). Table 3.2 lists the same concrete and crack strains converted to the *x* and *y* axes. The data from Tables 3.1 and 3.2 is plotted as Mohr's circles in Fig. 3.4.

3.3.3 Mechanics of Shear in Terms of Crack and Concrete Strain Components

Figure 3.4 provides a quantitative look at the fundamental mechanics of shear in reinforced concrete elements in terms of average strains. In particular:

- the concrete strain circle is much smaller than the crack strain circle, i.e., deformations due to the applied shear occur almost entirely at the cracks,
- comparing the three circles, it is apparent the only significant contribution from the concrete is in (or close to) the principal compression direction,
- at point 1 (elastic loading), the principal compression strain (ε_2) is almost entirely due to compression in the concrete; at point 2 (after yielding), about half of the principal compression strain is due to the crack strains: shear strain due to slip along the cracks (γ_{knp}) results in the crack strains contributing to the total principal compression strain (ε_2).
- the crack strains in the *x* and *y* directions are almost equal to the total *x* and *y* strains (which are equal to the reinforcement strains).

Figure 3.4 indicates the difficulty in capturing the shear response with cracked concrete modelled as a single material derived from plain (uncracked) concrete: since the strains due to deformations at the cracks (the crack strains) are much larger than the strains due to deformations in the concrete between the cracks (the concrete strains), the plain concrete model requires substantial modification. In fact, Fig. 3.4 indicates the crack strains are more closely related to the reinforcement strains than to the concrete strains.

Table 3.1 Example of concrete strains and crack strains, mε (relative to *n*, *p* axes)

	point 1: prior to yielding v_{xy} = 3.39MPa, $\theta_{c\sigma}$ = 40°, θ_k = 45° ε_x = .85, ε_y = 1.72, γ_{xy} = 3.25			point 2: after yielding v_{xy} = 4.91MPa, $\theta_{c\sigma}$ = 36°, θ_k = 45° ε_x = 1.61, ε_y = 7.63, γ_{xy} = 10.67		
	total	concrete	cracks	total	concrete	cracks
ε_n	2.910	0	2.910	9.955	0	9.955
ε_p	-.340	-.340	0	-.715	-.715	0
γ_{np}	-.870	-.060	-.810	-6.020	-.232	-5.788
ε_2	-.397	-.343	-.055	-1.506	-.733	-.780

Table 3.2 Example of concrete strains and crack strains, mε (relative to x, y axes)

	point 1: prior to yielding			point 2: after yielding		
	total	concrete	crack	total	concrete	crack
ε_x	.850	-.200	1.050	1.610	-.474	2.084
ε_y	1.720	- .140	1.860	7.630	- .241	7.871
γ_{xy}	3.250	.340	2.910	10.670	.715	9.955
θ_ε	37.5	.040	37.2	30.3	36	29.9

3.3.4 Sensitivity to the assumption $\varepsilon_{cn} = 0$

Of the three assumptions used to define the concrete strains, $\varepsilon_{cn} = 0$ is the least intuitive. Examining its influence on the calculated crack and concrete strains helps validate its use. For demonstration purposes, ε_{cn} is arbitrarily set at +0.13 mε (twice the cracking strain assuming $f_c' = 40$ MPa and $f_{cr} = 0.33\sqrt{f_c'}$) and −0.13 mε. With ε_{cn} non-zero, Eq. 3.10 becomes

$$\varepsilon_{kn} = \varepsilon_n - \varepsilon_{cn} \tag{3.13}$$

The other assumptions and equations are unchanged. The new concrete and crack strains for the two points from PP1 are listed in Tables 3.3 and 3.4.

Figure 3.5 compares the new strain circles to the ones resulting from $\varepsilon_{cn} = 0$. The crack strains being many times larger than the concrete strains, they are not significantly affected by the changes in ε_{cn}. This is particularly true after yielding.

The minimum principal concrete strain (ε_{c2}) is not significantly affected by a change in ε_{cn}. As the concrete strain circles show, the concrete strain state is anchored by ε_{cp}, which equals ε_p. Since the direction parallel to the cracks is close to the principal compression direction, ε_{c2} remains essentially unchanged.

Table 3.3 concrete and crack components assuming $\varepsilon_{cn} = +0.13$ mε

	point 1: prior to yielding $v_{xy} = 3.39$MPa, $\theta_{c\sigma} = 40°$, $\theta_k = 45°$ $\varepsilon_x = 0.85$, $\varepsilon_y = 1.72$, $\gamma_{xy} = 3.0$			point 2: after significant yielding $v_{xy} = 4.91$MPa, $\theta_{c\sigma} = 36°$, $\theta_k = 45°$ $\varepsilon_x = 1.61$, $\varepsilon_y = 7.63$, $\gamma_{xy} = 10.67$		
	total	concrete	crack	total	concrete	crack
ε_n	2.910	.130	2.780	9.955	.130	9.825
ε_p	-.340	-.340	0	-.715	-.715	0
γ_{np}	-.870	-.083	-.787	-6.020	-.275	-5.745
ε_2	-.397	-.344	-.055	-1.506	-.737	-.778

Table 3.4 concrete and crack components assuming $\varepsilon_{cn} = -0.13$ mε

	point 1: prior to yielding $v_{xy} = 3.39$MPa, $\theta_{c\sigma} = 40°$, $\theta_k = 45°$ $\varepsilon_x = 0.85$, $\varepsilon_y = 1.72$, $\gamma_{xy} = 3.0$			point 2: after significant yielding $v_{xy} = 4.91$MPa, $\theta_{c\sigma} = 36°$, $\theta_k = 45°$ $\varepsilon_x = 1.61$, $\varepsilon_y = 7.63$, $\gamma_{xy} = 10.67$		
	total	concrete	crack	total	concrete	crack
ε_n	2.910	-.130	3.040	9.955	-.130	10.085
ε_p	-.340	-.340	0	-.715	-.715	0
γ_{np}	-.870	-.037	-.833	-6.020	-.190	-5.830
ε_2	-.397	-.342	-.056	-1.506	-.730	-.782

3.4 DEFINING CRACK AND CONCRETE STRAINS: CRACKS IN TWO DIRECTIONS

With reverse-cyclic loading, cracks form in two opposite directions. During the transition from one direction of loading to the other, both sets of cracks are open at the same time. To define the crack and concrete strains, the closing crack strains and the concrete strains are defined using assumptions similar to cracks in one direction, while the opening crack strains result from compatibility with the other strains.

3.4.1 Cracks in Two Orthogonal Directions

The simplest case of cracks in two directions is when the two sets of cracks are orthogonal. This is the case with shear loading or shear with bi-axial compression equal in the two directions and is the case for the specimens used in this thesis. One set of axes is sufficient to define both sets of cracks: for this discussion, the crack axes are defined normal (n) and parallel (p) to the opening cracks which are determined by the direction of the applied shear stress (Fig. 3.6a).

For each set of cracks, deformations are represented by a normal strain (ε_{kn}) and a shear strain (γ_{np}) with the parallel strain (ε_{kp}) zero. Thus, for orthogonal cracks, the crack strain components are:

$\varepsilon_{kn} =$ strain normal to opening cracks + strain parallel to closing cracks (=0)

$\varepsilon_{kp} =$ strain parallel to opening cracks (=0) + strain normal to closing cracks

$\gamma_{np} =$ sum of shear strain on both sets of cracks

Unlike the solution for cracks in one direction, ε_{kp} is no longer zero. This makes the definition of the crack and concrete strains indeterminate to one degree, i.e., many different combinations of crack deformations will satisfy the strain compatibility requirements. Therefore, a constitutive relationship for the closing cracks is introduced; it defines the crack strain normal to the closing cracks as a function of the concrete compression stress normal to the closing cracks:

$$\varepsilon_{kp} = \varepsilon_{kp0} \cdot e^{\frac{\sigma_{cp}}{1-0.2\sigma_{cp}}} \tag{3.14}$$

where ε_{kp0} is the normal strain remaining at the end of unloading from the previous direction and σ_{cp} is the concrete compression stress normal to the closing cracks. The proposed function is derived from the experimental data in Chapter 4.

The remaining steps to define the crack and concrete strains are the same as for the case of cracks in one direction.

3.4.2 General Solution for Cracks in Two Directions

When the two sets of cracks are not orthogonal, two sets of axes are required. The positive axes are aligned with the cracks caused by positive shear stress and the negative axes are aligned with the cracks caused by negative shear stress (Fig. 3.6b). There are now four components of crack deformation: ε_{kn+}, γ_{knp+}, ε_{kn-}, γ_{knp-} (ε_{kp+} and $\varepsilon_{kp-} = 0$).

To solve the general case of cracks in two directions, the closing crack strains are transformed to the orientation of the opening cracks. To do this, the closing crack strains must be completely defined by three strain components: $\varepsilon_{kp} = 0$, ε_{kn} is obtained from the crack closing function (Eq. 3.14), and γ_{knp} is assumed to reduce at the same rate as the normal strain such that it also can be obtained from the crack closing function. After transforming the closing crack strains to the orientation of the opening cracks, the solution is analogous to the case with orthogonal cracks.

Unfortunately, there is no experimental data to verify this approach. To date, reverse-cyclic shear tests on membrane elements have been performed with pure shear or shear with biaxial compression (equal in both directions) resulting in cracks at ±45°.

3.5 PREDICTING TOTAL STRAINS FROM APPLIED STRESSES

To predict the complete load-deformation response, the total strains are found for each increment of applied stress. First, the stresses in the concrete and in the reinforcement required to equilibrate the applied loading are determined. From the stresses, strains are found by applying constitutive relationships for the concrete, the reinforcement and the closing cracks. Strain compatibility requirements then establish the deformations at the cracks and define the total strains from the concrete, crack, and reinforcement strains.

To solve the compatibility and equilibrium equations simultaneously, existing models use an explicit relationship between the local shear strain and the local shear stress at the cracks. Combined with the average stress-strain relationships in the two reinforcement directions and in the concrete principal directions, this provides a sufficient number of conditions to make an iterative solution possible. By comparison, the proposed model uses the principal concrete stress angle before yielding to first solve the equilibrium requirements and then solve the compatibility requirements. After yielding, the reinforcement

stress is known instead of the principal stress angle. This approach avoids the complicated and empirical relationships required to approximate local conditions at the cracks and is similar to the simplified solution procedure used for the CFT (Collins 1978).

The procedure for predicting total strains is first presented assuming the concrete has zero tension stress normal to the opening cracks. This is a reasonable assumption for well reinforced specimens subjected to reverse-cyclic shear such as SE8, SE9 and SE10. For cases with light reinforcement, concrete tension is added to the solution in Section 3.6. For this presentation, the cracks are assumed orthogonal and the crack axes are defined with respect to the opening cracks. The procedure described below is summarized in a flow chart in Fig. 3.7.

3.5.1 Predicting Strains Before Yielding of the Weak Reinforcement

Concrete Stress

The first step is to define the concrete stress state. From the equilibrium equations (see Eq. 2.5),

$$v_{cxy} = v_{xy} \tag{3.15}$$

and assuming no concrete tension normal to the cracks

$$\sigma_{cn} = 0 \tag{3.16}$$

To complete the definition of concrete stresses, the principal concrete stress angle, $\theta_{c\sigma}$, can be determined from the element properties and the loading characteristics. Baumann (1972) derived the following equation for the principal stress angle by using linear material properties, assuming no tension in the concrete, and applying strain compatibility and equilibrium requirements:

$$\left(1+\frac{1}{n\rho_y}\right)\tan^4\theta_{c\sigma} + \frac{\mu_y}{n\rho_y}\tan^3\theta_{c\sigma} - \frac{\mu_x}{n\rho_x}\tan\theta_{c\sigma} - \left(1+\frac{1}{n\rho_x}\right) = 0 \tag{3.17}$$

where $n = E_s/E_c$

$\mu_x = N_x/V_{xy}$

$\mu_y = N_y/V_{xy}$

ρ_x, ρ_y = reinforcement ratios in x and y directions

In developing the CFT, Collins (1978) derived a similar equation for the case of applied shear only :

$$\tan^4\theta_\sigma = \frac{\left(1+\dfrac{1}{n\rho_x}\right)}{\left(1+\dfrac{1}{n\rho_y}\right)} \tag{3.18}$$

where n, ρ_x and ρ_y are as defined above (with $\mu_x = \mu_y$=0, Eq. 3.17 reduces to Eq. 3.18).

Although these equations provide a good estimate of the principal stress angle, they consistently underestimate its value. This is because they are based on a model which assumes the principal stress angle and the principal strain angle are equal, resulting in a prediction which is an average of the two. This issue is reviewed in detail in Chapter 4, where the following adjustment is developed specifically to compensate for the equal angle assumption:

$$\theta_{c\sigma} = \theta_{\text{Eq. 3.17 or 3.18}} + \left(\rho_x/\rho_y - 1\right) \tag{3.19}$$

Equations 3.17 to 3.19 allow the principal concrete stress angle to be determined a-priori from the element and loading characteristics. The angle is assumed constant during loading up to yielding of the weak reinforcement and during unloading, for all cycles. This is consistent with the behaviour observed in Chapter 2 (Sec. 2.7).

With the concrete stresses fully defined by v_{cxy}, σ_{cn}, and $\theta_{c\sigma}$, transformation equations based on Mohr's circle are used to calculate the concrete stresses in the reinforcement directions, in the principal compression direction, and in the direction parallel to the opening cracks:

$$\sigma_{cx} = -v_{cxy}\left(\frac{1}{\tan 2\theta_{c\sigma}} + \frac{\cos(2\theta_k - 2\theta_{c\sigma})}{\sin 2\theta_{c\sigma}}\right) \tag{3.20}$$

$$\sigma_{cy} = +v_{cxy}\left(\frac{1}{\tan 2\theta_{c\sigma}} - \frac{\cos(2\theta_k - 2\theta_{c\sigma})}{\sin 2\theta_{c\sigma}}\right) \tag{3.21}$$

$$\sigma_{c2} = \frac{\sigma_{cx} + \sigma_{cy}}{2} - \frac{1}{2}\sqrt{(\sigma_{cy} - \sigma_{cx})^2 + (2v_{cxy})^2} \tag{3.22}$$

$$\sigma_{cp} = \sigma_{cx} + \sigma_{cy} - \sigma_{cn} \tag{3.23}$$

Concrete strains

The assumptions used to define the concrete and crack strains (Eqs. 3.5 and 3.7) define two components of the concrete strains: $\varepsilon_{cn} = 0$, $\theta_{c\varepsilon} = \theta_{c\sigma}$. The third component of strain is obtained from the stress-strain relationship for the concrete between the cracks. Since this stress-strain relationship does not include the influence of the cracks, a function similar to plain concrete is used. The presence of tensile strains transverse to the principal compression is assumed to soften the response compared to plain concrete (Vecchio and Collins 1986), therefore, a softened parabola is used to relate the principal concrete compression strain to the principal concrete compression stress:

$$\varepsilon_{c2} = \varepsilon_c'\left[1 - \sqrt{1 - \frac{\sigma_{c2}}{\beta_c f_c'}}\right] \tag{3.24}$$

where f_c' is the standard cylinder compression strength and β_c is a compression softening coefficient defined below. For cyclic loading, a linear unloading/re-loading path is used between the parabola and the origin.

Numerous functions have been proposed for the compression softening coefficient β (Duthinh 1999 compares 14 different functions); most are a function of the principal tension strain (some are a function of the principal tension stress or are constant). However, these functions were developed for cracked concrete as a single material — they relate the compression stress (σ_{c2}) to the total compression strain (ε_2) — and therefore include softening due to transverse tensile strains in the concrete between the cracks and due to shear slip along the cracks (Section 3.3).

For the proposed model, a new softening coefficient which excludes strains due to deformations at the cracks is required. The proposed coefficient, developed in Chapter 4, is:

$$\beta_c = 1 - 0.5\frac{\varepsilon_1}{.002 + \varepsilon_1} \tag{3.25}$$

where ε_1 is the principal tension strain.

With the concrete strains fully defined by ε_{cn}, $\theta_{c\varepsilon}$, ε_{c2}, the concrete strain parallel to the opening cracks (ε_{cp}) is calculated using the transformation equation:

$$\varepsilon_{cp} = \left[\varepsilon_{cn} - (\varepsilon_{cn} - 2\varepsilon_{c2})\cos(2\theta_k - 2\theta_{c\varepsilon})\right]\frac{1}{1 + \cos(2\theta_k - 2\theta_{c\varepsilon})} \tag{3.26}$$

Crack closing strain

The crack strain parallel to the opening cracks, and normal to the closing cracks, (ε_{kp}) is obtained from the crack closing function (Eq. 3.14) and the concrete compression stress σ_{cp} (Eq. 3.23). When added to the concrete strain, ε_{cp}, it defines the total strain parallel to the opening cracks:

$$\varepsilon_{cp} + \varepsilon_{kp} = \varepsilon_p \tag{3.27}$$

Reinforcement stress

The reinforcement stresses are obtained by rearranging the equilibrium equations (Eq. 2.5):

$$\sigma_{sx} = \frac{n_x - \sigma_{cx}}{\rho_x}, \quad \sigma_{sy} = \frac{n_y - \sigma_{cy}}{\rho_y} \tag{3.28}$$

where n_x and n_y are the applied normal stresses in the x and y directions and σ_{cx} and σ_{cy} are the concrete stresses in the x and y directions (Eqs. 3.20 and 3.21).

Reinforcement strains

In Chapter 2, the bare bar model was used for the analysis of the experimental data because of its simplicity and transparency. These qualities are equally desirable in the load-deformation model. In addition, the bare bar model does not require empirical

coefficients and is directly compatible with established flexure models – which is important if shear and flexure are to be later combined. The bare bar model is compared to alternative models in Chapter 4.

The reinforcement strains consist of an elastic component and a plastic component. The elastic reinforcement strains are obtained from the reinforcement stresses using the linear relationship

$$\begin{aligned} \varepsilon_{sx,elastic} &= \sigma_{sx} / E_s \\ \varepsilon_{sy,elastic} &= \sigma_{sy} / E_s \end{aligned} \tag{3.29}$$

The plastic strains are calculated at the end of a yield cycle and remain unchanged until more yielding occurs. The total reinforcement strains are

$$\begin{aligned} \varepsilon_{sx} &= \varepsilon_{sx,elastic} + \varepsilon_{sx,plastic} \\ \varepsilon_{sy} &= \varepsilon_{sy,elastic} + \varepsilon_{sy,plastic} \end{aligned} \tag{3.30}$$

Total strains

Applying the compatibility equations (Eqs. 3.3 and 3.4), the total strains are:

$$\varepsilon_x = \varepsilon_{sx}$$

$$\varepsilon_y = \varepsilon_{sy}$$

$$\varepsilon_p = \varepsilon_{cp} + \varepsilon_{kp}$$

The orientation of the principal strains (θ_ε) and the total shear strain (γ_{xy}) are calculated using the transformation equations:

$$\theta_\varepsilon = \begin{cases} \dfrac{1}{2}\tan^{-1}\left(\dfrac{\varepsilon_x + \varepsilon_y - 2\varepsilon_p - (\varepsilon_y - \varepsilon_x)\cos 2\theta_k}{(\varepsilon_y - \varepsilon_x)\sin 2\theta_k}\right); \varepsilon_y \neq \varepsilon_x \\ 45^\circ \cdot \dfrac{v_{xy}}{|v_{xy}|}; \varepsilon_y = \varepsilon_x \end{cases} \tag{3.31}$$

$$\gamma_{xy} = \begin{cases} (\varepsilon_y - \varepsilon_x)\tan 2\theta_\varepsilon ; \varepsilon_y \neq \varepsilon_x \\ (\varepsilon_y + \varepsilon_x - 2\varepsilon_p)\cdot \dfrac{v_{xy}}{|v_{xy}|} ; \varepsilon_y = \varepsilon_x \end{cases} \tag{3.32}$$

In this approach, shear strain at the crack interface is not explicitly determined. Unlike in existing models, shear slip along the cracks is considered a consequence and not a cause of deformations in the reinforcement and the concrete; shear slip occurs as needed to satisfy strain compatibility with the concrete and reinforcement.

3.5.2 Predicting strains During Yielding of the Weak Reinforcement

The weak reinforcement is assumed to yield when the stress σ_{sy} reaches the yield stress f_{yy}. From equilibrium (Eq. 2.5), during yielding the concrete stress in the y direction is

$$\sigma_{cy} = n_y - \rho_y f_{yy} \tag{3.33}$$

Equation 3.33, with $v_{cxy} = v_{xy}$, and $\sigma_{cn} = 0$ (assuming no tension), define the complete concrete stress state

During yielding, the ratio between concrete stress components varies such that the concrete stress angle estimated from the linear elastic section properties no longer applies. Instead, the concrete stress angle is calculated from

$$\theta_{c\sigma} = \frac{1}{2}\tan^{-1}\left[\frac{v_{cxy}(1-\cos 2\theta_k)}{\sigma_{cy} - \sigma_{cn} + v_{cxy}\sin 2\theta_k}\right] \tag{3.34}$$

The transformation equations (Eqs. 3.20, 3.22, and 3.23) are used to calculate the other concrete stress components: σ_{cx}, σ_{c2}, and σ_{cp}.

The concrete strains (ε_{cn}, $\theta_{c\varepsilon}$, ε_{c2}, and ε_{cp}) are derived from the concrete stresses using the same equations as before yielding (Eqs. 3.5, 3.7,3.24 and 3.26). The crack strain parallel to the opening cracks (ε_{kp}) is calculated using the crack closing function, Eq. 3.14 (although at this stage the closing cracks will typically be closed). The x reinforcement stress and strain are obtained from equilibrium (Eq. 3.28) and from the bare bar model (Eq. 3.29)

respectively. The perfectly plastic reinforcement model means the y reinforcement strain is indeterminate.

It was observed in Chapter 2 that the principal concrete stress angle ($\theta_{c\sigma}$) and the principal strain angle (θ_ε) rotate approximately in parallel after yielding. Assuming the difference between the two remains constant during yielding, the principal strain angle is

$$\theta_\varepsilon = \theta_{c\sigma} - \Delta\theta_{yield} \tag{3.35}$$

where $\theta_{c\sigma}$ is from Eq. 3.34 and the angle difference, $\Delta\theta_{yield}$, is defined as $\theta_{c\sigma} - \theta_\varepsilon$ at the point when yielding starts. This assumption is reviewed in Chapter 4.

The total strain state is defined by θ_ε, ε_x, and ε_p (Eqs. 3.35, 3.30, and 3.27). The total strain in the y direction (and the y-reinforcement strain) is calculated with the transformation equation

$$\varepsilon_y = \frac{\varepsilon_x[\cos(2\theta_k - 2\theta_\varepsilon) + \cos 2\theta_\varepsilon] - 2\varepsilon_p \cos 2\theta_\varepsilon}{\cos(2\theta_k - 2\theta_\varepsilon) - \cos 2\theta_\varepsilon} \tag{3.36}$$

The plastic strain in the reinforcement is updated after each load increment:

$$\varepsilon_{sy,plastic} = \varepsilon_y - \varepsilon_{yy} \tag{3.37}$$

where ε_{yy} is the strain at yielding (f_{yy}/E_s).

3.6 INCLUDING CONCRETE TENSION

The resistance of the concrete to the applied loads can be separated into a compression-only mechanism and a tension mechanism. The tension mechanism resists part of the applied load, up to the available tension strength, and the compression-only mechanism resists the remainder. The compression-only mechanism was defined in the previous sections, where concrete tension normal to the cracks was assumed to be zero. Referring to Mohr's circles, the total concrete stress can be divided into a compression stress circle and a tension stress circle (Fig. 3.8).

The concrete tension circle is characterized by the concrete tension normal to the opening cracks, $\sigma_{cn,t}$. The direction normal to the opening cracks is assumed to be the direction of

the principal applied tension, $\sigma_{c1,app}$ (Fig. 3.9). Before cracking, the concrete tension normal to the (future) opening cracks is equal to the principal applied tension, σ_{c1app} :

$$\sigma_{cn,t} = \sigma_{c1,app} \leq \sigma_{cr} \tag{3.38}$$

where σ_{cr} is the concrete cracking strength: Collins & Mitchell (1991) suggest

$$\sigma_{cr} = 0.33\sqrt{f_c'} \tag{3.39}$$

The principal stress applied to the concrete is calculated from

$$\sigma_{c1,app} = \frac{\sigma_{cx,app} + \sigma_{cy,app}}{2} + \frac{1}{2}\sqrt{(\sigma_{cy,app} - \sigma_{cx,app})^2 + (2v_{cxy,app})^2} \tag{3.40}$$

where $\sigma_{cx,app} = \sigma_x / (1 + \rho_x(n\text{-}1))$

$\sigma_{cy,app} = \sigma_y / (1 + \rho_y(n\text{-}1))$

$v_{cxy,app} = v_{xy}$

$n = E_s/E_c$

After cracking, the ability of the concrete to carry tension reduces quickly as the cracks open. The response of reinforced concrete in tension is reviewed in more detail in Chapter 4, leading to the development of a stress-strain function appropriate to reverse-cyclic shear and the bare bar reinforcement model. In the proposed function, the concrete tension capacity reduces with increasing average crack width, w:

$$\sigma_{cn} = \sigma_{cr}\left[1 - \frac{w}{0.12 + 0.76w}\right] \geq 0; \sigma_{cn,app} > \sigma_{cr} \tag{3.41}$$

and

$$w = (\varepsilon_n - \varepsilon_{cr}) \cdot s_{m\theta} \tag{3.42}$$

where ε_n= average strain normal to the cracks

ε_{cr} = average strain normal to the cracks at cracking (σ_{cr}/E_c)

$s_{m\theta}$= average crack spacing (mm)

The average crack spacing can be estimated using the equation presented for the MCFT (see Collins and Mitchell 1991):

$$s_{m\theta} = 1 \Big/ \left(\frac{\sin\theta_k}{s_{mx}} + \frac{\cos\theta_k}{s_{my}} \right) \tag{3.43}$$

where s_{mx} and s_{my} are the estimated crack spacings in each reinforcement direction, calculated with the CEB-FIP equation (CEB-FIP 1978; see also Collins and Mitchell 1991)

$$s_m = 2\left(c + \frac{s}{10} \right) + k_1 k_2 \frac{d_b}{\rho_{ef}} \tag{3.44}$$

where c = clear cover

s = maximum spacing between bars $\leq 15d_b$

d_b = bar diameter

$\rho_{ef} = A_s/A_{cef}$

A_s = area of steel reinforcement within A_{cef}

A_{cef} = area surrounding bars, $\leq 7.5d_b$ each side of bar

k_1 = 0.4 for deformed bars, 0.8 for plain bars

$k_2 = .25(\varepsilon_1+\varepsilon_2)/2\varepsilon_1$; strain gradient in embedment zone.

The complete concrete tension circle is defined by assuming it is proportional to the applied stress circle (Fig. 3.9):

$$\begin{aligned} \sigma_{cx,t} &= k \cdot \sigma_{cx,app} \\ \sigma_{cy,t} &= k \cdot \sigma_{cy,app} \\ v_{cxy,t} &= k \cdot v_{cxy,app} \\ \text{where } k &= \sigma_{cn} / \sigma_{c1,app} \leq 1.0 \end{aligned} \tag{3.45}$$

Figure 3.10 shows the concrete tension and compression stress states at various stages of loading for the case of monotonic shear. Before cracking (Fig. 3.10a), the concrete tension resists all the applied load. After cracking (Fig. 3.10b), the tension capacity reduces and the load is transferred to the compression mechanism. Except for very lightly reinforced

elements, once the weak reinforcement yields (Fig. 3.10c), the concrete tension capacity is essentially zero and all the resistance comes from the compression mechanism.

The total concrete stresses are the sum of the tension mechanism and the compression mechanism:

$$\begin{aligned} v_{cxy} &= v_{xy} \\ \sigma_{cn} &= \sigma_{cn,t} \\ &\text{and} \\ \sigma_{cx} &= \sigma_{cx,t} + \sigma_{cx,c} \\ &\text{or} \\ \sigma_{cy} &= \sigma_{cy,t} + \sigma_{cy,c} \end{aligned} \tag{3.46}$$

where $\sigma_{cx,c}$ and $\sigma_{cy,c}$ are the compression-only concrete stresses in the reinforcement directions, obtained from Eqs. 3.20 and 3.21 using the part of the applied load not resisted by the concrete tension.

The total concrete stress state is used to determine the concrete strains following the procedure described earlier. For completeness, the concrete strain normal to the opening cracks can be calculated as

$$\varepsilon_{cn} = \sigma_{cn} / E_c \tag{3.47}$$

instead of assuming zero as before. Note that this introduces an iterative element to the solution procedure. The remaining steps to obtain the total strains are the same as before.

3.7 FAILURE MODES AND CONCRETE SHEAR LIMIT

The shear failures observed in the experiments can be grouped into three types: concrete compression, reinforcement, and concrete shear. A concrete compression failure is a brittle failure which occurs when the concrete compression stress exceeds the concrete compression strength. A reinforcement failure occurs when both the x and y reinforcement yield, allowing the cracks to open with little restraint and resulting in a rapid deterioration of the shear strength. A concrete shear failure is relatively ductile and is the result of local damage along the cracks such as concrete splitting and crushing along the crack interface

and around the reinforcement; it is associated with large shear displacements along the cracks. Zararis (1988) characterises shear failures as resulting from tension splitting around the reinforcement. In existing monotonic models, concrete compression failures and concrete shear failures are combined in the stress-strain relationship for cracked concrete. Separating the cracks from the concrete allows the two failure modes to be evaluated independently.

Concrete compression failures and concrete shear failures have quite different characteristics. Compression failures are strength failures, determined by the compression strength of the concrete. In these failures, 90 to 100% of the total principal compression strain is from the concrete strains, i.e., $\varepsilon_{c2} \approx \varepsilon_2$. Concrete shear failures are deformation failures, occurring when the shear strains along the cracks become excessive. In concrete shear failures, the concrete compression strain is only a small part of the total compression strain, i.e., $\varepsilon_{c2} << \varepsilon_2$. This is illustrated in Fig. 3.11 using data from the LVDT instrumented specimens and from monotonic shear tests conducted by Vecchio and Collins (1982). (These additional specimens are described in Chapter 4 and selected experimental data is included in Appendix B.)

To capture concrete shear failures, a shear strain limit is defined. Since the local effects determining the shear strain at failure are difficult to quantify, an indirect approach is used: the maximum shear strain is defined as a function of the demand on the concrete which is expressed as the ratio of shear stress to concrete compression strength.

Figure 3.12 plots the ratio of shear strain at failure to shear strain at yielding versus the demand on the concrete. The proposed shear limit is a conservative lower bound to the experimental data:

$$\frac{\gamma_{xy,max}}{\gamma_{xy,yield}} = 4 - 12\frac{v_{cxy}}{f_c'} \geq 1.0 \tag{3.48}$$

where $\gamma_{xy,yield}$ is the shear strain when the weak reinforcement starts to yield. By using a function of the shear strain at yield, all the parameters which define the yield point – reinforcement ratios, concrete strength, applied loading – are included in the definition of the shear limit.

In summary, the proposed model for reverse-cyclic shear captures the three failure modes as follows:

concrete compression failure: $\sigma_{c2} \geq \beta_c f_c'$

concrete shear failure: $\gamma_{xy} \geq \gamma_{xy,max}$

reinforcement failure: $\sigma_{sx} = f_{xy}$ and $\sigma_{sy} = f_{yy}$

The model can be used to predict the load-deformation response until the occurrence of one of the three failure modes. The model does not include any post-peak response because the post-peak experimental data is questionable: failures were uncontrolled events, and in many cases, large post-peak deformations were localized along one or two major cracks or in one corner of the specimen making the assumptions of uniform stress and strain inappropriate.

3.8 EXPLAINING THE CONCRETE RESPONSE

Although developed primarily to model the relationships between reinforcement strains, crack strains and shear strains, the proposed model automatically captures the concrete response. The results of applying the model to the test specimens are presented in Chapter 5, however, it is convenient to use some results here to explain concrete compression softening and the bulge (region of tensile strain with compression stress) which appears during the load reversal.

Figure 3.13 examines the concrete response of PP1 in terms of σ_{c2} and ε_2: the concrete component and the crack component of the principal strain in the ε_2 direction are shown as a function of σ_{c2}. After yielding, the large increase in strains comes from the cracks while the concrete component follows the basic parabola (with softening from transverse strains only). The sum of the concrete and crack components gives an excellent prediction of the experimental result. As Fig. 3.13 indicates, the crack strains contribute significantly to the principal compression strain once the weaker reinforcement yields. This rational explanation is consistent with some of the early descriptions of the softening phenomenon by Collins (1978). Recently, Vecchio has modified the definition of cracked-concrete to exclude this effect (Vecchio 2000).

Figure 3.14 shows the concrete response for one reversal of loading for SE8 along with the concrete and crack components of the principal compression strain. The figure clearly shows the bulge in the concrete response is due to the deformations at the cracks.

3.9 SUMMARY OF THE PROPOSED MODEL FOR REVERSE-CYCLIC SHEAR

Table 3.5 summarizes the components of the proposed rational model for reverse-cyclic shear.

Table 3.5 Model components

Component	Assumption
Strain compatibility	concrete strains + crack strains = reinforcement strains = total strains
Equilibrium	concrete normal force + reinforcement force = applied normal force concrete shear force = applied shear force
Crack angle	fixed direction: may be estimated from principal stress direction at cracking
Principal concrete stress angle	before yielding: fixed direction estimated from a modified version of Baumann's equation (function of element properties and loading characteristics) after yielding: angle rotates as stress increases in x direction (concrete stress in direction of weak reinforcement is constant)
Principal strain angle	before yielding: independent of principal concrete stress angle after yielding: stress and strain angles rotate simultaneously (constant difference)
Concrete compression model	parabola for envelope, linear unloading/re–loading; softening due to transverse tensile strains
Concrete tension model	after cracking, concrete tension stress reduces as a function of crack width
Crack closing function	empirical relationship between crack opening and normal compression stress
Reinforcement model	bi–linear stress-strain relationship; bare bar yield strength used; plastic strains are cumulative from one shear direction to the other

4

Constitutive Relationships

The constitutive relationships introduced in Chapter 3 as part of the model development are derived from the experimental data in this Chapter. Constitutive relationships are defined for the closing cracks, the principal concrete stress angle before and after yielding of the weak reinforcement, the concrete in compression and in tension, and the reinforcement. Because the proposed model is based on a different strain compatibility requirement than existing models, new relationships were required for all but the reinforcement. Where applicable, the new relationships are compared to similar existing ones.

4.1 ADDITIONAL EXPERIMENTAL DATA

As part of the development of the MCFT, Vecchio and Collins (1982) tested 30 reinforced concrete panels in shear using the Panel Element Tester. Most of the panels were subjected to monotonic pure shear; other loading conditions included shear with biaxial compression (3 panels), shear with biaxial tension (1 panel), reversed-cyclic shear (1 panel), changing load ratios (1 panel), and uniaxial compression (2 panels, as references).

The panels were 890 mm square by 70 mm thick. They were reinforced with welded wire mesh (6.35 mm dia., 50 mm typical spacing), arranged in two layers. Concrete cylinder strengths varied from 14.5 MPa to 34.5 MPa.

Of the 30 specimens tested, 15 were selected as additional specimens for this research (13 were discounted in the original study due to edge failures or poor casting, and the 2

reference specimens loaded in uniaxial compression are not used). Details for the 15 specimens and important data points are included in Appendix B. A more complete table summarising the tests is provided in Vecchio and Collins (1986).

4.2 CRACK CLOSING FUNCTION

The crack closing function defines the crack strain normal to the closing cracks as a fraction of the residual crack strain at the end of unloading: in effect, it defines the distribution of the total crack strain between the closing and the opening cracks when they are both open. The closing of the cracks is assumed to be a function of the concrete compression stress normal to the closing cracks. Assuming orthogonal cracks and using the notation of Chapter 3 where the crack axes are defined relative to the opening cracks, the strain normal to the closing cracks is also the strain parallel to the opening cracks, ε_{kp}.

At the end of an unloading segment, the concrete strains are essentially zero thus the residual crack strain ε_{kp0} is equal to the total residual strain ε_{p0}. As the load is applied in the new direction, the total strain normal to the closing cracks includes both crack and concrete components. The concrete component is estimated from

$$\varepsilon_{cp} = \frac{\varepsilon_{cn} - (\varepsilon_{cn} - 2\varepsilon_{c2})\cos(2\theta_k - 2\theta_{c\varepsilon})}{1 + \cos(2\theta_k - 2\theta_{c\varepsilon})} \tag{4.1}$$

where $\varepsilon_{cn} = 0$, $\theta_{c\varepsilon} = \theta_{c\sigma}$, and the principal concrete strain ε_{c2} is obtained from the principal stress σ_{c2} using the parabolic function of Sec.2.9, Eq. 2.11. Removing the concrete strain from the total strain leaves the crack strain normal to the closing cracks ε_{kp}. Data from the four reverse-cyclic specimens (SE8, SE9, SE10, PDV2) is shown in Fig. 4.1.

For simplicity, the following crack closing function is proposed (see Fig. 4.1):

$$\varepsilon_{kp} = \varepsilon_{kp0} \cdot e^{\frac{\sigma_{cp}}{1-0.2\sigma_{cp}}} \tag{4.2}$$

where ε_{kp} is the crack strain normal to the closing cracks, ε_{kp0} is the residual crack strain at the end of unloading, and σ_{cp} is the concrete compression stress normal to the closing

cracks. Equation 4.2 does not go to zero to avoid any discontinuity in the model and to represent some residual crack strains due to the cracks not closing perfectly.

A crack closing function developed by Matsuzaki et al. (1989) is included in Fig. 4.1. It was derived from tests on small concrete specimens subjected to tension and compression – shear slip along the cracks was not included. Using the notation of Eq. 4.2, their proposed relationship for the crack strain is

$$\varepsilon_{kp} = \varepsilon_{kp0} \cdot [1 - 0.196 \ln(1 - 29.1\sigma_{cp})] \tag{4.3}$$

4.3 PRINCIPAL CONCRETE STRESS ANGLE - BEFORE YIELDING

It was observed in Chapter 2 that before yielding of the reinforcement and during unloading, the response to reverse-cyclic shear is essentially linear-elastic and constant for all cycles. This linear-elastic behaviour is assumed to have a constant principal stress orientation. Kupfer (1964) is generally credited with providing the first solution for the principal stress angle. Baumann (1972) then developed a more general solution which has been widely referenced. In formulating the CFT, Collins (1978) also noted linear-elastic behaviour before yielding and formulated an equation for the principal stress angle for the case of pure shear loading.

Baumann (1972) developed the following equation for the principal stress angle by assuming the principal strain and principal stress angles are equal, assuming a linear concrete stress-strain relationship, neglecting tension in the concrete, and applying strain compatibility and equilibrium requirements:

$$\left(1 + \frac{1}{n\rho_y}\right)\tan^4\theta_{c\sigma} + \frac{\mu_y}{n\rho_y}\tan^3\theta_{c\sigma} - \frac{\mu_x}{n\rho_x}\tan\theta_{c\sigma} - \left(1 + \frac{1}{n\rho_x}\right) = 0 \tag{4.4}$$

where $n = E_s/E_c$

$\mu_x = N_x/V_{xy}$

$\mu_y = N_y/V_{xy}$

For the case of pure shear, μ_x and μ_y are zero and Eq. 4.16 simplifies to the form presented by Collins (1978):

$$\tan^4\theta_{c\sigma} = \frac{\left(1+\dfrac{1}{n\rho_x}\right)}{\left(1+\dfrac{1}{n\rho_y}\right)} \tag{4.5}$$

A derivation of Eqs 4.4 and 4.5 is included in Appendix A.2.

Figure 4.2(a) compares the angle predicted by Eq. 4.4 with the experimental stress angle at yielding of the weak reinforcement. Baumann's solution is most applicable just before the weak reinforcement yields since at that point the principal stress and strain angles are relatively close and tension in the concrete is minimal. As Fig. 4.2(a) indicates, Eq. 4.4 consistently underestimates the principal concrete stress angle, although by less than 5°.

4.3.1 Influence of concrete tension stress

Baumann's equation underestimates the experimental angle partly because it ignores the influence of tension stresses in the concrete. Equation 4.4 is re-derived in Appendix A.2 with the principal concrete tension stress (σ_{cl}) included. The resulting equation is:

$$\tan^4\theta_{c\sigma} - \alpha + \mu_1\left(\alpha\tan\theta_{c\sigma} - \tan^3\theta_{c\sigma}\right) + \frac{\mu_y}{1+n\rho_y}\tan^3\theta_{c\sigma} - \mu_x\frac{\rho_y}{\rho_x}\left(\frac{1}{1+n\rho_y}\right)\tan\theta_{c\sigma} = 0 \tag{4.6}$$

where

$$\alpha = \tan^4\theta_{c\sigma,\text{ no tension}} = \frac{\left(1+\dfrac{1}{n\rho_x}\right)}{\left(1+\dfrac{1}{n\rho_y}\right)}$$

$$\mu_1 = \frac{\sigma_{cl}}{v_{xy}} \qquad \mu_x = \frac{N_x}{V_{xy}} \qquad \mu_y = \frac{N_y}{V_{xy}}$$

and $n = E_s/E_c$

Figure 4.3 shows the influence of concrete tension on the principal stress angle for the case of pure shear loading. As expected, the angle tends towards 45° as σ_{c1}/v_{xy} approaches 1.0 which is uncracked concrete. The influence of the concrete tensile stress on the principal stress angle can be easily estimated by

$$\theta = \theta_{\text{no tension}} + \mu_1^{1.5}(45 - \theta_{\text{no tension}}) \tag{4.7}$$

Equation 4.7 is shown on Fig. 4.3 for $\rho_x/\rho_y = 12$; it provides an equally good fit at the other reinforcement ratios. For the case of pure shear, Eq. 4.7 can be used with Eq. 4.5 as an alternative to solving Eq. 4.6.

Figure 4.2(b) compares the principal stress angle predicted by Eq. 4.6 with the experimental data. For these predictions, the tension ratio μ_1 is taken as the principal tension stress at yielding of the reinforcement divided by the shear stress at yielding (see Appendix B for data values). For these specimens, μ_1 is less than 0.28, therefore including concrete tension does not significantly change the predicted stress angle.

4.3.2 Influence of Assuming $\theta_\varepsilon = \theta_{c\sigma}$

The derivation of Eqs. 4.4, 4.5, and 4.6 assumes the principal stress angle is equal to the principal strain angle. The result is a predicted angle which is the average of the experimental stress and strain angles. Tables 4.1 and 4.2 compare the angle predicted by Eq. 4.6 with the experimental values at the point where the reinforcement yields. Monotonic models which include this equal angle assumption, like the MCFT, predict an average angle over the entire load-deformation response.

The difference between the predicted angle (Eq. 4.6) and the average of the experimental stress and strain angles is typically less than 1° (see Fig. 4.2c). For the LVDT instrumented specimens, the difference between the experimental concrete stress angle and the experimental strain angle varies from 1.5° for SE8 to 6.8° for PDV3. The error due to the equal angle assumption is half that difference or 0.75° to 3.4°. Results for the Vecchio-Collins specimens are similar. Figure 4.2(c) indicates that the predicted principal stress angle is underestimated primarily as a result of the equal angle assumption.

Table 4.1 Comparison of principal angles: LVDT instrumented specimens

Specimen	$\theta_{\sigma,exp}$	$\theta_{\varepsilon,exp}$	$\theta_{\sigma,exp} - \theta_{\varepsilon,exp}$	$\frac{1}{2}(\theta_{\sigma,exp} + \theta_{\varepsilon,exp})$	$\theta_{\sigma,pred.}$ (Eqn 4.18)
SE8	39.4	37.9	1.5	38.65	38.1
SE9	48.3	43.5	4.8	45.90	45.0
SE10	42.1	38.4	3.7	40.25	39.6
PP1	41.1	36.6	4.5	38.85	38.3
PDV1	43.3	40.5	2.8	41.90	42.1
PDV2	43.1	41.2	1.9	42.15	42.0
PDV3	45.1	38.3	6.8	41.70	42.3

Table 4.2 Comparison of principal angles: Vecchio–Collins, 1982 specimens

Specimen	$\theta_{\sigma,exp}$	$\theta_{\varepsilon,exp}$	$\theta_{\sigma,exp} - \theta_{\varepsilon,exp}$	$\frac{1}{2}(\theta_{\sigma,exp} + \theta_{\varepsilon,exp})$	$\theta_{\sigma,pred.}$ (Eq. 4.18)
PV4	45.0	43.4	1.6	44.2	45.0
PV6	45.1	43.4	1.6	44.3	45.0
PV10	44.0	37.9	6.1	41.0	41.7
PV11	40.5	39.7	0.8	40.1	43.1
PV12	38.3	33.5	4.9	35.9	37.5
PV16	45.0	43.4	1.6	44.2	45.0
PV18	39.2	29.6	9.5	34.4	35.6
PV19	43.2	34.6	8.6	38.9	39.9
PV20	45.2	35.8	9.4	40.5	41.1
PV21	46.8	39.2	7.6	43.0	43.2
PV26	44.8	38.5	6.4	41.7	41.6
PV29	44.9	38.0	6.8	41.5	40.9
PV30	46.5	39.2	7.3	42.9	41.7

To compensate for the equal angle assumption, half the difference between the principal stress and principal strain angles can be added to the predicted angle. The difference

between the principal angles is assumed to be a function of the relative reinforcement ratio ρ_x/ρ_y, as shown in Fig. 4.4. The proposed linear relationship:

$$\Delta\theta = 2(\rho_x/\rho_y - 1) \tag{4.8}$$

provides a good fit to the LVDT based data. The Vecchio-Collins test data is more scattered with a group of data points shifted by roughly 5°.

The angle predicted by Eq. 4.6 can then be adjusted by adding half the angle difference from Eq. 4.8, i.e.,

$$\theta_{c\sigma} = \theta_{\sigma,\text{Eq. 4.6}} + (\rho_x/\rho_y - 1) \tag{4.9}$$

Figure 4.2(d) compares the adjusted angle (Eq. 4.9) with the unadjusted angle (Eq. 4.6). The prediction for experimental angles below 45° is noticeably improved by the adjustment. For experimental angles greater than 45°, the angle is still underestimated, however, since these specimens were loaded in shear or shear with bi-axial compression, there is no theoretical basis for an angle greater than 45°. To match these experimental values would require a purely empirical adjustment.

4.3.3 Influence of Other parameters

The derivation of Baumann's equation assumes the principal concrete tension is zero. In the proposed model, it is the concrete stress normal to the cracks which is assumed, introducing the crack angle into the prediction of the concrete stress angle. The influence of the crack angle is reviewed in Appendix A.2 and found to be negligible (for $\theta_k - \theta_{c\sigma} < 15°$) such that Baumann's equation can be used. The influence of the modular ratio, *n*, on the predicted angle is also examined in Appendix A.2 and found to be negligible.

4.4 CONSTANT ANGLE DIFFERENCE DURING YIELDING

To predict the total strains after the weak reinforcement yields, the proposed model assumes the principal concrete stress angle and the principal strain angle rotate in parallel after yielding. This assumption is examined in Fig. 4.5 for specimens PP1 and PDV1 and in Fig. 4.6 for the seven Vecchio-Collins specimens where the weak reinforcement yielded. The

reverse-cyclic specimens are not included because the yielding segment of each cycle is too short to be meaningful.

Specimen PP1 in particular supports the assumption of a constant angle difference. The PV specimens show more scatter as expected from only a few manual measurements. Overall, Figs. 4.5 and 4.6 indicate it is reasonable to assume the principal angles rotate in parallel after yielding of the weak reinforcement.

Rotation of the principal concrete stress angle occurs because after the y reinforcement yields and the y-direction concrete stress is fixed, the x-direction concrete stress must increase in compression to equilibrate any increase in shear stress (see Fig. 2.26). Meanwhile, the y-reinforcement strain increases faster than the x-reinforcement strain, causing the principal strain angle to also rotate towards the x axis.

4.5 CONCRETE IN COMPRESSION

The stress-strain response of concrete in compression is normally measured in the principal direction, i.e., σ_{c2} vs ε_2. The response of concrete subjected to uniaxial compression such as in a standard plain concrete cylinder test is often approximated by a simple parabola (Collins and Mitchell 1991; Park and Paulay 1975) as shown in Fig. 4.7 (a).

The response of concrete under biaxial loading where there is principal compression and tension, such as caused by shear loading, has a lower peak compressive stress (is weaker), and a greater principal compressive strain (is softer) than the uniaxial response (Vecchio and Collins 1986); see Fig. 4.7(b). This is attributed to two effects:

- transverse strains reduce the ability of the concrete to carry compression (Vecchio and Collins 1986),
- strains from deformations at the cracks include a strain component in the principal compression direction which becomes very large after yielding of the reinforcement (see Fig. 3.4).

Since the softened response still has a parabolic shape, it is typically represented by the basic parabola, modified by a compression softening coefficient (β). Some models also reduce the strain at peak stress (ε_c') by the same, or a similar softening coefficient. As noted in Chapter 1, a large number of equations exist for the softening coefficient β. This is due to

differences in how β is calculated from the experimental data, to differences in the orientation of the reinforcement relative to the cracks, and to differences in the base curve used to represent the plain concrete response. All the functions modify the plain concrete response to obtain the desired relationship between the principal concrete stress σ_{c2} and the principal strain ε_2.

For the case of reverse-cyclic shear, the concrete response appears very complicated. In addition to softening from transverse strains and from shear slip along the cracks, the response includes a region of tensile strains associated with compressive stress, a bulge (see Sec. 2.9). Current reverse-cyclic shear models use a single stress-strain relationship to capture all three effects requiring a complicated, empirical function with many rules. Because of the region of tensile strains, it combines both concrete compression and concrete tension relationships. As an example, the relationship proposed by Stevens et al. (1987) is shown in Fig. 4.7(c); it is defined by 18 equations. Mansour, Hsu and Lee (2000) use a similar relationship defined by 11 different equations.

In the proposed model for reverse-cyclic shear, the influence of the cracks is considered separately from the concrete, therefore, the concrete stress-strain function relates the principal concrete stress σ_{c2} to the principal concrete strain ε_{c2} and not to the principal total strain ε_2. Since the concrete function includes only the softening due to transverse tensile strains, the simple parabola, modified by a softening coefficient β_c is sufficient even for the complex reverse-cyclic case:

$$\sigma_{c2} = \beta_c f_c' \left[\frac{2\varepsilon_{c2}}{\varepsilon_c'} - \left(\frac{\varepsilon_{c2}}{\varepsilon_c'} \right)^2 \right] \tag{4.10}$$

where β_c is the concrete-only softening coefficient (excludes influence of the cracks).

Since existing functions for the softening coefficient are related to the principal total strain, a new function is required, related to the principal concrete strain. Figure 4.8 illustrates the difference between the two by plotting the concrete response for specimen PV21 in terms of both ε_2 and ε_{c2}. When ε_{c2} is less than ε_2 – which occurs primarily after yielding – the calculated softening coefficient is smaller.

The concrete-only softening coefficient was calculated from the experimental data by solving Eq. 4.10 for β_c at each data point. The principal concrete strain can be estimated from the total strains using

$$\varepsilon_{c2} = \frac{1}{4}\left[\varepsilon_1 + \varepsilon_2 - (\varepsilon_1 - \varepsilon_2)\cos(2\theta_k - 2\theta_\varepsilon)\right]\left(1 + \frac{1}{\cos(2\theta_k - 2\theta_\sigma)}\right) \tag{4.11}$$

and the principal concrete stress was defined by Eq. 2.6.

The calculated softening coefficients are plotted in Fig. 4.9(a) as a function of the principal tensile strain. Since the model assumes all the tensile strains occur at the cracks (Sec. 3.3), the total principal tension strain is used instead of a concrete-only tensile strain.

In Fig. 4.9(a), β_c reduces to about 0.6 as ε_1 increases to 6 mε. Beyond 6 mε, β_c is relatively constant. A principal tension strain of 6 mε corresponds to yielding of the weak reinforcement (with ε_{yy} = 2 mε) in an element subjected to pure shear. This indicates that the large increase in ε_1 which occurs after yielding of the reinforcement has little effect on the softening of the concrete between the cracks.

The proposed concrete-only softening function is

$$\beta_c = 1 - 0.5\frac{\varepsilon_1}{0.002 + \varepsilon_1} \tag{4.12}$$

Equation 4.12 is plotted against all the data points in Fig. 4.9(a) and against only the failure points in Fig. 4.9(b). (See appendix B for the failure point data.) The function averages the compression failure points.

Equation 4.12 is compared to existing softening functions in Fig. 4.10; the existing functions are listed in Table 4.3. Note that the other functions are applied to a concrete stress-strain function which uses the principal total compression strain ε_2 whereas the proposed function is used with the principal concrete compression strain ε_{c2}.

The Belarbi and Hsu function is similar to the proposed function at principal tensile strains less than 6 mε. It was derived from tension-compression tests with the reinforcement parallel to the loading, thus ε_{c2} is approximately equal to ε_2. The Vecchio-Collins function shows increasing softening at tensile strains greater than 5 mε. This agrees with ε_2 becoming

larger than ε_{c2} as shear slip along the cracks becomes large. Miyahara et al. proposed a linear function with a lower limit at $\beta = 0.6$. It is used in conjunction with a shear transfer model and thus may also exclude softening due to shear slip along the cracks.

Separating the deformations at the cracks from the concrete reduces the sources of compression softening to only one: transverse tensile strains. This offers the potential to bring together the various tests used to estimate softening functions.

Table 4.3 Existing Softening Functions (partial listing)

Vecchio and Collins (1993) Model B	$\beta = \dfrac{1}{1+0.27(\varepsilon_1/\varepsilon_0 - 0.37)}$
Belarbi and Hsu (1995)	$\beta = \dfrac{0.9}{\sqrt{1+400\varepsilon_1}}$
Miyahara et al (1988)	$\beta = 1.0$ $\quad \varepsilon_1 \le 0.0012$ $\beta = 1.15\text{-}125\varepsilon_1$ $\quad 0.0012 \le \varepsilon_1 \le 0.0044$ $\beta = 0.60$ $\quad 0.0044 \le \varepsilon_1$
Shirai and Noguchi (1989)	$\beta = \dfrac{1}{0.27+0.96(\varepsilon_1/\varepsilon_0)^{0.167}}$
Kollegger and Mehlhorn (1987)	$\beta = 1.0;$ $\quad 0 \le f_{c1}/f_t \le 0.25$ $\beta = 1.1\text{-}0.4f_{c1}/f_t$ $\quad 0.25 \le f_{c1}/f_t \le 0.75$ $\beta = 0.8$ $\quad 0.75 \le f_{c1}/f_t \le 1.0$

4.6 CONCRETE IN TENSION

There are two components to the concrete tension stresses: residual tension and tension stiffening (Fig. 4.11; from Fronteddu 1993). Residual tension represents the ability of plain concrete to resist axial tension (or principal tension in a bi-axial stress state). It typically decreases quickly after cracks form. Tests on plain concrete measure the residual tension stresses. The other component, tension stiffening, represents the tension which occurs in the concrete surrounding reinforcing bars under tension. Bond between the reinforcing bar and the surrounding concrete allows the applied tension to be shared between the two. This reduces the strain in the embedded bar compared to a bare bar subjected to the same applied tension — the bar is stiffened by the concrete. Tension stiffening remains after cracking since the reinforcement is still bonded to the concrete between the cracks. Tests on

reinforced concrete specimens measure the combined effects of residual tension and tension stiffening. For reverse-cyclic loading, the bond between the reinforcement and the surrounding concrete degrades as the load is cycled which leads to a degradation of the tension stiffening effect.

The concrete tension is examined in Fig. 4.12 for the LVDT instrumented specimens. The concrete tension stress normal to the opening cracks (σ_{cn}), normalized by the stress at first cracking, is plotted versus the total strain normal to the cracks(ε_n). In specimens SE8, SE9 and SE10, the first load cycles cause a sudden drop in the tension stress bringing it below zero before the reinforcement yields. For the more lightly reinforced specimens, PDV1, PDV2 and PDV3, concrete tension stresses are still present when the reinforcement yields. Note that, as discussed in Chapter 2 (Sec. 2.2), the concrete tensile stress is dependent on the assumed reinforcement stress-strain model.

Based on Fig. 4.12, it is reasonable to ignore tension stiffening in the proposed model for reverse-cyclic shear and consider only residual tension. Existing concrete tension functions relate the tension stress to the principal tensile strain (Vecchio and Collins 1986; Belarbi and Hsu 1994), however, Fig. 4.13 indicates the residual tension is more closely related to the average crack width.

The proposed function for the residual tension stress normal to the cracks is

$$\sigma_{cn} = f_{cr}\left[1 - \frac{w}{0.12 + 0.76w}\right] \geq 0 \tag{4.13}$$

where w = average crack width, in mm (Eq. 3.42), and f_{cr} is the concrete cracking stress.

Equation 4.13 reduces gradually to 0 at a crack width of 0.5mm to avoid any significant discontinuity in the model predictions. For simplicity it is assumed applicable to both monotonic and reverse-cyclic shear.

A straight line reducing to 0 at an average crack width of 0.2 mm can be used as a simpler alternative function well suited to hand calculations or simplified estimates of the concrete tension:

$$\sigma_{cn} = 1 - 5w \geq 0 \tag{4.14}$$

Equations 4.13 and 4.14 are shown in Fig. 4.14. In Fig. 4.15, the proposed function (Eq. 4.13) is compared to the concrete tension function proposed by Vecchio and Collins (1986)

$$f_{c1} = f_{cr}\left(\frac{1}{1+\sqrt{200\varepsilon_1}}\right) \tag{4.15}$$

and the function proposed by Belarbi and Hsu (1994)

$$f_{c1} = f_{cr}\left(\frac{.0001}{\varepsilon_1+.0001}\right)^{0.4} \tag{4.16}$$

where f_{c1} is the principal tension stress, ε_1 is the principal tension strain and f_{cr} is the cracking stress. Equations 4.15 and 4.16 combine both residual tension and tension stiffening. An example of the tensile response of plain concrete, from Gopalaratnam and Shah (1985) is also shown.

In the models where Eqs. 4.15 and 4.16 are used, the cracks are assumed to rotate normal to the principal tension stress, therefore f_{c1} is equivalent to σ_{cn}. Equations 4.15 and 4.16 are converted to crack widths by assuming average crack spacings of 50, 100 and 150 mm.

The function proposed by Belarbi and Hsu (Eq. 4.15) is derived from tests where monotonic tension and compression are applied in two orthogonal directions parallel to the reinforcement. After an initial reduction, the function levels off as tension stiffening reaches equilibrium. The Vecchio-Collins function (Eq. 4.16) is derived from elements subjected to shear loading with the reinforcement at 45° to the principal tension and compression stresses. The decrease in tension stress is less pronounced than with loading parallel to the reinforcement.

4.7 REINFORCEMENT STRESS–STRAIN MODEL

The average stress-strain response of a reinforcing bar embedded in concrete is different than a bare bar subjected to the same loading. Under tension, the embedded bar will transfer some stress to the surrounding concrete. At a crack, the ability of the surrounding concrete to carry any tension is severely reduced, thus the bar alone must resist the applied load. When the reinforcement yields locally at the cracks, the average stress in the bar will

be less than the yield stress and the difference between the average stress and the local stress in the reinforcement is a function of the tension stress in the concrete (Stevens, Uzumeri, and Collins 1987; Kaufmann and Marti 1998; Belarbi and Hsu 1994). The tension in the concrete is influenced by factors such as the number and spacing of cracks and the bond between reinforcement and concrete.

Most shear models, including the one proposed here, require a constitutive relationship for the reinforcement which relates average stresses to average strains. The experimental data measures the total average stress — reinforcement plus concrete — and the average strain. How the total average stress is divided between the reinforcement and the concrete in tension is somewhat arbitrary. This is illustrated in Fig. 4.16.

For the MCFT, Vecchio and Collins (1986) use the bare bar stress-strain model for the average stress and strain in the reinforcement and a separate function for the tension in the concrete. A "crack check" is performed to reduce the tension in the concrete as the reinforcement approaches yield, ensuring the total stress at a crack is no greater than the yield stress of the reinforcement. Part of their justification for using the bare bar model is that due to strain hardening — which is ignored — local stresses at a crack will be greater than the yield stress and thus the average stress will be close to the yield stress.

An alternative to using the bare bar model is to define an average yield stress which is less than the bare bar yield stress where the reduction is a function of the concrete tensile strength. Stevens et al. (1987) used this approach in order to eliminate the "crack check" which is not suitable to a Finite Element formulation.

In order to be more conceptually correct, Hsu and colleagues (Belarbi and Hsu 1994; Pang and Hsu 1995) and Kaufmann and Marti (1998) also developed stress-strain relationships with a reduced yield stress where the reduction is derived from an assumed bond stress distribution and the tension capacity of plain concrete. A separate function is used for the average tension stress in the concrete. In theory, the sum of the two functions gives the correct total average stress. In practice, Stevens et al. (1987) and Belarbi and Hsu (1994) added an empirical factor to obtain the desired result.

The bare bar model is used in the proposed model because it is simple and transparent, and because it is compatible with established axial and flexural strength models:

$$\sigma_s = E_s \cdot \varepsilon_s \leq f_{sy} \tag{4.17}$$

where the steel modulus E_s is typically 200,000 MPa and f_y is the bare bar yield stress (strain hardening is ignored). Unloading and re-loading of the stress occurs at a slope of E_s.

Equation 4.17 applies only to tension stresses which is sufficient for reverse-cyclic shear loading since for this case the reinforcement is always in tension. More complete reinforcement models which cycle between tension and compression stresses and include the Baushinger effect are available, e.g., Kent and Park (1973).

5

Model Predictions

The fundamental principles and the constitutive relationships of the proposed model have been implemented in a computer program that can predict the complete load-deformation response of a membrane element subjected to reverse-cyclic shear. Using only the section properties, concrete strength and reinforcement arrangement, as input, the program predicts the shear strain at each step of a prescribed loading history. In this Chapter, the model predictions are compared to the experimental data.

The model is also used to examine the sensitivity of the predicted response to the constitutive relationships used for the reinforcement, the principal stress angle, the crack closing function, concrete in tension, and concrete in compression.

5.1 MODEL IMPLEMENTATION

The procedure for predicting the load-deformation response of reinforced concrete membrane elements subjected to reverse-cyclic shear presented in Chapter 3 has been implemented in a computer program. Cycling of the load is controlled by target strain values: the loading is increased in one direction (by 0.1 MPa at each step) until the shear strain reaches a target value, then the load is reduced to zero and re-applied in the direction of the next target (opposite direction for reverse-cycling, same direction for positive-only cycling) until the next strain target is reached. The target values are arbitrary and can be experimental data points or, for example, the strain at specified ductility or deflection

values. The prediction is terminated when the last target is reached or when failure occurs based on the three criteria defined in Section 3.7: concrete compression strength is exceeded, the shear strain limit is reached, or both x and y reinforcement yield.

The algorithm used to implement the model is summarized as a flow chart in Fig. 5.1. The model is divided into two parts: before yielding (which includes unloading) and yielding. The solution algorithm is essentially the same for both parts except that before yielding, the principal concrete stress angle is known from the element properties, while after yielding, the y-reinforcement stress is known. Within each part there are three iteration loops. The outer loop increments the shear stress until the next strain target is reached or failure occurs. The second loop iterates on the strain normal to the cracks which is used to define the average crack width and thus the concrete tension stress. The inner loop iterates on the principal tension strain which is used to define the compression softening coefficient. The two inner iteration loops could be eliminated by using a sufficiently small increment of stress so that the strain values from the previous increment can be used with minimal error.

5.2 MODEL PREDICTIONS

5.2.1 Input Values

The section properties used as input to the program are listed in Table 5.1. The estimated principal concrete stress angle and average crack spacing are listed in Table 5.2. Because some of the specimens were tested at an early age, when the tensile strength may have been relatively high, experimental values are used for the cracking stress, f_{cr} (see Table 5.3). The experimental shear strain at the peak shear stress of each cycle are used as the strain targets.

Table 5.4 compares the predicted and experimental failure modes. Because the shear strain limit has been defined conservatively, it tends to dominate. For a more complete comparison with the experimental data, predictions are also made with the shear strain limit turned off.

Table 5.1 Input Values - Section Properties

Parameter	PP1	SE8	SE9	SE10	PDV1	PDV2	PDV3
f_c'	-27	-37	-44.2	-34	-26.8	-23.7	-34.1
ε_c'	-0.00217	-0.003	-0.003	-0.002	-0.0016	-0.002	-0.002
E_c	26000	30400	33200	29200	25900	24300	29200
ρ_x	0.0195	0.0294	0.0294	0.0294	0.0182	0.0182	0.0182
ρ_y	0.0065	0.0098	0.0294	0.0098	0.0091	0.0091	0.0091
f_{yx}	480	492	422	422	282	282	282
f_{yy}	480	479	422	479	282	282	282
E_s	200000	200000	200000	200000	200000	200000	200000
Shear Loading	Mono-tonic	Reverse cyclic	Reverse cyclic	Reverse cyclic	Mono-tonic	Reverse cyclic	Cyclic
Normal Loading	0	0	0	$-1/3\|V_{xy}\|$	$-0.4\|V_{xy}\|$	$-0.4\|V_{xy}\|$	$-0.4\|V_{xy}\|$

Table 5.2 Input Values – Calculated Properties

Parameter	PP1	SE8	SE9	SE10	PDV1	PDV2	PDV3
$\theta_{c\sigma}$ (Eq. 3.19), deg.	39.9	40.1	45	41.6	42.7	42.7	42.7
$s_{m\theta}$ (Eq. 3.43), mm	212	145	109	195	71	71	71

Table 5.3 Concrete tension (MPa)

Specimen	$f_{t,experimental}$	$0.33\sqrt{f_c'}$ (for comparison)
PP1	1.55	1.71
SE8	2.07	2.01
SE9	2.18	2.19
SE10	2.08	1.92
PDV1	2.12	1.71
PDV2	2.2	1.61
PDV3	2.7	1.93

Table 5.4 Failure Modes

specimen	experimental failure mode[1]	predicted failure mode[1]	
		with shear strain limit	without shear strain limit
PP1	shear	shear	reinforcement
SE8	shear	shear	none[3]
SE9	compression	shear[2]	reinforcement[2]
SE10	shear	shear	compression
PDV1	reinforcement	shear	reinforcement
PDV2	reinforcement	shear	reinforcement
PDV3	reinforcement	shear	reinforcement

[1]the failure modes are:
shear = shear strain limit exceeded
compression = concrete compression strength exceeded
reinforcement = reinforcement in both direction reaches yield
[2]SE9: misses compression failure by .5MPa (1.9 %)
[3]none: no failure after reaching a shear strain 10 times the maximum experimental strain

5.2.2 Predicted Response

PP1 (Fig. 5.2)

The model gives a good prediction of the monotonic shear response of PP1. The influence of concrete tension is under-estimated during the cracking stage, possibly because the residual tension function was derived from reverse-cyclic data.

SE8 (Fig. 5.3)

The predicted response for SE8 agrees very well with the experimental data. Yielding in the model is less rounded than in the experimental response which is expected from the bi-linear reinforcement model. The peak shear stress for each cycle and the pinching of the hysteresis loops are well predicted.

Despite the simple approach used for the principal concrete stress angle (Fig. 5.3b), the predicted principal strain angle closely follows the experimental data (Fig. 5.3c). For the y reinforcement, modelling the plastic strains as fully cumulative results in greater predicted strains (Fig. 5.3d). The predicted concrete response (Fig. 5.3e) agrees well with the

experimental data at the peak stresses. The constant stress angle results in a linear unloading segment. The prediction reduces to zero stress and has smaller tensile strains as a result of neglecting minor residuals. The "bulge" (tensile strain with compressive stress) is represented, although it is less prevalent than in the experimental data, likely due to the simple concrete model and the simple stress angle assumption. The pinching of the shear loops is well captured.

SE9 (Fig. 5.4)

For SE9, equal x and y reinforcement results in predicted stress and strain angles of 45°; both reinforcement have equal stresses and strains and both yield at the same time. The experimental data, however, reflects some unevenness between the two reinforcements, with the y reinforcement yielding before the x reinforcement.

The y reinforcement strain is well predicted (Fig. 5.4d), except for the slight yielding seen in the experimental data. The predicted concrete response is stiffer than the experimental response (Fig. 5.4e) because the model does not include the additional softening due to elastic cycling of the load.

SE10 (Fig.5.5)

For SE10, the model predicts a concrete shear failure before yielding of the weak reinforcement. With the shear strain limit turned off, the model gives a good prediction of the complete experimental response. The shear limit may be too conservative when the loading includes bi-axial compression such as for SE10.

The individual components (Fig. 5.5 b, c, d, e) show good agreement with the experimental data. As with SE9, the predicted concrete response is stiffer than the experimental data because there is no additional softening from cycling of the load.

PDV series (Fig. 5.6)

The envelope to the response is very well predicted for all three PDV specimens. The linear unloading and reloading used in the concrete model is apparent in the cycles for PDV2 and

PDV3. These cycles occur at low concrete stresses and strains, where the minor residuals due to cracks not closing completely are more noticeable.

5.3 SENSITIVITY ANALYSIS

This section examines the sensitivity of the model predictions to the key assumptions in the constitutive relationships. This helps evaluate the importance of each parameter and validate the model assumptions.

5.3.1 Influence of Bi-Linear Steel Model

In the experimental data, yielding of the reinforcement occurs gradually, possibly because of rounding in the actual reinforcement stress-strain response and local yielding at multiple cracks not all at once. For comparison purposes, a stress-strain relationship which includes gradual yielding was defined:

$$\varepsilon_s = \frac{f_s}{E_s}\left(1+\left(\frac{f_s}{f_y}\right)^{15}\right)^{1/3} \tag{5.1}$$

where the exponents were selected to approximate the results from SE8.

Model predictions using Eq. 5.1 are shown in Fig. 5.7 for PP1 and SE8. The predicted shear response follows the experimental response more closely than when the bi-linear reinforcement model is used, however, key parameters such as shear stiffness and peak shear stress are not affected. The improvements in the prediction are not sufficient to justify the added complexity and the empirical coefficients required for the gradual yield model.

5.3.2 Influence of Concrete Tension

In the model, concrete tension stresses influence the uncracked stage and the cracking stage when crack widths are small. For well reinforced elements such as PP1 (Fig. 5.8a) and SE8 (Fig. 5.8b), the influence of concrete tension is negligible by the time the reinforcement yields. For lightly reinforced specimens such as PDV3 (Fig. 5.8c), concrete tension influences the shear stress beyond the point at which yielding occurs. In all cases, including concrete tension improves the prediction.

5.3.3 Influence of Principal Concrete Stress Angle

The sensitivity of the model predictions to the principal concrete stress angle is examined in Fig. 5.9 for PP1 and Fig. 5.10 for SE8. The angle calculated by Eq. 3.19 is arbitrarily changed by ±2° or approximately 5%. Increasing the concrete stress angle by 2° reduces the shear stress at yield by 6% in PP1 and 7% in SE8. Decreasing the stress angle by 2° increases the shear stress at yield by 8% in PP1 and by 10% in SE8.

Increasing the angle rotates the principal compression closer to the *y* reinforcement. This increases the demand on the *y* reinforcement and causes yielding to occur at a lower shear stress. Conversely, reducing the angle increases the demand on the *x* reinforcement, allowing a greater shear stress to be reached before the *y* reinforcement yields.

The calculation of the principal concrete stress angle includes an adjustment to compensate for the equal angle assumption (Eq. 3.19). For PP1 and SE8, the adjustment is +2° therefore neglecting the adjustment is equivalent to reducing the stress angle by 2° (Fig. 5.9 for PP1 and Fig. 5.10b for SE8). Without the adjustment, the stress angle is under-estimated and the peak shear stress is over-estimated which is typically unconservative. Since the adjustment has a rational basis it should be included in the calculation of the principal concrete stress angle.

5.3.4 Influence of Concrete Compression Softening

If concrete compression softening is ignored (β_c = 1.0), the predicted shear response is stiffer than the experimental response (Fig. 5.11a). Without softening, the stiffer concrete means a greater concrete stress and a greater stress and strain in the *y* reinforcement are required to reach a given shear strain. Note that the principal concrete stress angle is unchanged and the shear stress at yielding is not affected since it is governed by the reinforcement yield strength.

The influence of compression softening is relatively minor when the concrete stresses are low (e.g., PP1 and SE8). When the compression stresses in the concrete are higher (e.g., SE9), the difference between the softened and unsoftened response is more significant (Fig. 5.11b).

As noted earlier, specimens SE9 and SE10 show softening of the concrete response due to cycling of the load. This effect can be modelled with an equation such as

$$\beta_{cyclic} = 1 - 0.5\frac{\sum\left|\varepsilon_{c2}\right|}{\left|\varepsilon_c'\right|} \geq 0.7 \tag{5.2}$$

Where the cyclic softening coefficient, β_{cyclic}, is a function of the cumulative sum of the concrete principal strain ε_{c2}. The cumulative sum is one measure of the amount of cycling the concrete has experienced. The coefficients in Eq. 5.2 have been selected to approximate the concrete response of SE9.

Figure 5.11c shows the predicted response when using Eq. 5.2 to add cyclic softening. The concrete response follows the experimental data more closely, although some further refinement is required at peak stresses. The shear stress-strain response also follows the experimental data more closely, however, this improved fit is partly coincidental. In the experiment, the shear strain includes yielding of the *y* reinforcement. In the model, the increased shear strain is due to additional concrete softening.

Due to limited data, the need for a more complex concrete stress-strain formulation and the constraint of knowing the complete load history, cyclic softening is not implemented.

5.3.5 Influence of Crack Closing Function

The crack closing function affects the load reversal stage when cracks are open in two directions. The pinching of the shear loops and the "bulge" in the concrete response are the two components most sensitive to the crack closing function. This is seen in Fig. 5.12 where the response using Eq. 3.14 is compared to the response using a linear crack closing function which reduces to zero at a compression stress of 6 MPa. The linear function results in slower closing of the cracks. This increases the shear stress through the reversal and increases the size of the bulge in the concrete response.

6

Simplified Model for Design

The model for reverse-cyclic shear presented in Chapters 3 and 4 – called the general model in this Chapter – can be simplified for application in structural analysis and design. Knowledge of the important characteristics of the response can be used to select appropriate simplifications which can then be verified with the general model, resulting in simple transparent models with a rational basis.

The simplified model presented here consists of an envelope to the response and a simple function to define the loops, including pinching. The simplified model includes an equation to determine the cracked section shear stiffness from the section properties of the element.

A sensitivity analysis using the simplified model examines the influence of different parameters (reinforcement ratio, modular ratio, axial load, concrete tension, crack angle, principal stress angle) on the predicted shear stress and shear strain at yielding and on the cracked section shear stiffness. This indicates the relative importance of each parameter and confirms the validity of the simplifying assumptions.

6.1 CURRENT APPROACHES TO SEISMIC SHEAR DESIGN - SELECTED EXAMPLES

Current approaches for including seismic shear in the design of concrete structures do not reflect the actual behaviour and lack a rational basis. For example, the concrete design code ACI 318-02 (ACI Committee 318 2002), uses the empirical $V_s + V_c$ approach based on a

45° truss analogy. For seismic design, V_c is assumed to be zero and the transverse reinforcement (which gives V_s) is selected to remain elastic. Yielding of the transverse reinforcement is generally equated with a shear failure. Figure 6.1 compares this approach with a more sophisticated one which includes shear yielding.

For shear-dominated elements, the conservative shear strength approach of ACI 318-02 may actually result in the brittle shear failure it aims to avoid. Depending on the ratio of transverse to longitudinal reinforcement, the compression stresses in the concrete may be oriented at less than 45° to the longitudinal reinforcement resulting in larger concrete stresses than assumed in the 45° truss analogy. Conversely, stresses in the transverse reinforcement are lower than assumed. This can result in a brittle concrete compression failure before the transverse reinforcement yields. In some cases, the shear reinforcement prescribed by the conservative strength model can be detrimental to the performance of shear-dominated elements.

The seismic loads in shear-dominated structures or elements are a function of the shear stiffness, however, this is not addressed in ACI 318-02 (ACI Committee 318 2002). The UBC building code (ICBO 1997) states that "stiffness properties of reinforced concrete and masonry elements shall consider the effects of cracked sections" but provides no guidance. The Seismic Rehabilitation Pre-standard, FEMA 356 (ASCE 2000), prescribes a reduced flexural stiffness for cracked walls versus uncracked walls, but, for the shear stiffness, it suggests the gross or uncracked section shear stiffness for both uncracked and cracked walls.

Using the uncracked section shear stiffness in the analysis of structures and structural elements can lead to incorrect estimates of load magnitudes and distributions and to inaccurate predictions of failure modes. When applied to existing structures, this can lead to expensive retrofits. As seen in this thesis, the cracked section shear stiffness can be one-tenth the uncracked stiffness. Using the wrong shear stiffness undermines the accuracy of the latest analysis techniques, including non-linear dynamic and pushover analyses.

Although complete reverse-cyclic models are outside the scope of design codes, they are needed for detailed seismic analysis. Current models are either empirical – Saatcioglu (1991) reviews hysteretic models for reinforced concrete – or semi-empirical. For example,

Pincheira et al (1999) use the Modified Compression Field Theory to define the envelope and empirical rules to define the cycles. Empirical models are typically expressed directly in terms of shear stress vs shear strain (or shear force vs shear displacement) making them relatively easy to implement in analysis tools. They are typically based on specific tests and some require that parameters such as pinching and strength decay be "assigned by the analyst" (Saatcioglu 1991) which limits their general application.

6.2 ENVELOPE MODEL

The envelope to the load-deformation response of a membrane element subjected to reverse-cyclic shear can be approximated by a simple bi-linear or tri-linear model. As shown in Fig. 6.2a, the tri-linear model captures all three stages of the response: uncracked, cracking and yield. If the uncracked stage is ignored, a bi-linear model can be used. The envelope model assumes no post-yield strength gain. This is conservative for the monotonic case (Fig. 6.2b).

The tri-linear envelope is defined by 3 points:

1. the cracking point; shear stress and shear strain at cracking, $v_{xy,cr}$ and $\gamma_{xy,cr}$,
2. the yield point; shear stress and shear strain at yield, $v_{xy,yld}$ and $\gamma_{xy,yld}$,
3. the failure point; shear stress or shear strain at failure, $v_{xy,max}$ or $\gamma_{xy,max}$.

The cracking point is where the principal applied tensile stress reaches the concrete cracking strength. The yield point is where the stress in the weak reinforcement reaches the yield stress. The failure point is the first occurrence of either a concrete compression failure, a shear failure, or a reinforcement failure.

The cracked section shear stiffness is an important result of the simplified model. It is defined as the secant stiffness to the yield point:

$$G_{cr} = v_{xy,yld} / \gamma_{xy,yld} \tag{6.1}$$

To model the complete reverse–cyclic response, a simplified equation for the hysteresis loops is added to the envelope. It defines the loops directly in terms of shear stress and shear strain and is derived from the general model. The complete reverse-cyclic model, shown in Fig. 6.2c, has the following characteristics:

- yielding occurs at $v_{xy,yld}$ for each cycle,
- the cracked section shear stiffness (G_{cr}) is constant for each cycle
- unloading occurs at a slope of G_{cr},
- the shear strain remaining at the end of unloading, $\gamma_{xy,plastic}$, is cumulative from one direction to the other
- the shear strain during re-loading is the shear strain corresponding to the shear stress plus a component due to accumulated plastic strain (described in Sec. 6.6)

6.3 CRACKING POINT

The concrete cracking stress can be estimated by the equation suggested by Collins and Mitchell (1991),

$$f_{cr} = 0.33\sqrt{f_c'} \text{ (MPa)} \tag{6.2}$$

The uncracked shear stiffness can be estimated, as suggested by Park & Paulay (1975), by

$$G_{cr} = 0.4E_c \tag{6.3}$$

where, from Collins and Mitchell (1991),

$$E_c = 4730\sqrt{f_c'} \text{ (MPa)} \tag{6.4}$$

For homogeneous uncracked concrete, neglecting the influence of the reinforcement, the shear stress at cracking is approximately

$$v_{xy,cr} = \sqrt{(f_{cr} - n_x)(f_{cr} - n_y)} \tag{6.5}$$

where n_x and n_y are the applied normal stresses in the reinforcement directions.

The shear strain at cracking is approximately

$$\gamma_{xy,cr} = v_{xy,cr}/0.4E_c \tag{6.6}$$

6.4. YIELD POINT

6.4.1 Shear Stress at Yield, $v_{xy,yld}$

From a Mohr's circle of concrete stress, the shear stress is expressed as a function of the stress normal to the cracks (σ_{cn}) and the stress in the y direction (σ_{cy}):

$$v_{xy} = (\sigma_{cn} - \sigma_{cy}) \frac{\sin 2\theta_{c\sigma}}{\cos(2\theta_k - 2\theta_{c\sigma}) - \cos 2\theta_{c\sigma}} \tag{6.7}$$

where $\theta_{c\sigma}$ is the concrete principal stress angle (Eq. 3.19) and θ_k is the crack orientation. When the y reinforcement yields, from equilibrium considerations (Eq. 2.5),

$$\sigma_{cy} = n_y - \rho_y f_{yy} \tag{6.8}$$

Substituting for σ_{cy} in Eq. 6.7, the shear stress at yield is

$$v_{xy,yld} = (\sigma_{cn} + \rho_y f_{yy} - n_y) \frac{\sin 2\theta_{c\sigma}}{\cos(2\theta_k - 2\theta_{c\sigma}) - \cos 2\theta_{c\sigma}} \tag{6.9}$$

Equation 6.9 is a general equation for the shear strength, taking into account tension in the concrete, axial load, and a fixed crack orientation. As an approximation, the cracks can be assumed parallel to the principal concrete compression, i.e., $\theta_k = \theta_{c\sigma}$, eliminating the need to calculate the crack angle. This is equivalent to the "rotating crack" approach used in the MCFT and similar existing models. Replacing θ_k with $\theta_{c\sigma}$ in Eq. 6.9 yields

$$v_{xy,yld} = (\sigma_{cn} + \rho_y f_{sy} - n_y) \cot\theta_{c\sigma} \tag{6.10}$$

Equation 6.10 is equivalent to the shear strength equation obtained from the MCFT (Vecchio and Collins 1986).

At yielding, the residual tension stress normal to the cracks (σ_{cn}) can be assumed to be zero which is conservative since the shear stress at yield will be under-estimated. This is reasonable for well reinforced elements but may be overly-conservative for lightly reinforced elements. Alternatively, σ_{cn} can be related to the crack width by Eq. 3.41, where the

average crack width is a function of the strain normal to the cracks at yield ($\varepsilon_{n,yld}$) and the average crack spacing. In Appendix A.3, it is shown that, with no axial load, $\varepsilon_{n,yld}$ can be estimated by

$$\varepsilon_{n,yld} = \frac{f_{yy}}{E_s}\left[1+\left(\frac{\rho_x}{\rho_y}\right)^{-0.56} + n\rho_y\left(\frac{\rho_x}{\rho_y}\right)^{0.3}\right] \tag{6.11}$$

where f_{yy} is the y-reinforcement yield stress, ρ_x and ρ_y are the reinforcement ratios and n is the modular ratio E_s / E_c. A more detailed equation which includes the influence of axial loads is included in Appendix A.3.

6.4.2 Shear Strain at Yield, $\gamma_{xy,yld}$

From a Mohr's circle of strain, the shear strain is related to the strain in each reinforcement direction (ε_x and ε_y) and to the strain parallel to the open cracks (ε_p) by the equation

$$\gamma_{xy} = \frac{\varepsilon_x}{\tan\theta_k} + \varepsilon_y \tan\theta_k - \varepsilon_p\left(\tan\theta_k + \frac{1}{\tan\theta_k}\right) \tag{6.12}$$

where θ_k is the crack angle.

Using linear stress-strain relationships for the concrete in compression and in tension, using a linear relationship for the reinforcement, and applying the equilibrium equations, the strains in Eq. 6.12 can be related to the stresses (see Appendix A.4). The result is the general equation:

$$\begin{aligned}\gamma_{xy} = \frac{v_{xy}}{\sin 2\theta_{c\sigma}} & \left[\frac{\cos(2\theta_k - 2\theta_{c\sigma}) + \cos 2\theta_{c\sigma}}{E_s\rho_x \tan\theta_k} + \frac{\tan\theta_k\left(\cos(2\theta_k - 2\theta_{c\sigma}) - \cos 2\theta_{c\sigma}\right)}{E_s\rho_y} + \frac{2\cos(2\theta_k - 2\theta_{c\sigma})}{E_c}\left(\tan\theta_k + \frac{1}{\tan\theta_k}\right)\right] \\ & -\sigma_{cn}\left[\frac{1}{E_s\rho_x \tan\theta_k} + \frac{\tan\theta_k}{E_s\rho_y} + \frac{1}{E_c}\left(\tan\theta_k + \frac{1}{\tan\theta_k}\right)\right] \\ & + \frac{n_x}{E_s\rho_x \tan\theta_k} + \frac{n_y \tan\theta_k}{E_s\rho_y}\end{aligned} \tag{6.13}$$

The relative importance of the concrete tension term at yield is examined using SE8 as a numerical example. At the point where the y reinforcement yields, v_{xy} = 5.64 MPa, σ_{cn} = 0.06 MPa, $\theta_{c\sigma}$=39.4°, σ_{c2} = -11.43 MPa. For SE8, $n_x = n_y = 0$, $\theta_k = 45°$, $\rho_x = 3\%$, $\rho_y = 1\%$, n=6.7. Substituting these values into Eq. 6.13:

$$\begin{aligned}
\gamma_{xy} &= \frac{1}{E_s}\left\{v_{xy}\left[\frac{1}{\rho_x}\left(1+\frac{1}{\tan 2\theta_{c\sigma}}\right)+\frac{1}{\rho_y}\left(1-\frac{1}{\tan 2\theta_{c\sigma}}\right)+4n\right]-\sigma_{cn}\left[\frac{1}{\rho_x}+\frac{1}{\rho_y}+\frac{n}{\tan^2 2\theta_{c\sigma}}\right]\right\} \\
&= \frac{1}{E_s}\{5.64[39.9+80.2+26.8]-0.06[33.3+100+0.26]\} \\
&= \frac{1}{E_s}\{5.64[147]-0.06[134]\} \\
&= \frac{1}{E_s}(829-8) \\
&= 0.0041
\end{aligned}$$

This compares well with the experimental value of 0.0048. In this example, the shear stress accounts for 99% of the shear strain at yielding and the concrete tension for only 1%.

With the approximation $\theta_k = \theta_{c\sigma}$, Eq. 6.13 reduces to

$$\begin{aligned}
\gamma_{xy} = &\frac{v_{xy}}{E_s}\left[\frac{1}{\rho_x \tan^2\theta_{c\sigma}}+\frac{\tan^2\theta_{c\sigma}}{\rho_y}+n\left(\tan\theta_{c\sigma}+\frac{1}{\tan\theta_{c\sigma}}\right)^2\right] \\
&-\frac{\sigma_{cn}}{E_s}\left[\frac{1}{\rho_x \tan\theta_{c\sigma}}+\frac{\tan\theta_{c\sigma}}{\rho_y}+n\left(\tan\theta_{c\sigma}+\frac{1}{\tan\theta_{c\sigma}}\right)\right] \\
&+\frac{n_x}{E_s\rho_x \tan\theta_{c\sigma}}+\frac{n_y \tan\theta_{c\sigma}}{E_s\rho_y}
\end{aligned} \tag{6.14}$$

For the case of pure shear ($n_x = n_y = 0$), neglecting concrete tension ($\sigma_{cn} = 0$), and substituting Collins' equation (Eq. 3.18) for $\theta_{c\sigma}$, Eq. 6.14 reduces to the equation developed by Collins in formulating the CFT (Collins 1978):

$$\gamma_{xy} = \frac{2v_{xy}}{E_c}\left[1+\sqrt{\left(1+\frac{1}{n\rho_x}\right)\left(1+\frac{1}{n\rho_x}\right)}\right] \tag{6.15}$$

Concrete Modulus

To reduce the complexity of the shear strain equation (Eq. 6.13), a linear stress-strain relationship was assumed for the concrete in compression:

$$\varepsilon_{c2} = f_{c2}/E_c \tag{6.16}$$

This linear approximation is generally considered valid for a compression stress below $0.6f_c'$. As f_{c2} approaches f'_c, the linear function under-estimates the principal strain by up to 50% (Fig. 6.3)

To improve the estimate of the concrete strain at yielding, the secant modulus is assumed to vary as a function of the principal compression stress and is adjusted to include compression softening:

$$E_c^* = \alpha\beta_c E_c \tag{6.17}$$

where α is a function of the principal compression stress (σ_{c2}) and β_c is the compression softening coefficient.

In Eq. 6.17, α varies from 1.0 for $\sigma_{c2} = 0$ to 0.5 for $\sigma_{c2} = f_c'$. At yielding, the principal compression stress can be related to the weak reinforcement: ignoring concrete tension and assuming pure shear loading,

$$\sigma_{c2} = \frac{\rho_y f_{yy}}{\sin^2\theta_{c\sigma}} \tag{6.18}$$

Recognizing that $1/\sin^2\theta_{c\sigma}$ varies from 2 for $\rho_x/\rho_y = 1$ ($\theta_{c\sigma} = 45°$) to 4 for $\rho_x/\rho_y = 12$ ($\theta_{c\sigma} \approx 30°$), it can be approximated by $2(\rho_x/\rho_y)^{0.3}$, then α can be defined as

$$\alpha = 1 - \left(\frac{\rho_x}{\rho_y}\right)^{0.3} \frac{\rho_y f_{yy}}{f_c'} \geq 0.5 \tag{6.19}$$

The compression softening coefficient, β_c, was derived in Chapter 4 as a function of the principal tension strain, ε_1:

$$\beta_c = 1 - 0.5\frac{\varepsilon_1}{0.002 + \varepsilon_1} \tag{6.20}$$

For simplicity, ε_1 is assumed equal to ε_n which can be estimated with Eq. 6.11. Alternatively, a lower bound value of 0.6 can be assumed for β_c: this corresponds approximately to yielding of an element subjected to pure shear, where the reinforcement yield strain is 0.002.

Figure 6.3 compares the linear concrete model with the typical parabolic relationship and with the softened response typical of specimens loaded in shear. Where the modular ratio is used instead of the concrete modulus, the softened modular ratio $n^* = E_c^*/E_c$ should be used:

$$n^* = \frac{n}{\alpha\beta_c} \tag{6.21}$$

6.5 FAILURE POINT

Concrete Compression Failure

To avoid a concrete compression failure, the principal compression stress in the concrete (σ_{c2}) must be less than the softened concrete compression strength ($\beta_c f_c'$). From a Mohr's circle of concrete stress, the principal concrete compression stress is

$$\sigma_{c2} = \sigma_{cn} - v_{cxy}\frac{1 + \cos(2\theta_k - 2\theta_{c\sigma})}{\sin 2\theta_{c\sigma}} \tag{6.22}$$

where σ_{cn} is the tensile stress normal to the cracks, v_{cxy} is the concrete shear stress, $\theta_{c\sigma}$ is the principal concrete stress angle and θ_k is the crack orientation.

To check against compression failures, an upper–bound estimate of σ_{c2} is used: Eq. 6.22 is a maximum when the stress normal to the opening cracks is neglected and the cosine

term is taken equal to 1.0. Taking a low estimate of 30° for $\theta_{c\sigma}$, the concrete principal stress is

$$\sigma_{c2} = -2.3v_{cxy} \tag{6.23}$$

Assuming $\beta_c = 0.6$, with f_c' taken positive, the maximum allowable shear stress is

$$\begin{aligned} v_{xy\max} &\leq \frac{0.6f_c'}{2.3} \\ &\approx 0.25f_c' \end{aligned} \tag{6.24}$$

Equation 6.24 is consistent with the limit specified in AASHTO (American Association of State Highway and Transportation Officials 1998, Sec. 5.8.3.3) and CSA A23.3 (Canadian Standards Association Committee A23.3 1994, Eq. 11-17).

Reinforcement Failure

The shear stress at which both the x and y reinforcement yield, neglecting tension in the concrete, is approximately:

$$v_{xy,\max} = \sqrt{(n_y - \rho_y f_{yy})(n_x - \rho_x f_{yx})} \tag{6.25}$$

For pure shear loading and equal reinforcement yield stress, Eq. 6.25 simplifies to

$$v_{xy,\max} = f_y\sqrt{\rho_x \rho_y} \tag{6.26}$$

Concrete Shear Failure

A concrete shear failure occurs when the shear strain reaches the maximum shear strain, as defined in Chapter 3 (Sec. 3.7, Eq. 3.48). Since both the shear strain limit and the check for a compression failure (Eq. 6.24) are based on the ratio of shear stress to concrete strength, they can be combined into one expression (Fig. 6.4):

$$\gamma_{xy,\max} = \gamma_{xy,yld}\left(4 - 12\frac{v_{xy,yld}}{f_c'}\right); \frac{v_{xy,yld}}{f_c'} \leq 0.25 \tag{6.27}$$

6.6 CRACKED SECTION SHEAR STIFFNESS

As noted earlier (Eq. 6.1), the cracked section shear stiffness (G_{cr}) is defined as the secant stiffness to the yield point. Using Eq. 6.10 for the shear stress and 6.14 for the shear strain (both include the θ_k=$\theta_{c\sigma}$ approximation), G_{cr} is:

$$G_{cr} = \frac{E_s}{A+B}$$

$$A = \frac{1}{\rho_x \tan^2\theta_{c\sigma}} + \frac{\tan^2\theta_{c\sigma}}{\rho_y} + n\left(\tan\theta_{c\sigma} + \frac{1}{\tan\theta_{c\sigma}}\right)^2 \tag{6.28}$$

$$B = \frac{1}{(\sigma_{cn} + \rho_y f_{yy} - n_y)}\left[\frac{n_x - \sigma_{cn}}{\rho_x} + \frac{(n_y - \sigma_{cn})\tan^2\theta_{c\sigma}}{\rho_y} - \frac{n\sigma_n}{\cos^2\theta_{c\sigma}}\right]$$

Park and Paulay (1975) derived an equation for the cracked section shear stiffness in concrete beams based on a truss mechanism. They assumed $n_x = n_y = 0$, $\theta_k = \theta_{c\sigma} = 45°$, σ_{cn}= 0, and that the horizontal struts (x-direction reinforcement) are infinitely rigid, i.e., $\rho_x = \infty$. Applying these assumptions to Eq. 6.28 results in the same expression as Park and Paulay (1975):

$$G_{cr} = \frac{E_s \rho_y}{1 + 4n\rho_y} \tag{6.29}$$

They derived a second equation with $\theta_k = \theta_\sigma$ but not necessarily 45°: in this case, Eq. 6.28 reduces to

$$G_{cr} = \frac{E_s \rho_y \sin^4\theta_{c\sigma} \cot^2\theta_{c\sigma}}{\sin^4\theta_{c\sigma} + n\rho_y} \tag{6.30}$$

which is similar to the expression presented by Park and Paulay (1975).

6.7 HYSTERESIS LOOP EQUATION

The residual shear strain at the end of unloading reflects the cracks which remain open and the plastic strain in the weak reinforcement. Given that the plastic strain in the

reinforcement is maintained during the reversal, it follows that the residual shear strain will have the same magnitude but opposite direction at the end of the reversal, i.e., the shear strain associated with the cracks goes from $+\gamma_{xy,plastic}$ to $-\gamma_{xy,plastic}$. Assuming this occurs at the same rate as the closing of the cracks, the crack closing function presented in Chapter 3 (Eq. 3.14) can be used to characterize the shear strain reversal. Using Eq. 3.14 to define a function which varies from +1 to −1 and applying it to the residual shear strain,

$$\gamma_{xy,crack} = \gamma_{xy,plastic}\left[2\exp\left(\frac{2v_{xy}}{\sin 2\theta_{c\sigma} - 0.4v_{xy}}\right) - 1\right] \tag{6.31}$$

where $\gamma_{xy,plastic}$ is the residual shear strain at the end of unloading. The total shear strain at any point is the sum of the shear strain from Eq. 6.31 and the elastic shear strain due to the increasing shear stress:

$$\gamma_{xy} = \gamma_{xy,concrete} + \gamma_{xy,crack} \tag{6.32}$$

where $\gamma_{xy,concrete} = v_{xy}/G_{cr}$.

Equations 6.31 and 6.32 provide a model for the hysteresis loops which is defined in terms of shear stress and shear strain. Indirectly, this simple model has the same rational basis as the general model presented in Chapter 3: the stiffness decay is due to the accumulation of plastic strain in the *y* reinforcement and pinching of the loops is a function of the crack closing and of the plastic strain in the *y* reinforcement. Unlike empirical models, these effects are captured automatically, without the need for coefficients provided by the analyst.

6.8 PARAMETRIC STUDY USING THE YIELD POINT EQUATIONS

The influence of the various parameters on the shear stress at yield, the shear strain at yield, and the cracked section shear stiffness is examined with a parametric study. The study is based mostly on the general equations, Eqs. 6.9 and 6.13, with the approximation $\theta_k = \theta_{c\sigma}$ (Eqs. 6.10, 6.14) examined at the end. The parametric study does not include the failure checks.

For all cases, f_{yy} = 400 MPa is assumed. Unless noted otherwise, $f_c' \approx$ 40 MPa, f_{cr} = 2.1 MPa, E_c = 29,850 MPa, n=6.7, and $G_{gr} \approx$ 12,000 MPa (0.4E_c). Pure shear loading and zero concrete tension are assumed ($n_x = n_y = 0$ and $\sigma_{cl} = 0$). The crack angle, θ_k, is perpendicular to the principal direction of the applied tension at cracking. The concrete stress angle $\theta_{c\sigma}$ is calculated from Eq. 3.19.

The results of the parametric study are summarized in Table 6.1 and in Figs. 6.5 to 6.14.

6.9 COMPARISON WITH EXPERIMENTAL DATA

The simplified equations (Eqs. 6.10 and 6.14) are used to estimate the shear stress at yield, the shear strain at yield and the cracked section shear stiffness. The section properties used in the equations and the calculated values are summarized in Tables 6.2 and 6.3.

Yield Point

In Fig 6.15, the predicted yield points are compared to the graphically determined yield points (Appendix B.4). This effectively compares the bi-linear envelope model to an equivalent experimental bi-linear response.

For the LVDT instrumented specimens, all three predicted values, shear stress at yield (Fig. 6.15a), shear strain at yield (Fig. 6.15b) and cracked section shear stiffness (Fig. 6.15c) are within 15% of the experimental values. The Vecchio-Collins specimens show somewhat more scatter. Given the simplicity of the approach, the predictions are quite good.

Envelope Model

In Figs 6.16 to 6.18, the simple bi–linear and tri-linear envelope models are compared to the experimental shear response for the seven LVDT instrumented specimens. The input parameters are f_c', ρ_x, ρ_y, and $\theta_{c\sigma}$ (see Chapter 5, Tables 5.1 and 5.2). As in Chapter 5, experimental values for the cracking stress σ_{cr} are used (see Table 5.3). For the reverse-cyclic specimens, the envelope is applied to the positive-shear side only.

For SE8 (Fig. 6.16a), the envelope models provide a very good prediction of the overall response.

Table 6.1 Parametric study using the yield point equations

Parameter examined	Figure	Comments
reinforcement ratios, ρ_x and ρ_y	6.5	• shear stress and shear strain increase linearly with *y* reinforcement ratio
ratio of reinforcement, ρ_x/ρ_y	6.6	• shear stress, shear strain, and shear stiffness are a maximum when $\rho_x/\rho_y = 1.0$ • all three decrease rapidly as the relative ratio increases to about 3
modular ratio, *n*	6.7	• shear stress at yield is essentially independent of *n* • shear strain at yield increases linearly with *n* • shear stiffness reduces almost linearly with increasing *n;* the reduction is more significant for greater amounts of reinforcement
axial loads, n_x and n_y [1]	6.8	• shear stress at yield is more sensitive to tension in the *y* direction than in the *x* direction • shear stress at yield can be significantly increased by compression in the *y* direction • influence of n_x appears independent of n_y
residual concrete tension, σ_{cn}	6.9	• shear stress at yield and shear stiffness increase with increasing residual tension • shear strain increases slightly with increasing tension: the decrease in strain due to tension in the concrete is offset by the increase in shear stress at yield
crack angle, θ_k: $\theta_k = 45°$ is exact angle for $\rho_x/\rho_y = 1, \theta_{c\sigma} = 45°$ for $\rho_x/\rho_y = 3, \theta_{c\sigma} = 38°$	6.10	• shear stress and shear strain at yield are a minimum at $\theta_k = \theta_{c\sigma}$ and are not sensitive to a crack angle within $\pm 10°$ of $\theta_{c\sigma}$ • shear stiffness is essentially independent of θ_k
stress angle, $\theta_{c\sigma}$ [2]	6.11	• for $\rho_x/\rho_y = 1$, shear stiffness is independent of $\theta_{c\sigma}$ • for $\rho_x/\rho_y > 1$, stiffness reduces linearly as $\theta_{c\sigma}$ increases
simplifying approximation, $\theta_k = \theta_{c\sigma}$ [3]	6.12 - 6.14[4]	• simplified equations conservative for shear stress • simplified equations diverge only at low amounts of *y* reinforcement

[1] The case of bi-axial compression and equal reinforcement is not shown because it increases the shear stress at yield too much relative to the other curves, and may prevent yielding altogether
[2] For each ratio of reinforcement, adjusted angle is from Eq. 3.19 and base angle is from Eq. 3.17
[3] Compares the general equations (Eqs. 6.9 and 6.13) with the simplified equations (Eqs. 6.10 and 6.14); the simplified equations are exact for $\rho_x = \rho_y$ ($\theta_{c\sigma} = 45°$) and pure shear loading ($\theta_k = 45°$).
[4] Figure 6.14 compares the equations for different values of n_x with $n_y = 0$; this is representative of walls supporting vertical gravity loads where horizontal loads tend to be negligible.

For PP1 (Fig. 6.16b), as expected the model under-estimates the shear stress after yielding.

For SE9 (Fig. 6.17a), the reinforcement is predicted to yield simultaneously in both direction, causing failure before any post-yield response occurs.

For SE10 (Fig. 6.17b), the model predicts a compression failure almost immediately after yielding (for this case, the compression failure criteria may be overly conservative).

For the PDV specimens (Fig. 6.18), the model gives a reasonable representation of the response and the failure is conservatively predicted.

Reverse-cyclic Model

The simplified hysteretic model (Eq. 6.32) is applied to SE8 (Fig. 6.19a) and to SE10 (Fig. 6.19b). For SE10, the compression failure check is ignored to allow yield cycles to occur. The figures show this simple model, derived from rational fundamentals, is able to capture the important characteristics of the reverse-cyclic response.

Table 6.2 Yield Point Parameters, LVDT specimens

	ρ_x (%)	ρ_y (%)	f_{yy} (MPa)	n_x, n_y (MPa)	n Eq. 6.21	$\theta_{c\sigma}$ (deg.)	σ_{cn} (MPa)	$v_{xy,yld}$ (MPa) Eq. 6.10	$\gamma_{xy,yld}$ ($x10^{-3}$) Eq. 6.14	G_{cr} (MPa)
SE8	2.94	0.98	479	0	12.6	40.06	0.00	5.58	4.78	1166
SE9	2.94	2.94	422	0	13.8	45.00	0.00	11.05	6.79	1625
SE10	2.94	0.98	479	-2.56	13.5	41.59	0.00	8.47	5.82	1453
PP1	1.95	0.65	480	0	14.5	39.89	0.00	3.73	4.46	836
PDV1	1.82	0.91	282	-2.46	13.1	42.73	0.55	5.96	3.76	1584
PDV2	1.82	0.91	282	-2.34	14.2	42.75	0.57	5.93	3.95	1499
PDV3	1.82	0.91	282	-2.68	11.3	42.68	0.71	6.27	3.55	1766

Table 6.3 Yield Point Parameters, PV specimens

specimen*	ρ_x (%)	ρ_y (%)	f_{yy} (MPa)	n_x, n_y (MPa)	n Eq. 6.21	$\theta_{c\sigma}$ (deg.)	σ_{cn} (MPa)	$v_{xy,yld}$ (MPa) Eq. 6.10	$\gamma_{xy,yld}$ ($x10^{-3}$) Eq. 6.14	G_{cr} (MPa)
PV4	1.056	1.056	242	0	12.7	45.00	0.40	2.96	3.11	949
PV6	1.785	1.785	266	0	13.2	45.00	0.32	5.07	3.95	1281
PV10	1.785	0.999	276	0	20.1	42.18	0.24	3.30	3.59	919
PV11	1.785	1.306	235	0	18.9	43.45	0.29	3.55	3.42	1036
PV12	1.785	0.446	269	0	15.9	39.12	0.31	1.86	2.31	803
PV16	0.74	0.74	255	0	14.0	45.00	0.19	2.07	3.10	669
PV18	1.785	0.315	412	0	15.2	38.46	0.17	1.84	2.84	648
PV19	1.785	0.713	299	0	15.8	40.64	0.26	2.79	3.11	896
PV20	1.785	0.885	297	0	16.1	41.56	0.26	3.25	3.41	953
PV21	1.785	1.296	302	0	17.7	43.38	0.22	4.37	4.24	1029
PV29	1.785	0.885	324	0	15.4	41.53	0.23	3.50	3.66	953

*specimens which failed in concrete compression before yielding have been omitted

7

Conclusions

The fundamental mechanisms governing the load-deformation response of reinforced concrete membrane elements subjected to seismic (reverse-cyclic) shear identified in this research are summarized below. The important concepts used in the rational model developed to capture these mechanisms are reviewed and compared with existing models. Conclusions from the development of simplified models are also presented in this Chapter.

7.1 FUNDAMENTAL MECHANISMS OF THE REVERSE-CYCLIC SHEAR RESPONSE

The shear response of reinforced concrete is the end result of complex interactions between the reinforcement and the concrete. To investigate these interactions, experimental data was examined in detail, focussing on the relationships between various stress and strain components. From this investigation, important relationships emerged: these were presented in Chapter 2. Developing a rational model to capture these relationships led to an understanding of the fundamental mechanisms governing the reverse-cyclic shear response.

Shear deformation occurs primarily at the cracks: The crack strains are much greater than the concrete strains and are almost equal to the total strains, except in the principal compression direction (Sec. 3.3; Fig. 3.4). This is particularly true after yielding of the reinforcement which results in large deformations at the cracks and large shear deformation of the element. The crack strain in each reinforcement

direction is approximately equal to the reinforcement strain which is equal to the total strain.

Crack strains, and thus the shear strain, are controlled primarily by compatibility with the reinforcement: This is evident in the simultaneous occurrence of yielding in the weak reinforcement, rapidly increasing crack strains and yielding of the element in shear. It is also demonstrated by the linear relationships between the reinforcement strain and the shear strain (Sec. 2.5; Fig. 2.17) and between the crack strains and the shear strain (Sec. 2.6; Fig. 2.22).

Pinching of the hysteresis loops is a function of plastic strain in the reinforcement: At the end of an unloading segment, cracks remain open in proportion to the plastic strain in the reinforcement. As loading is applied in the reverse direction, the previous-direction cracks close and the new-direction cracks open with the sum of the two essentially constant and proportional to the plastic strain in the reinforcement. Since this process occurs at the same applied stress for each cycle, the pinching becomes more pronounced as plastic strain accumulates in the reinforcement and the shear strain must reverse over a greater range. (Sec. 3.1; Fig. 3.1)

Principal angles deviate during the reversal: Before yielding, the principal strain angle follows the principal stress angle closely throughout the cycle (the response is essentially linear elastic). After yielding, when there is plastic strain in the reinforcement, the cracks remain open at the end of unloading. As loading is applied in the new direction, the orientation of the principal stress changes to the new direction, however, the orientation of the principal strain does not fully change direction until the previous-direction cracks close and the new-direction cracks open. As a result, the principal strain angle lags the principal stress angle (Sec. 2.8; Fig. 3.31). This lag is a function of plastic strain in the reinforcement.

Concrete compression softening is largely due to shear slip along the cracks: Shear slip along the cracks results in a compressive strain component in the minimum principal strain (ε_2) direction, which becomes particularly large after the reinforcement yields (Sec. 2.9; Fig. 2.33 and Sec. 3.3; Fig. 3.4). Because of this, the concrete compression response, when measured as the principal concrete compression stress (σ_{c2}) versus the minimum total principal strain (ε_2), appears to soften considerably after yielding. A more appropriate measure of the concrete response is to consider the concrete principal stress versus the concrete-only principal strain (ε_{c2}).

The complex concrete response is due to crack deformations during the load reversal: The concrete response, when measured as a function of the total principal strain (ε_2), includes a region of compressive stress associated with tensile strain – seen as a bulge in the response (Sec. 3.8; Fig. 3.14). During the reversal, when both sets of cracks are open, the total crack strains are greater than the concrete strains, resulting in a tensile minimum principal strain (ε_2).

7.2 RATIONAL MODEL FOR REVERSE-CYCLIC SHEAR

To understand the complex behaviour of reinforced concrete membrane elements subjected to reverse-cyclic shear, a simple model was formulated in terms of average stresses and average strains. In this model, deformations at the cracks are a consequence of deformations in the concrete and in the reinforcement as they maintain strain compatibility and equilibrate the applied loading.

7.2.1 Strain Compatibility

To model the relationships observed in the experimental data, the deformations at the cracks are separated from the deformations in the concrete between the cracks. The corresponding strain compatibility requirement in terms of average strains is:

concrete strains + crack strains = total strains = reinforcement strains

The key to a simple and transparent model formulation is in the definition of the crack and concrete strain components. In particular, it is assumed that the concrete strain normal to the opening cracks is negligible compared to the crack strain normal to the cracks. This leads to a formulation which does not require defining the more complex shear strain at the crack interface.

7.2.2 Constitutive Relationships

Constitutive relationships relate stresses to strains, linking the strain compatibility and equilibrium requirements. The use of these relationships is fundamental to the model formulation. The specific equations, however, are not and therefore the proposed functions presented in Chapter 4 are not repeated here. Important characteristics of the constitutive relationships include:

- a simple bi-linear (bare bar) model is used for the reinforcement; a reinforcement model with gradual yielding is not needed,
- plastic strains in the weak reinforcement are cumulative from one direction of shear to the other,
- the principal concrete stress angle before yielding is calculated from a linear elastic model; an adjustment to compensate for the equal angle assumption is added,
- compression softening of the concrete excludes the strain component due to shear slip along the cracks,
- only the residual concrete tension is specifically included; this is sufficient for reverse-cyclic shear,
- a crack closing function is used to define the rate of crack closing during the reversal,
- concrete shear failures and concrete compression failures are modelled separately using a shear strain limit defined in terms of average stress and a reduced peak compression strength respectively.

7.2.3 Comparison with Existing Models

Existing rational models treat cracked concrete as a single material. The proposed model separates deformations at the cracks from deformations in the concrete. This "cracks plus concrete" approach is the most significant departure from existing "cracked concrete" models. With this approach:

- deformations at the cracks are governed by the reinforcement (through strain compatibility) instead of by the concrete model,
- pinching of the loops is automatically captured by having the reinforcement plastic strains control the crack closing/opening during the reversal,
- principal stress and strain angles can deviate as required to maintain equilibrium and compatibility,
- concrete softening due to shear slip along the cracks is automatically captured, requiring no adjustment of the concrete model,
- the "bulge" in the concrete response is automatically captured, eliminating the need for a complex empirical formulation to describe cracked concrete.

Existing rational models include an explicit measure of shear strain at the crack interface, usually as a local effect. Until now, shear strain at the crack interface has been viewed as a controlling parameter in the shear deformation of reinforced concrete elements. In this Thesis, shear deformation along the cracks is treated as a consequence of other deformations; it occurs as needed to maintain equilibrium and strain compatibility.

This thesis formulates a model entirely in terms of average stresses and strains. It uses a linear elastic solution to determine the concrete stress angle. And it includes a shear strain limit in terms of average strains. These concepts were part of the Compression Field Theory (Collins 1978). They were dropped in the formulation of the Modified Compression Field Theory (Vecchio and Collins 1986) and subsequent models.

7.3 APPLICATION TO DESIGN

The proposed model for reverse-cyclic shear can be used to develop simpler models more easily applied in structural analysis and design of reinforced concrete structures. The more detailed general model provides a rational basis for selecting and verifying simplifications and approximations.

This thesis includes two simplified models: an envelope to the reverse-cyclic response and a shear stress vs shear strain function for the cycling. The following conclusions result from developing these simple models:

- the envelope to the response can be approximated by three points: the shear at first cracking, the shear at yielding of the weak reinforcement and the shear at failure; these three points can be estimated from the section properties,
- assuming rotating cracks is a valid simplification for a wide range of section properties,
- with appropriate assumptions, the reverse-cyclic loops can be defined by a simple function of shear stress, shear strain, and residual (plastic) shear strain,
- with a shear strain limit defined, shear ductility can be explicitly considered,
- the cracked section shear stiffness can be determined from the section properties
- a modified linear stress-strain relationship for the concrete in compression can improve the estimated shear strains and can include the effect of compression softening.

A parametric study of the shear stress at yield, the shear strain at yield, and the cracked section shear stiffness determined that, for the elements studied:

- shear stress at yield is independent of the concrete strength,

- shear stress at yield is more sensitive to axial load in the weak reinforcement direction than axial load in the strong reinforcement direction,
- assuming a rotating crack angle results in a conservative estimate of the shear stress at yield,
- shear strain at yield reduces linearly with increasing concrete strength,
- cracked section shear stiffness is independent of the crack angle.

7.4 RECOMMENDATIONS FOR FURTHER RESEARCH

7.4.1 Experimental Research

Additional experimental data would be beneficial to verify or better define the constitutive relationships presented here. Data is particularly needed from specimens with:

- low reinforcement ratios typical of walls, e.g., $\rho = 0.25\%$,
- crack orientations other than $\pm 45°$, e.g., non-orthogonal cracks can result from a combination of shear and constant axial compression in only one direction, similar to a wall with vertical dead load and in-plane shear,
- reverse-cyclic shear combined with axial loading other than bi-axial compression, such as, compression on one face and tension on the other, bi-axial tension, or reversing axial loads.

7.4.2 Analytical Research

The following additional analytical research is recommended:

The proposed model for shear should be combined with a model for flexure. The resulting model would be able to predict the load-deformation response of beams and columns in addition to membrane elements. Since the proposed model for shear assumes uniform stresses and strains, the combined shear-flexure model would be suitable for regions of beams and columns where this assumption is valid, typically regions away from discontinuities in geometry or loading (B-regions). Vecchio and Collins successfully extended the Modified Compression Field Theory from

membrane elements (Vecchio and Collins 1982) to beams and columns (Vecchio and Collins 1986). Their approach may provide some useful guidance.

The shear-flexure model for B-regions should then be extended to the regions around discontinuities (D-regions). At discontinuities in loading (e.g., under a point load) or in geometry (e.g., fixed-end support), cracks due to shear tend to form a "fan"; they radiate from one point, each at a different angle. The author believes the fundamental concepts developed in this research are sufficiently general and rational to be applied to D-regions. This will require some means to account for the variation of stress, strain and crack orientation at each section. For example, it may be possible to integrate the response from the proposed model over a range of principal stress angles to find the average response at each section.

Figures

Figure 1.1 Shear failures in reinforced concrete structures during recent earthquakes: Northridge, 1994 (a, f, g) and Kobe, 1995 (b, c, d, e)

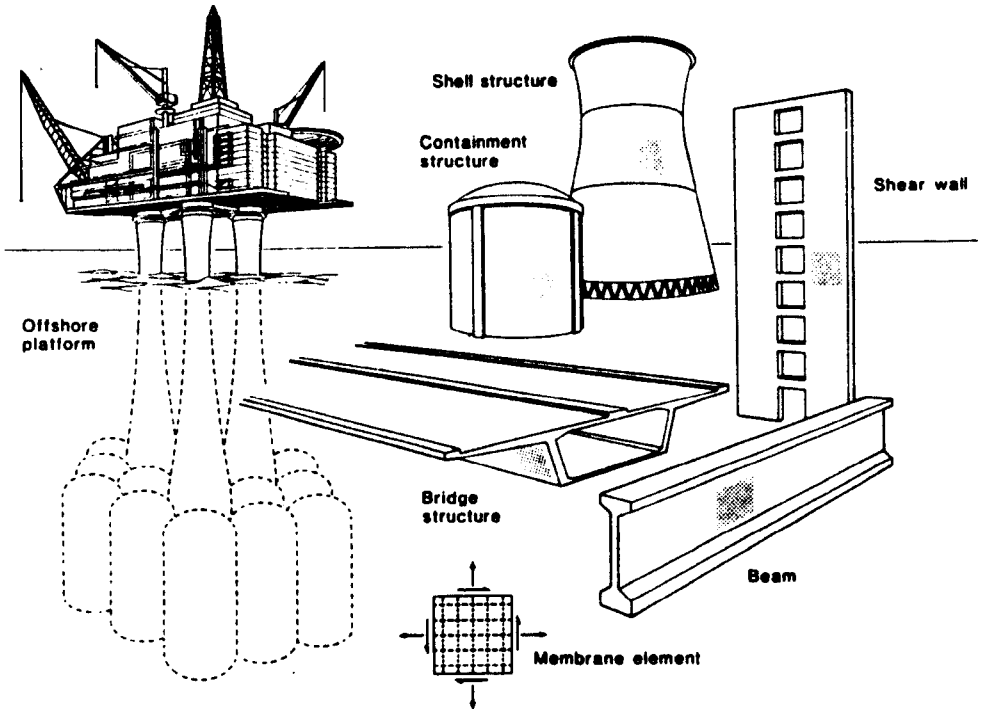

Figure 1.2 Structures idealized as an assemblage of membrane elements (from Vecchio and Collins, 1986)

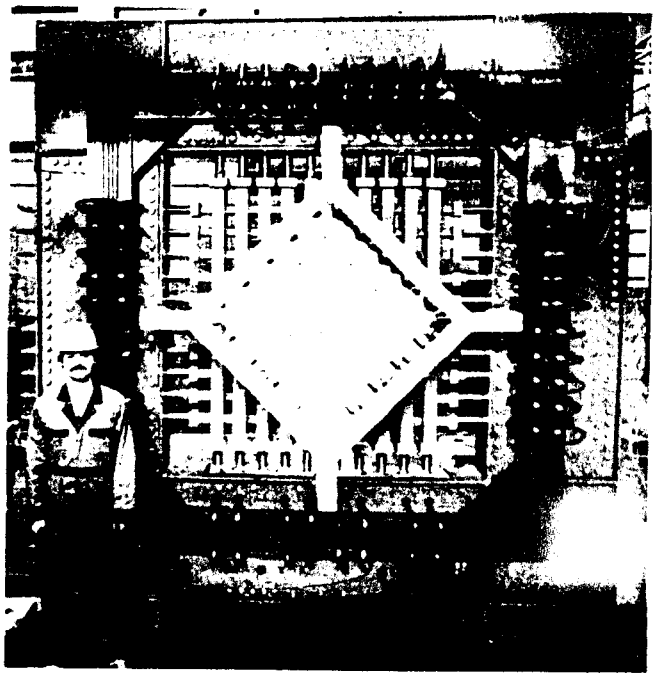

Figure 1.3 The University of Toronto Panel Element Tester (From Vecchio and Collins, 1986)

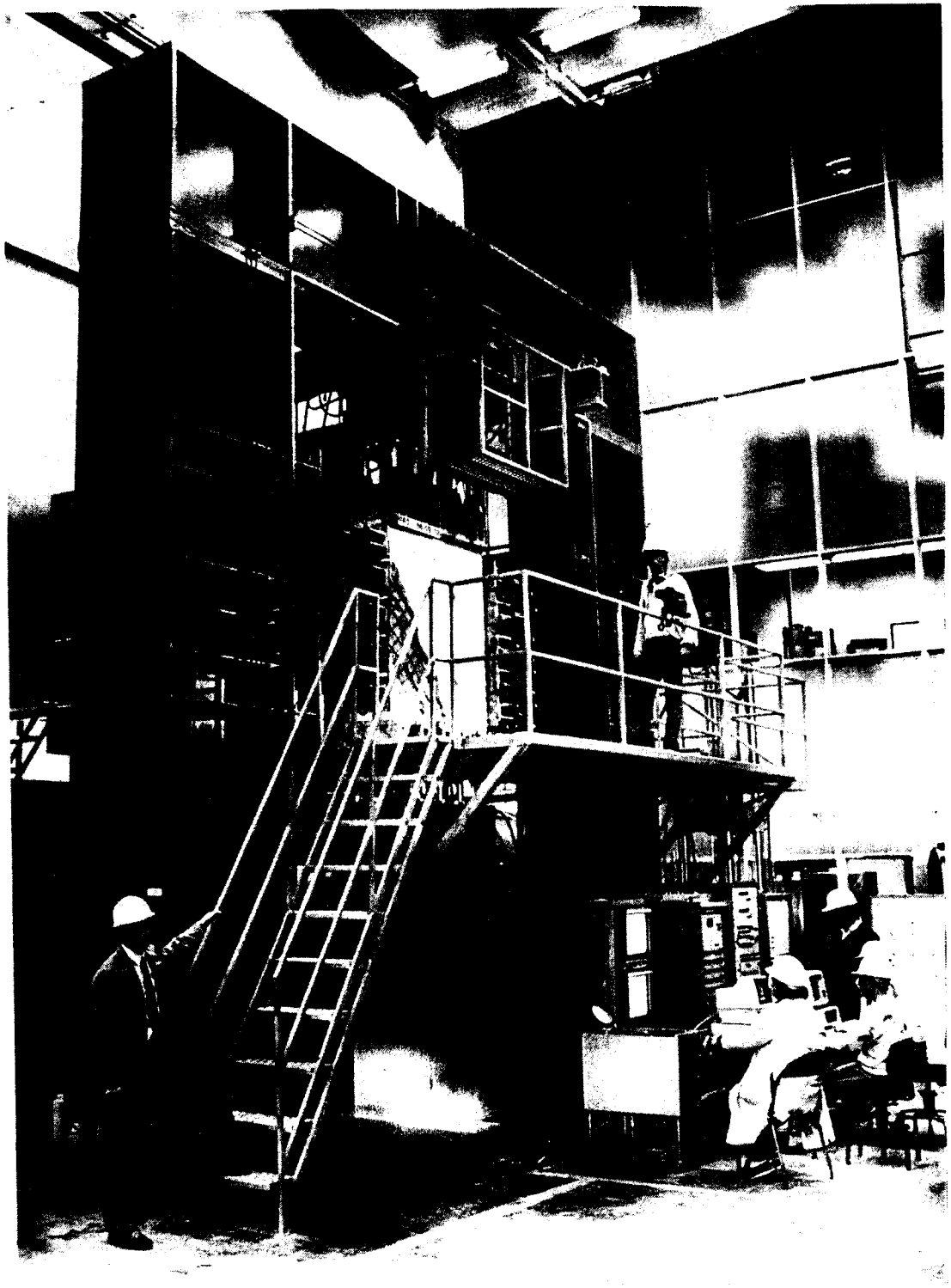

Figure 1.4 The University of Toronto Shell Element Tester (From Meyboom, 1987)

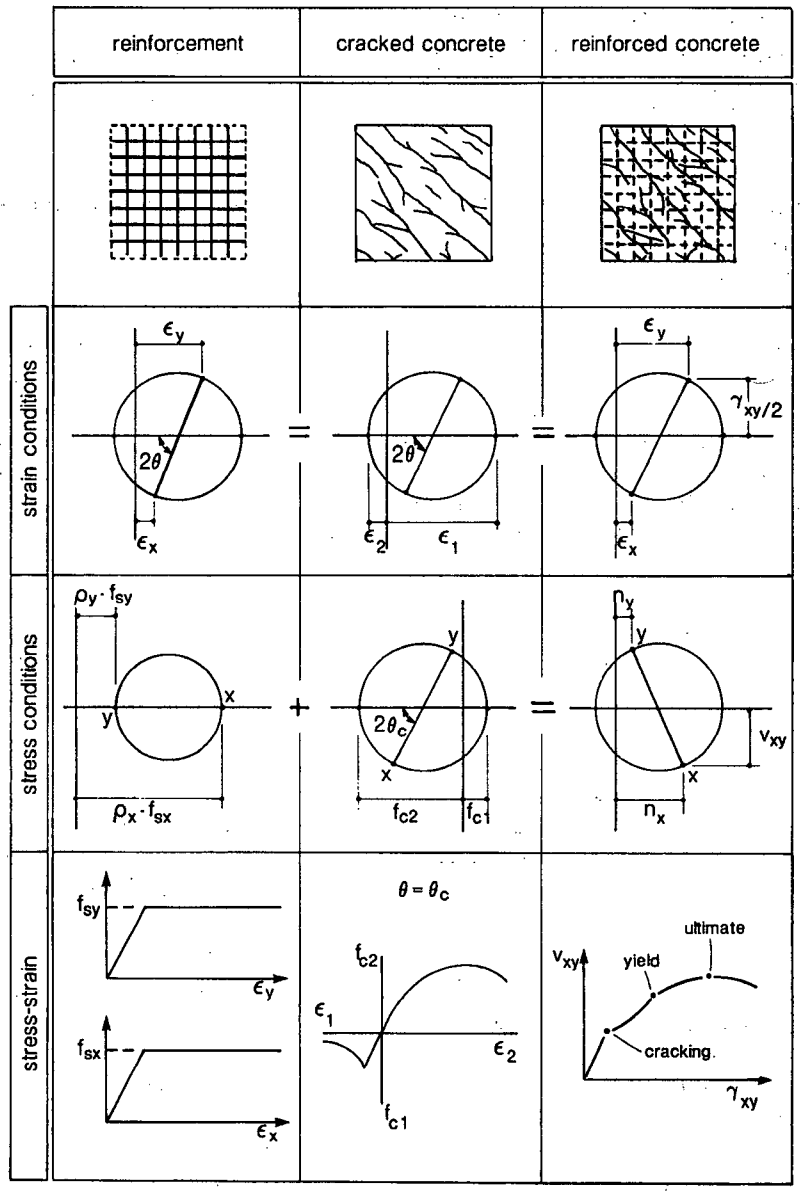

Figure 1.5 Summary of the Modified Compression Field Theory (from Collins and Mitchell, 1991)

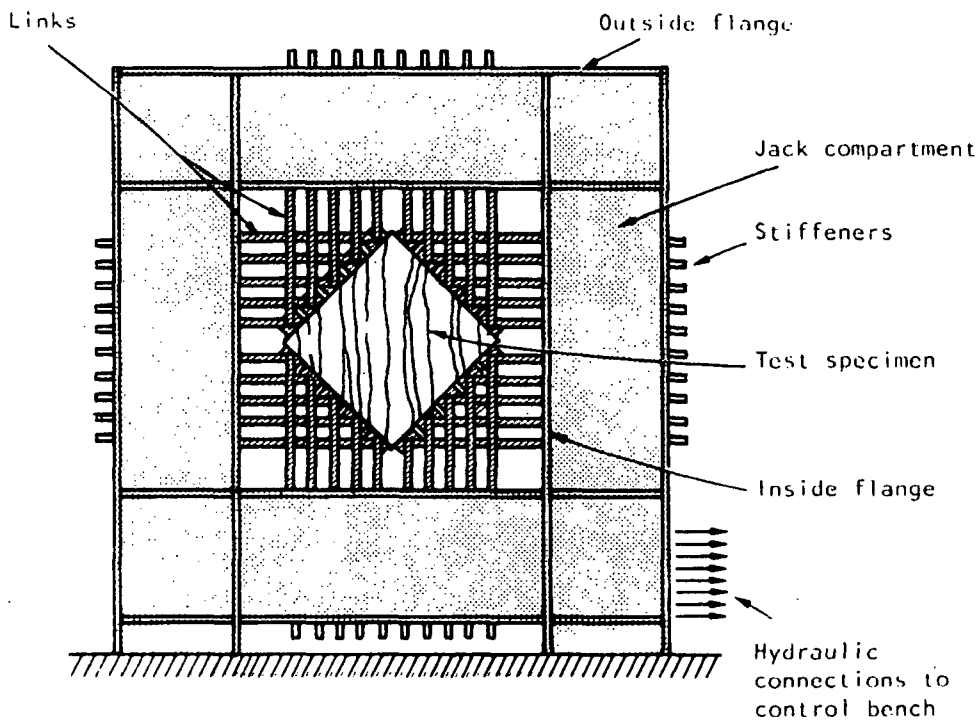

Figure 2.1 The University of Toronto Panel Element Tester - diagram (From Vecchio and Collins, 1982)

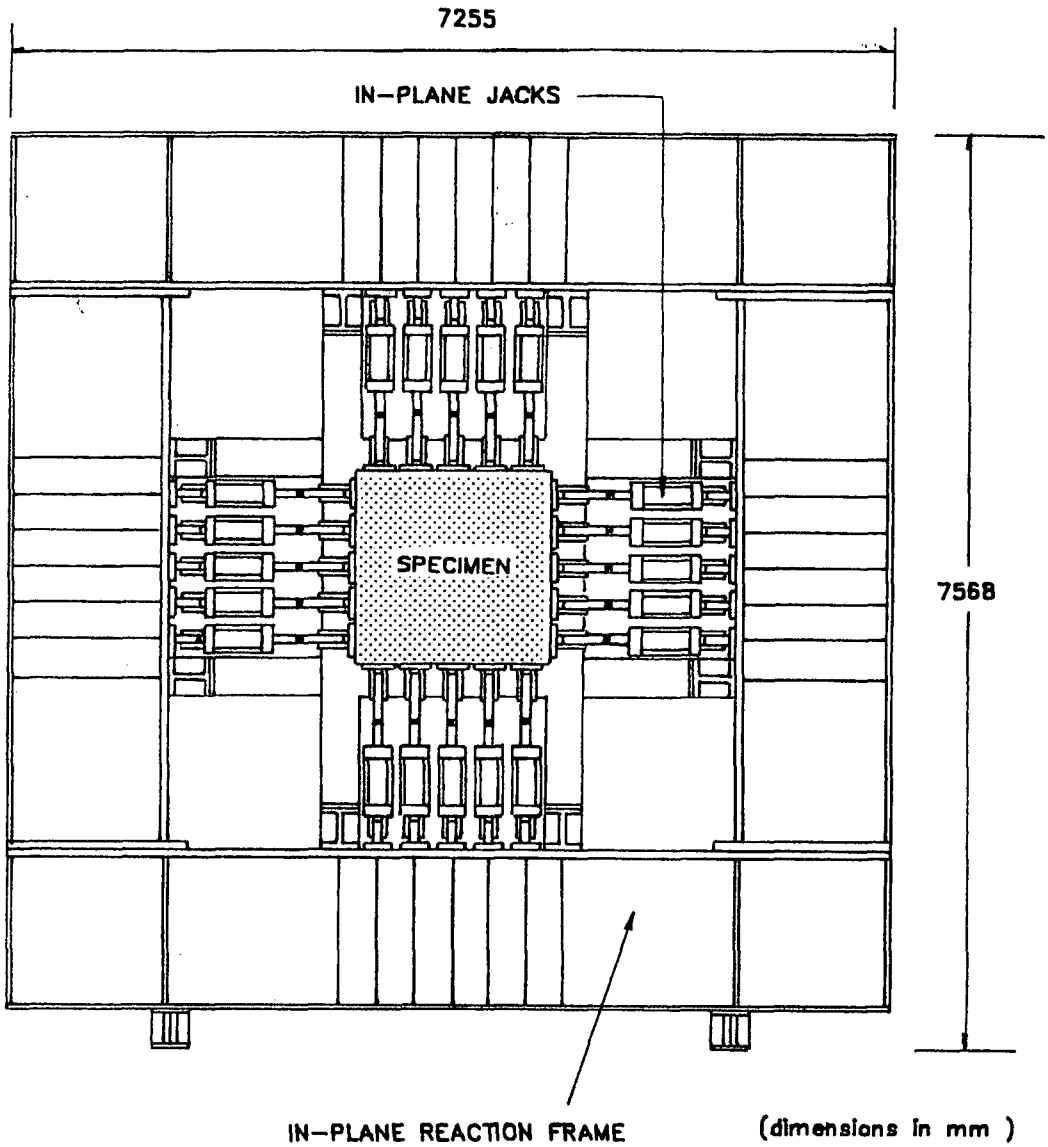

Figure 2.2 The University of Toronto Shell Element Tester - diagram (From Meyboom, 1987)

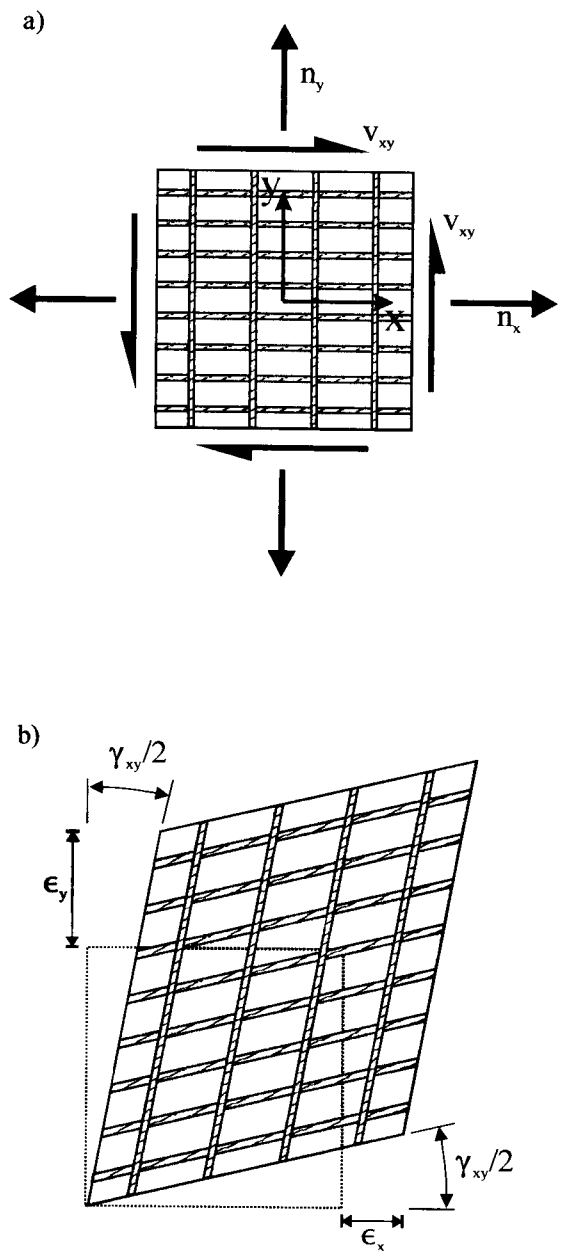

Figure 2.3 Membrane element: a) applied stresses, b) resulting strains

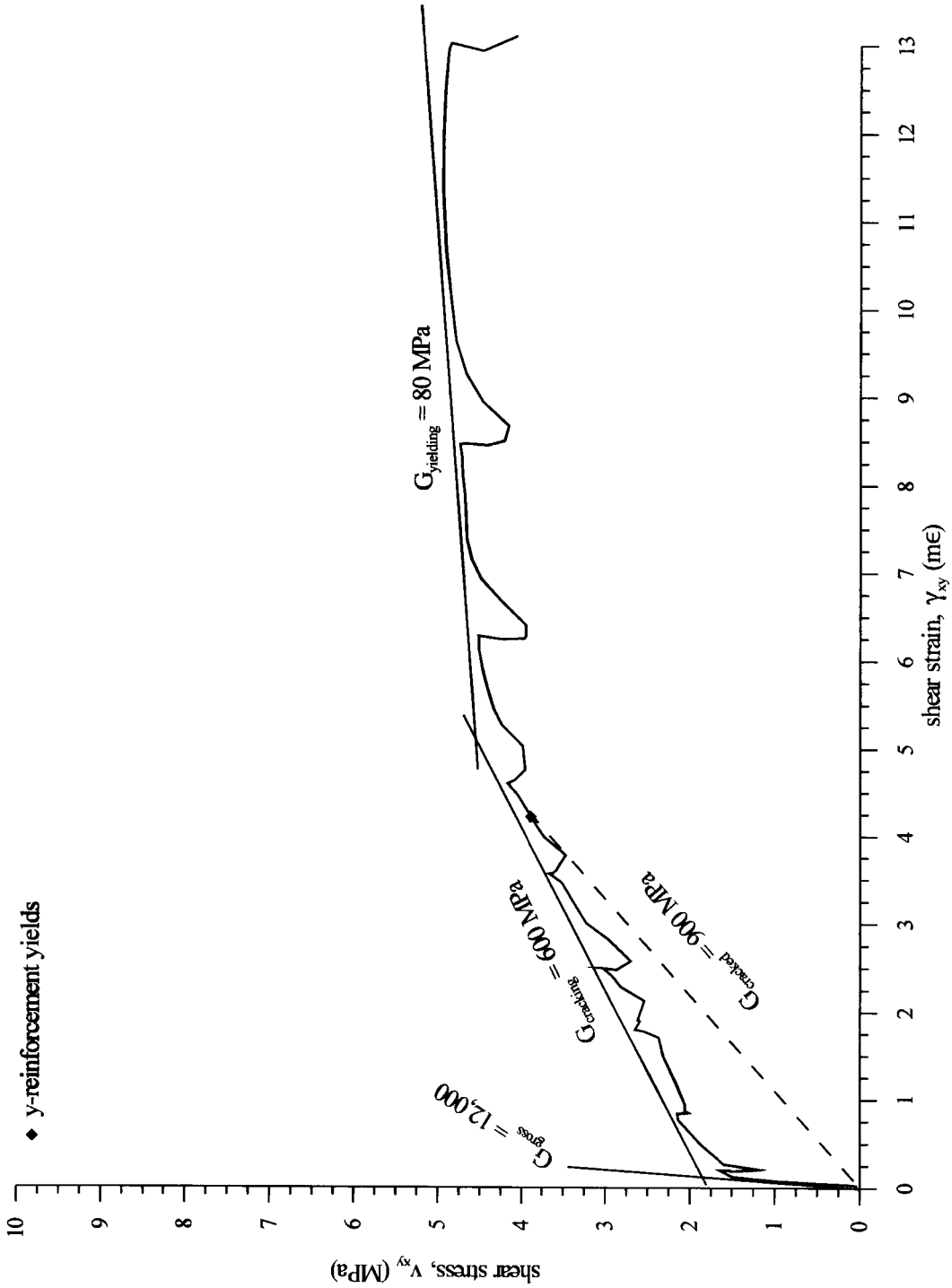

Figure 2.4 Shear stress vs shear strain: PP1

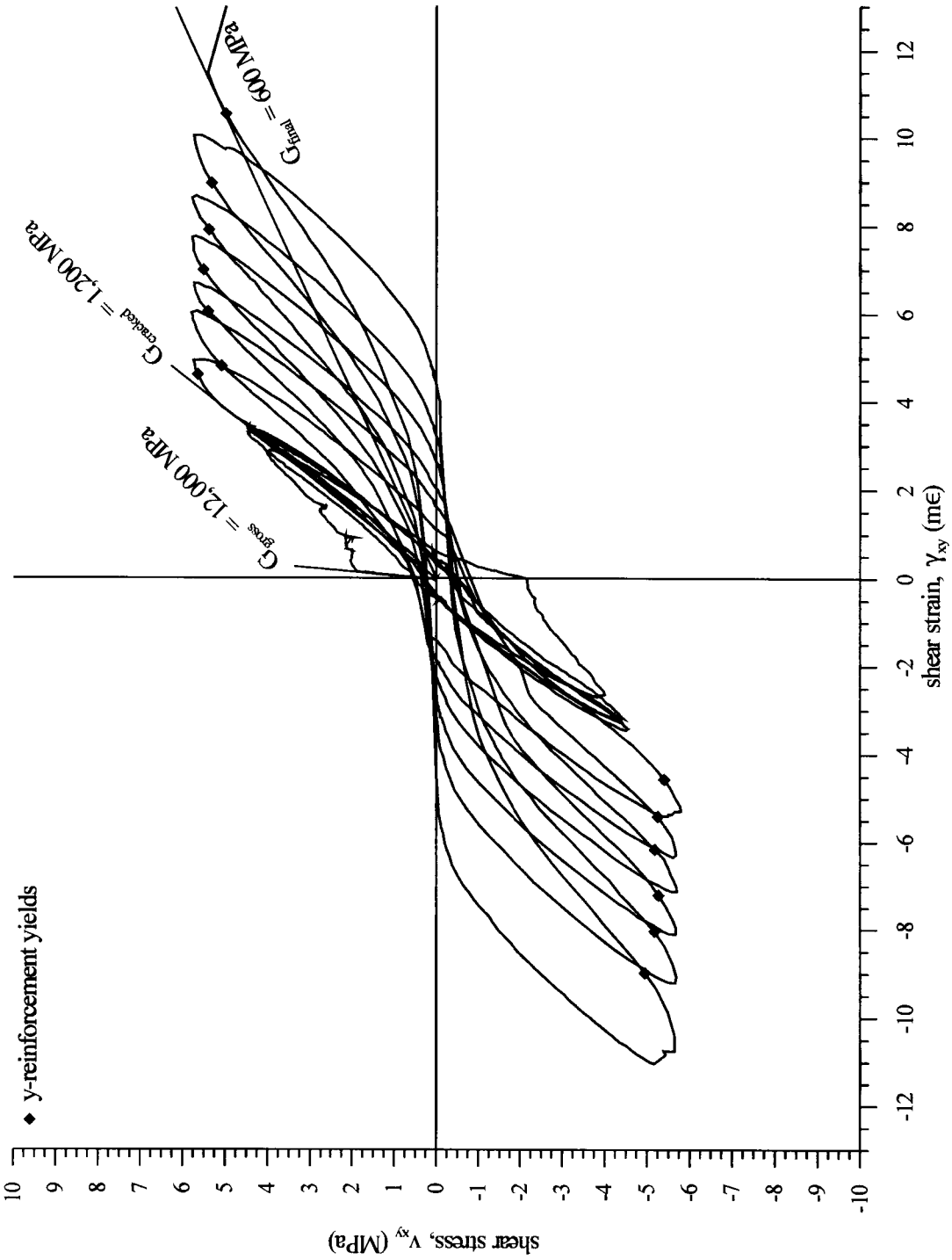

Figure 2.5 Shear stress vs shear strain: SE8

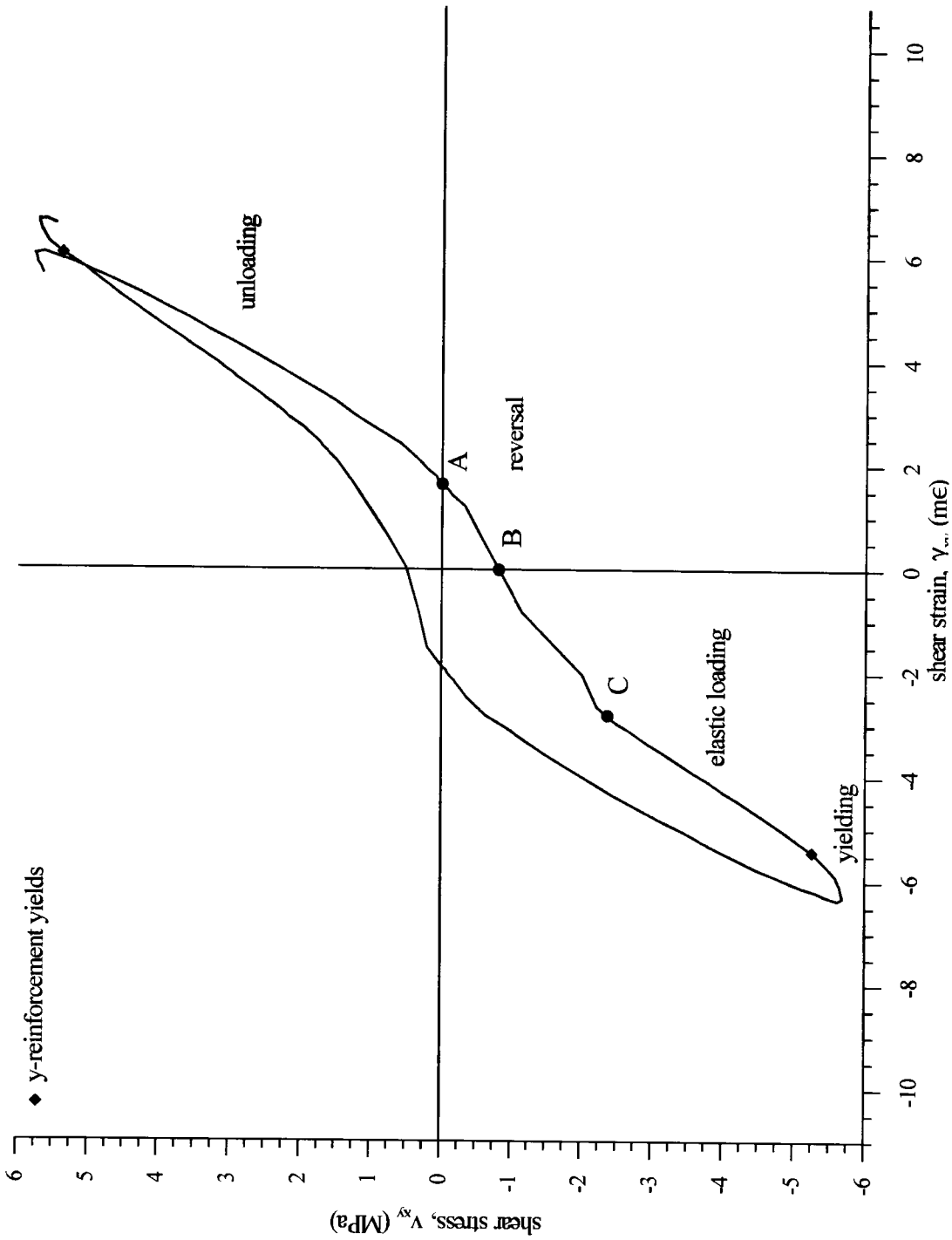

Figure 2.6 Shear stress vs shear strain: single cycle of SE8

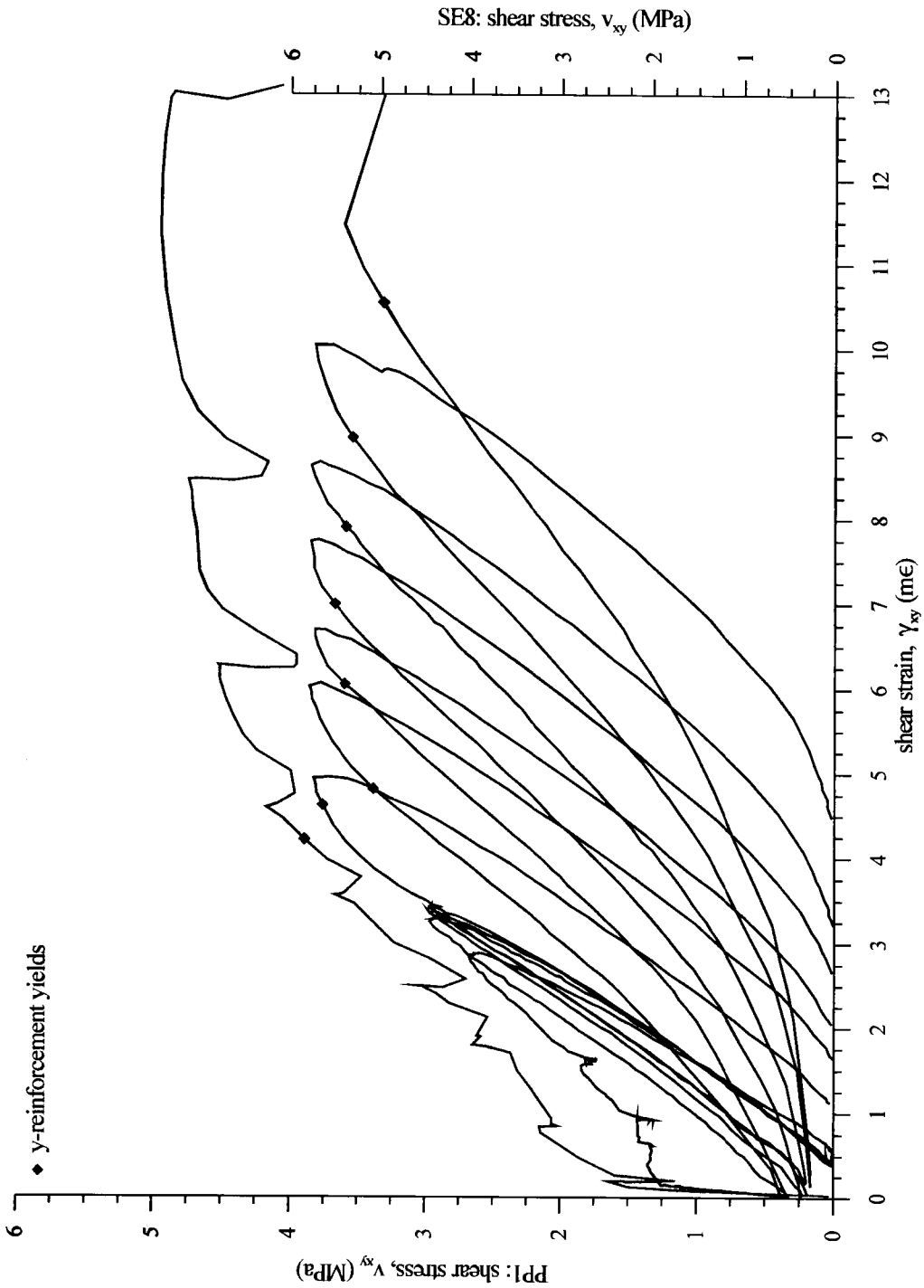

Figure 2.7 Shear stress vs shear strain: monotonic (PP1) vs reverse-cyclic (SE8) (shear stress for PP1 scaled by 1.5)

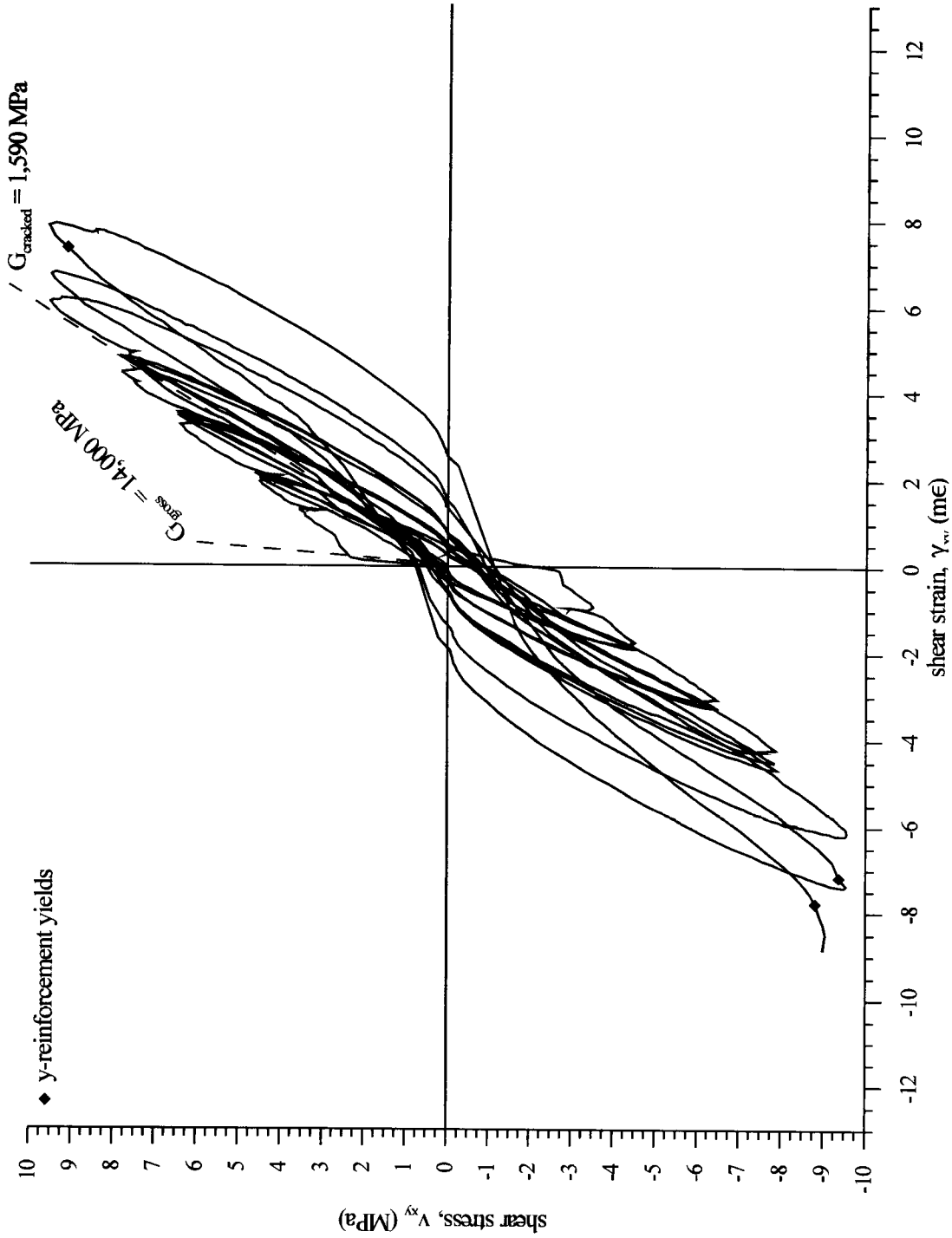

Figure 2.8 Shear stress vs shear strain: SE9

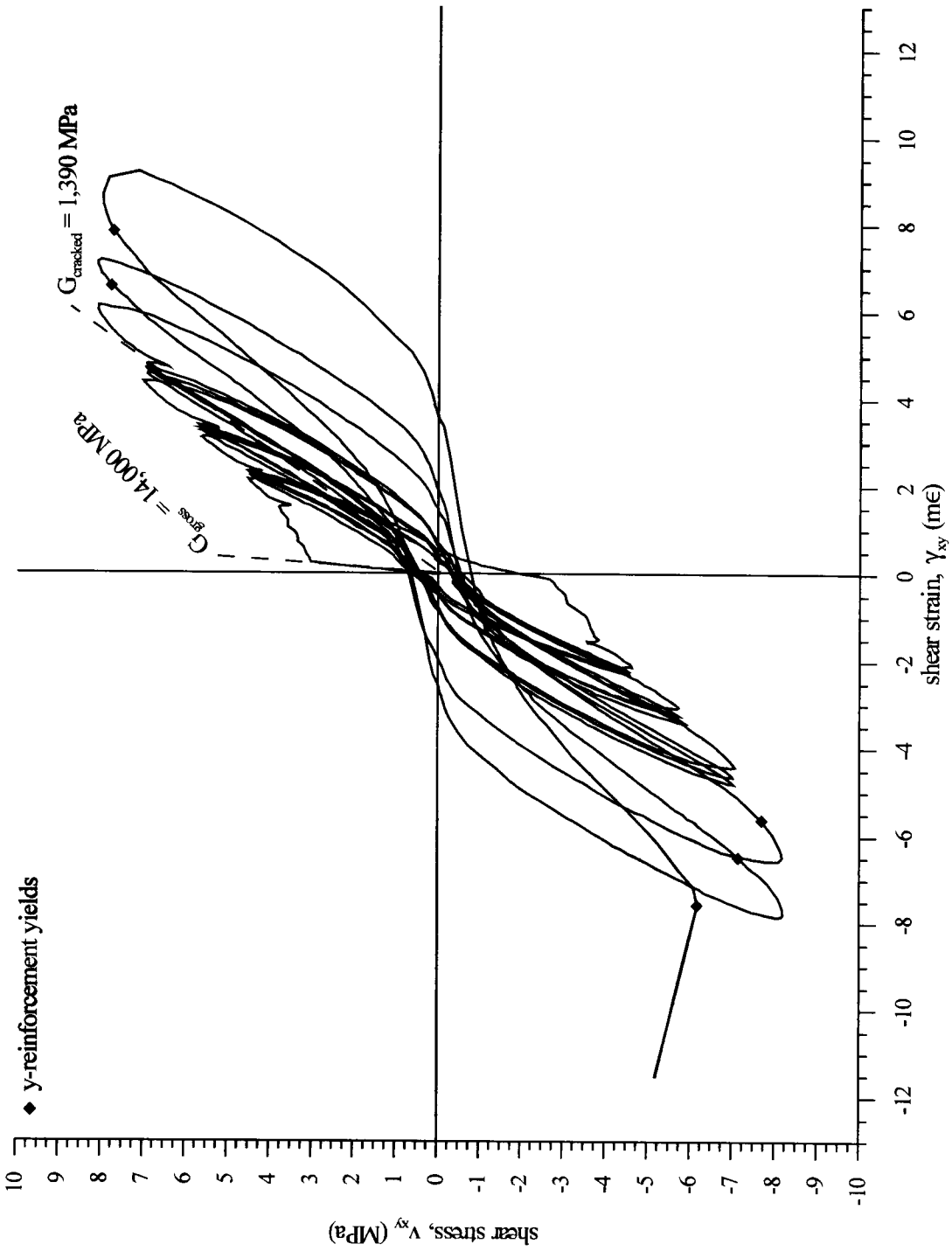

Figure 2.9 Shear stress vs shear strain: SE10

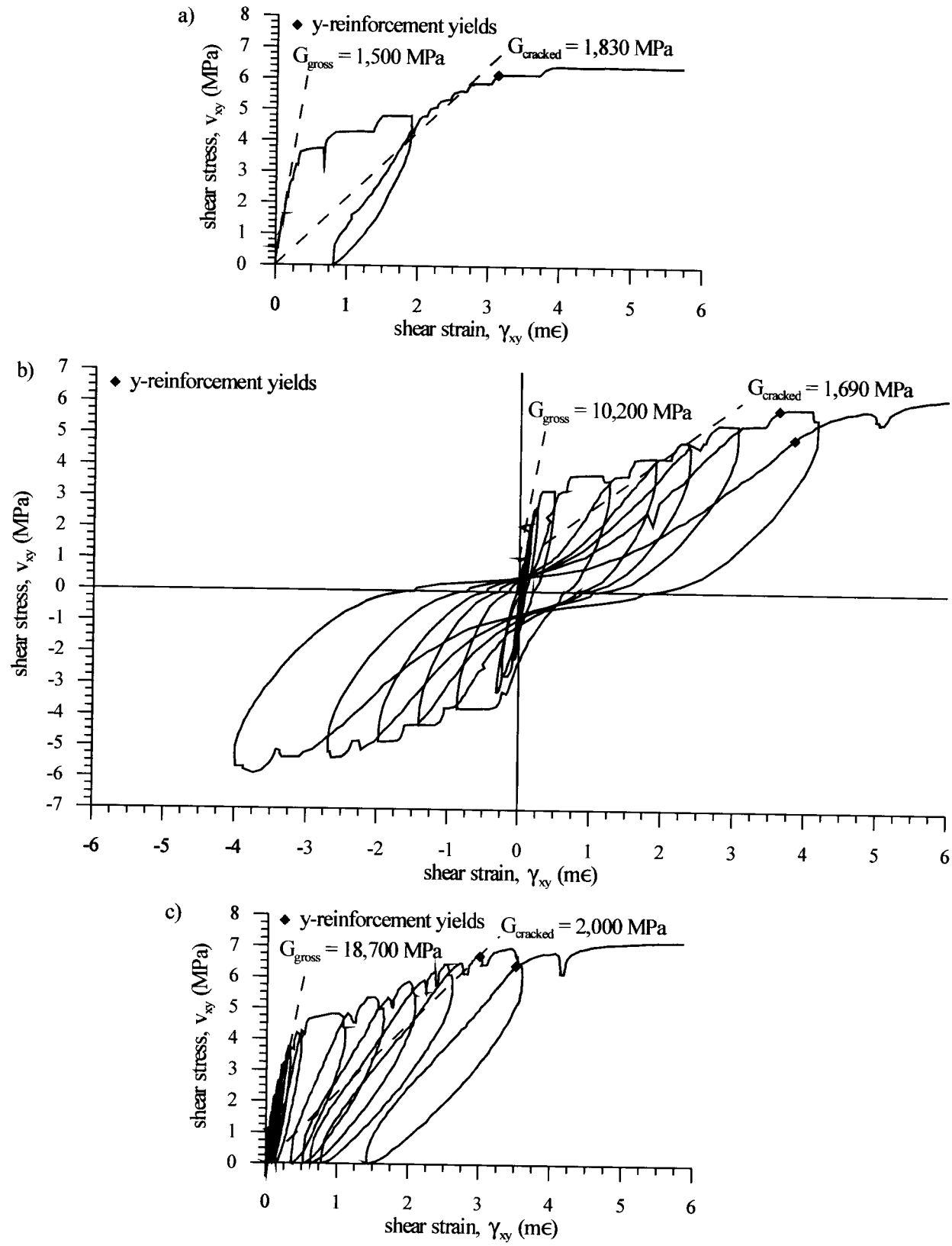

Figure 2.10 Shear stress vs shear strain: a) PDV1, b) PDV2, c) PDV3

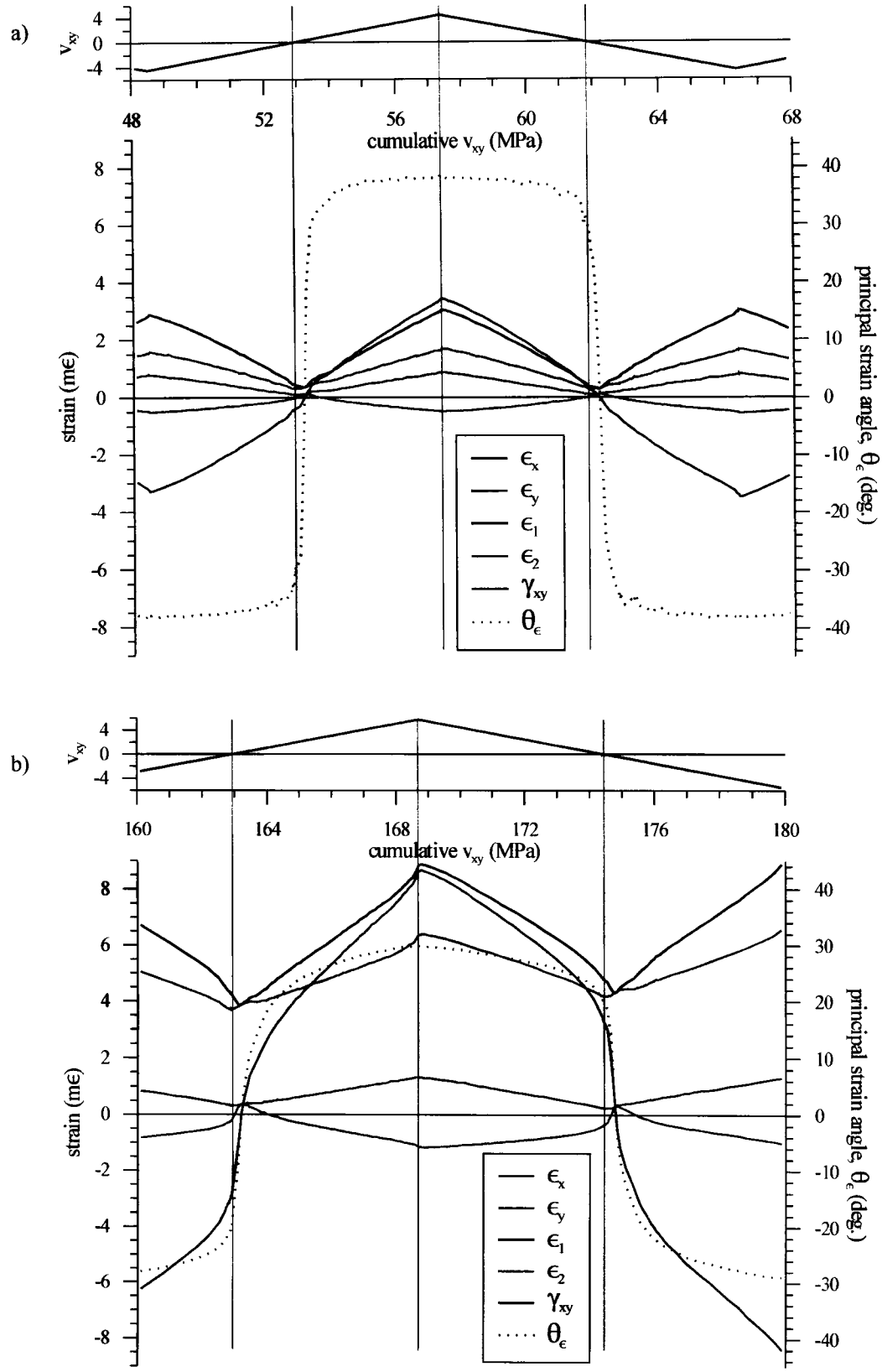

Figure 2.11 Measured strains, SE8: a) elastic cycle, b) plastic cycle

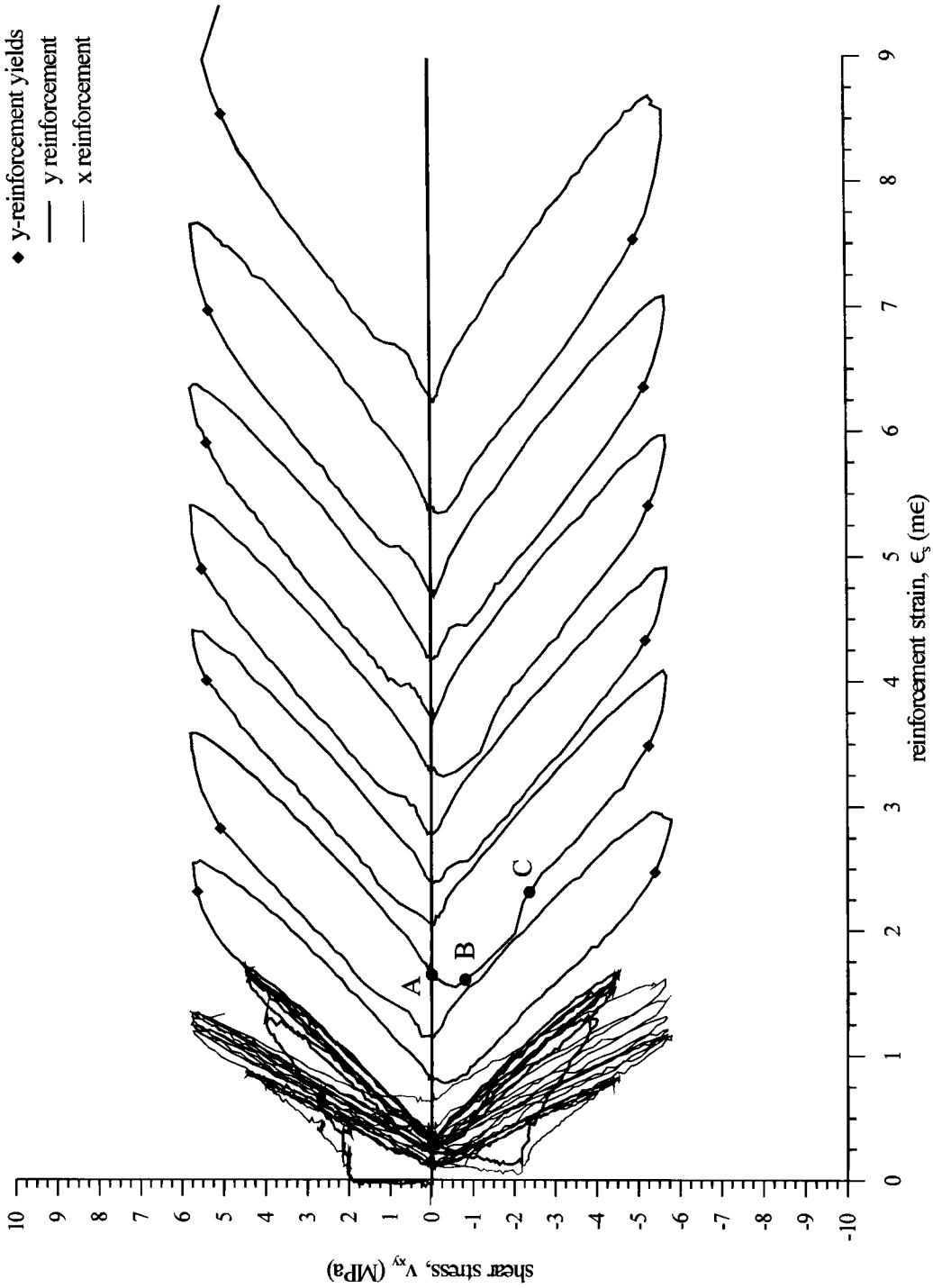

Figure 2.12 Shear stress vs reinforcement strain: SE8

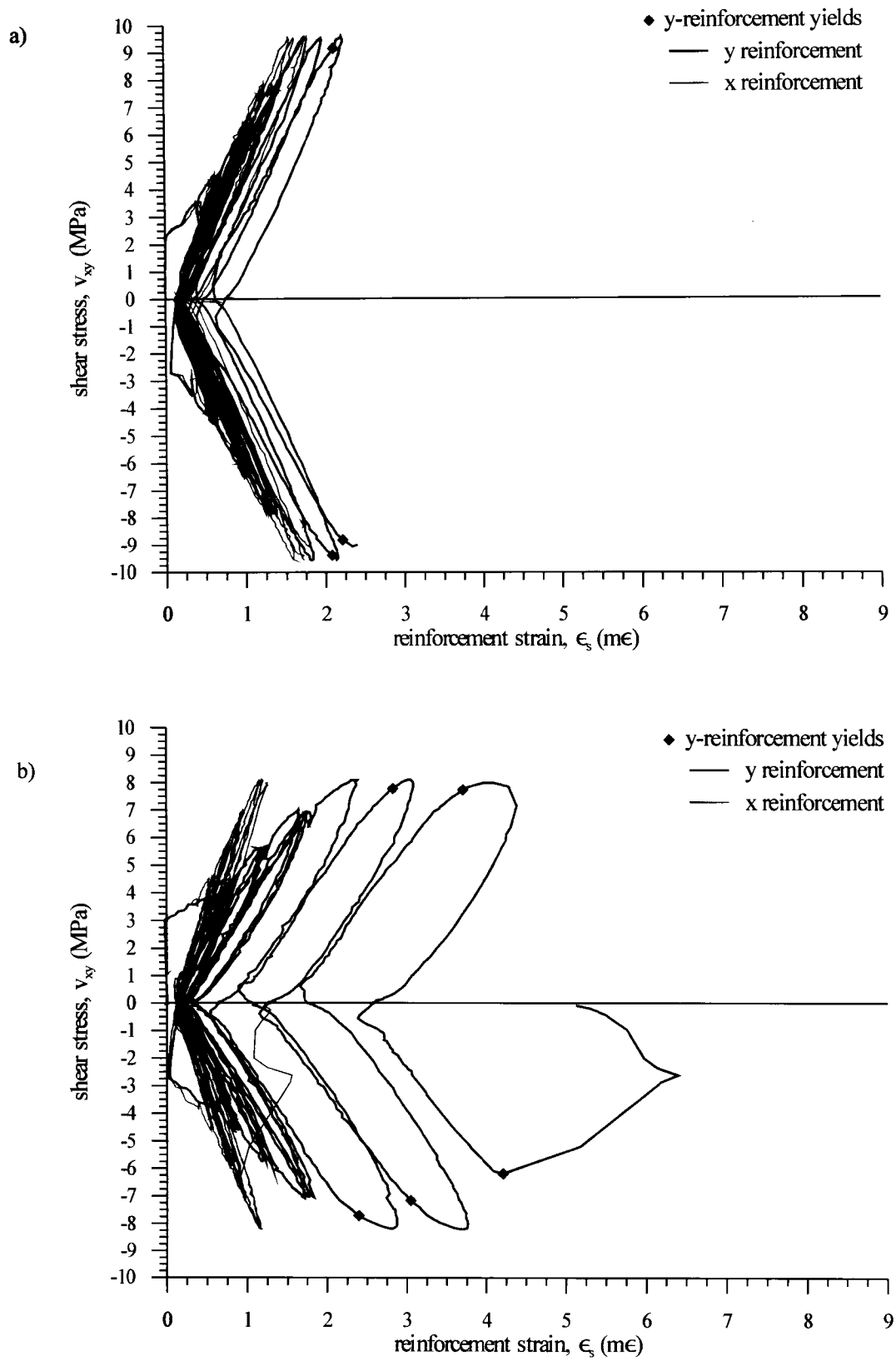

Figure 2.13 Shear stress vs reinforcement strain: a) SE9, b) SE10

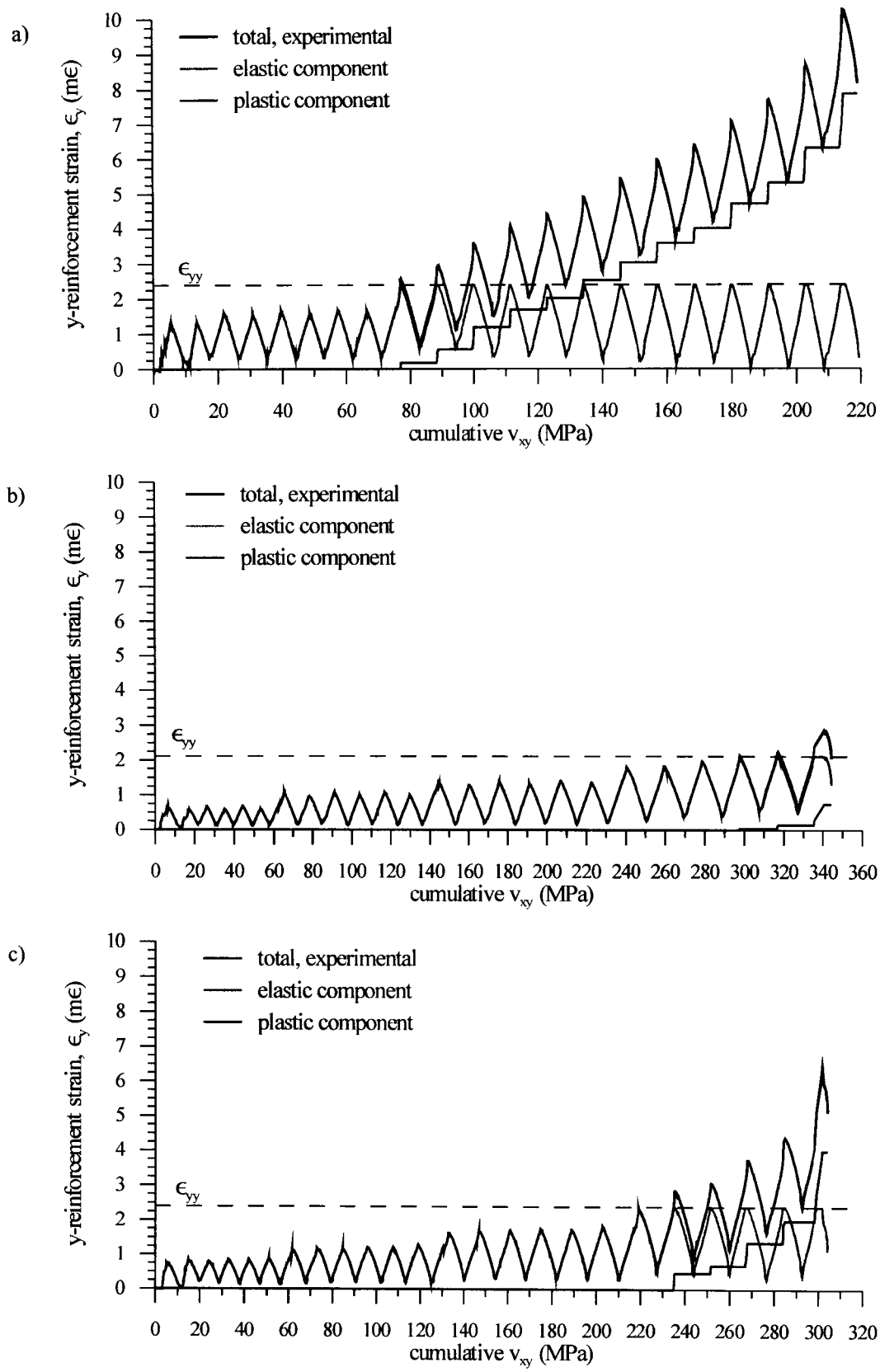

Figure 2.14 Elastic and plastic reinforcement strains: a) SE8, b) SE9, c) SE10

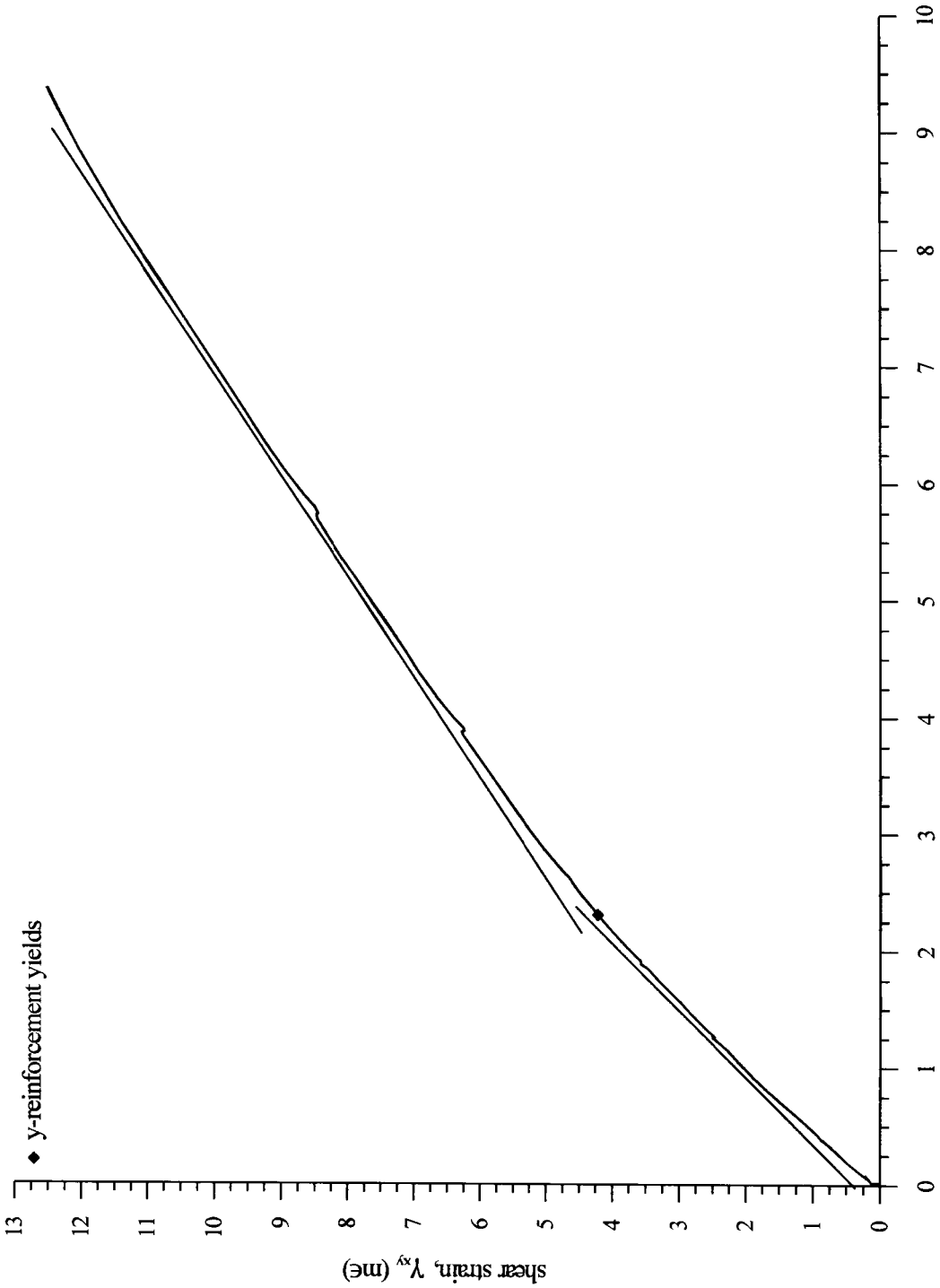

Figure 2.15 Shear strain vs reinforcement strain: PP1

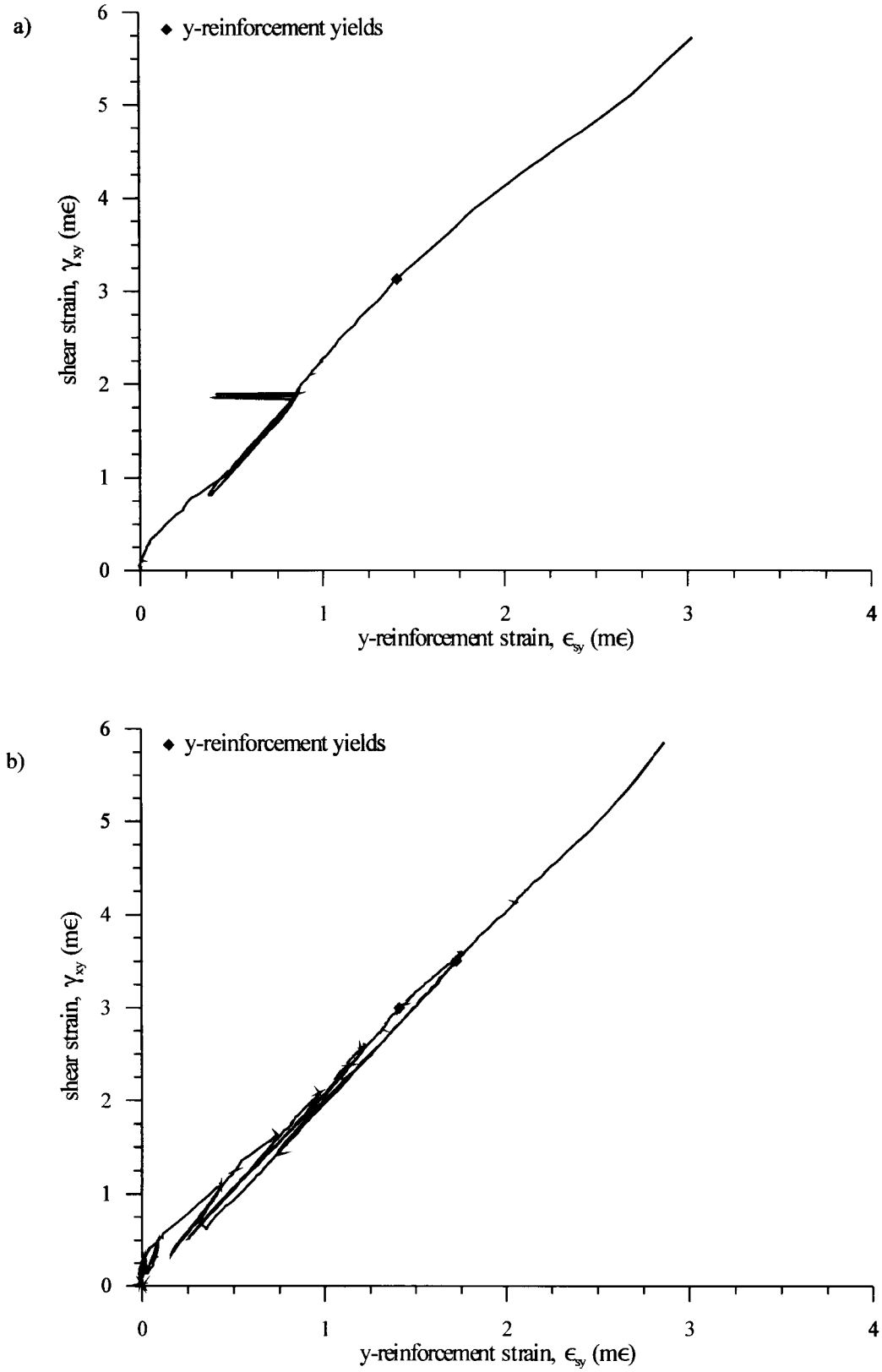

Figure 2.16 Shear stress vs reinforcement strain: a) PDV1, b) PDV3

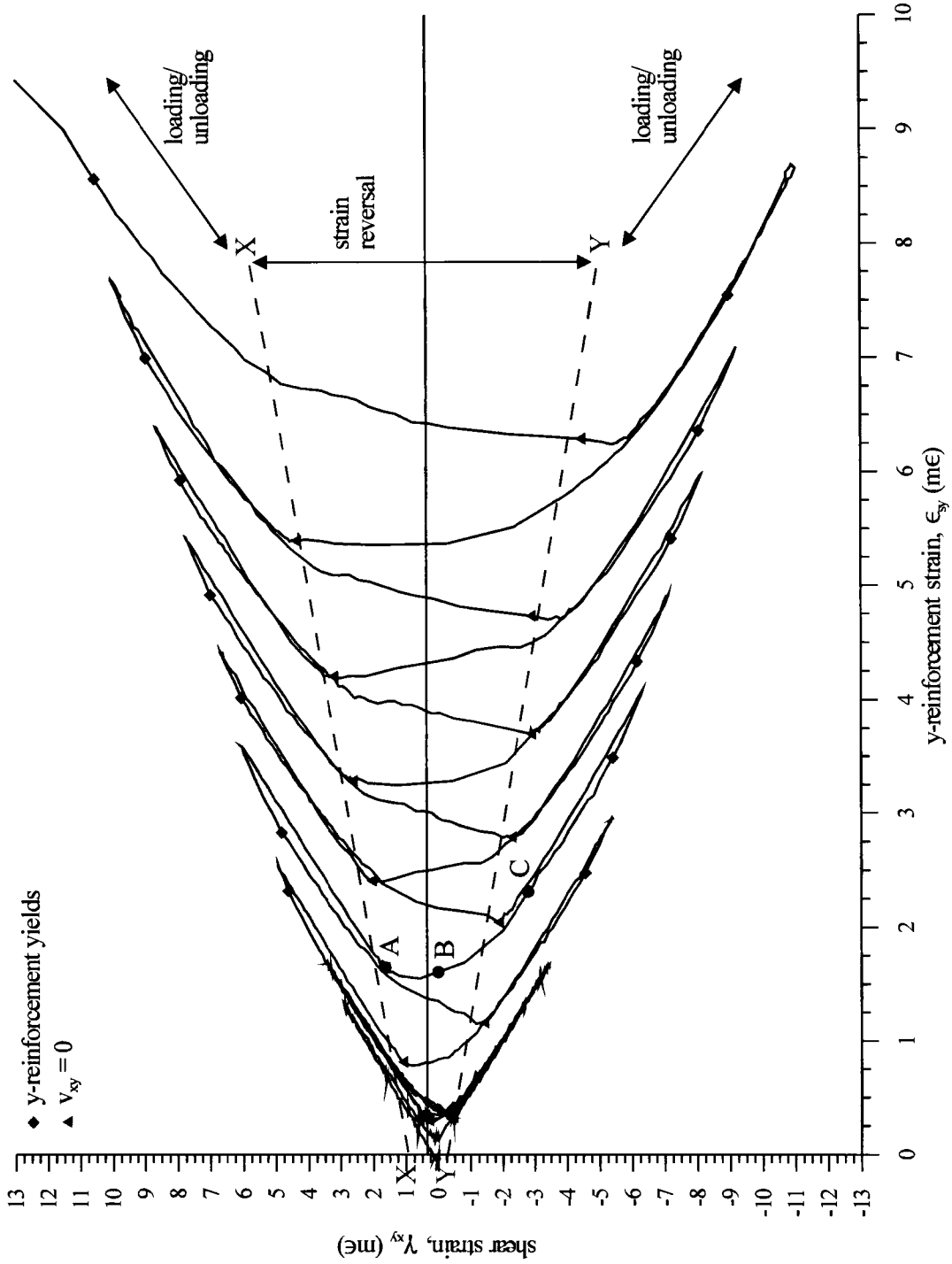

Figure 2.17 Shear strain vs reinforcement strain: SE8

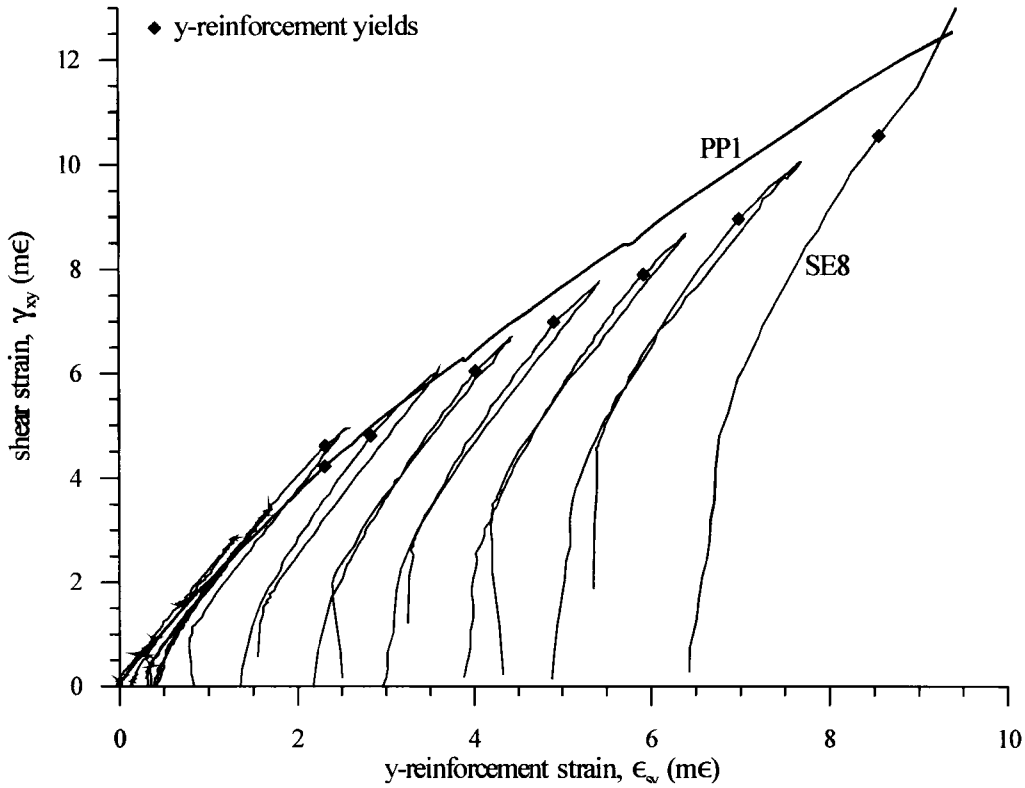

Figure 2.18 Shear strain vs reinforcement strain: monotonic (PP1) vs reverse-cyclic (SE8)

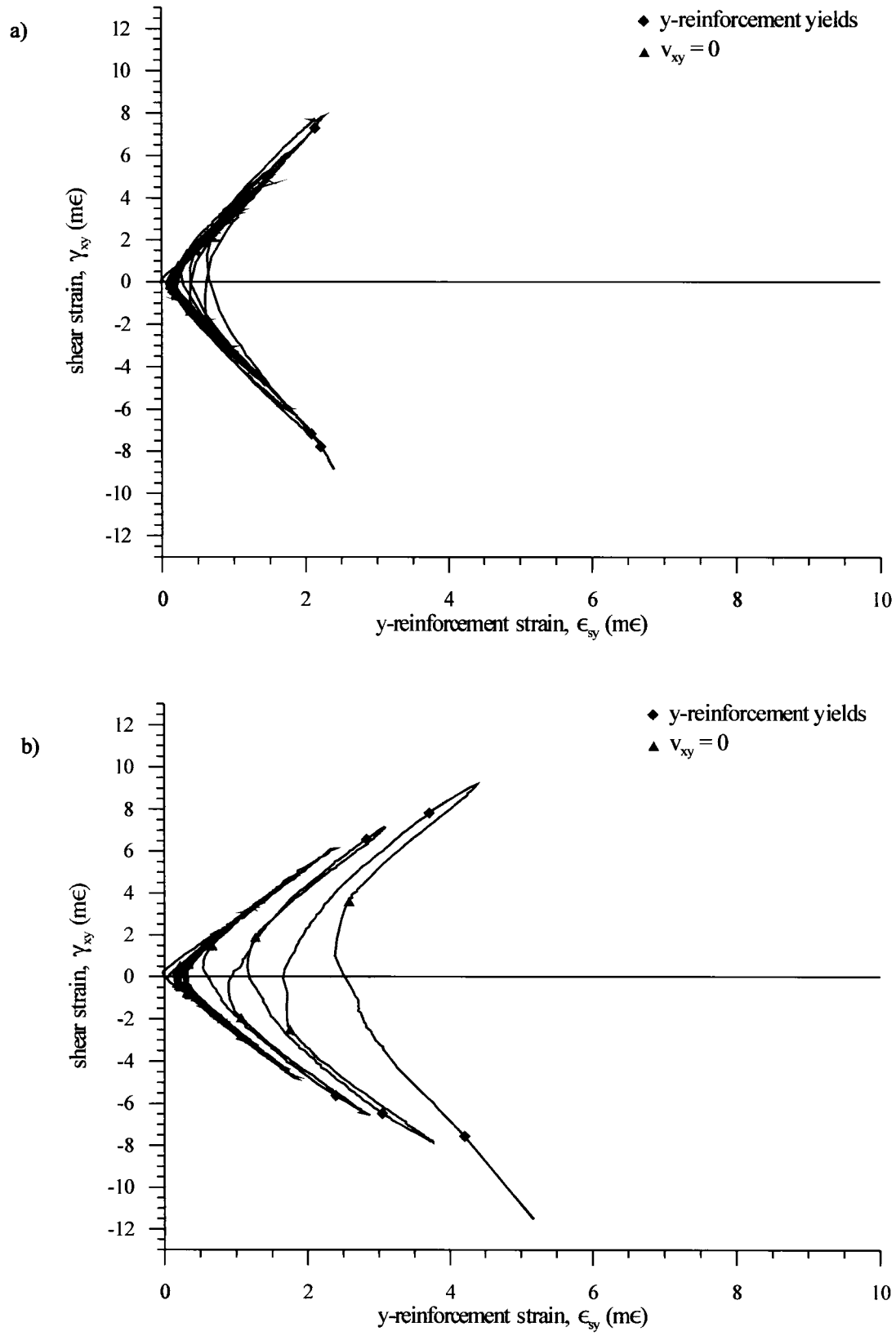

Figure 2.19 Shear strain vs reinforcement strain: a) SE9, b) SE10

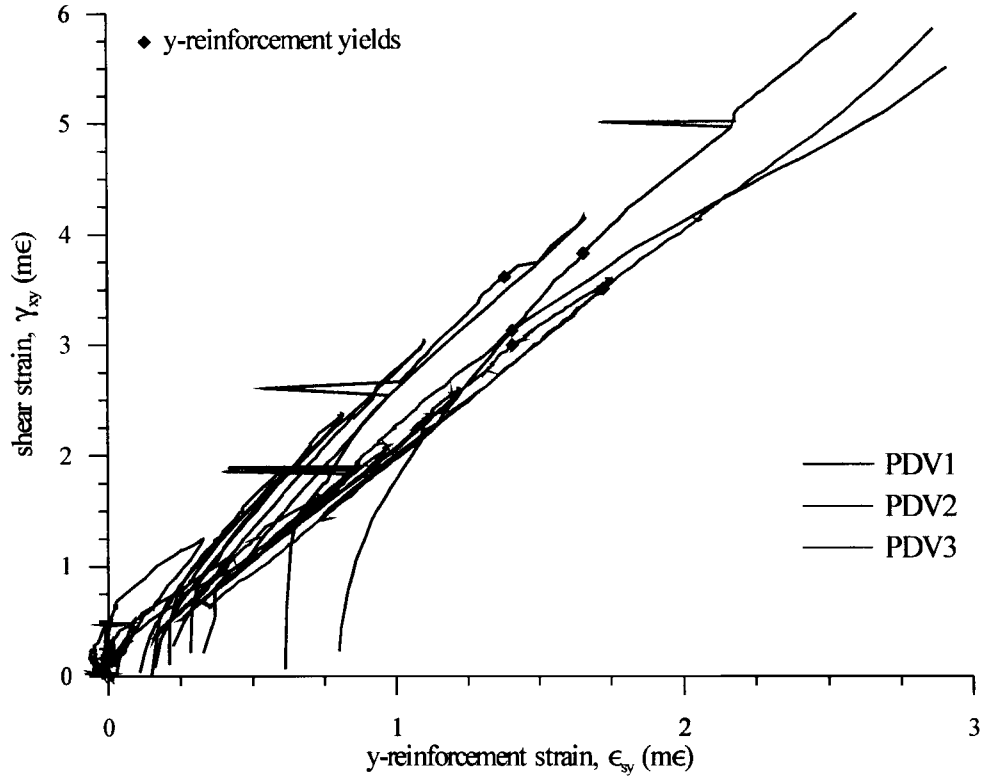

Figure 2.20 Shear strain vs reinforcement strain: monotonic (PDV1), reverse-cyclic (PDV2), and cyclic (PDV3)

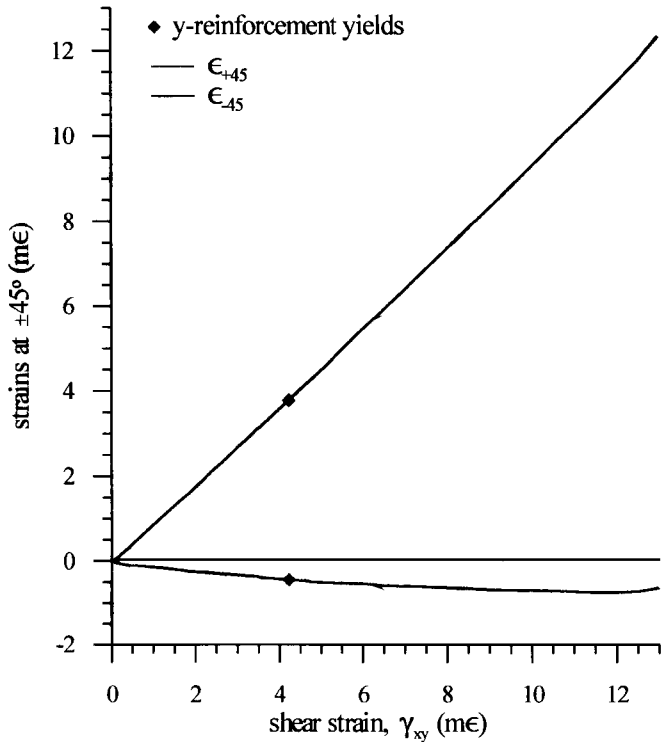

Figure 2.21 Strains at 45 deg. vs shear strain: PP1

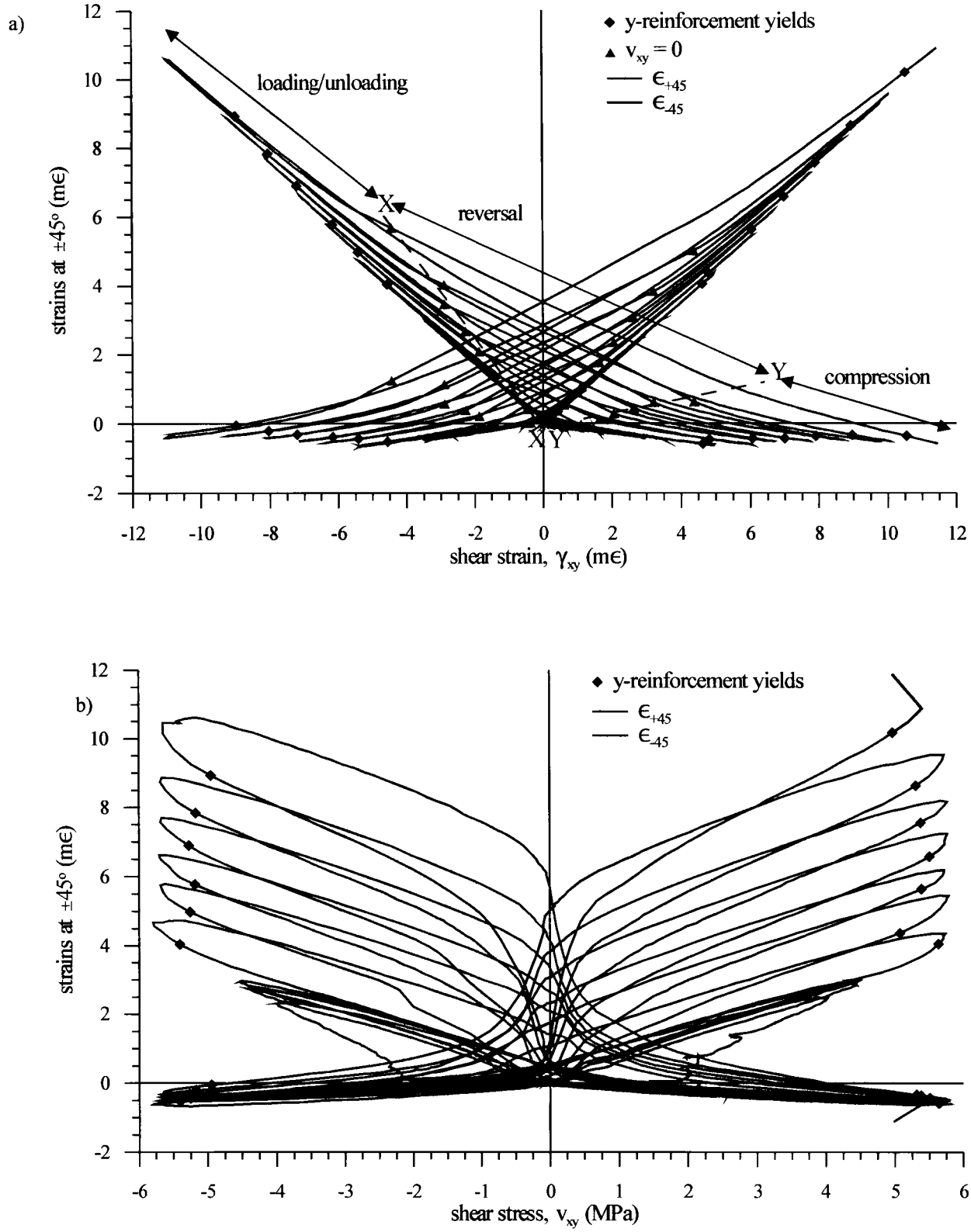

Figure 2.22 Strains at 45 deg., SE8: a) vs shear strain, b) vs shear stress

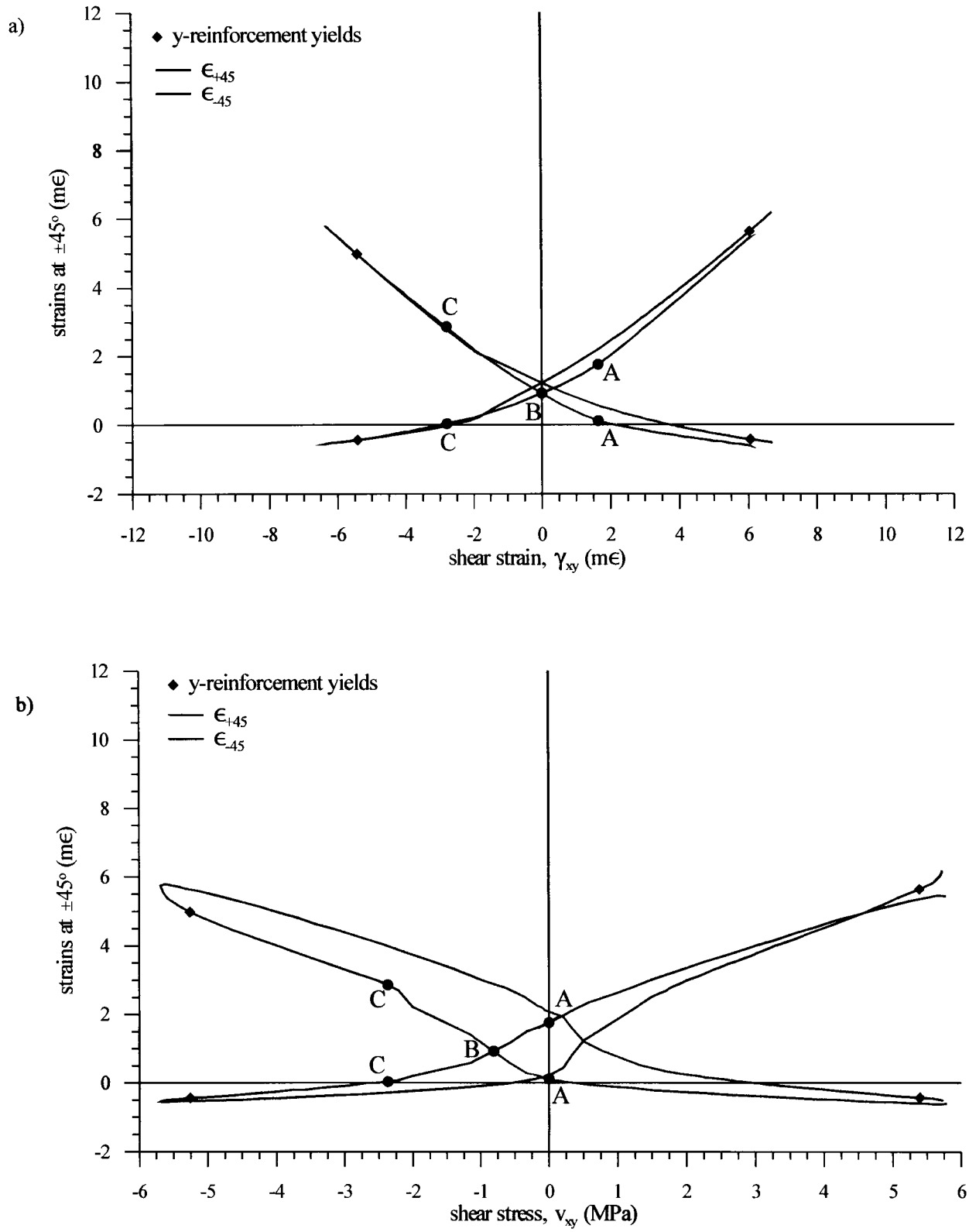

Figure 2.23 Strains at 45 deg., single cycle of SE8: a) vs shear strain, b) vs shear stress

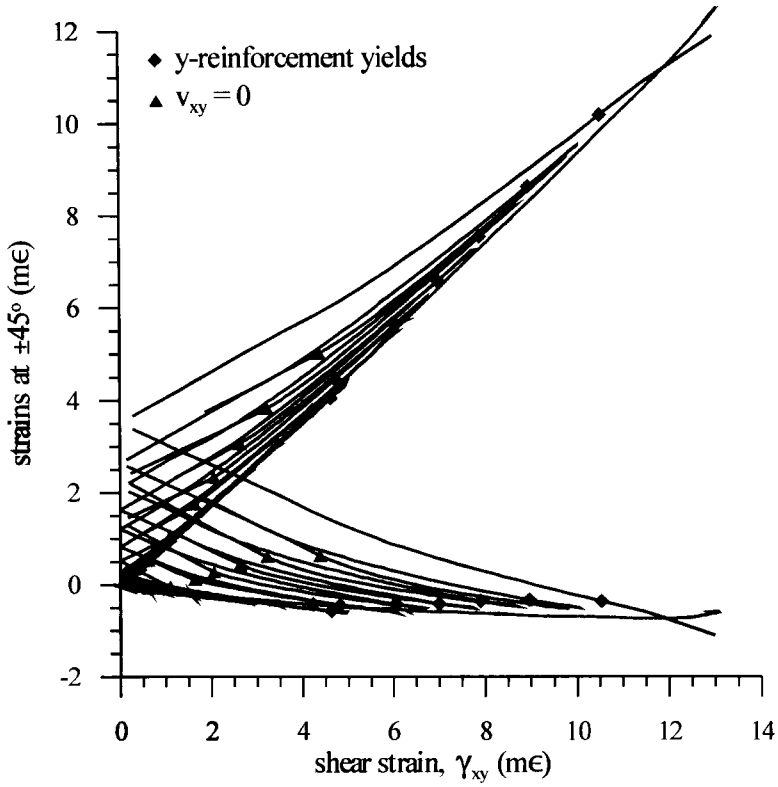

Figure 2.24 Strains at 45 deg. vs shear strain: monotonic (PP1) vs reverse-cyclic (SE8)

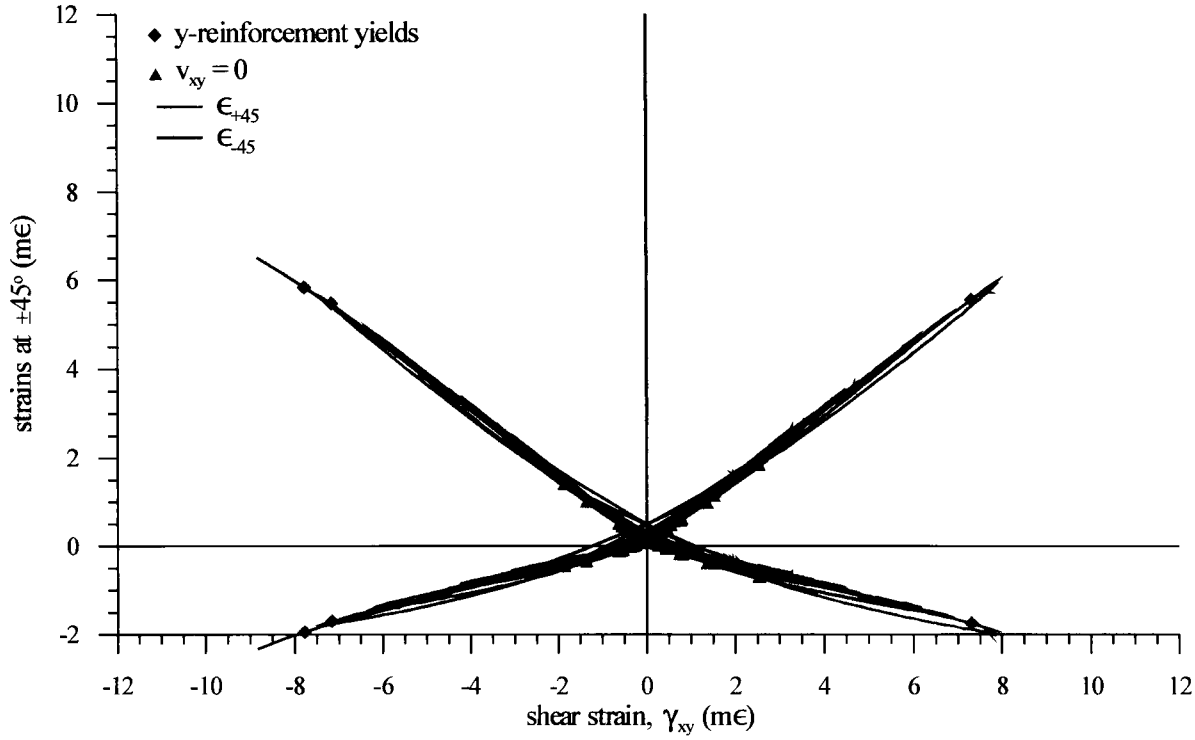

Figure 2.25 Strains at 45 deg. vs shear strain: SE9

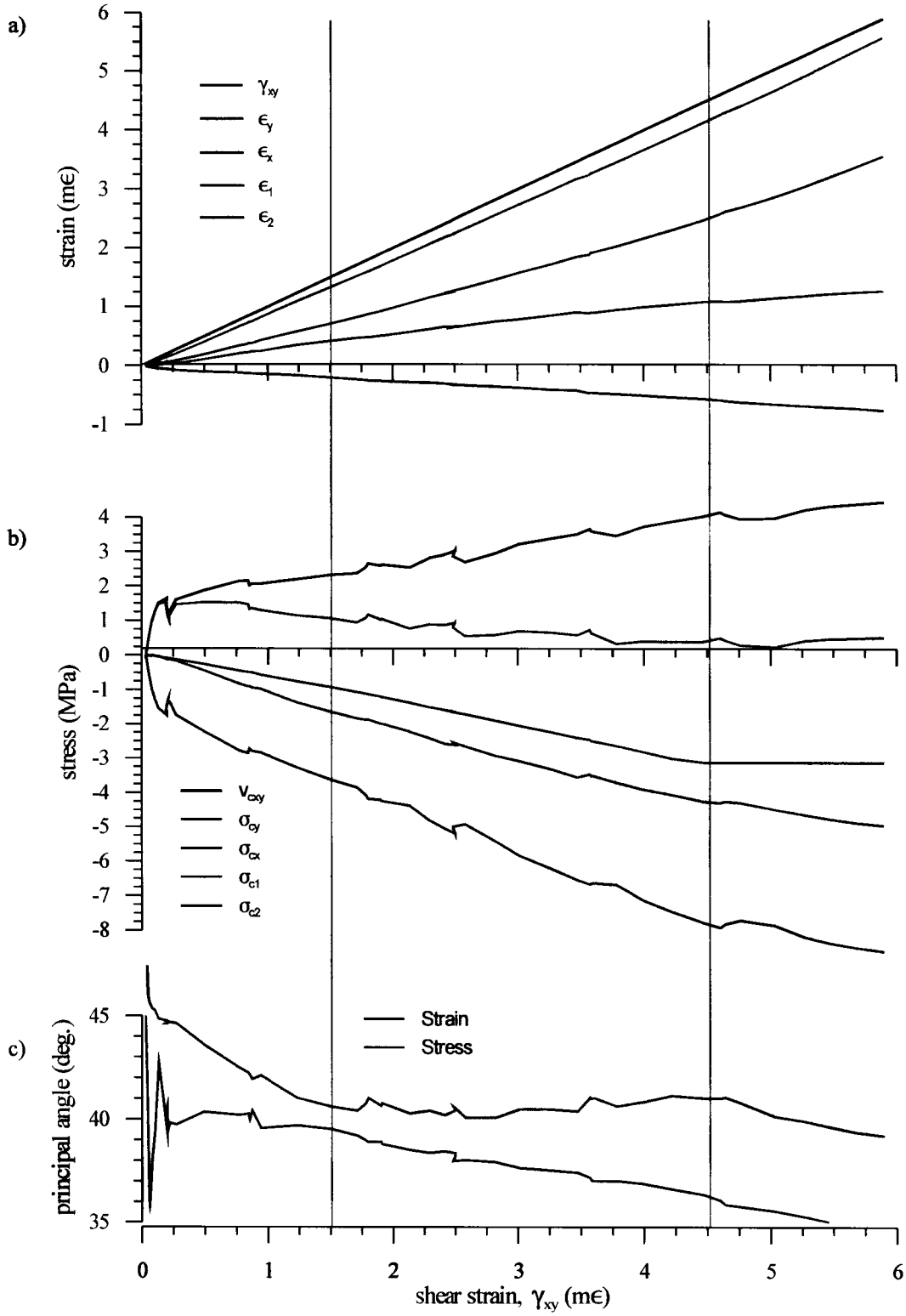

Figure 2.26 Stress and strain components during elastic loading: PP1: a) strains, b) stresses, c) principal angles

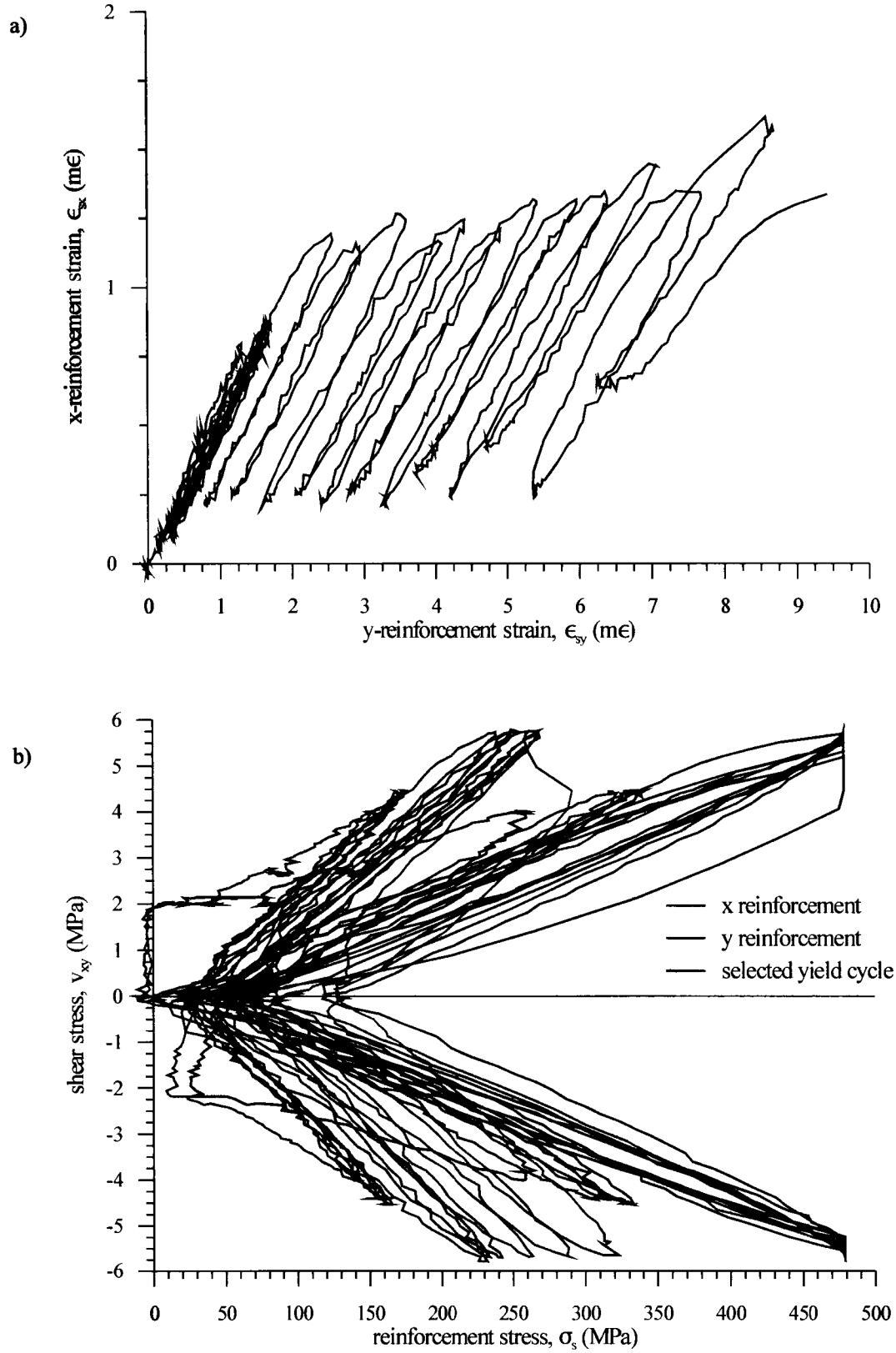

Figure 2.27 Reinforcement stresses and strains, SE8: a) strains, b) stresses

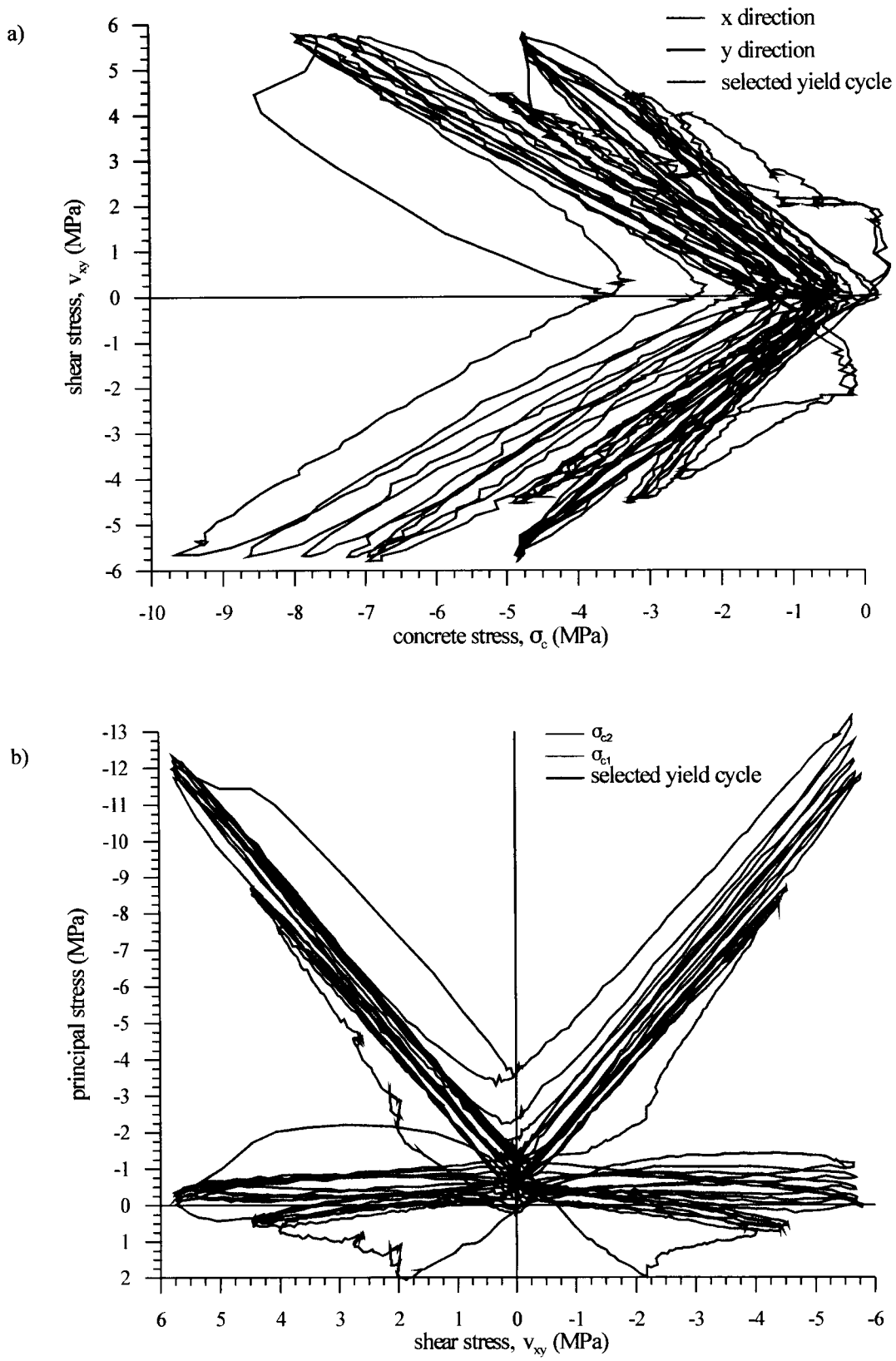

Figure 2.28 Concrete stresses, SE8: a) in the reinforcement directions, b) in the principal directions

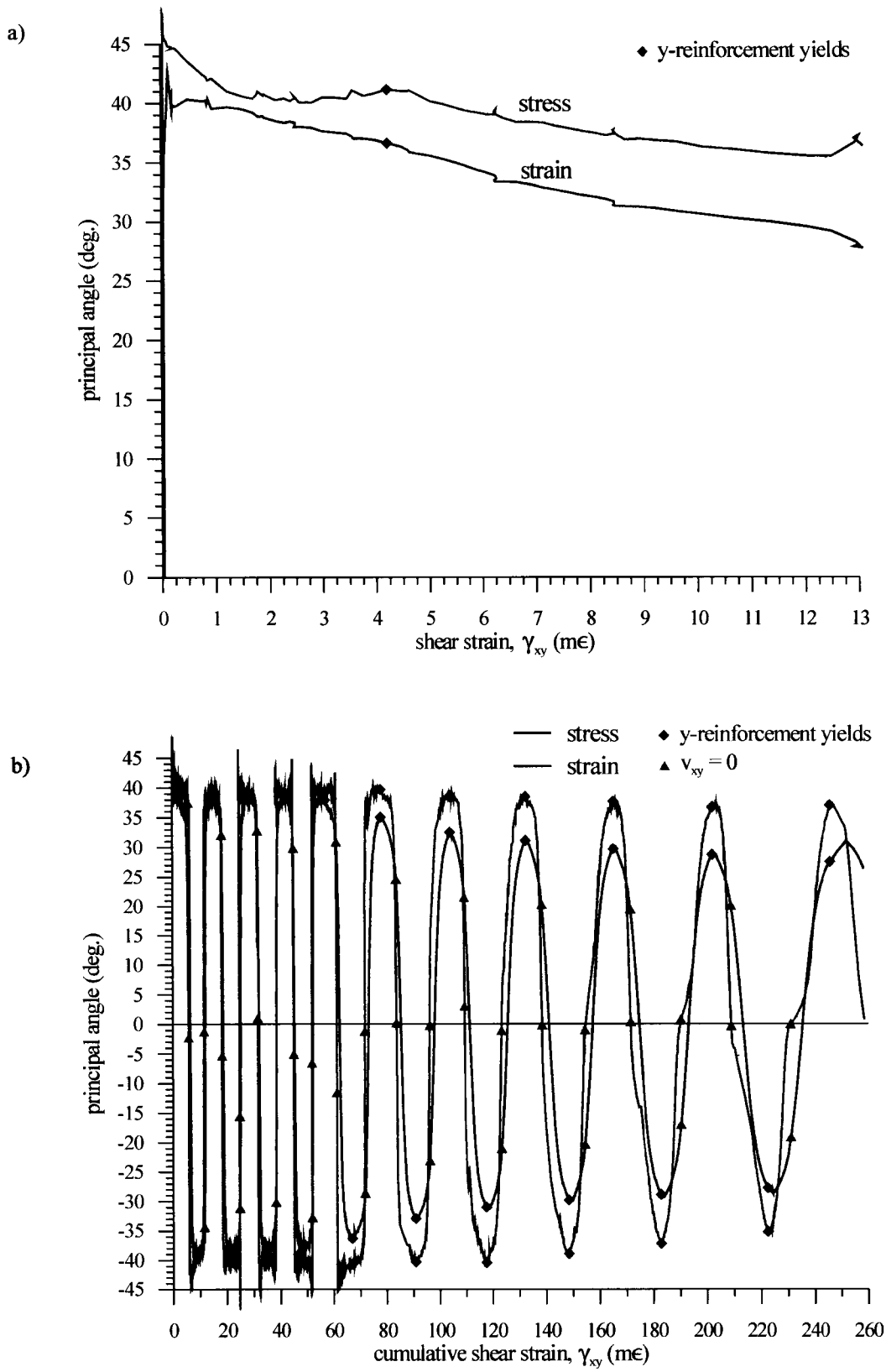

Figure 2.29 Principal stress and strain angles: a) PP1, b) SE8

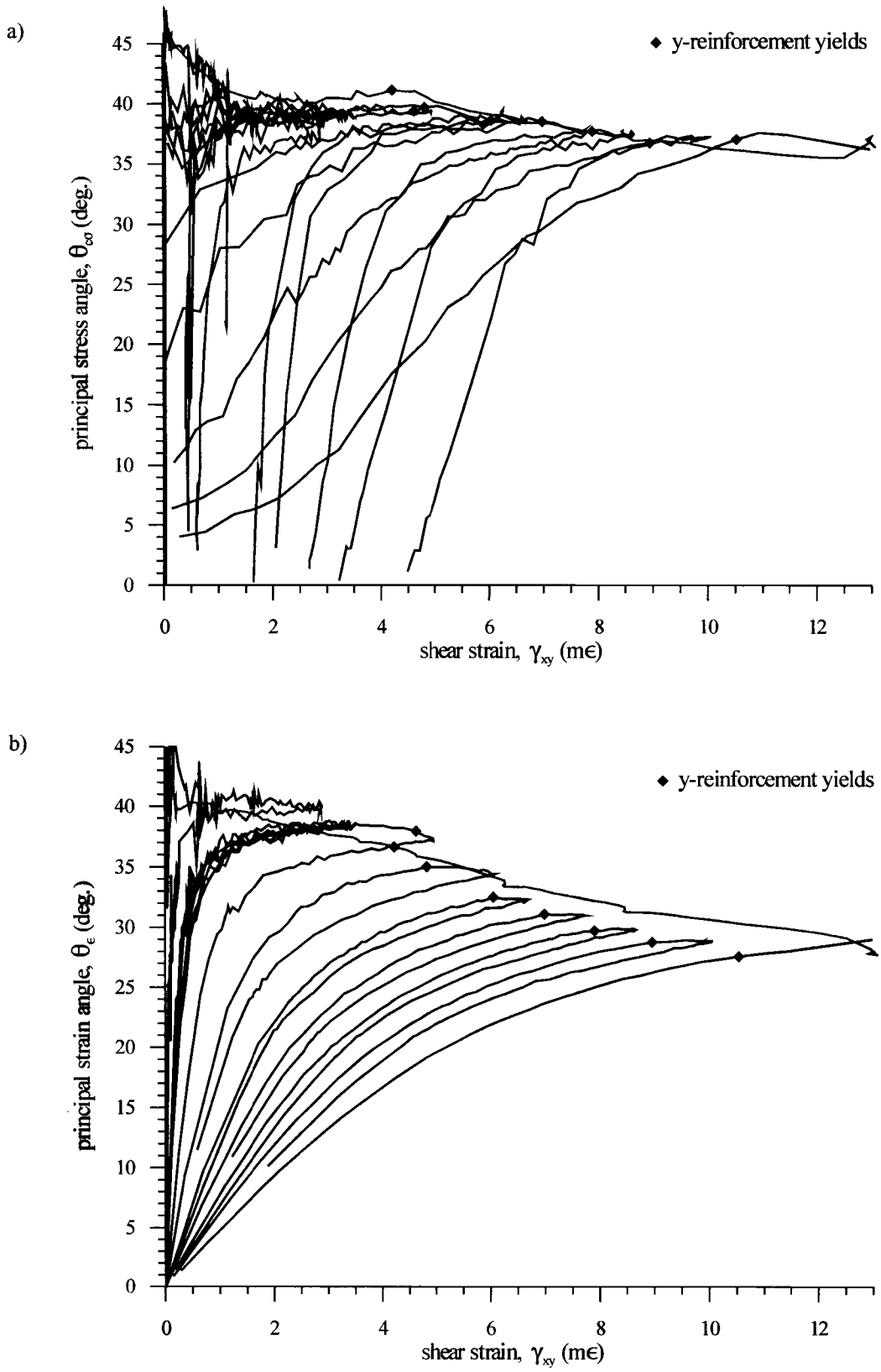

Figure 2.30 Principal stress and strain angles, monotonic (PP1) vs reverse-cyclic (SE8)
a) principal stress angle, b) principal strain angle

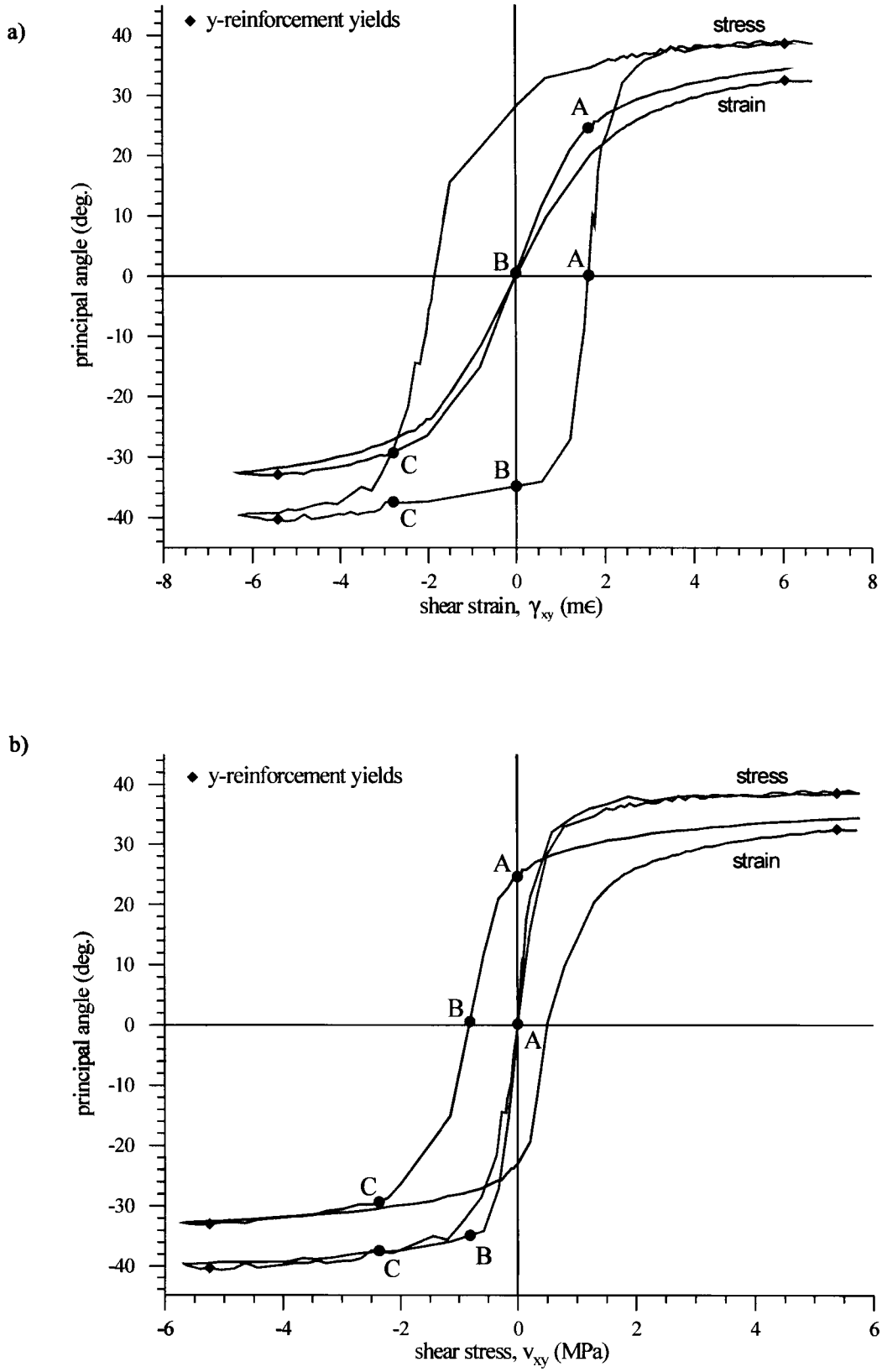

Figure 2.31 Principal stress and strain angles, single cycle of SE8: a) vs shear strain, b) vs shear stress

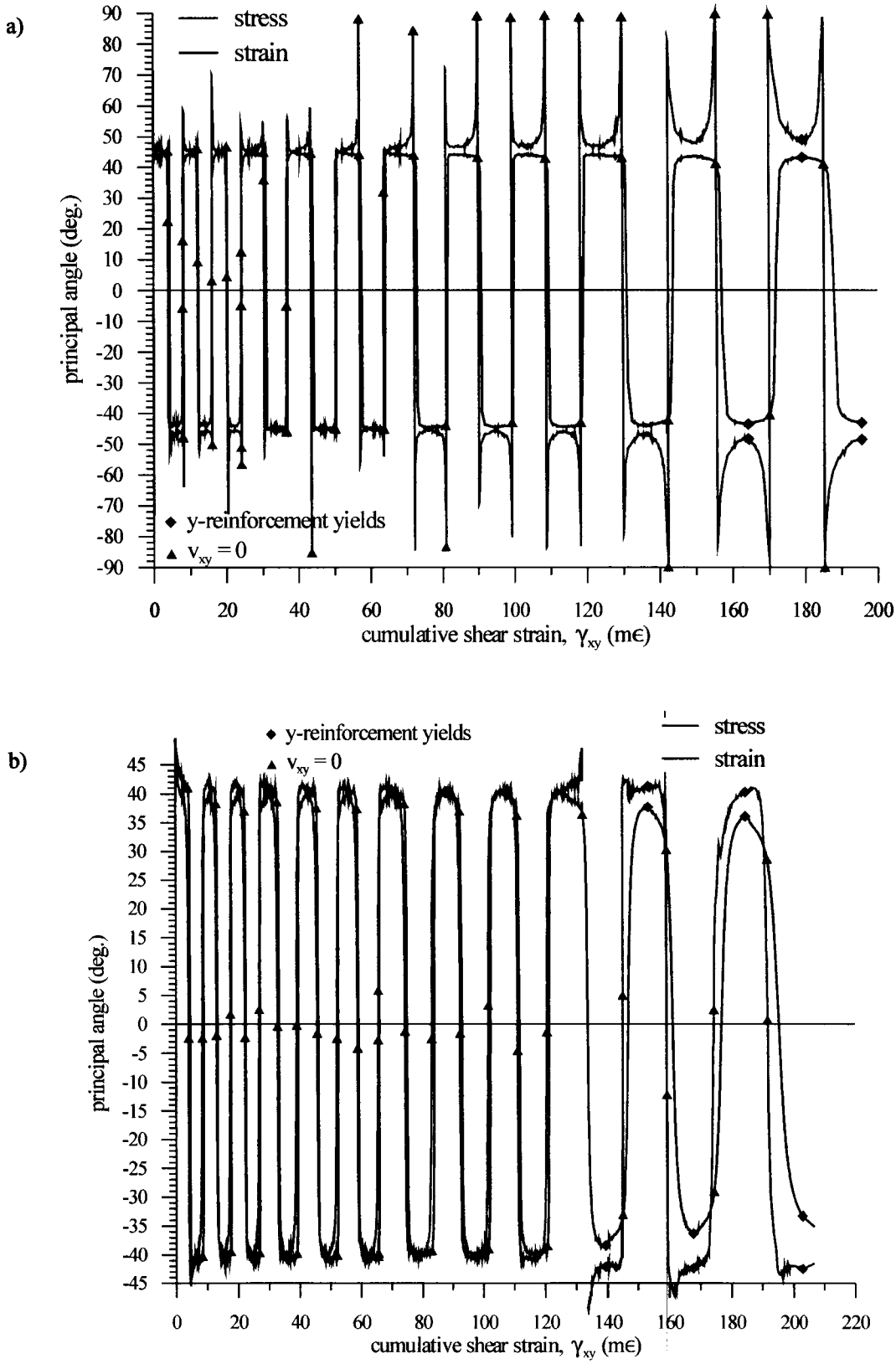

Figure 2.32 Principal stress and strain angles: a) SE9, b) SE10

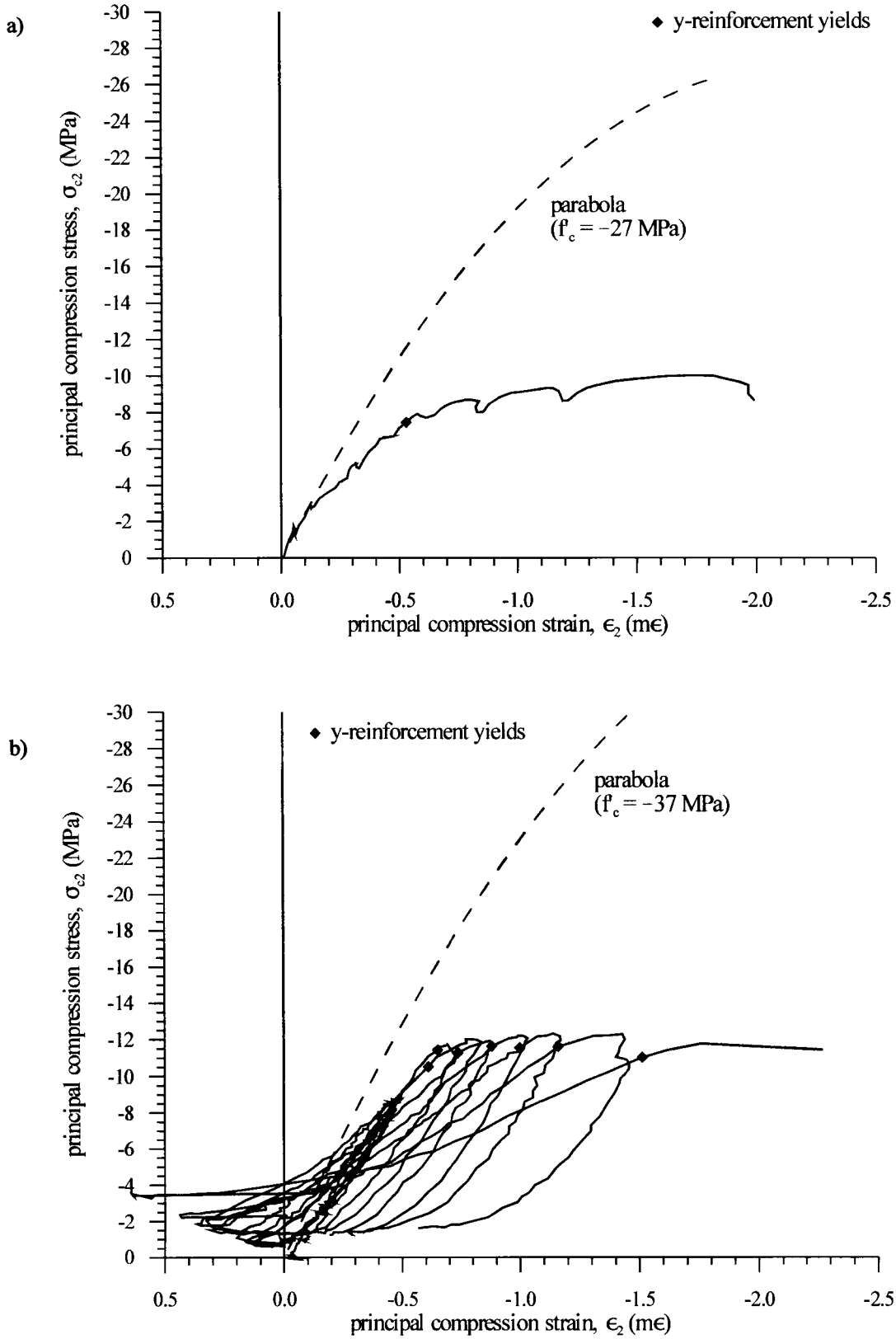

Figure 2.33 Principal concrete compression stress vs minimum principal strain: a) PP1, b) SE8 (for clarity, only positive shear cycles shown)

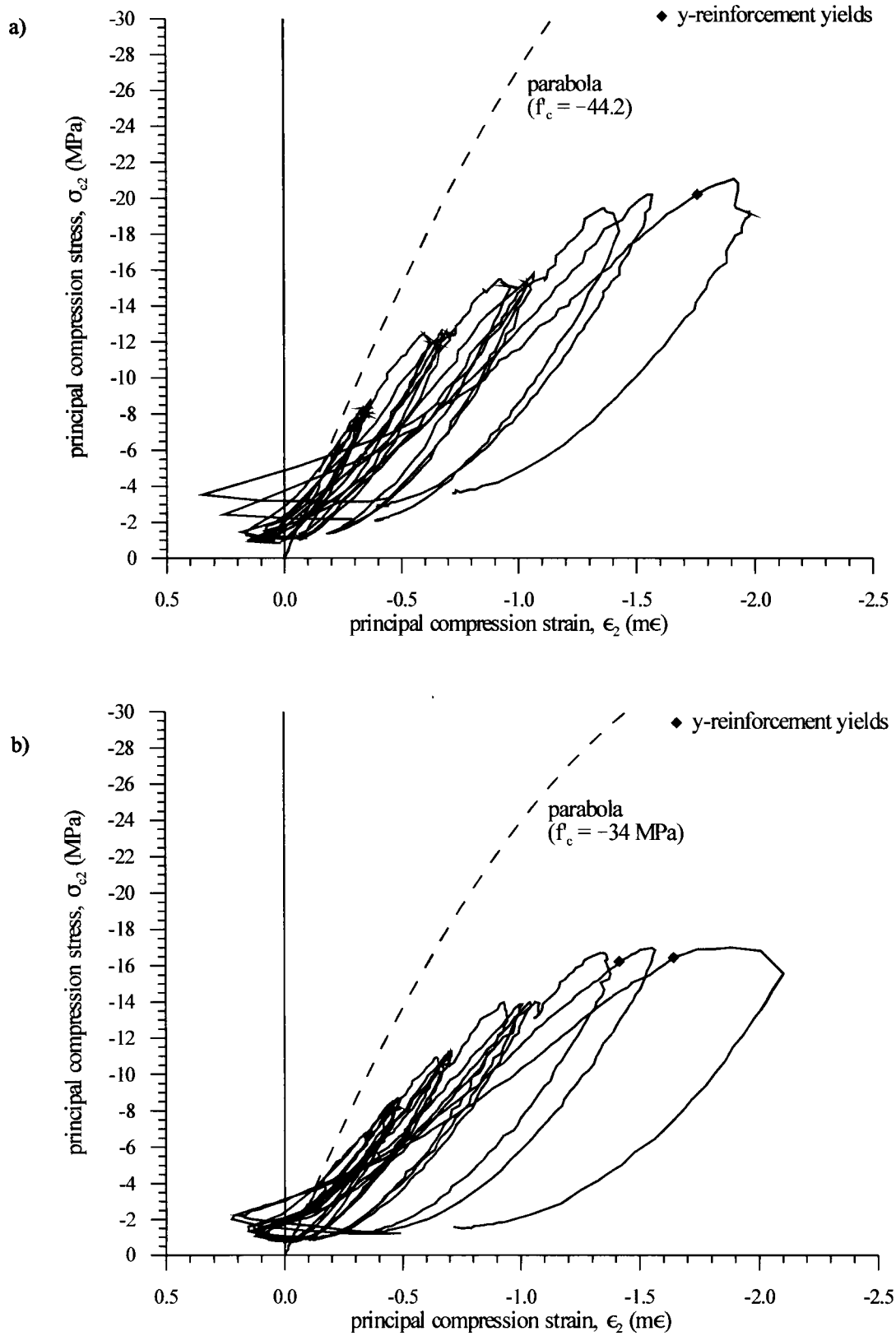

Figure 2.34 Principal concrete compression stress vs minimum principal strain: a) SE9, b) SE10 (for clarity, only positive shear cycles shown)

a)

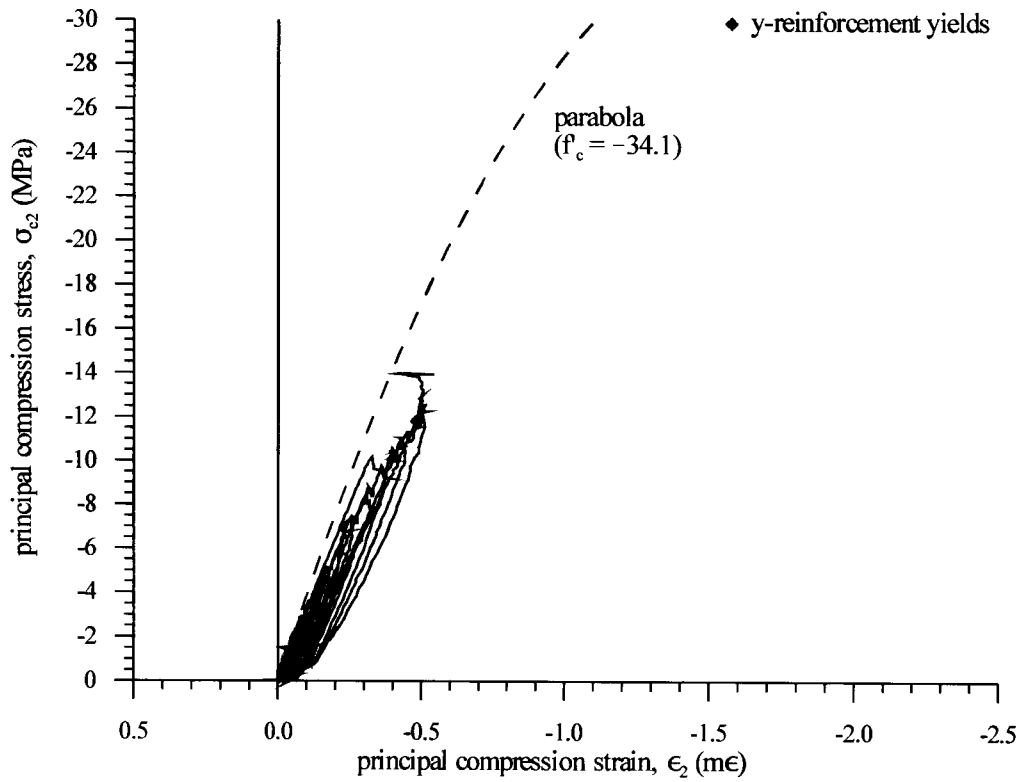

Figure 2.35 Principal concrete compression stress vs minimum principal strain: PDV3

b)

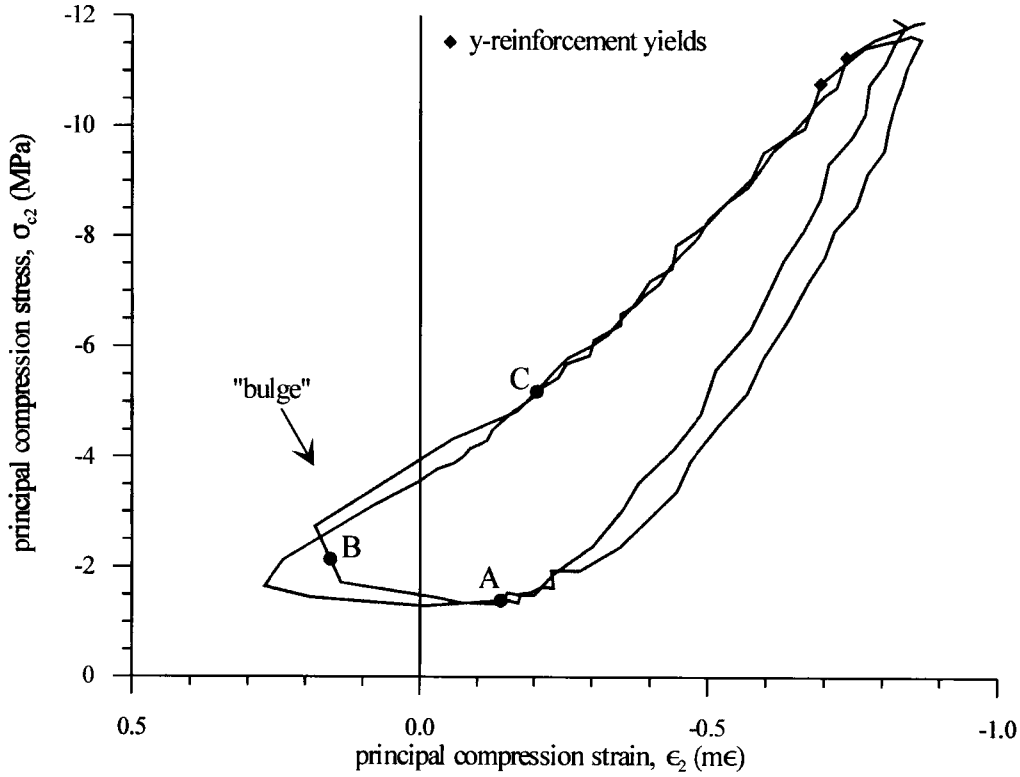

Figure 2.36 Principal concrete compression stress vs minimum principal strain: single cycle of SE8

a) **POINT A Shear stress = 0**

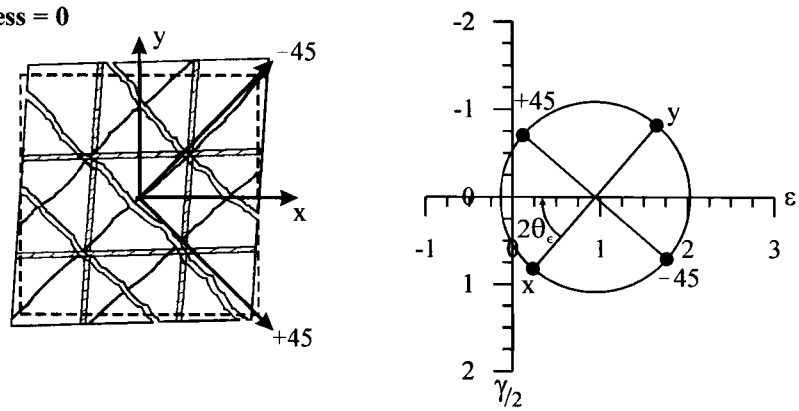

b) **POINT B Shear strain = 0**

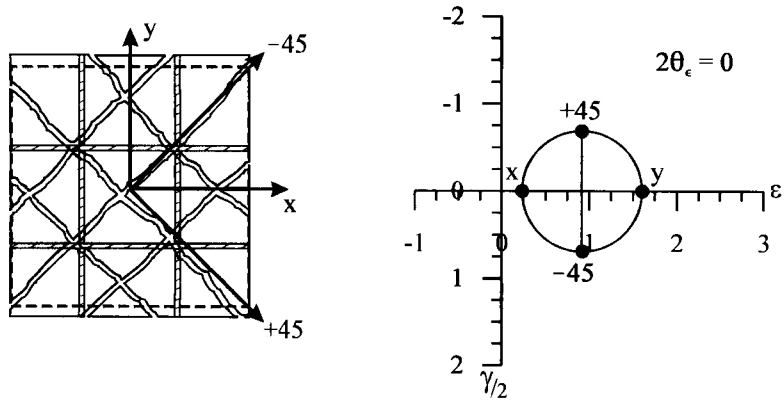

c) **POINT C Previous cracks closed**

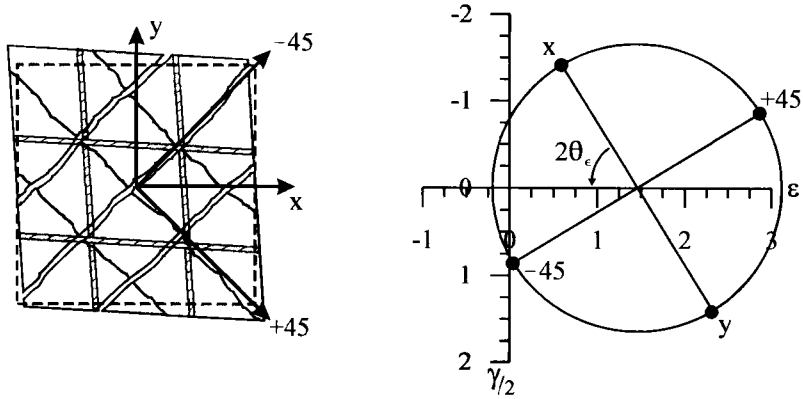

Figure 3.1 Physical model for shear strain reversal

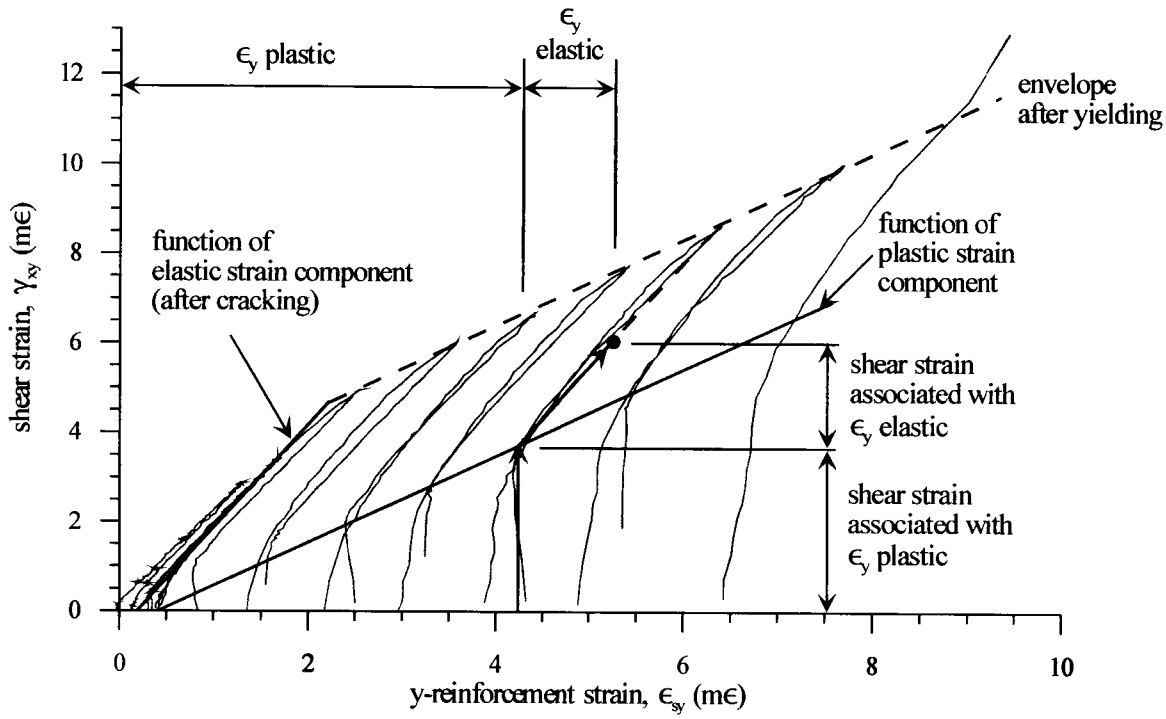

Figure 3.2 Illustration of relationship between shear strain and weak reinforcement strain (based on SE8)

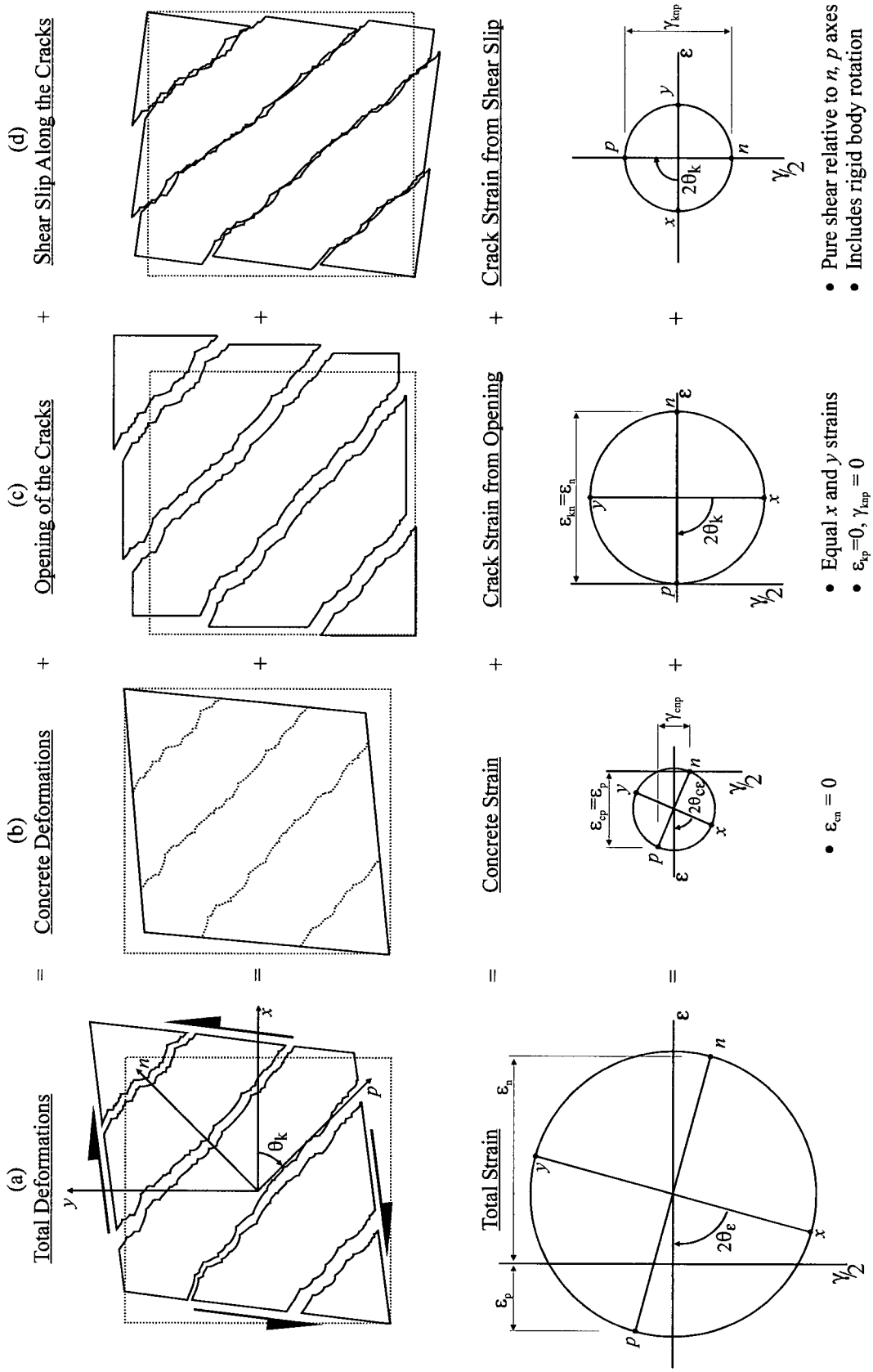

Figure 3.3 Representing total strains by concrete and crack strains

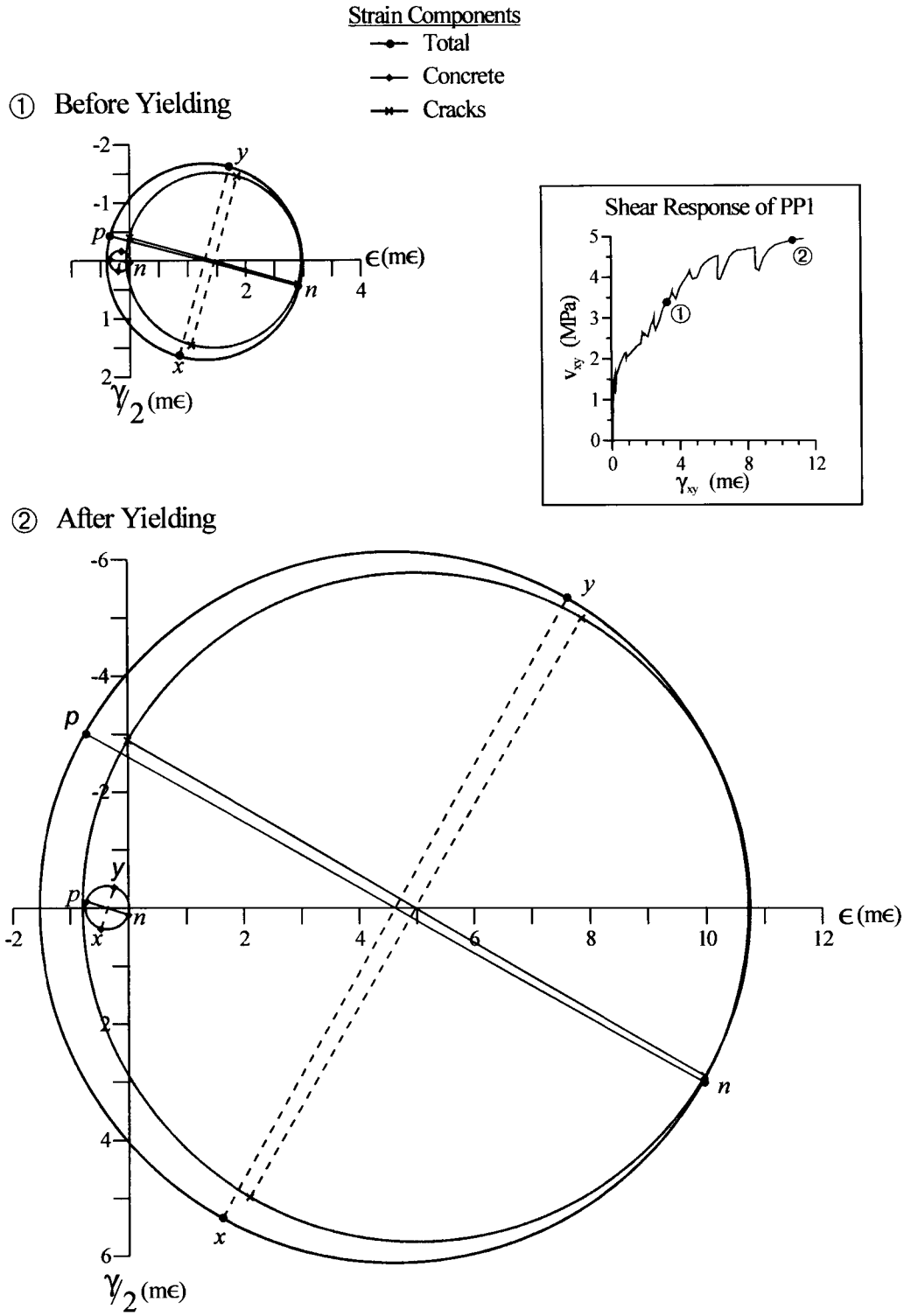

Figure 3.4 Concrete and crack strains: example using PP1

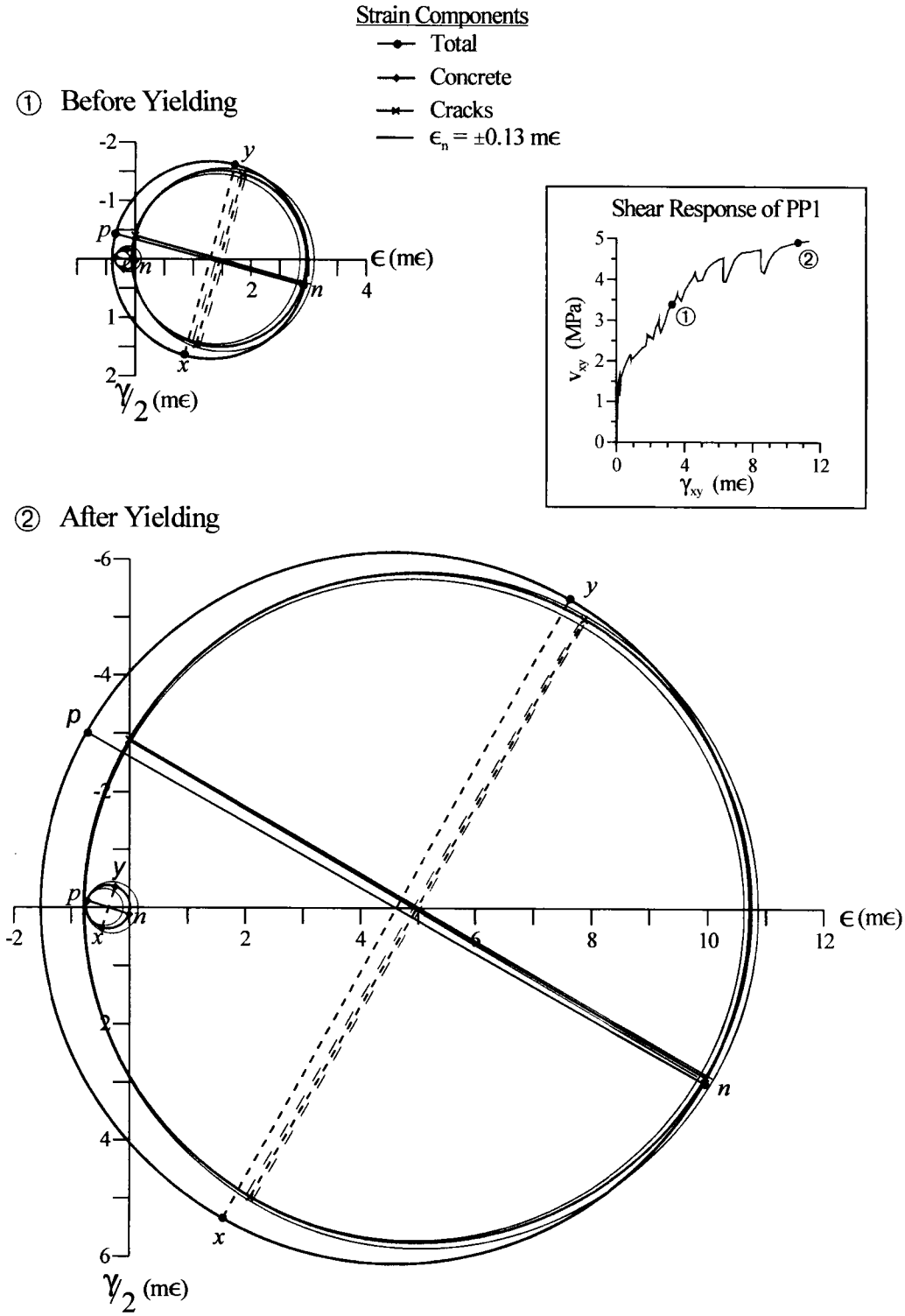

Figure 3.5 Concrete and crack strains: sensitivity to assumed concrete tension strain

a) orthogonal cracks (defined with respect to opening cracks)

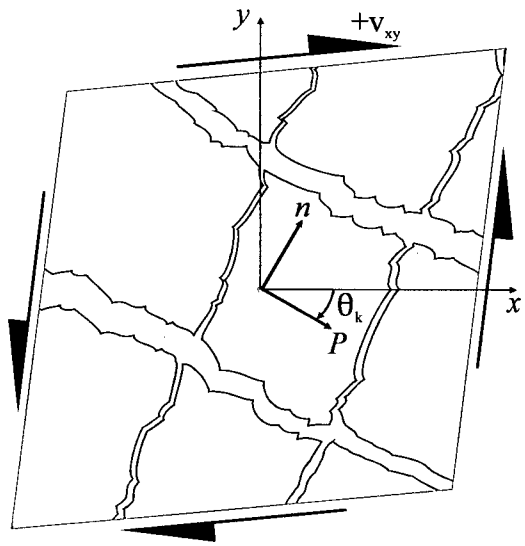

b) general case (defined with respect to applied shear stress

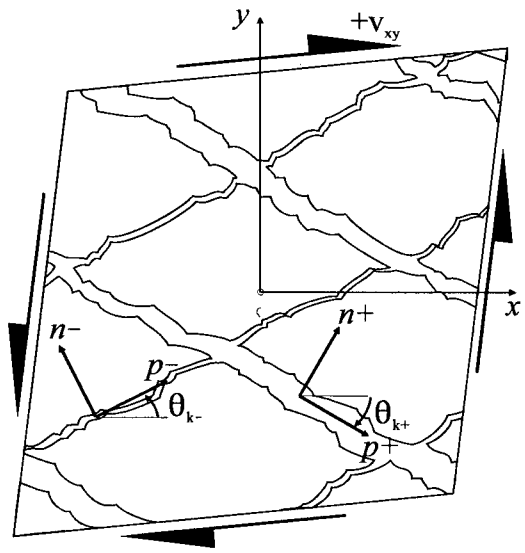

Figure 3.6 Crack orientations and axes: a) orthogonal cracks (defined with respect to opening crack), b) general case (defined with respect to shear stress)

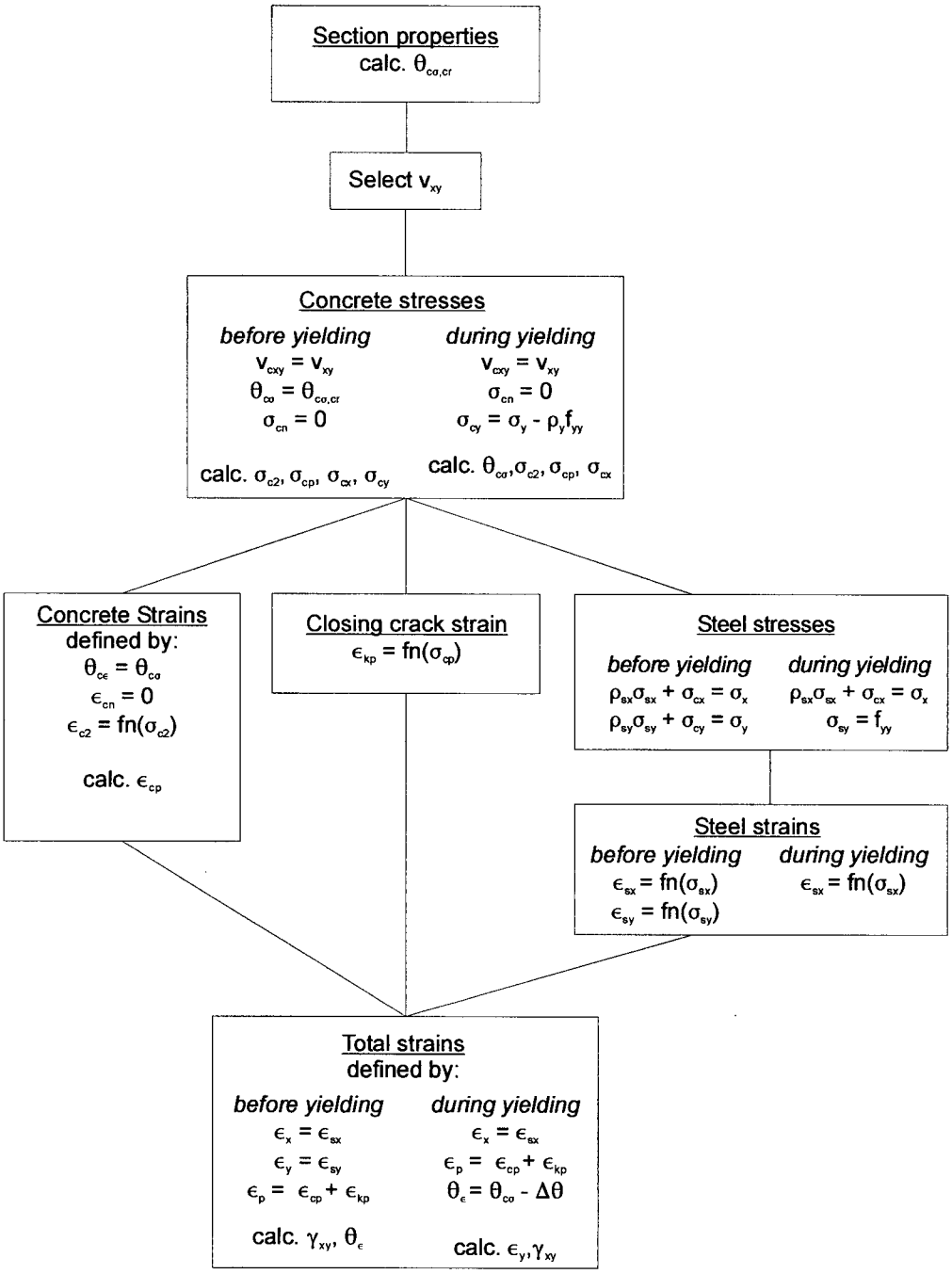

Figure 3.7 Basic solution algorithm for predicting strains: cracks in two directions, no concrete tension

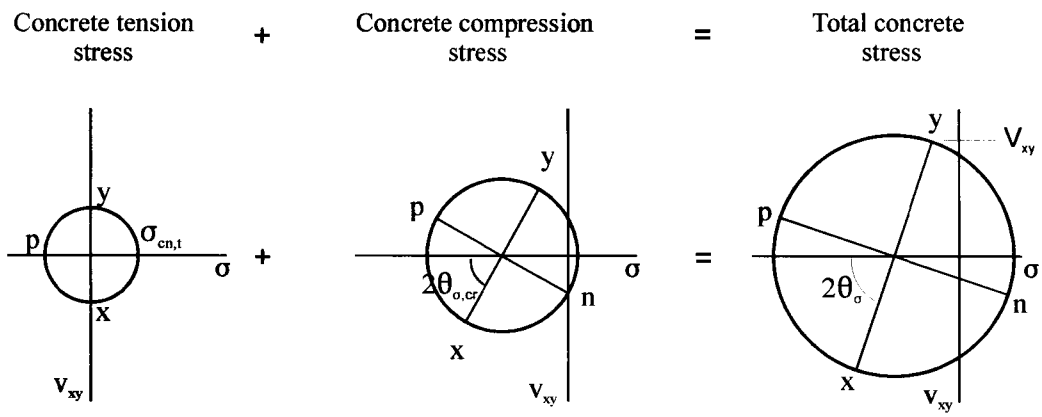

Figure 3.8 Superposition of concrete compression and tension stresses: pure shear applied loading

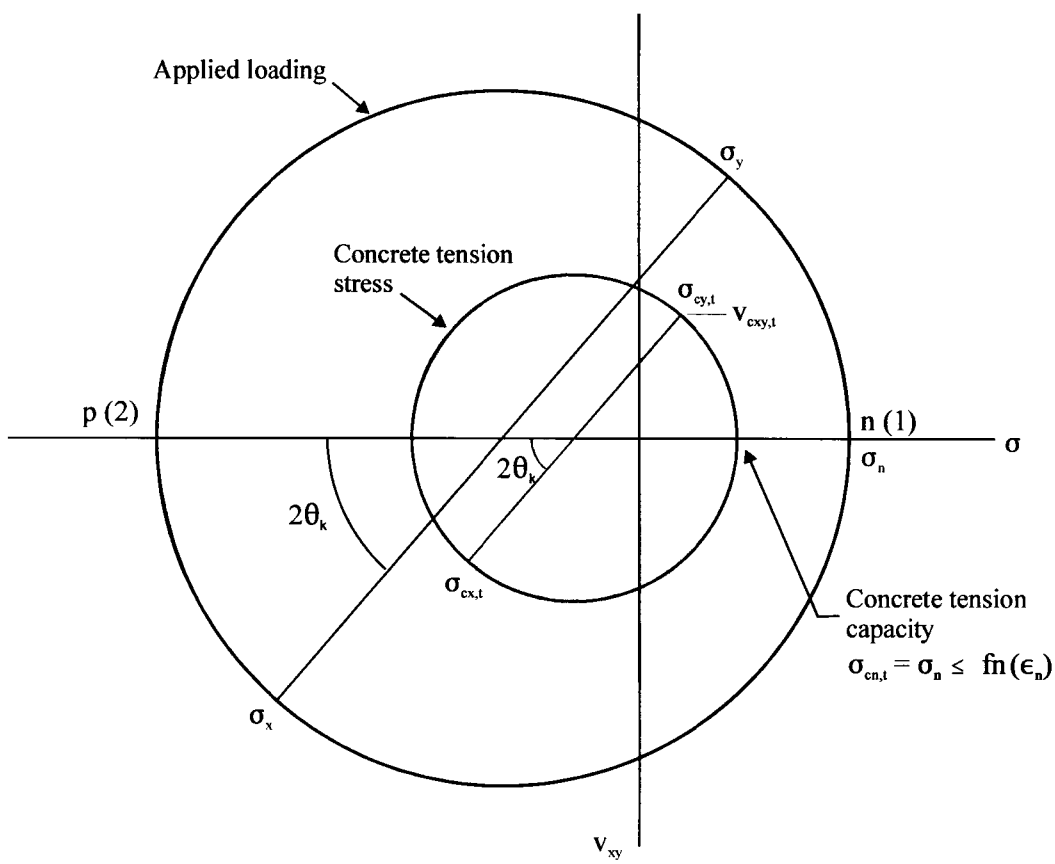

Figure 3.9 Defining the load carried by concrete tension

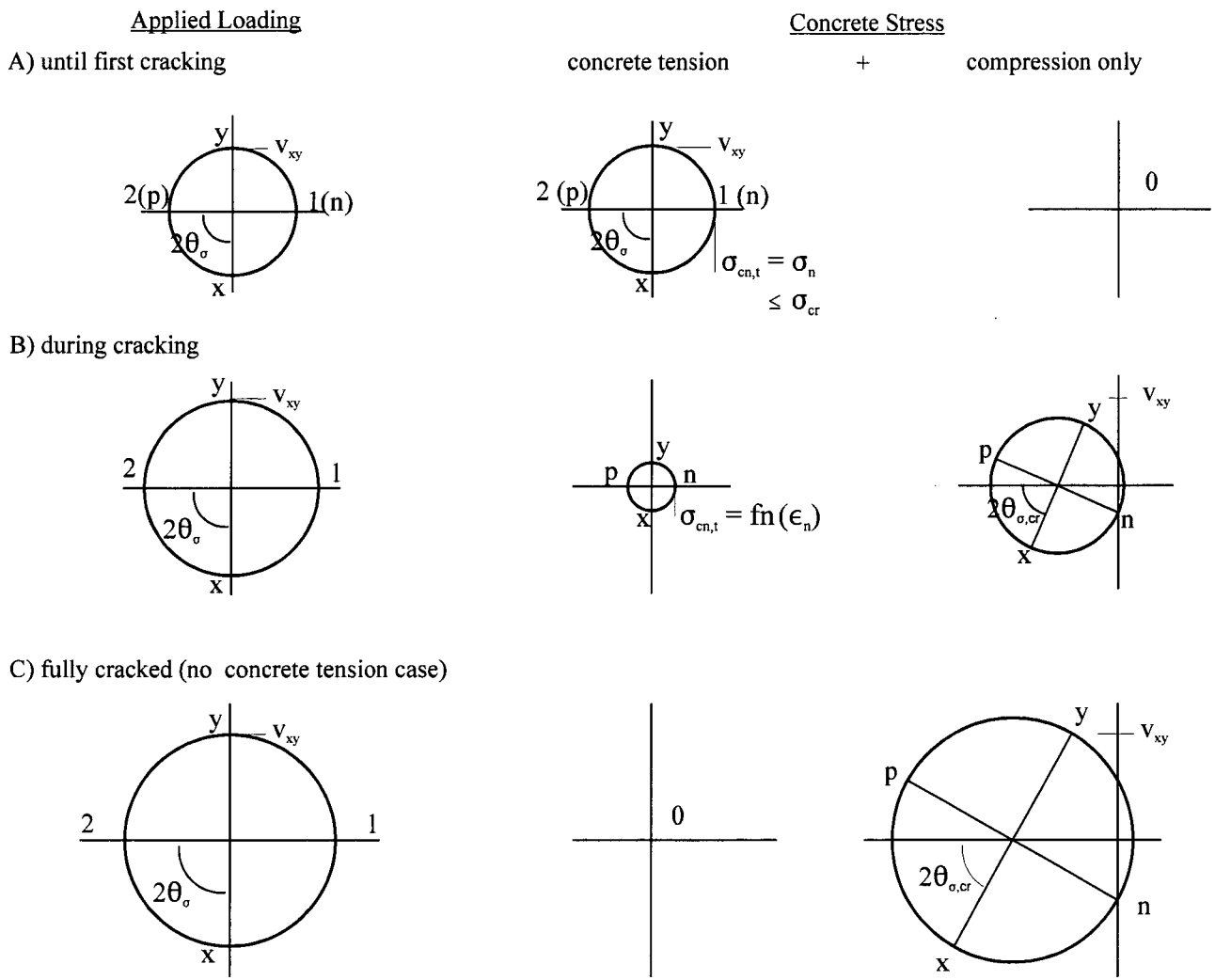

Figure 3.10 Variation of concrete stresses with increasing loading: pure shear case

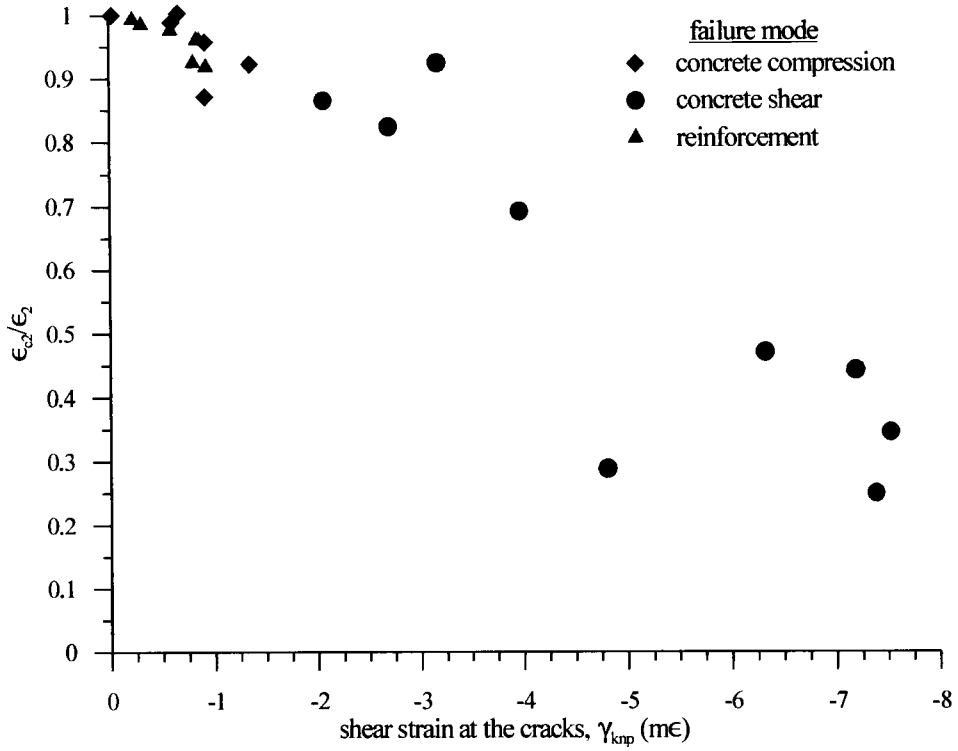

Figure 3.11 Differentiating shear failures: shear strain at the crack interface

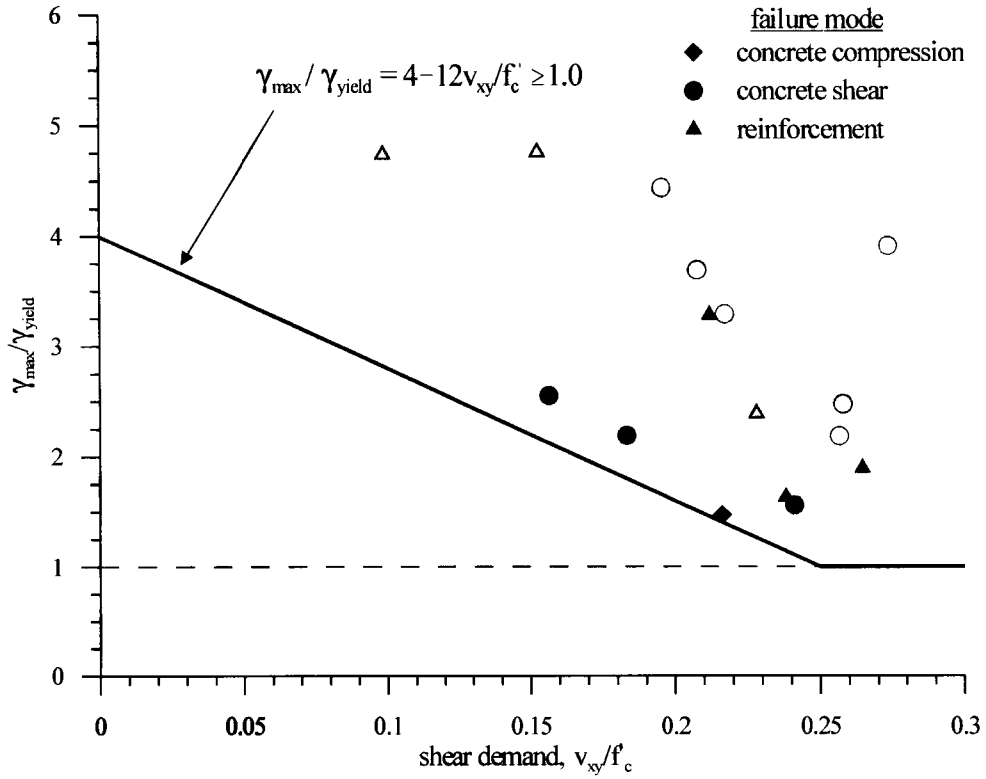

Figure 3.12 Proposed shear strain limit (solid = LVDT data, hollow = Vecchio-Collins, 1982 data)

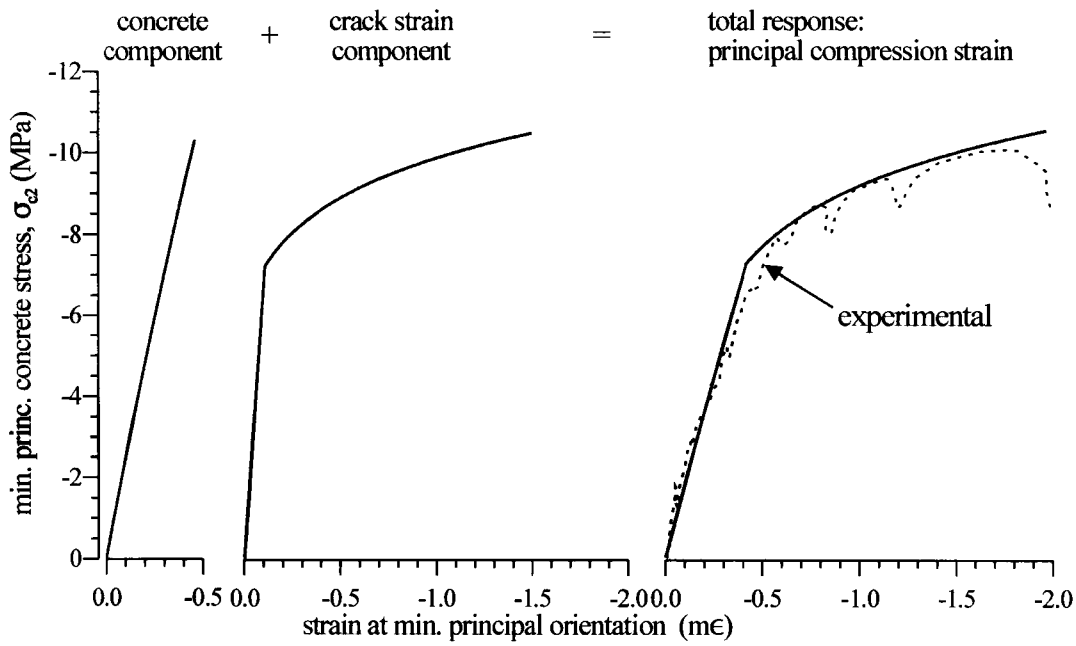

Figure 3.13 Concrete and crack strains: concrete compression softening

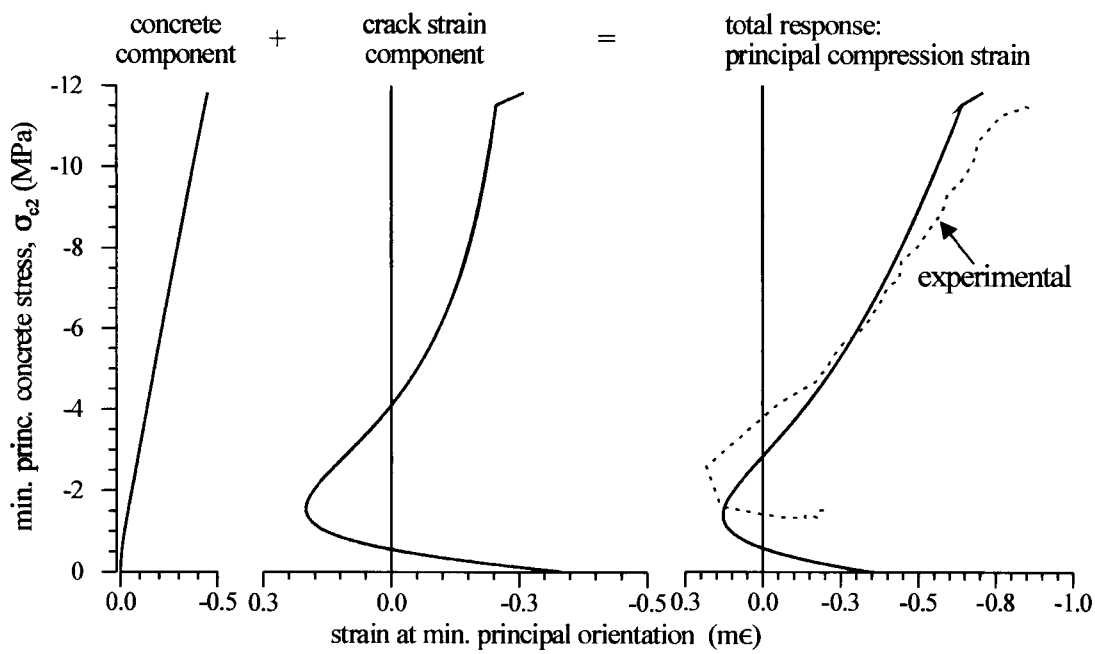

Figure 3.14 Concrete and crack strains: complex concrete response (bulge)

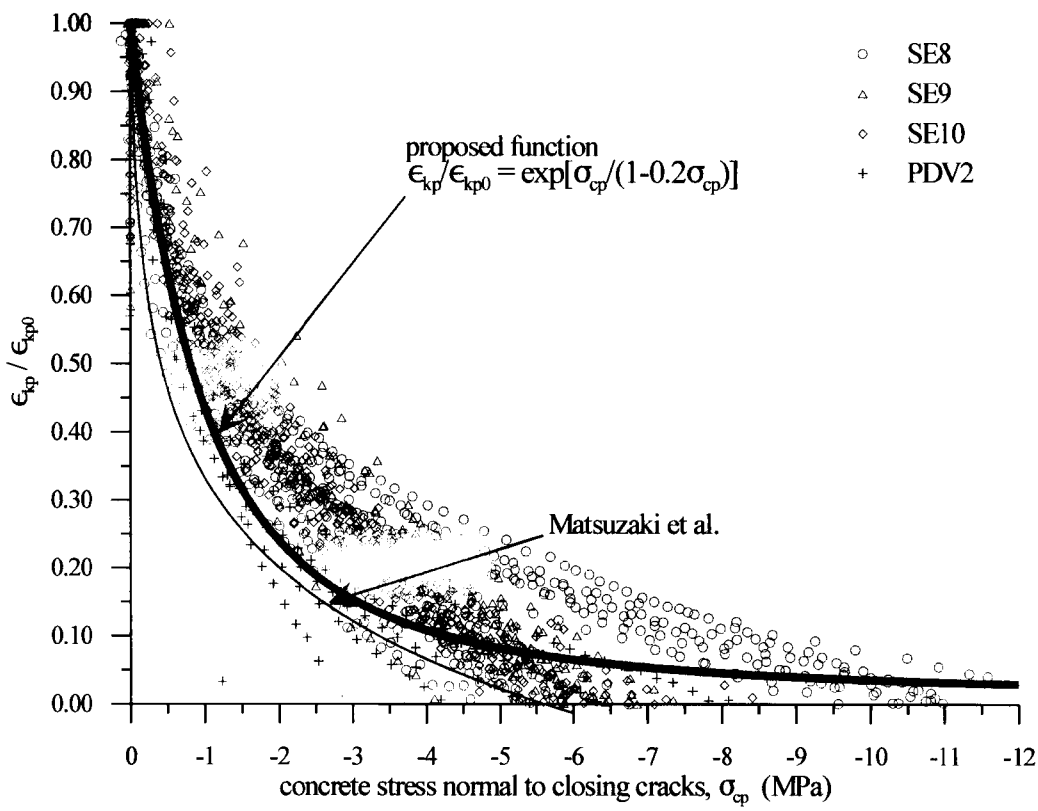

Figure 4.1 Crack closing function

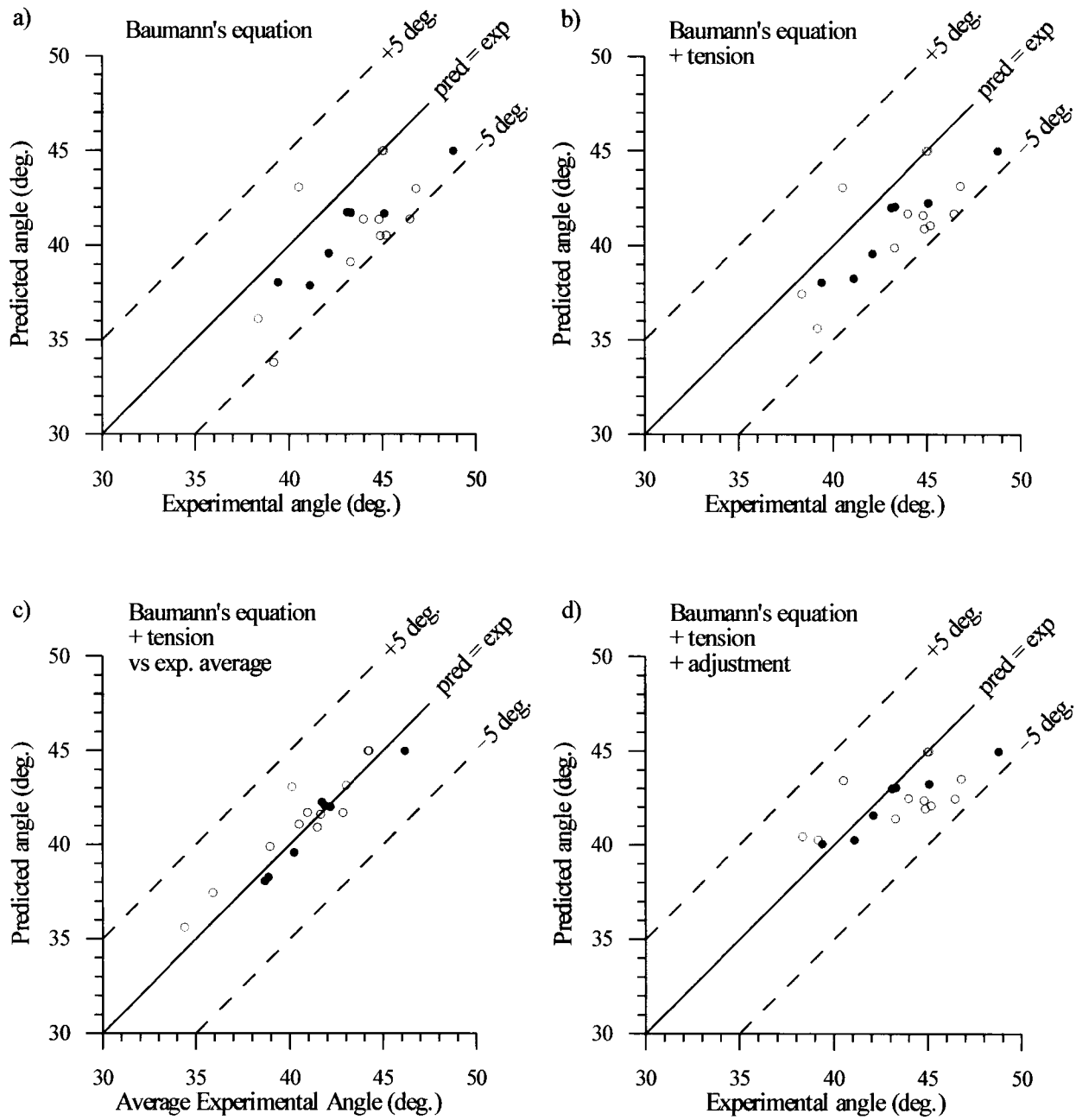

Figure 4.2 Predicted principal stress angle: a) using Baumann's equation, b) including concrete tension, c) compared to average of experimental stress and strain angles, d) with adjustment for ratio of reinforcement (solid = LVDT data, hollow = Vecchio-Collins, 1982 data)

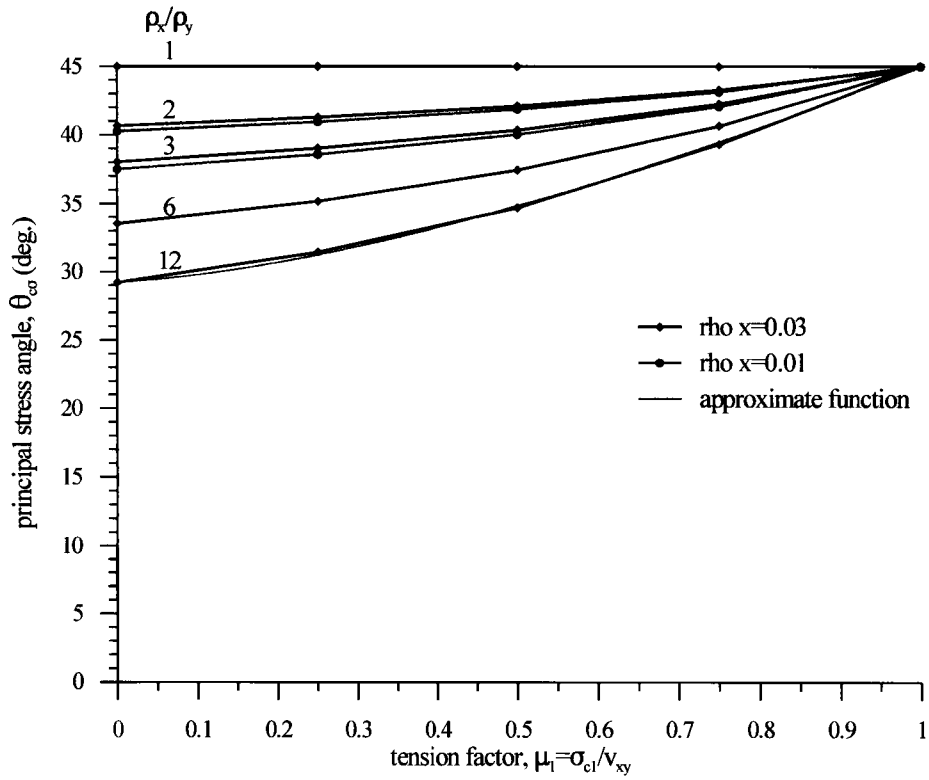

Figure 4.3 Influence of concrete tension stress on predicted principal stress angle ($n_x = n_y = 0$)

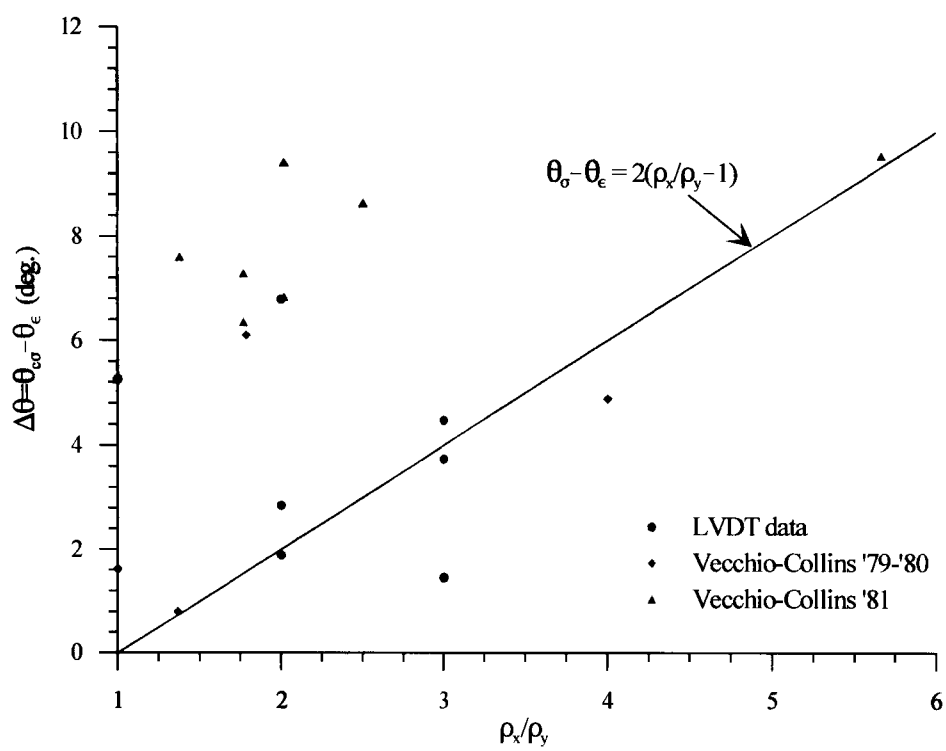

Figure 4.4 Difference between stress and strain angles, as a function of ratio of reinforcement

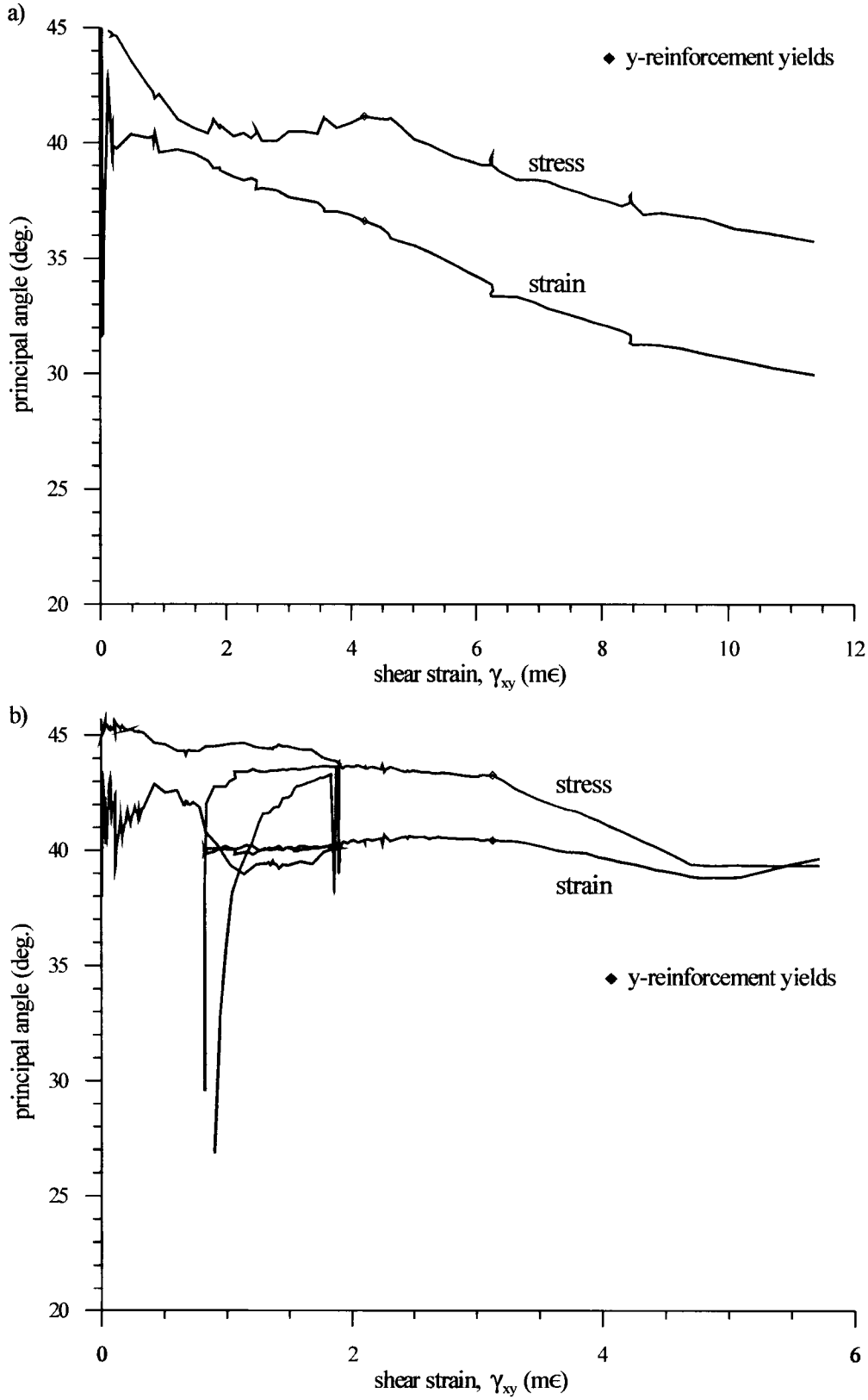

Figure 4.5 Rotation of principal angles: a) PP1, b) PDV1

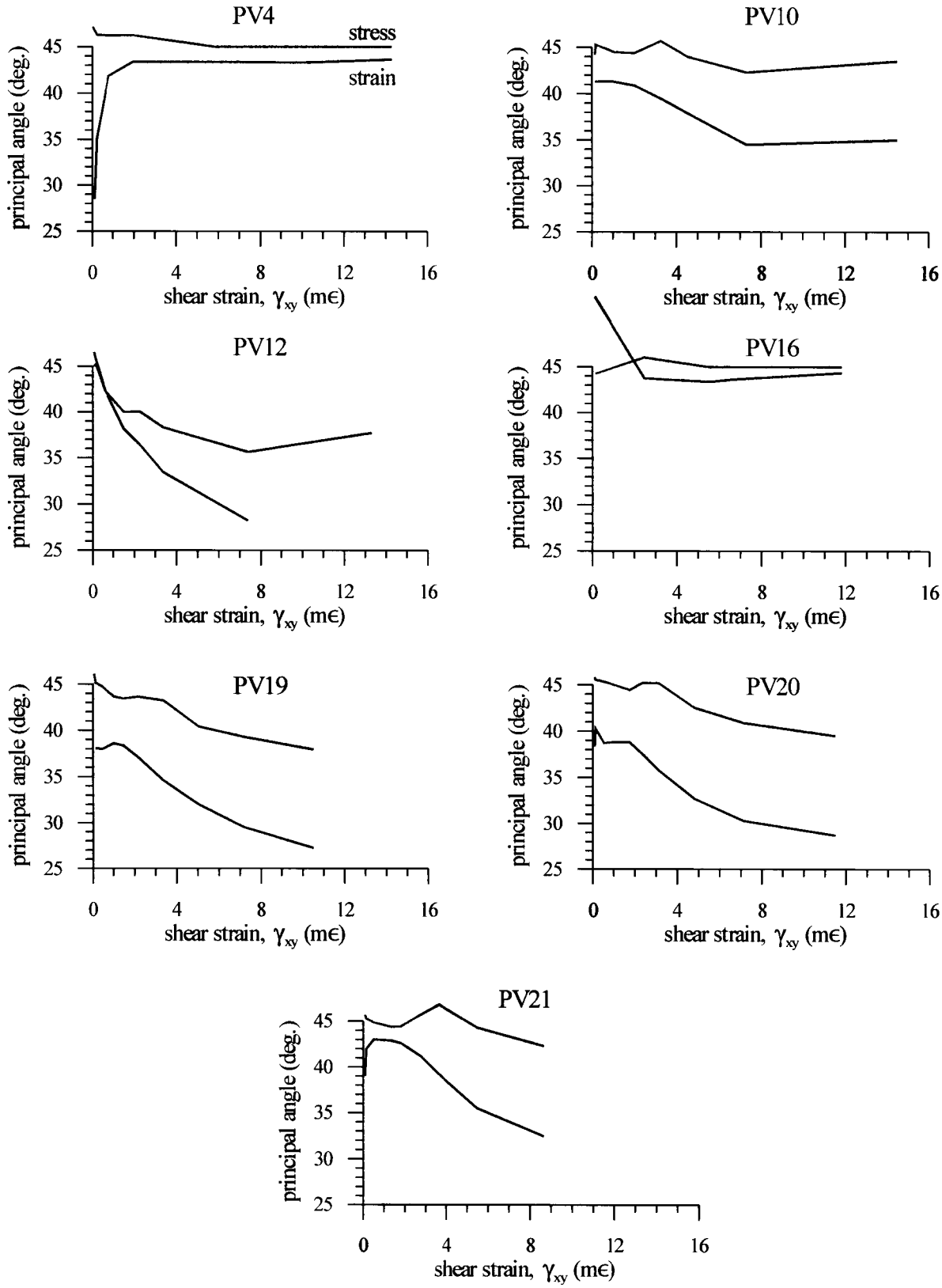

Figure 4.6 Rotation of principal angles: specimens from Vecchio-Collins, 1982 (monotonic loading only)

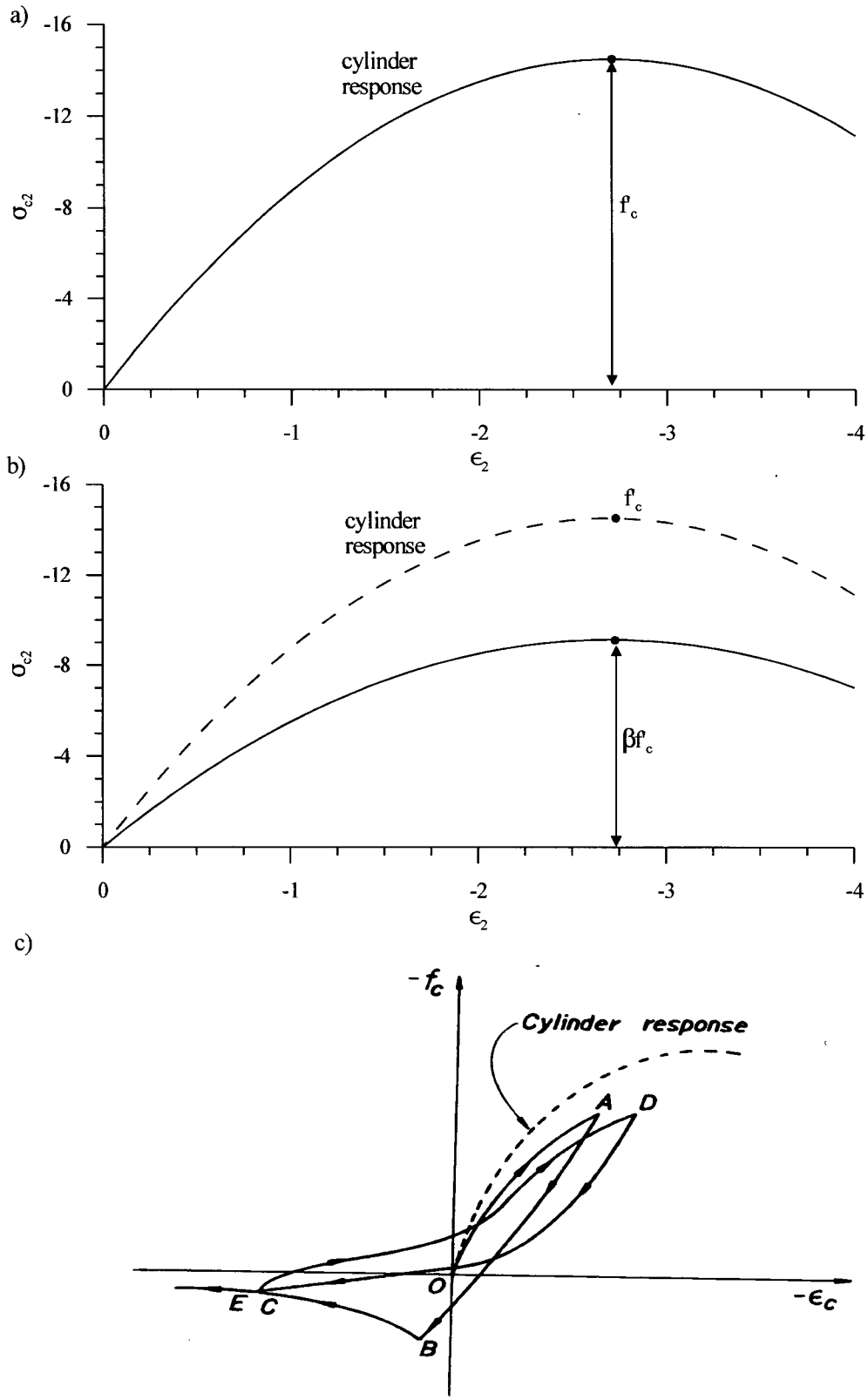

Figure 4.7 Representing concrete in compression: a) uniaxial compression, b) principal compression with transverse tension (e.g., from monotonic shear loading), c) associated with reverse-cyclic shear loading (from Stevens, 1987)

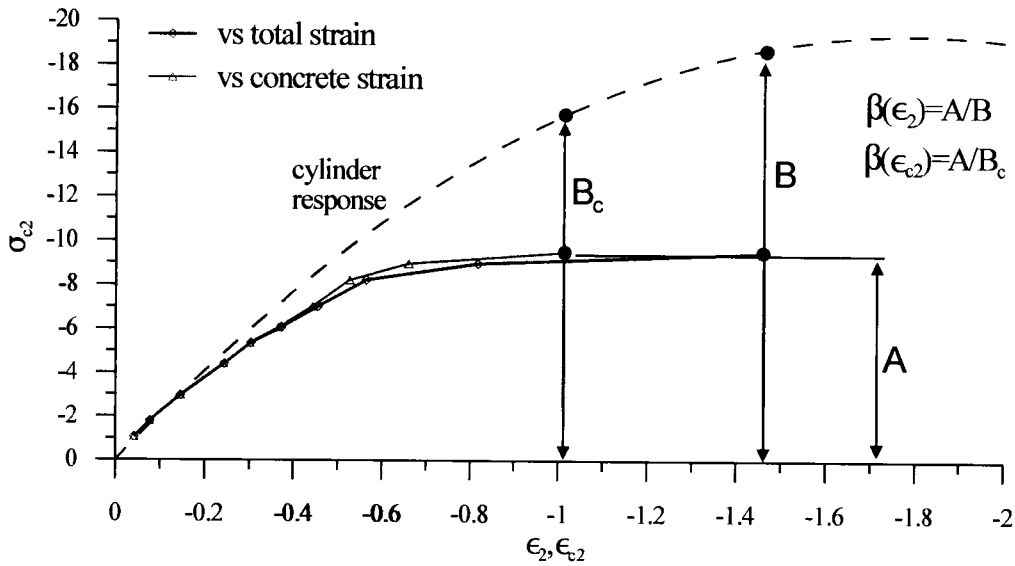

Figure 4.8 Comparing concrete principal strain and total principal strain (PV21)

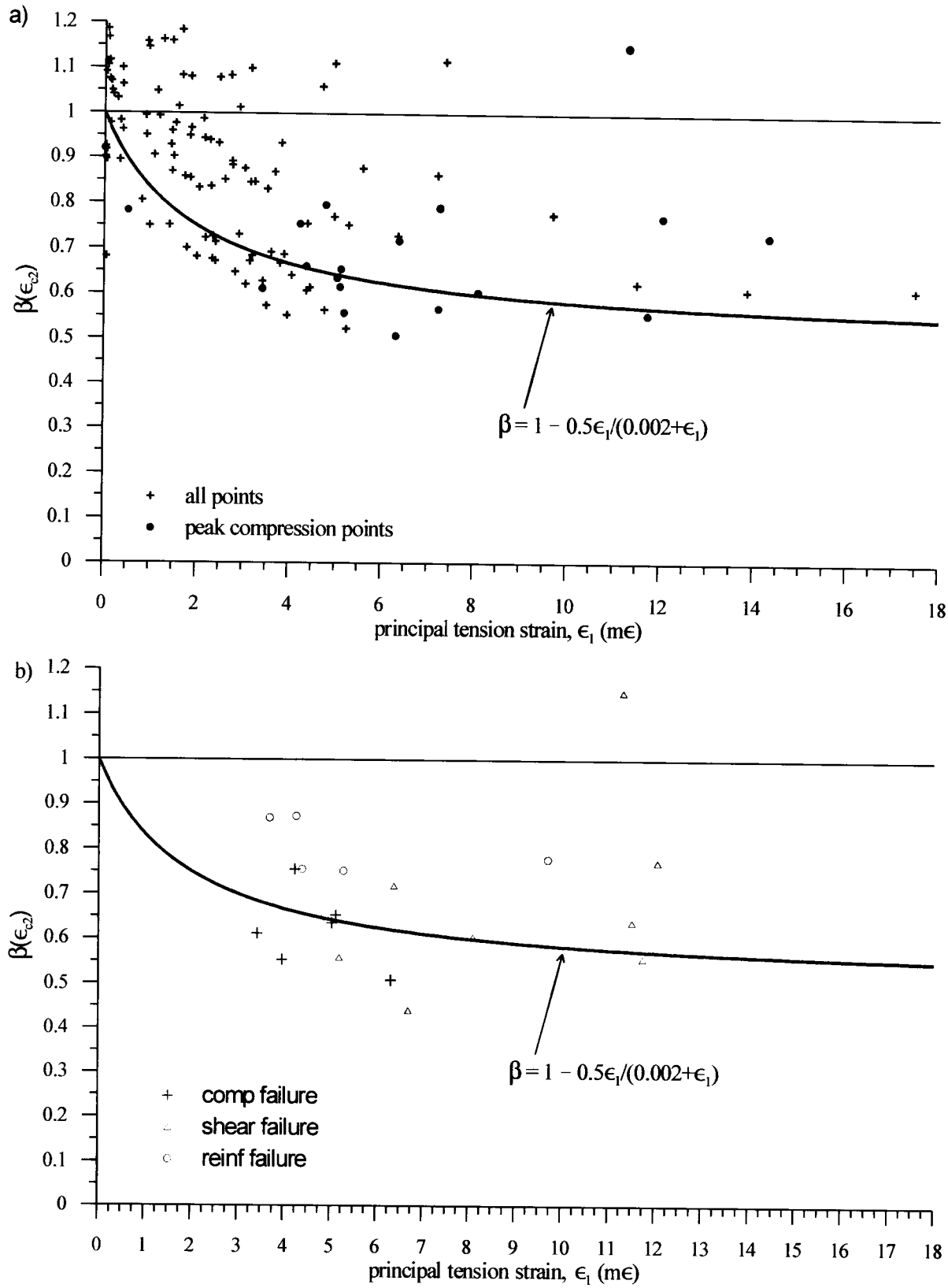

Figure 4.9 Concrete compression softening function: a) all data points, b) failure points only

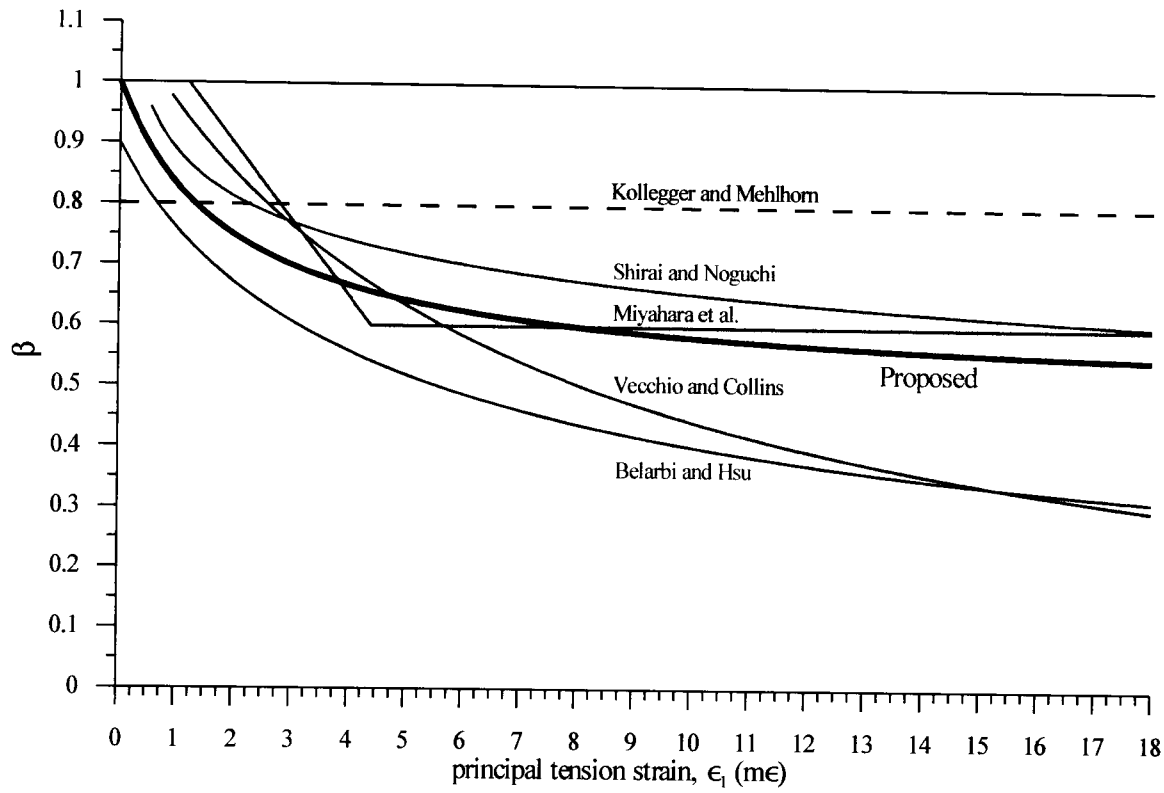

Figure 4.10 Comparison of concrete compression softening functions

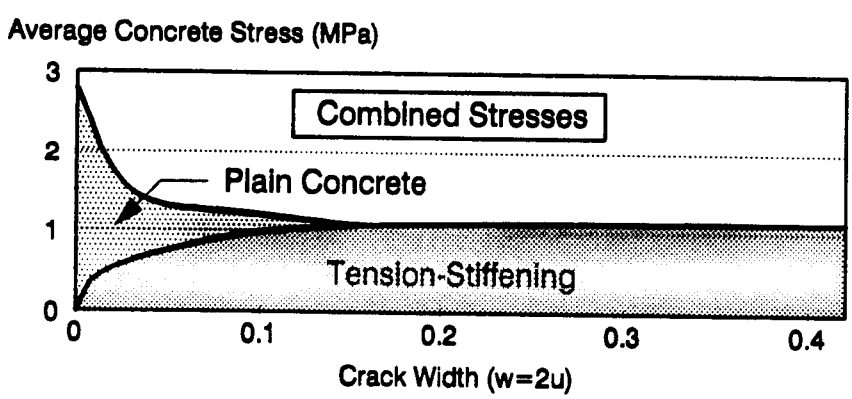

Figure 4.11 Average tensile stresses in reinforced concrete (from Fronteddu, 1993)

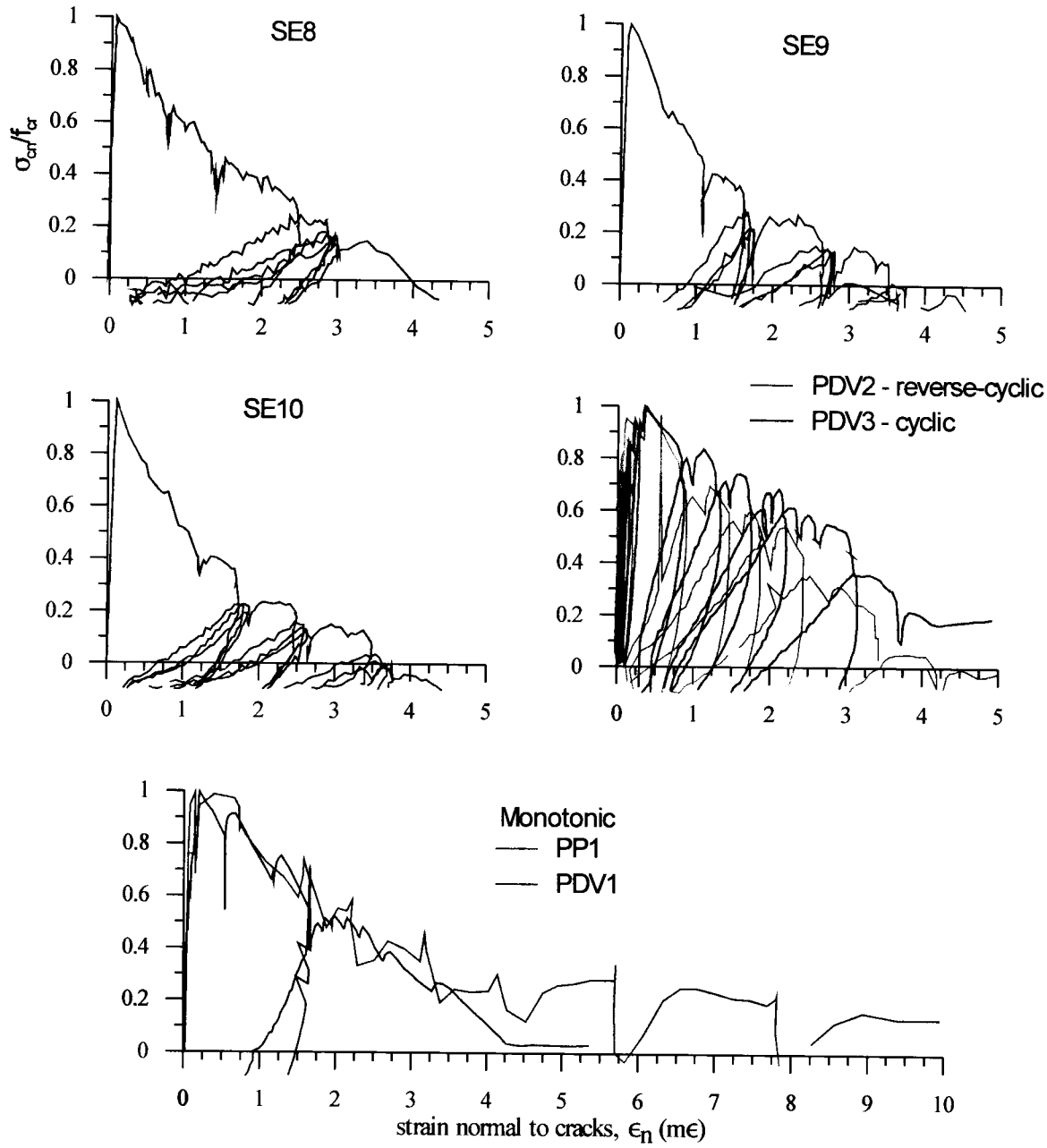

Figure 4.12 Principal concrete tension stress: LVDT data

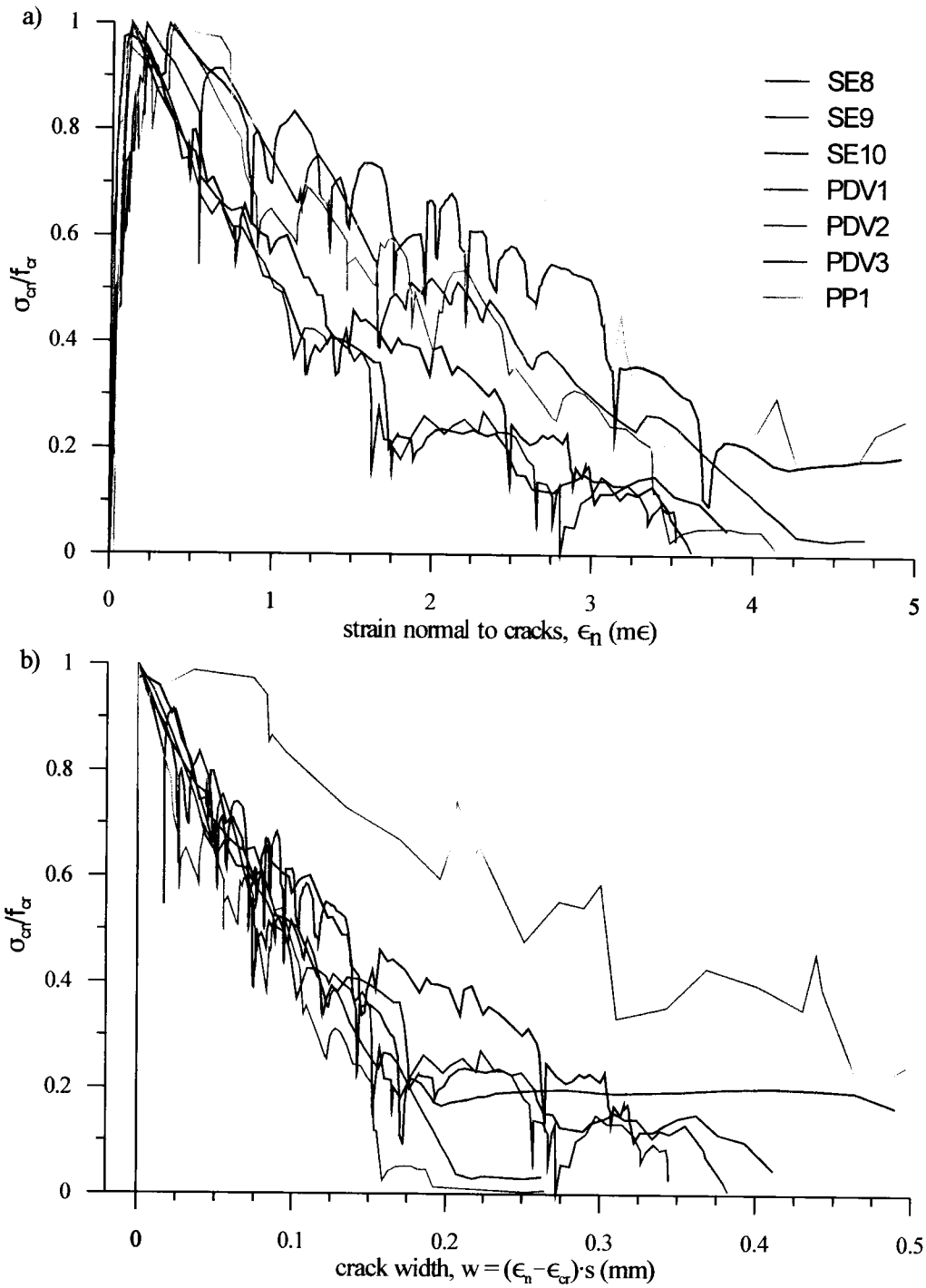

Figure 4.13 Principal concrete tension stress: a) vs strain normal to cracks, b) vs estimated crack width

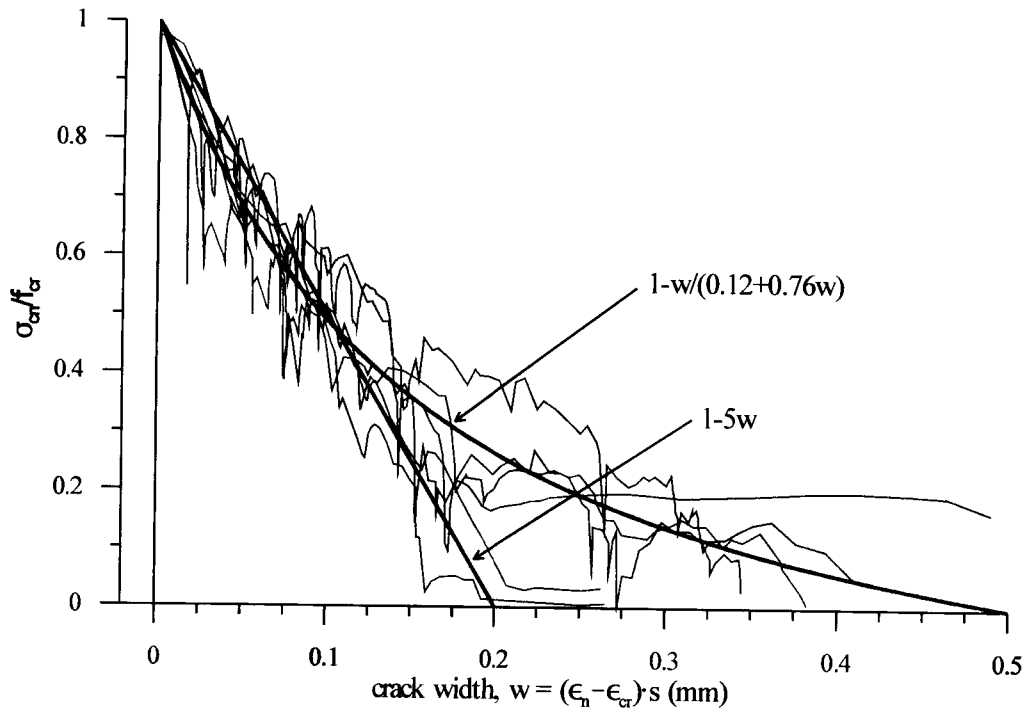

Figure 4.14 Residual concrete tension function

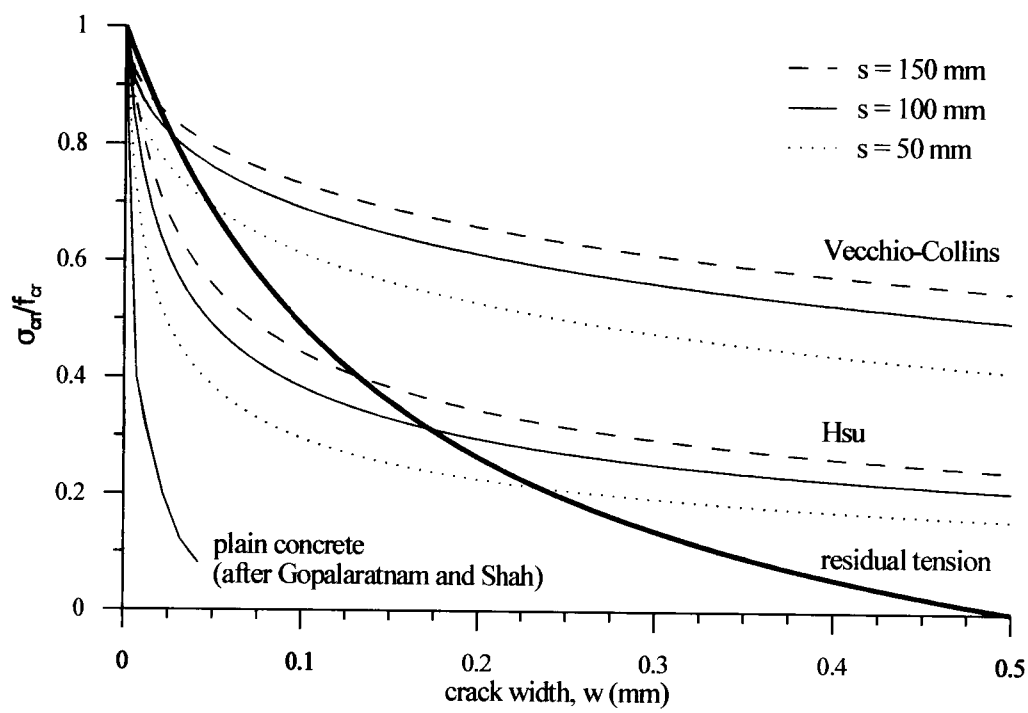

Figure 4.15 Comparison of concrete tension functions

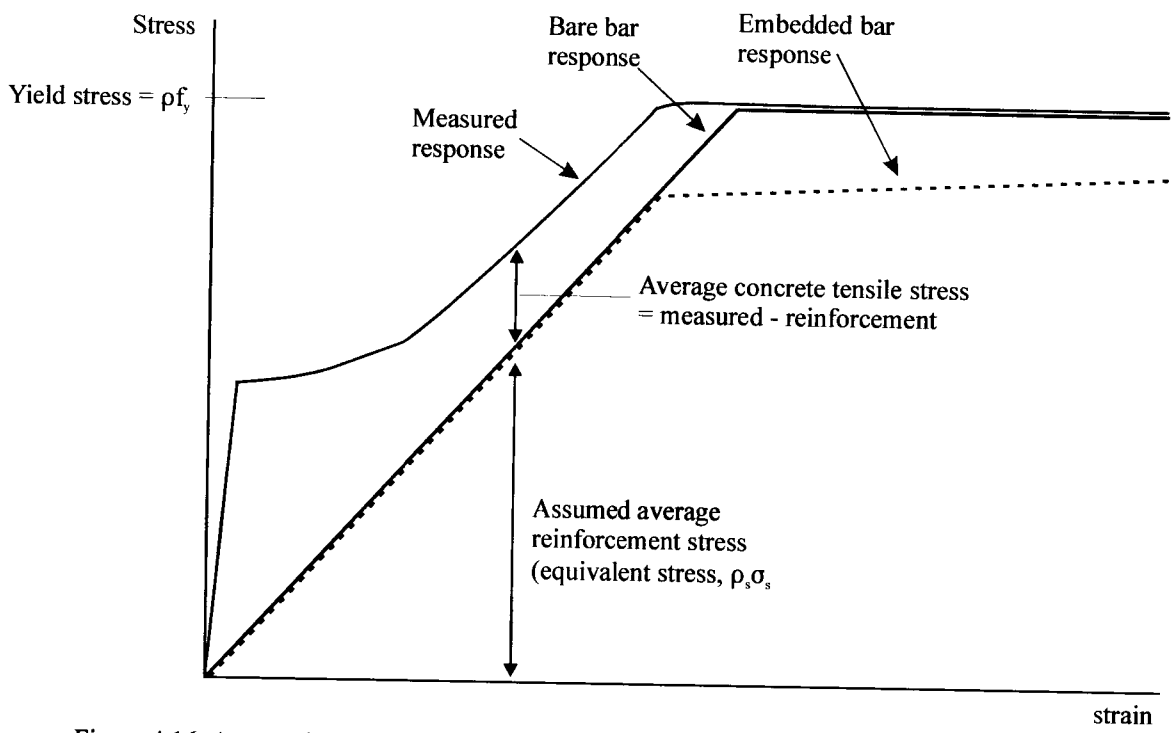

Figure 4.16 Assumed reinforcement stresses: bare bar vs embedded bar (reduced yield stress)

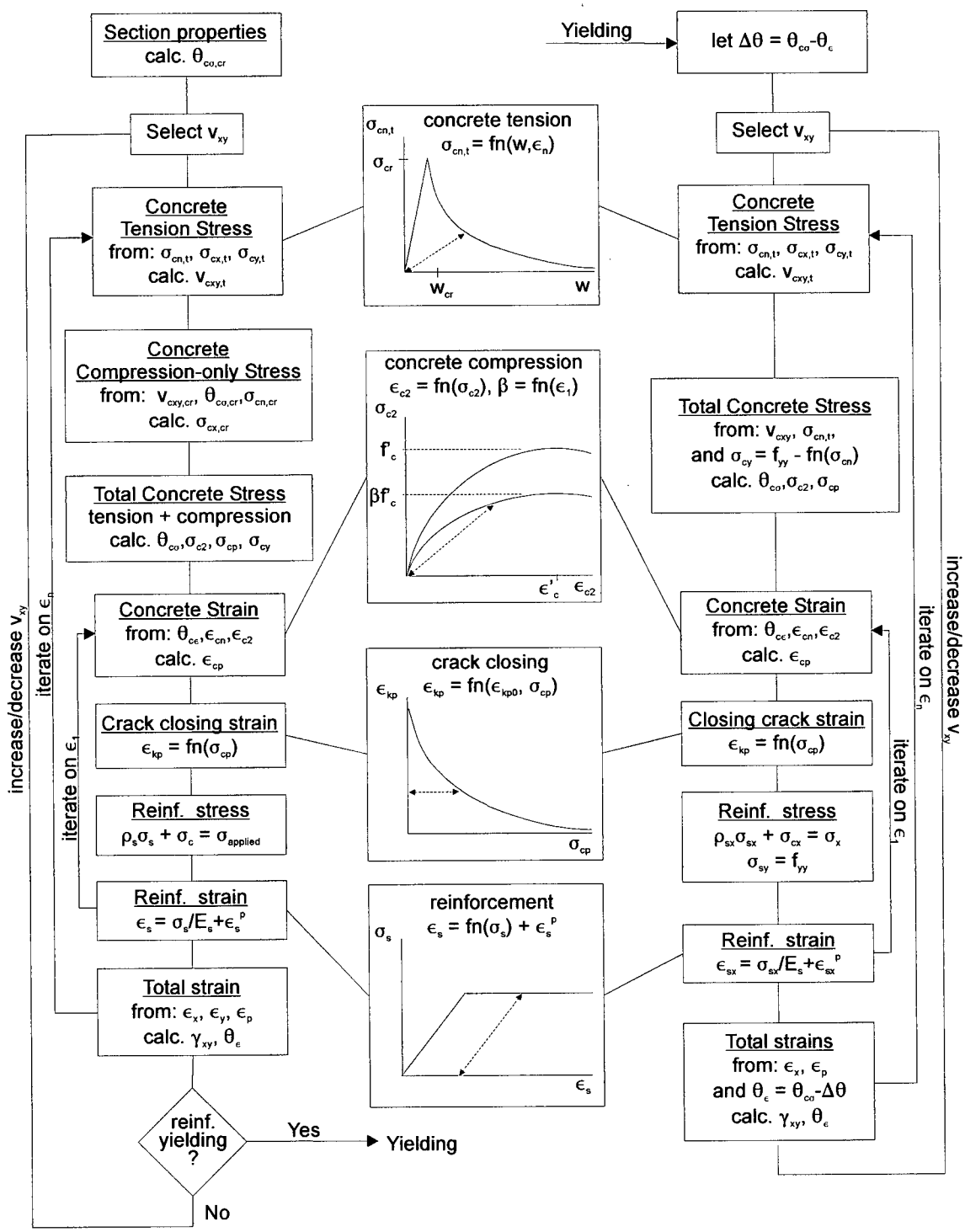

Figure 5.1 Solution algorithm for proposed model (as implemented in computer program)

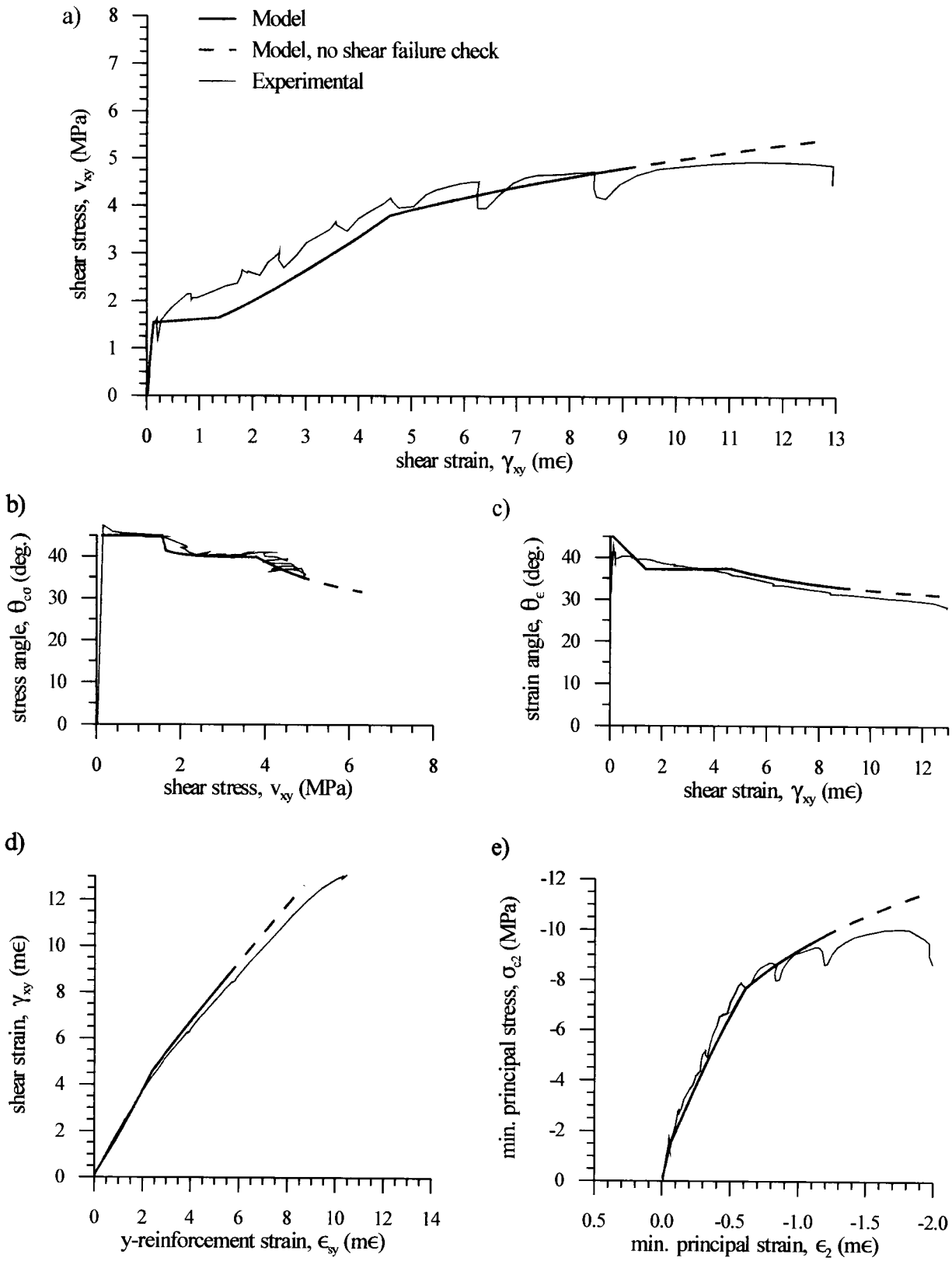

Figure 5.2 Model prediction, PP1: a) shear stress, b) principal stress angle, c) principal strain angle, d) *y*-reinforcement strain, e) concrete compression stress

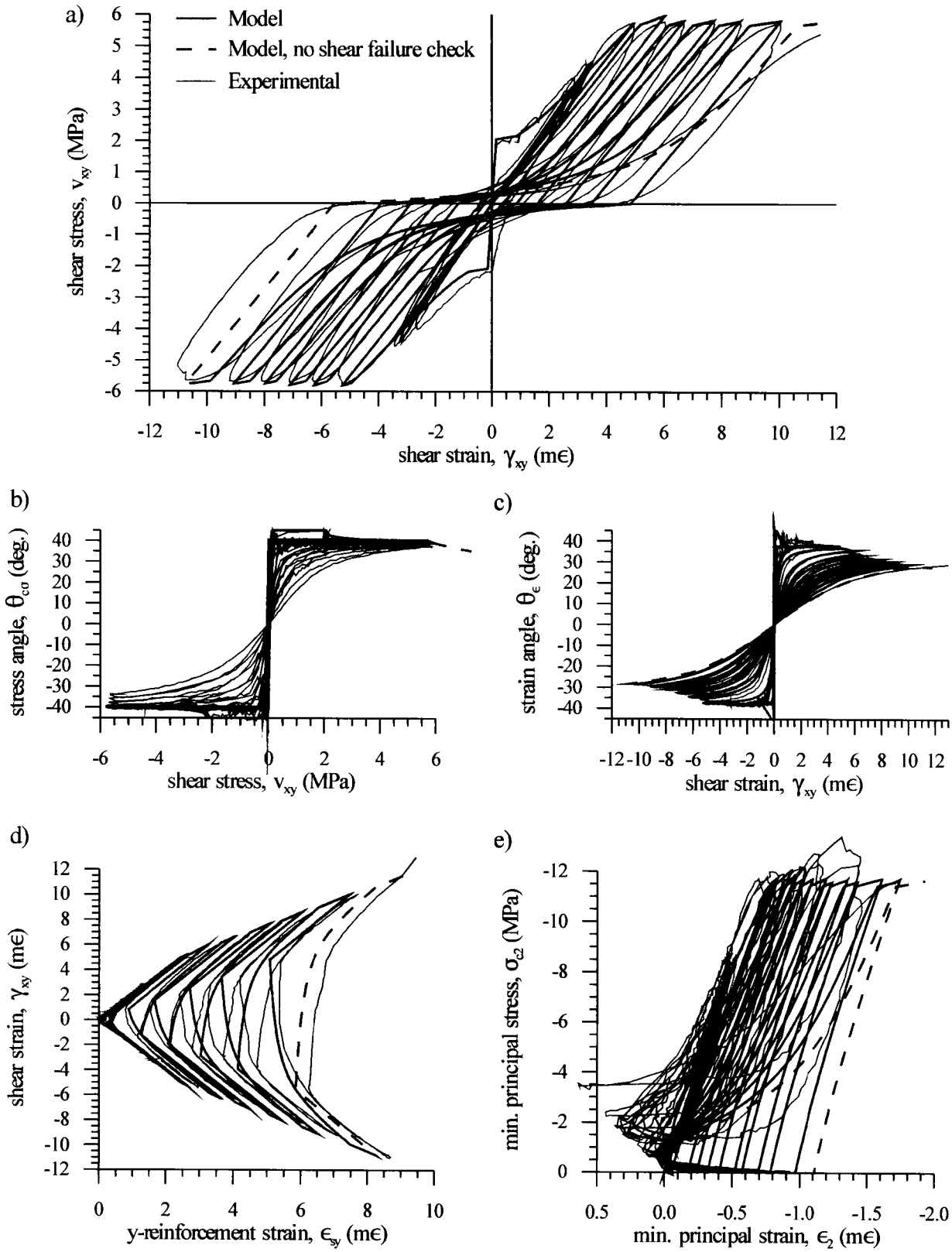

Figure 5.3 Model prediction, SE8: a) shear stress, b) principal stress angle, c) principal strain angle, d) *y*-reinforcement strain, e) concrete compression stress

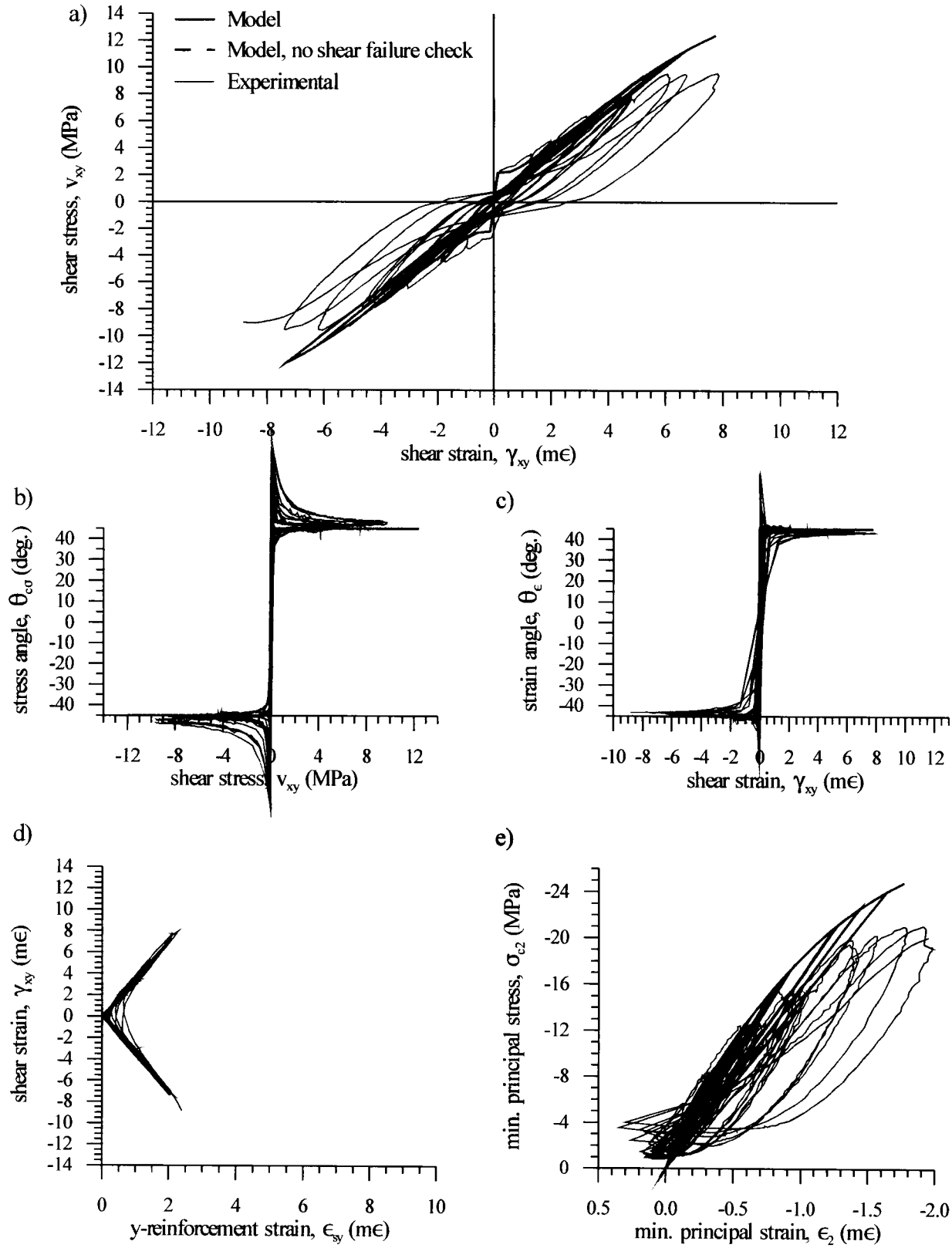

Figure 5.4 Model prediction, SE9: a) shear stress, b) principal stress angle, c) principal strain angle, d) *y*-reinforcement strain, e) concrete compression stress

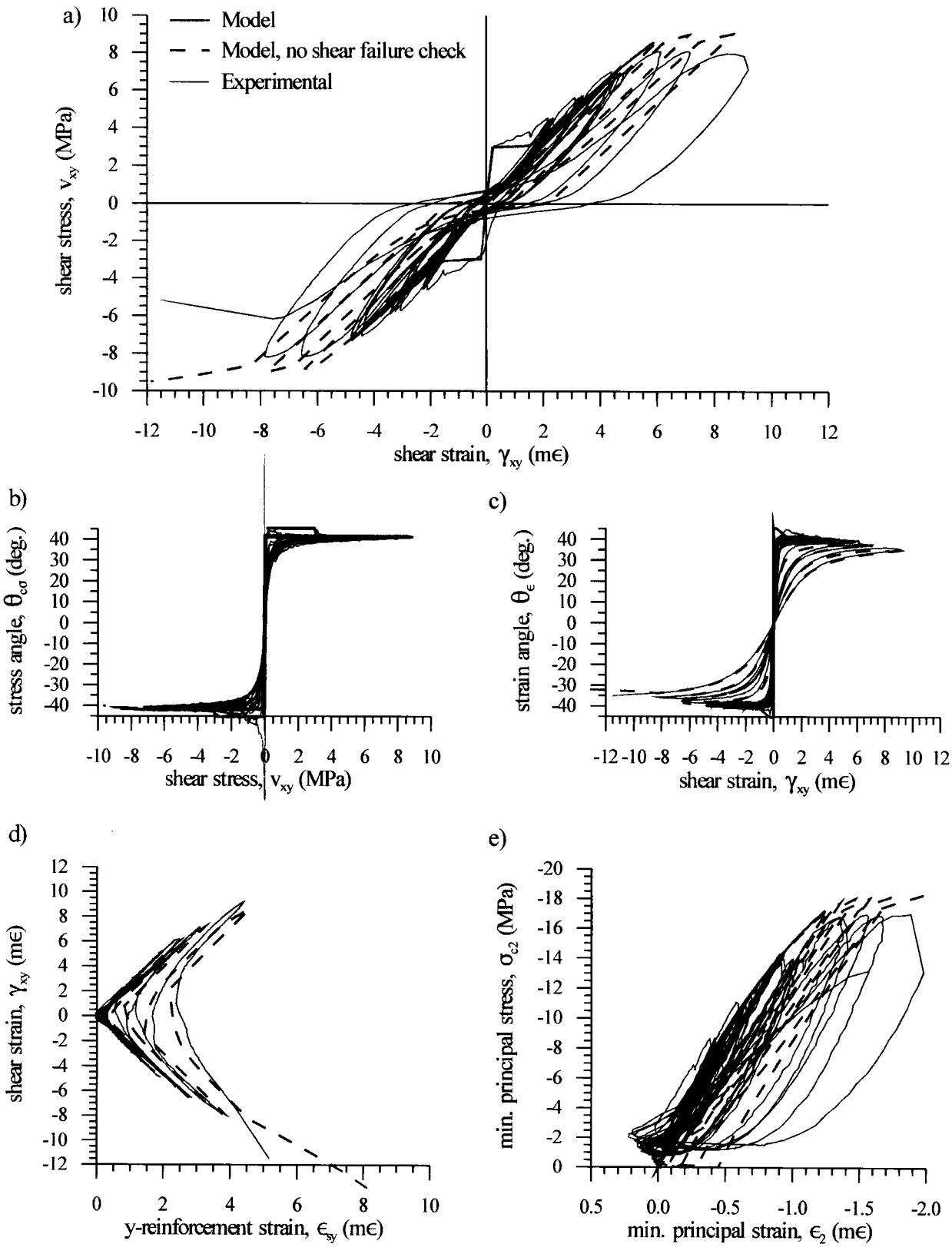

Figure 5.5 Model prediction, SE10: a) shear stress, b) principal stress angle, c) principal strain angle, d) *y*-reinforcement strain, e) concrete compression stress

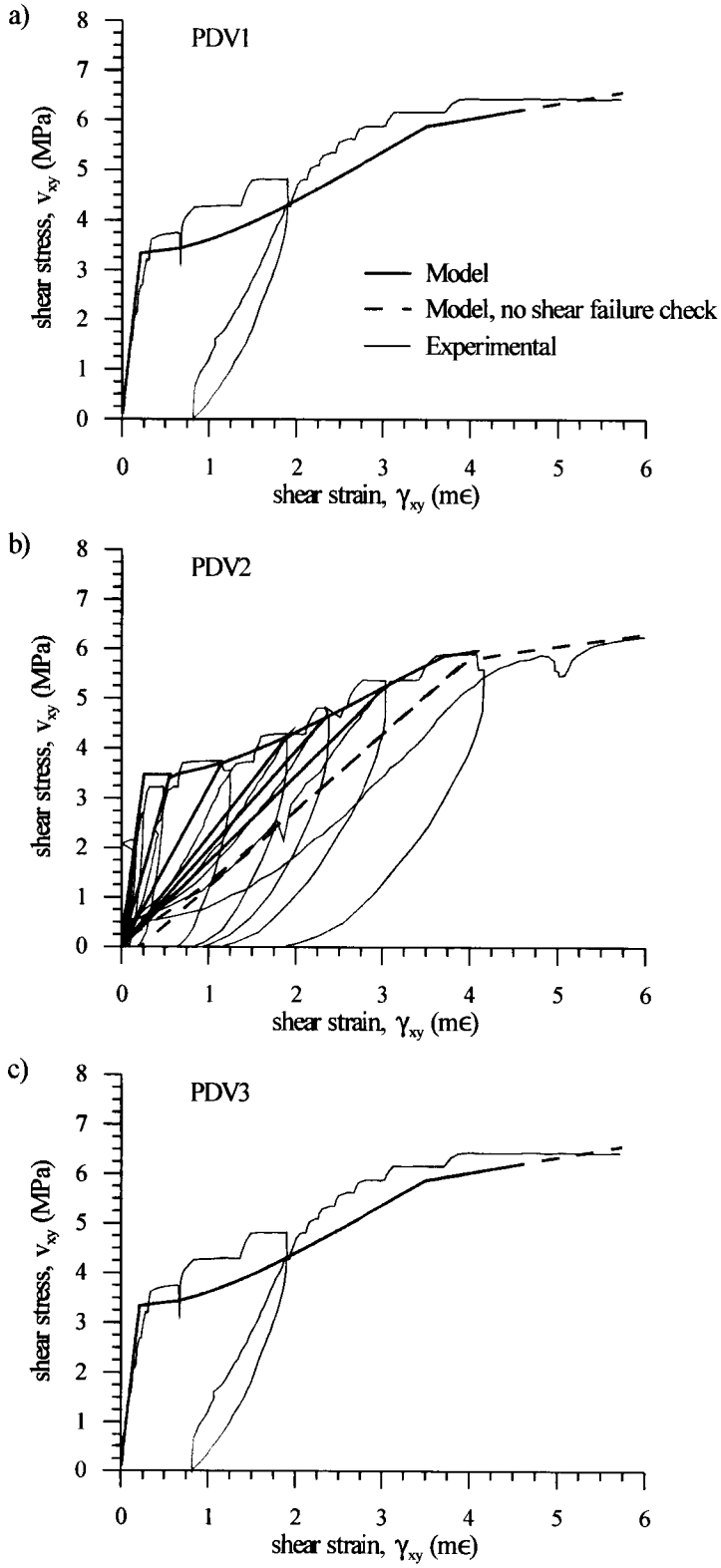

Figure 5.6 Model prediction, shear stress vs shear strain:
a) PDV1, b) PDV2, c) PDV3

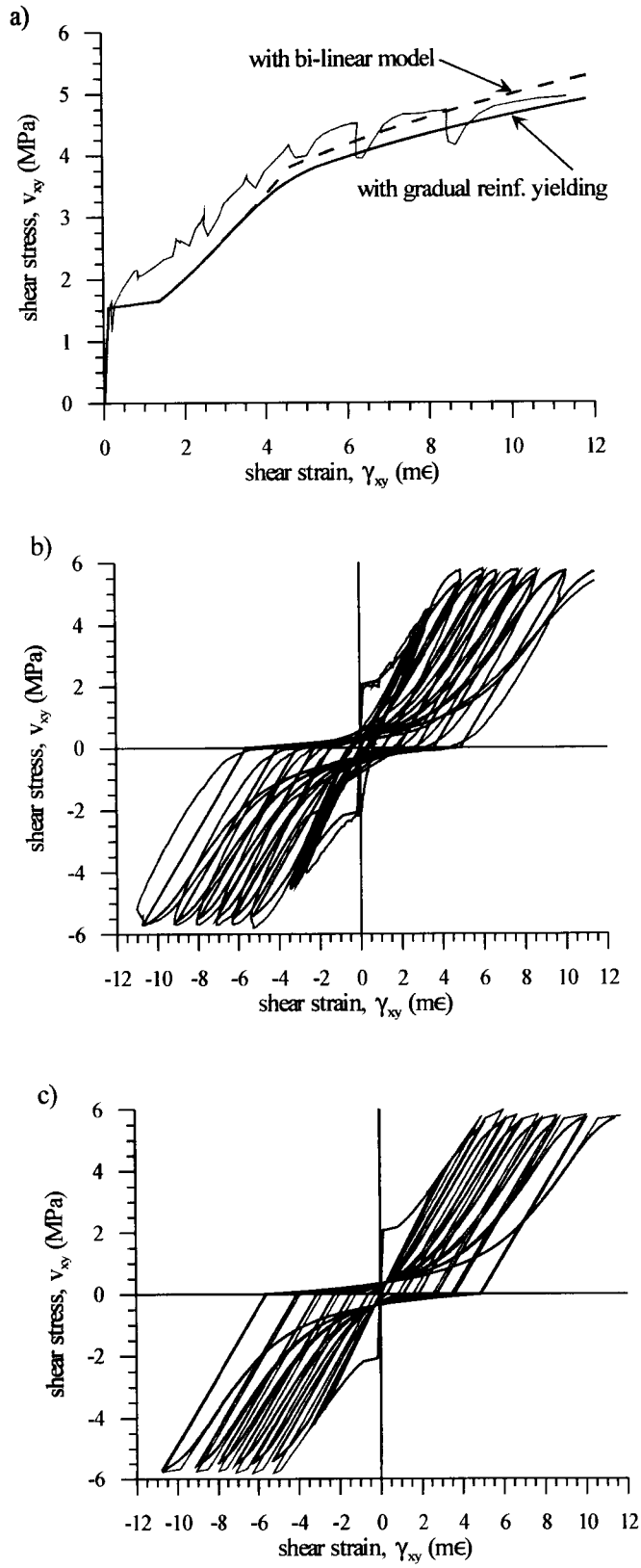

Figure 5.7 Model predictions using gradual-yield reinforcement model: a) PP1, b) SE8 - compared to experimental, c) SE8 - compared to bi-linear reinforcement model

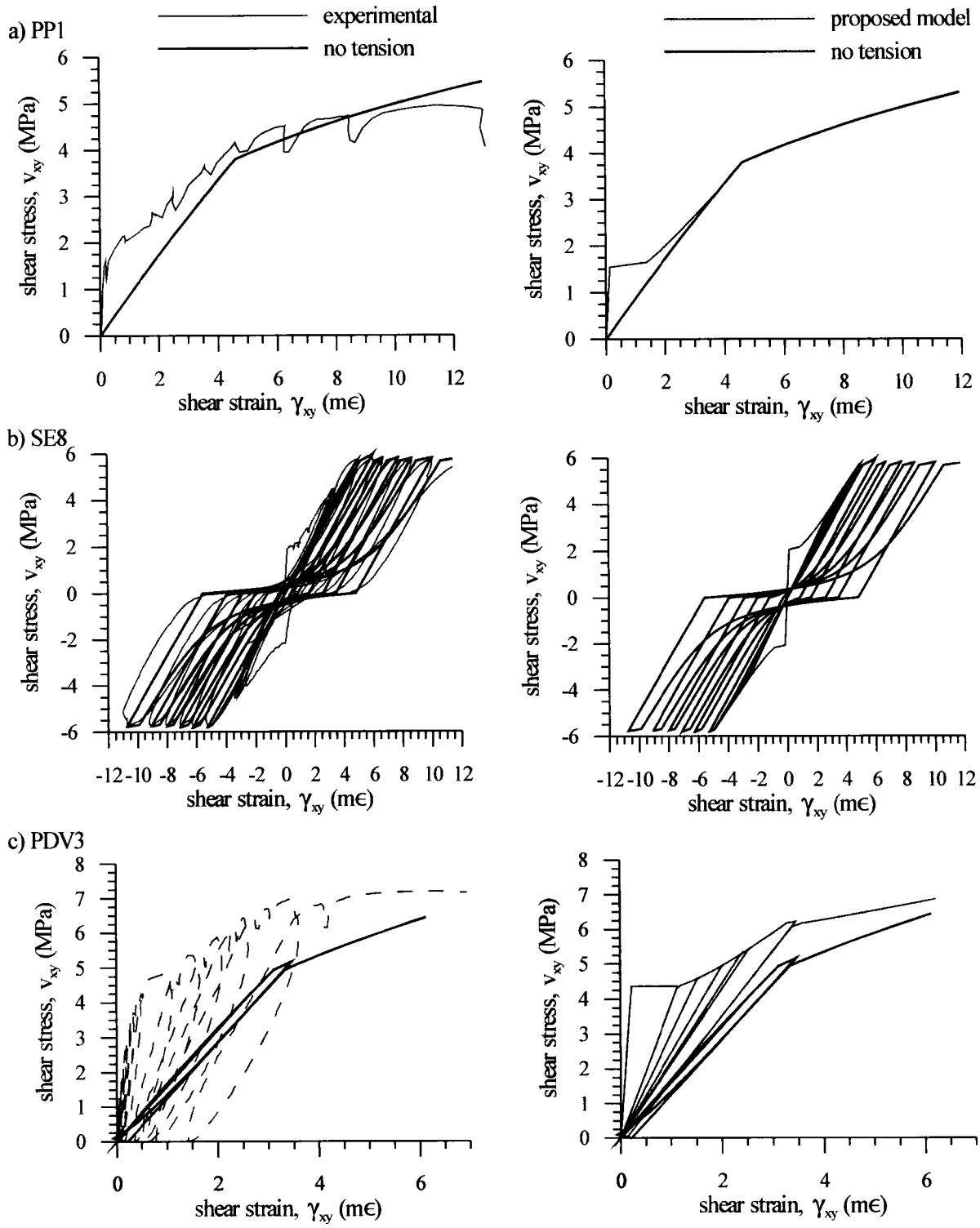

Figure 5.8 Model predictions without concrete tension: a) PP1, b) SE8, c) PDV3

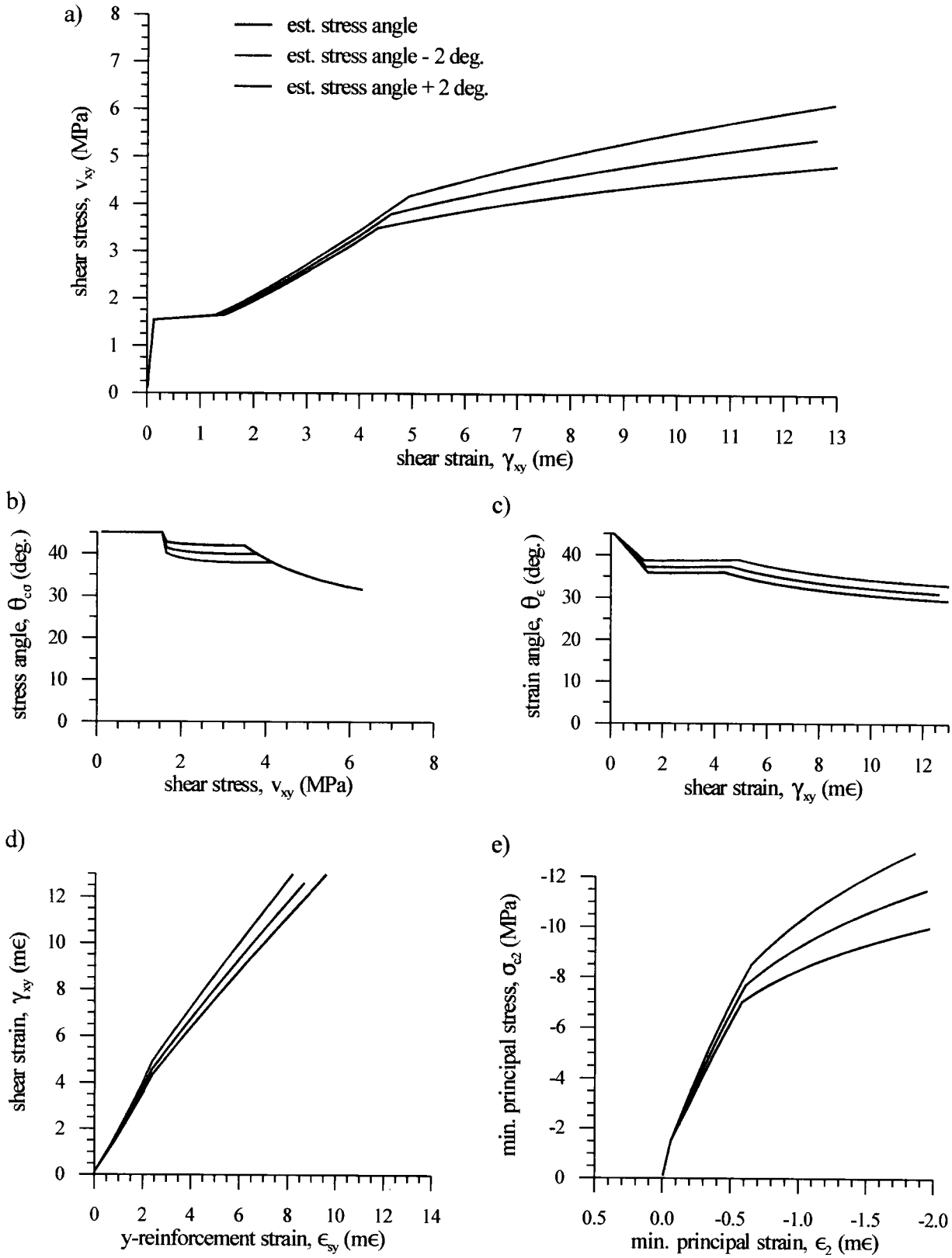

Figure 5.9 Sensitivity of predicted values to principal stress angle, PP1: a) shear stress, b) principal stress angle, c) principal strain angle, d) *y*-reinforcement strain, e) concrete compression stress

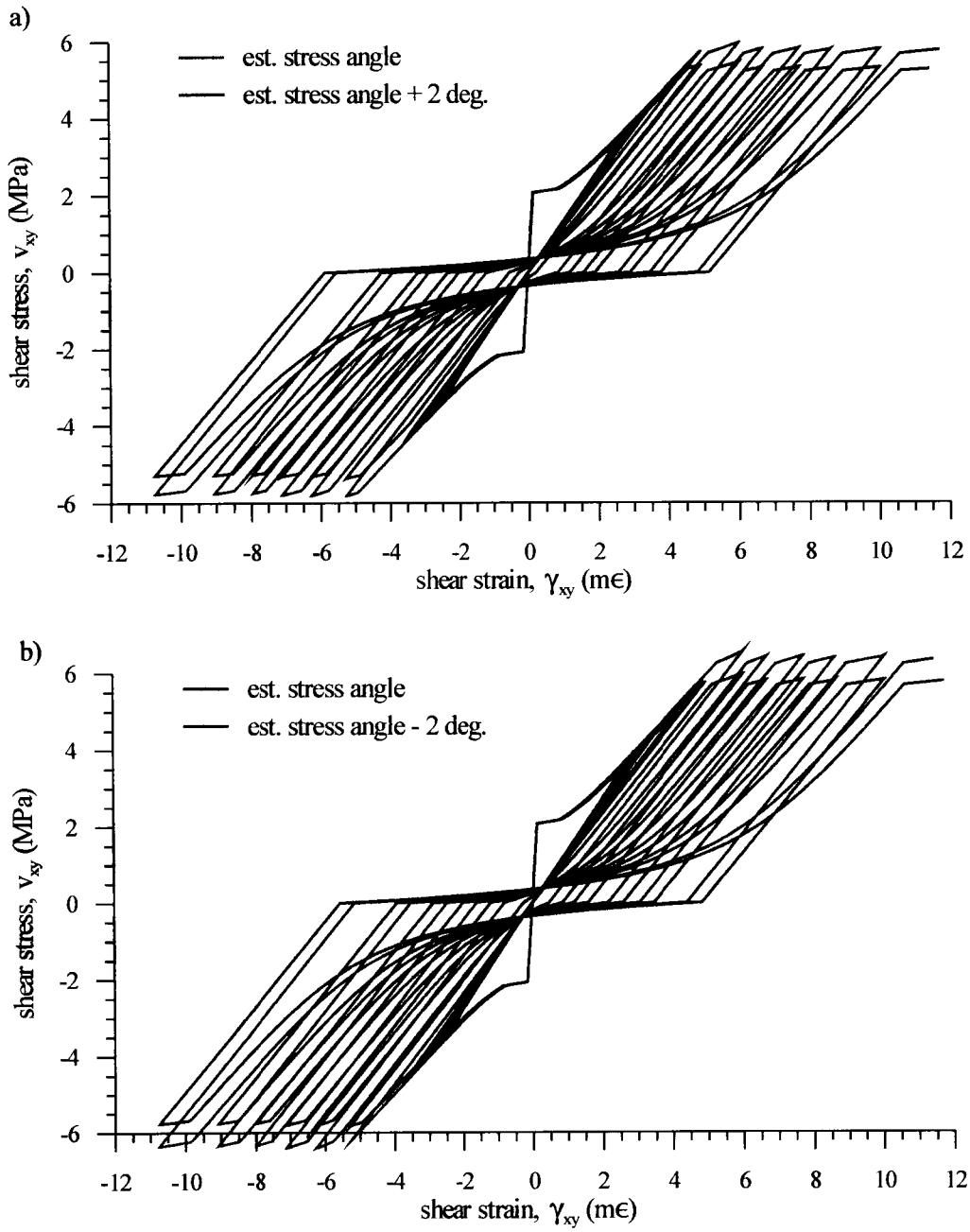

Figure 5.10 Sensitivity of predicted values to principal stress angle, SE8: a) calculated angle + 2°, b) calculated angle - 2°

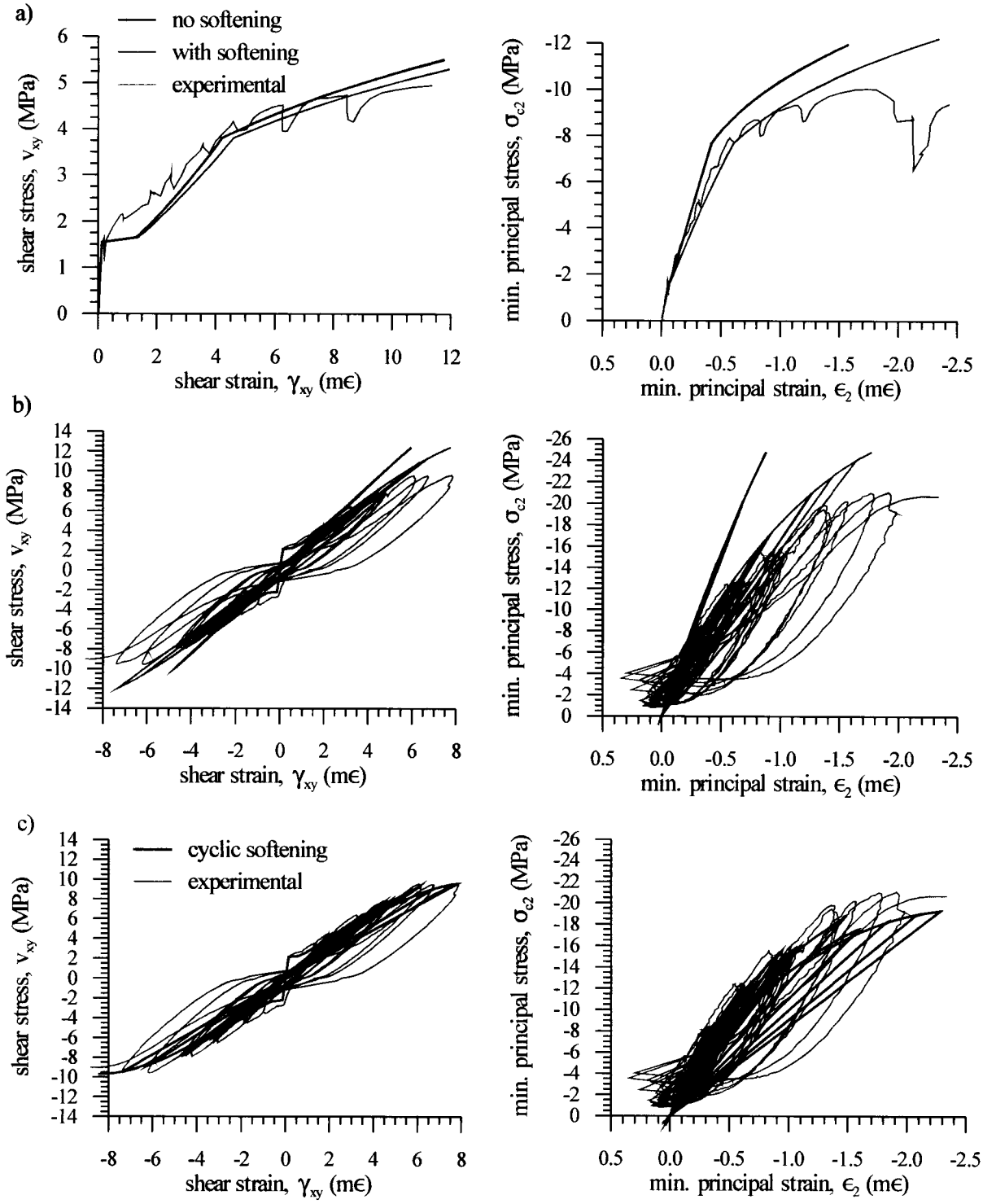

Figure 5.11 Influence of concrete compression softening: a) PP1 - no softening, b) SE9 - no softening, c) SE9 - cyclic softening

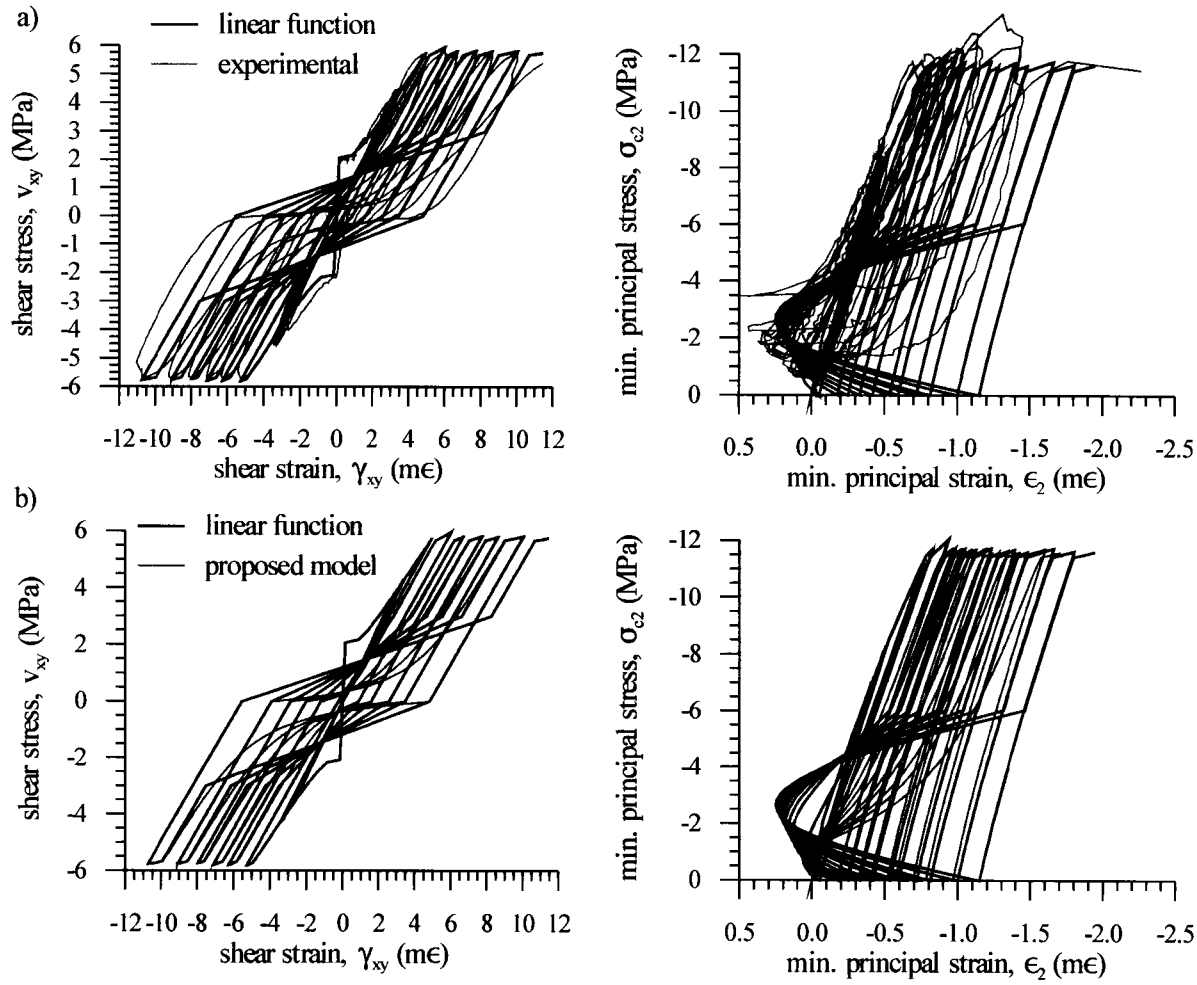

Figure 5.12 Influence of crack closing function on shear stress and concrete compression stress, SE8: a) compared to experimental, b) compared to proposed model

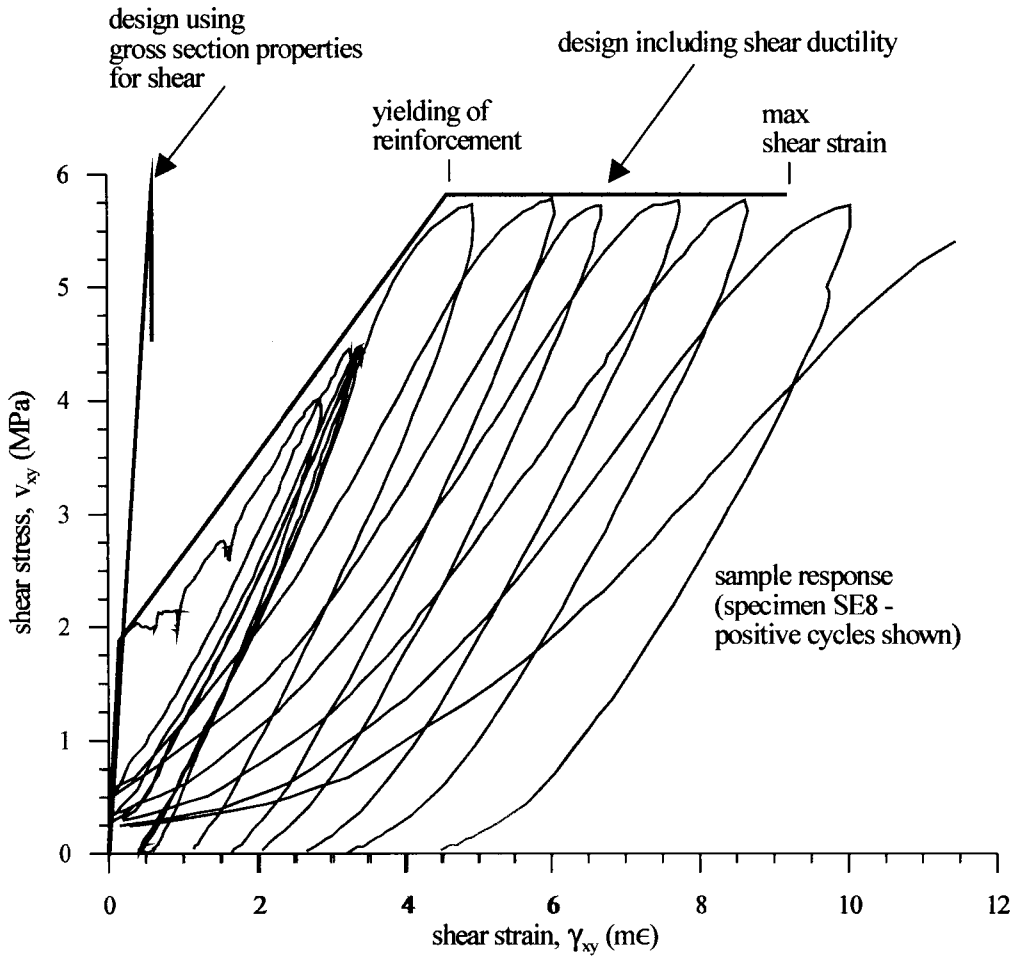

Figure 6.1 Designing for a ductile shear response

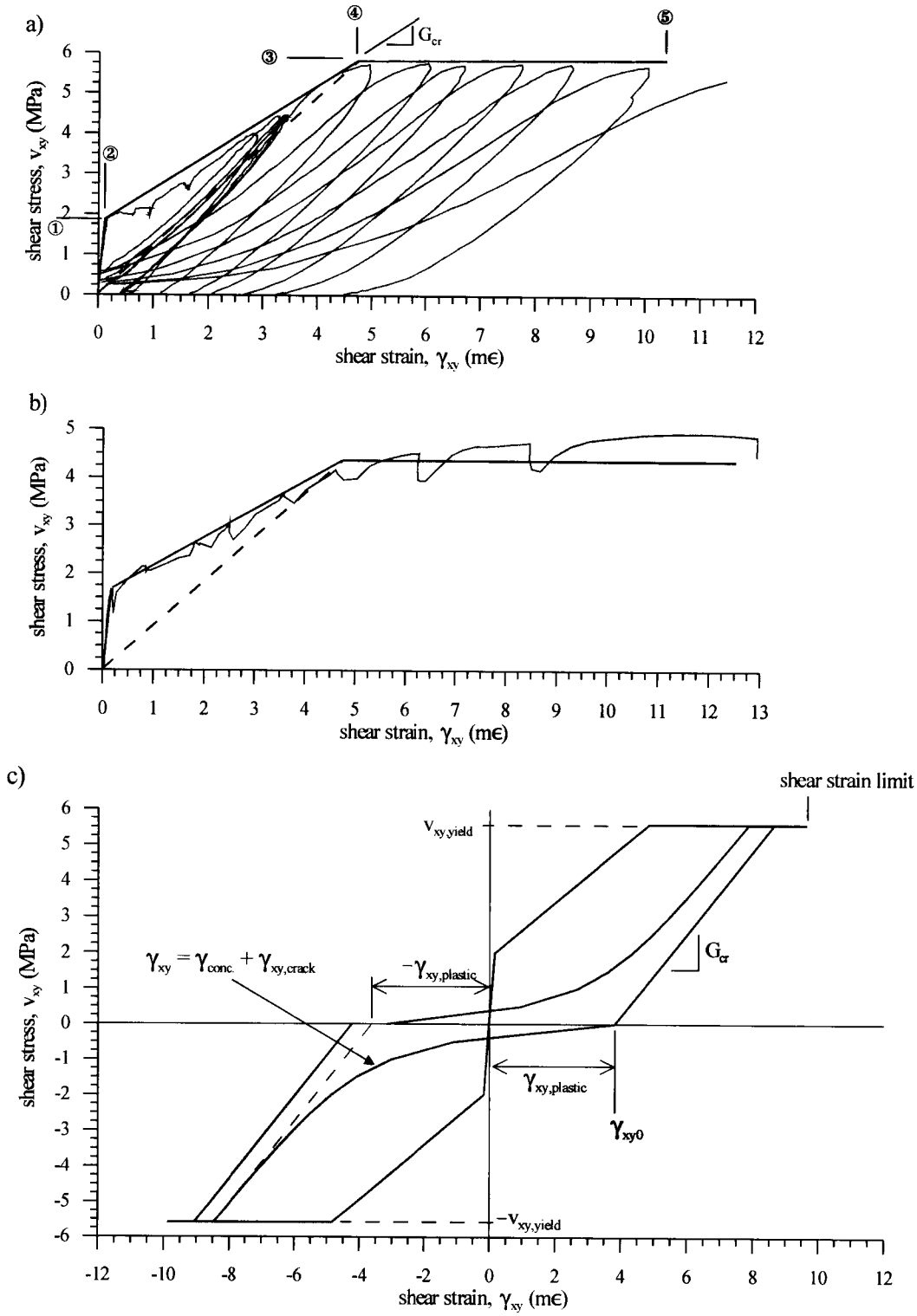

Figure 6.2 Simplified models: a) linear envelope applied to SE8, b) linear envelope applied to PP1, c) reverse-cyclic model

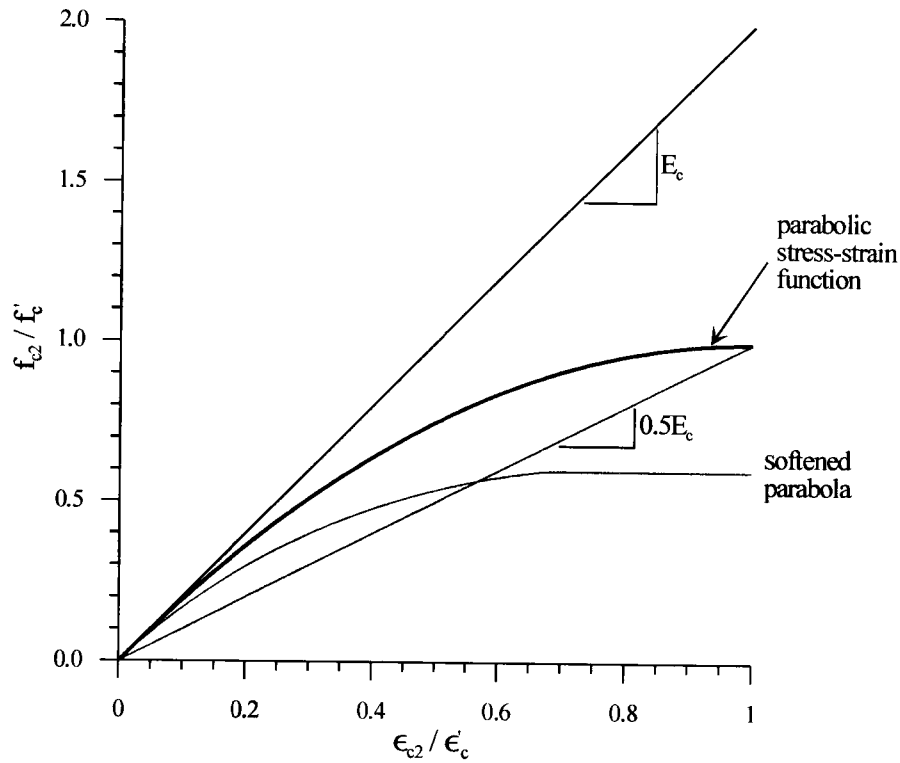

Figure 6.3 Linear approximation for the concrete in compression

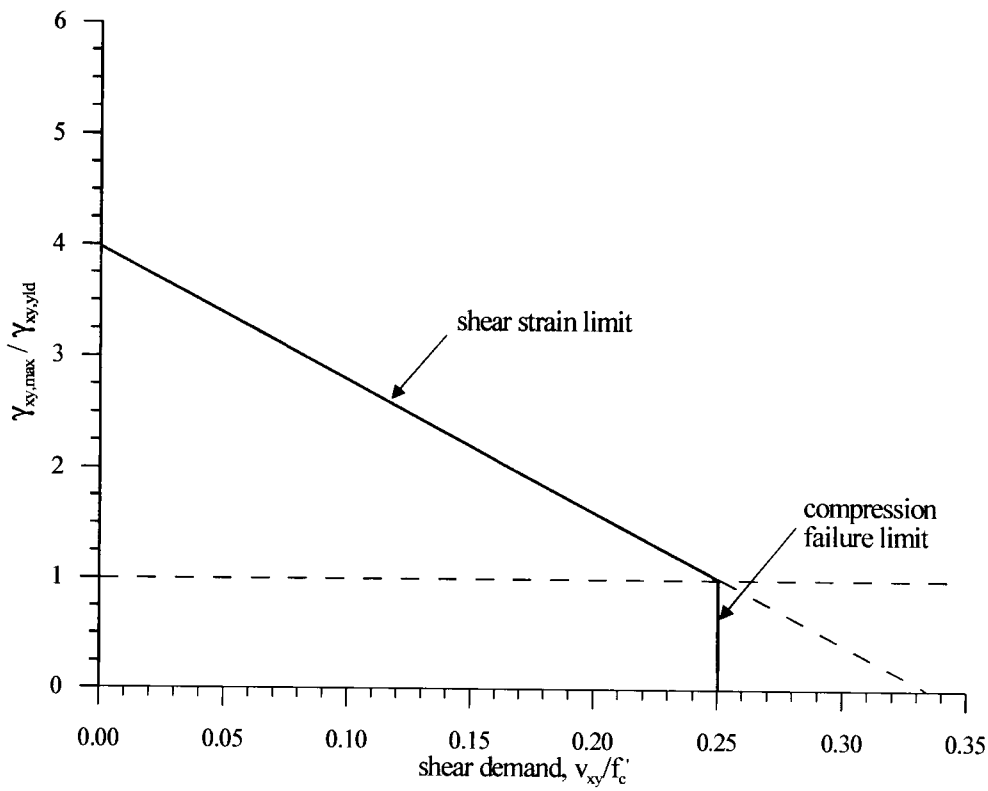

Figure 6.4 Shear strain limit, combined with compression failure check

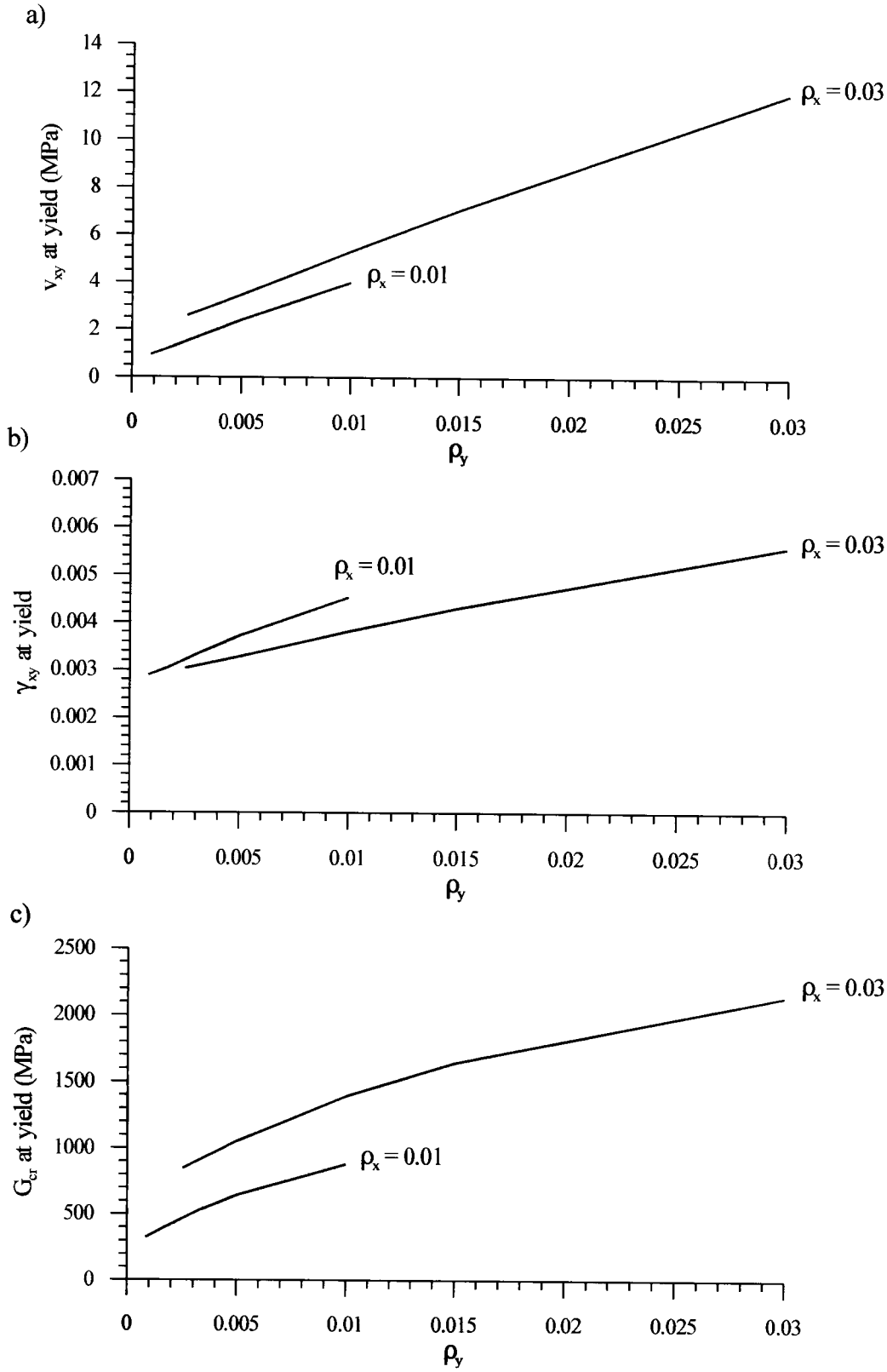

Figure 6.5 Influence of reinforcement ratios: a) on shear stress at yield, b) on shear strain at yield, c) on cracked section shear stiffness

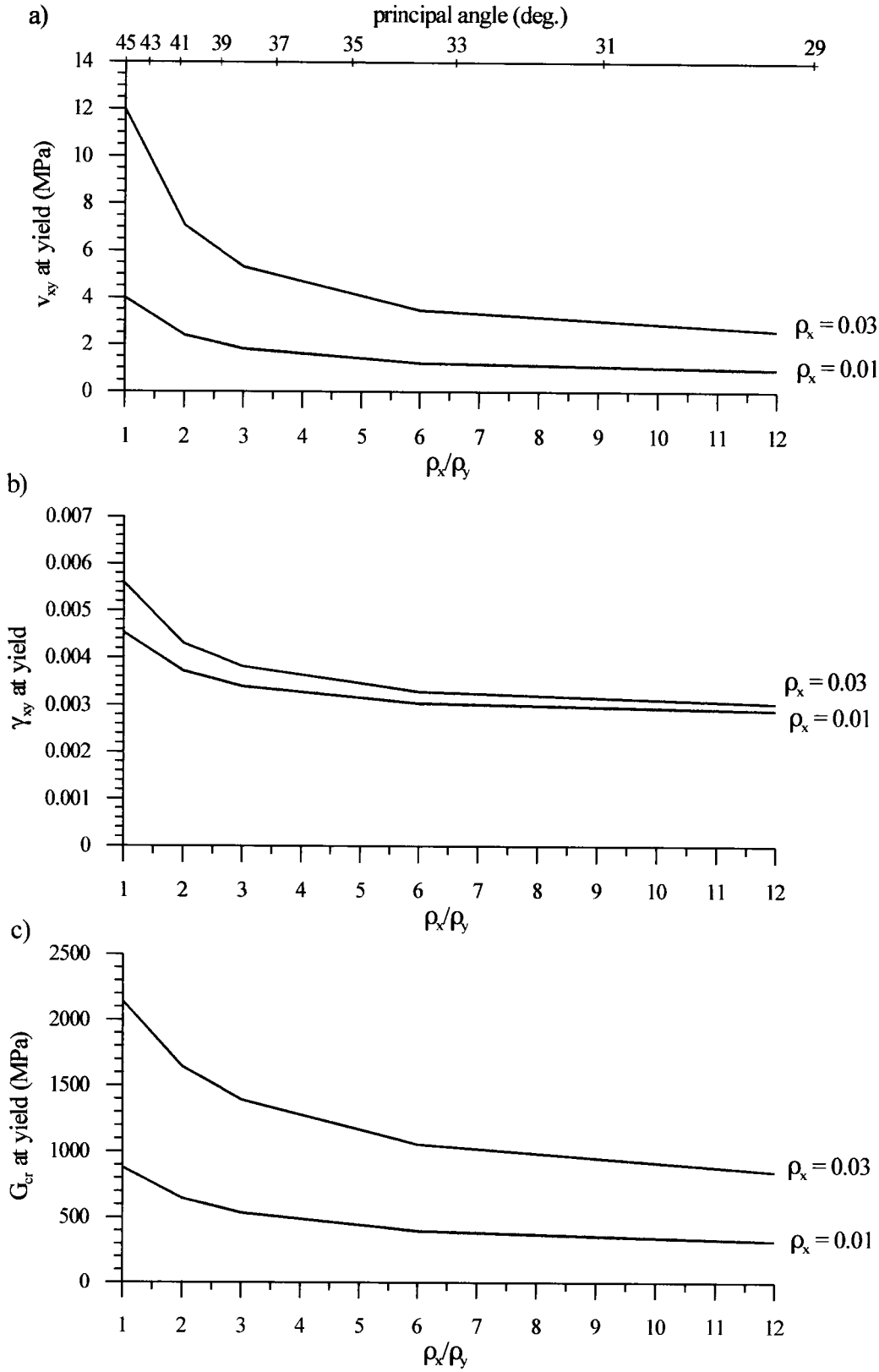

Figure 6.6 Influence of relative reinforcement ratios: a) on shear stress at yield, b) on shear strain at yield, c) on cracked section shear stiffness

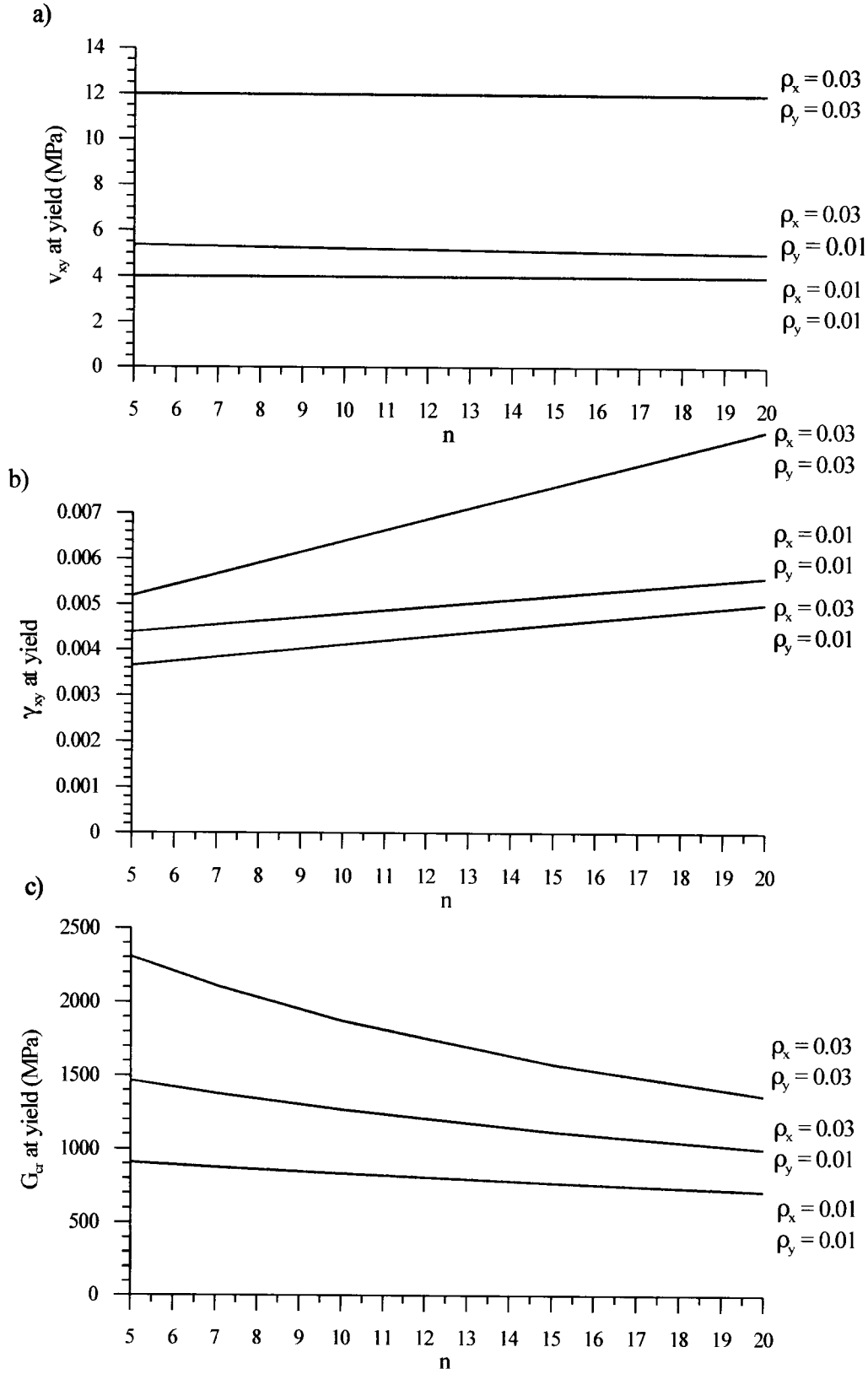

Figure 6.7 Influence of modular ratio, n: a) on shear stress at yield, b) on shear strain at yield, c) on cracked section shear stiffness

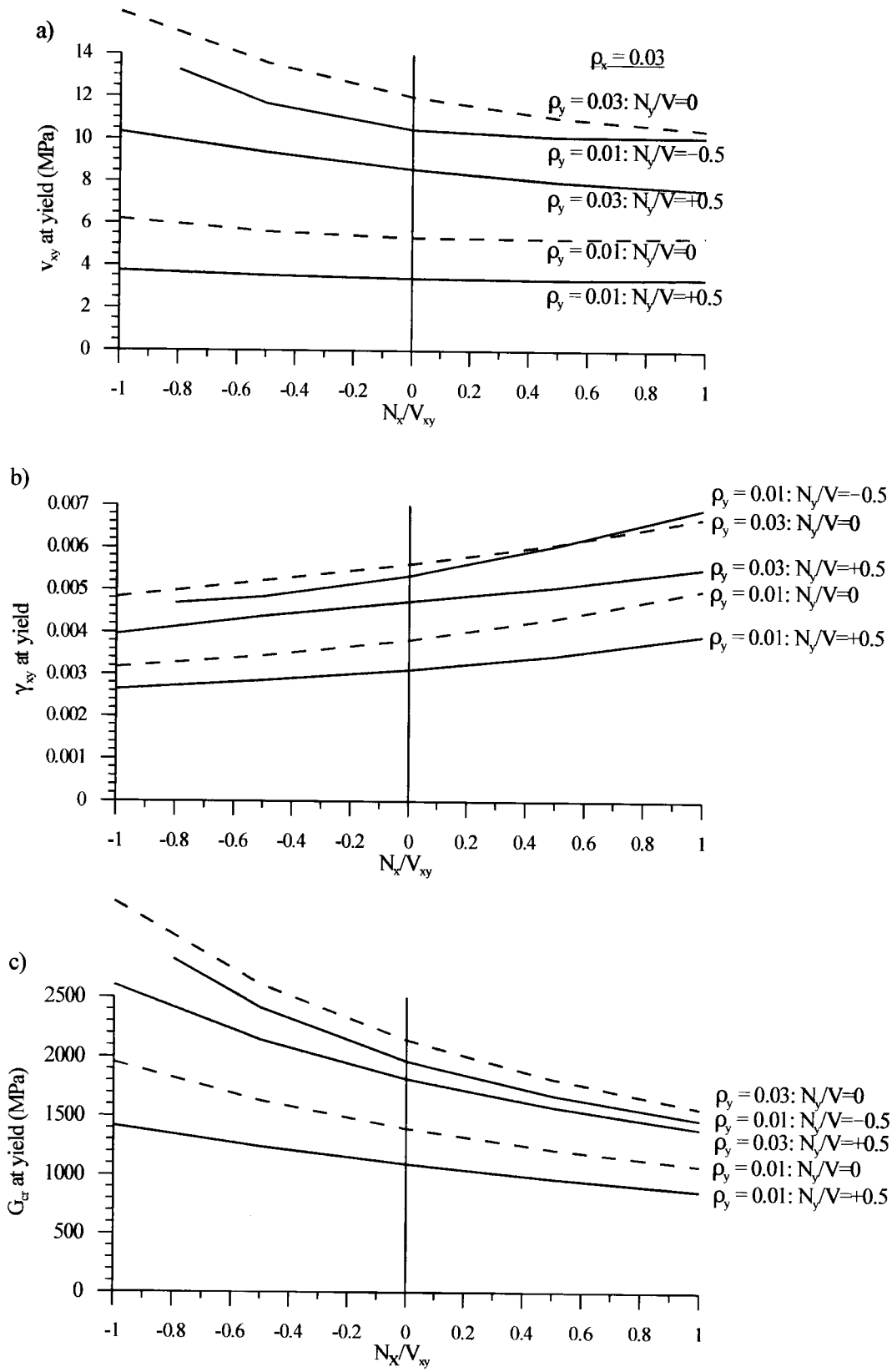

Figure 6.8 Influence of axial loads: a) on shear stress at yield, b) on shear strain at yield, c) on cracked section shear stiffness

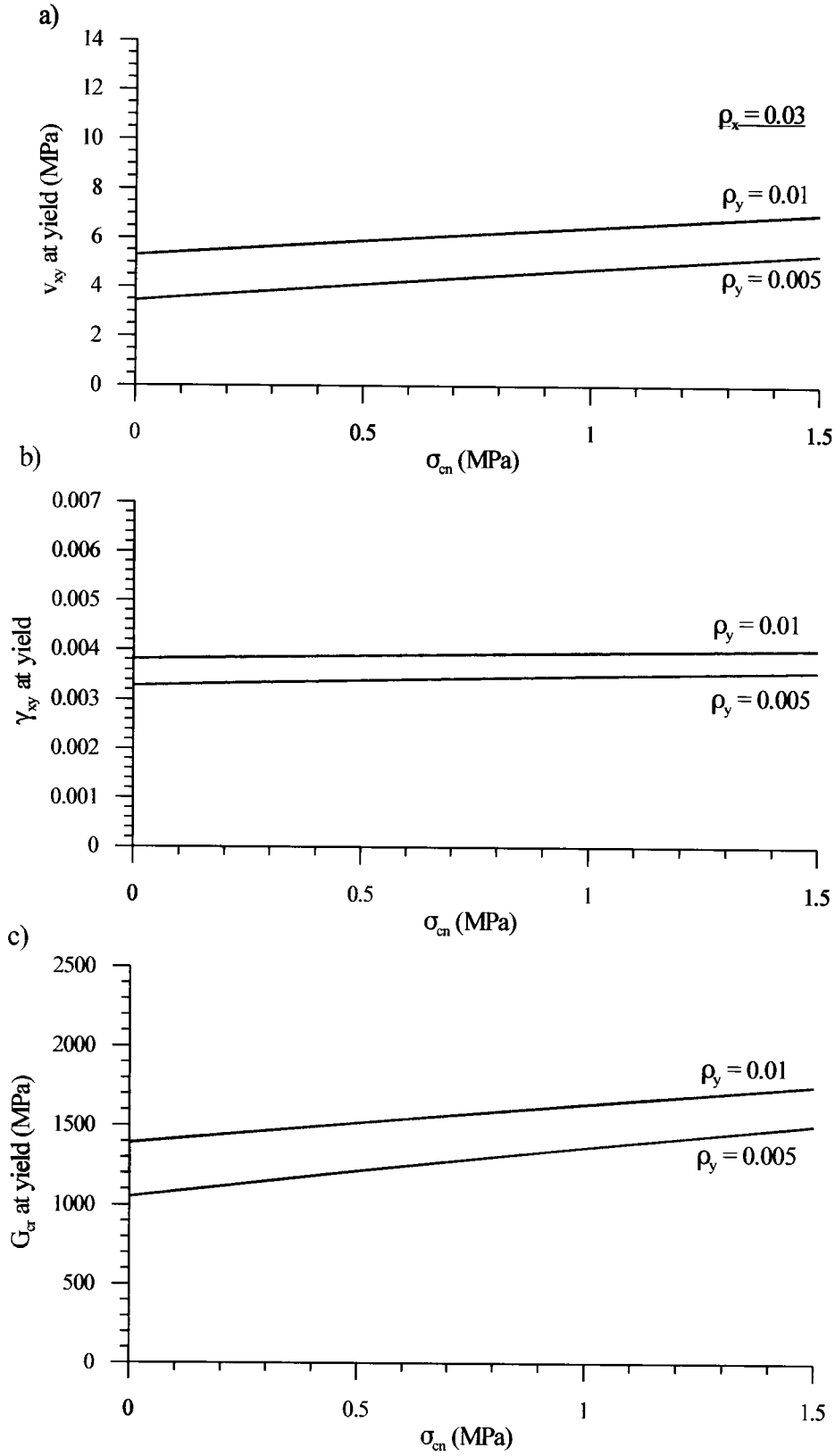

Figure 6.9 Influence of residual concrete tension stress ($\rho_x = 0.03$): a) on shear stress at yield, b) on shear strain at yield, c) on cracked section shear stiffness

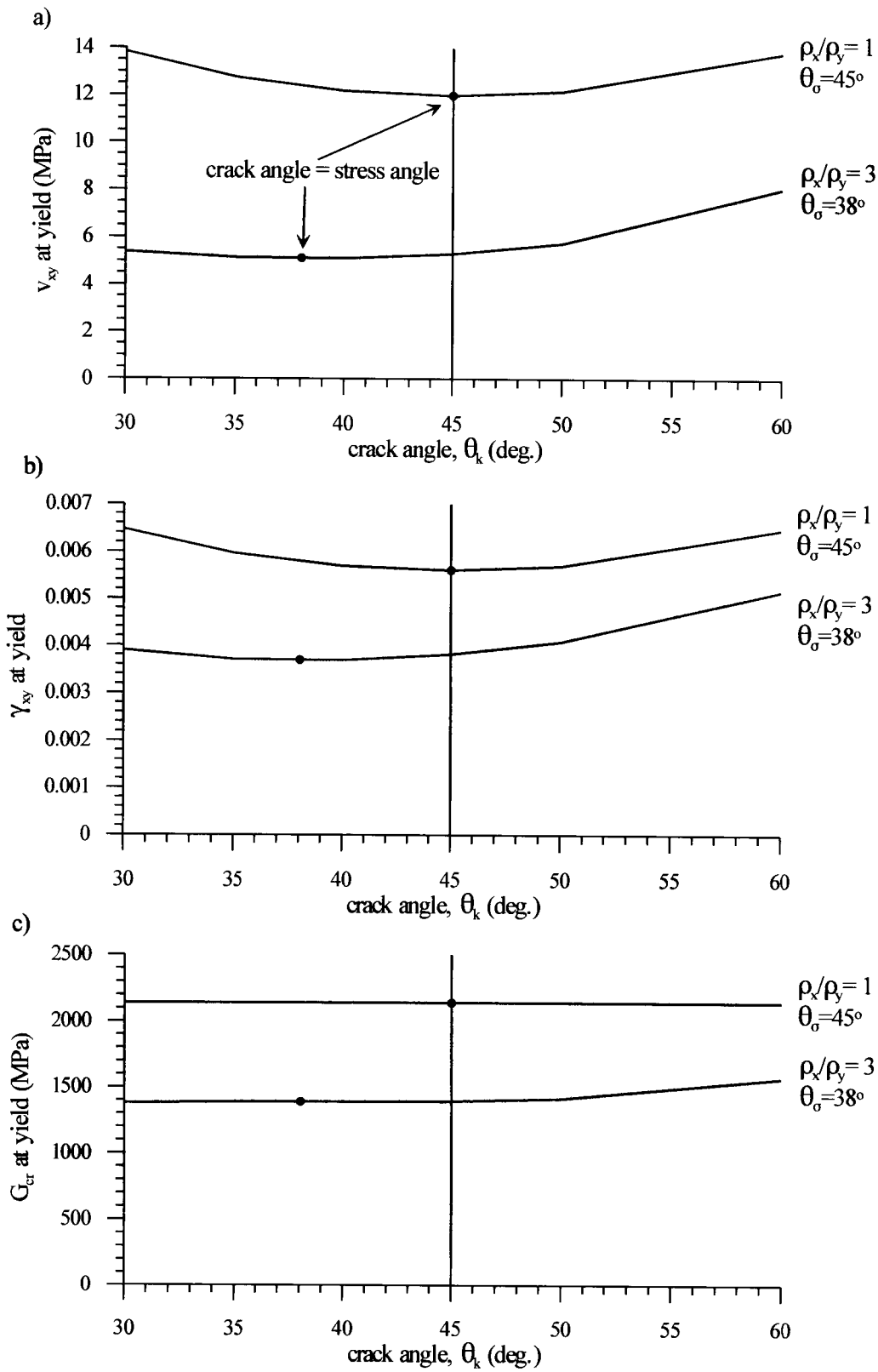

Figure 6.10 Influence of crack angle: a) on shear stress at yield, b) on shear strain at yield, c) on cracked section shear stiffness

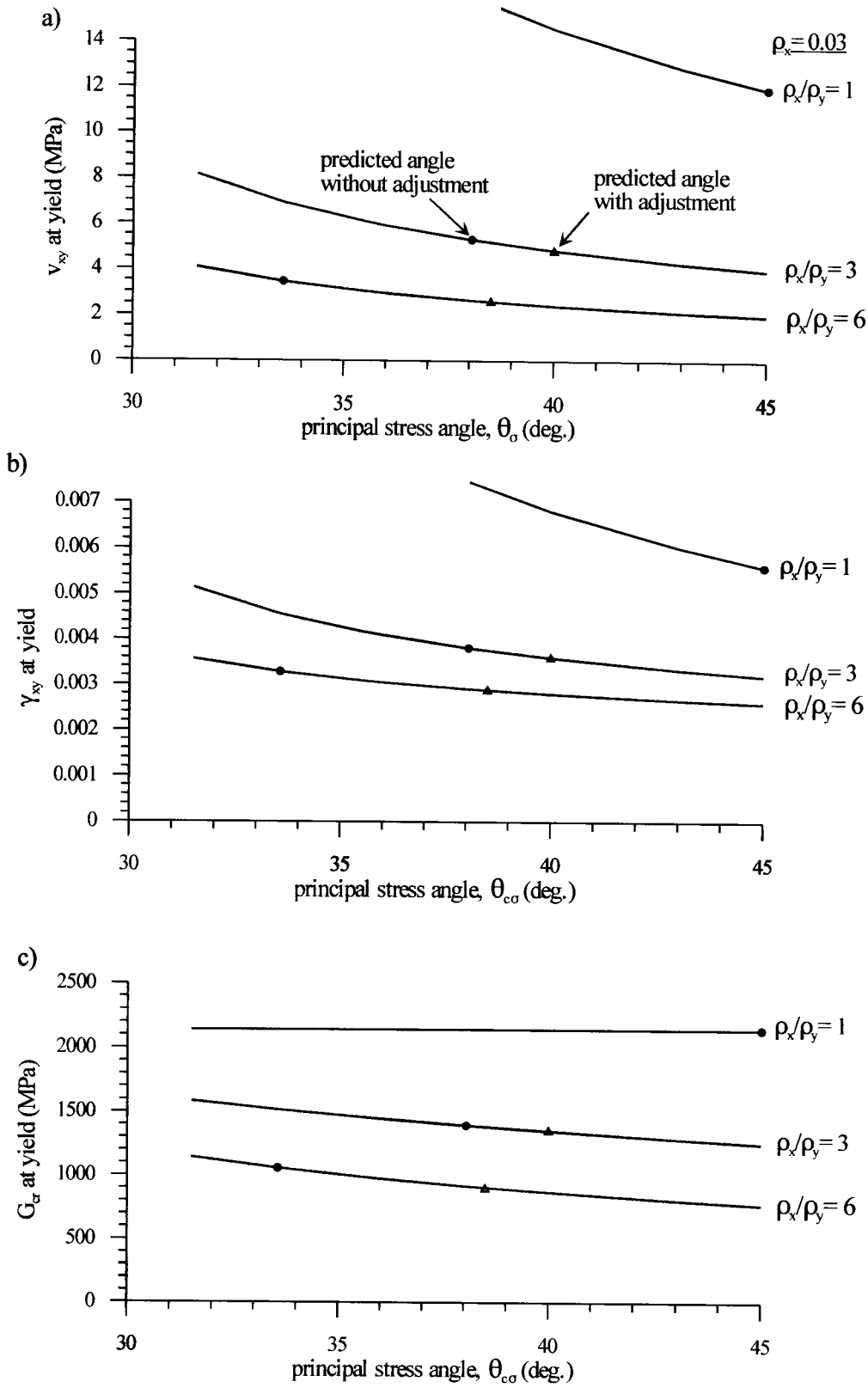

Figure 6.11 Influence of principal stress angle ($\rho_x = 0.03$): a) on shear stress at yield, b) on shear strain at yield, c) on cracked section shear stiffness

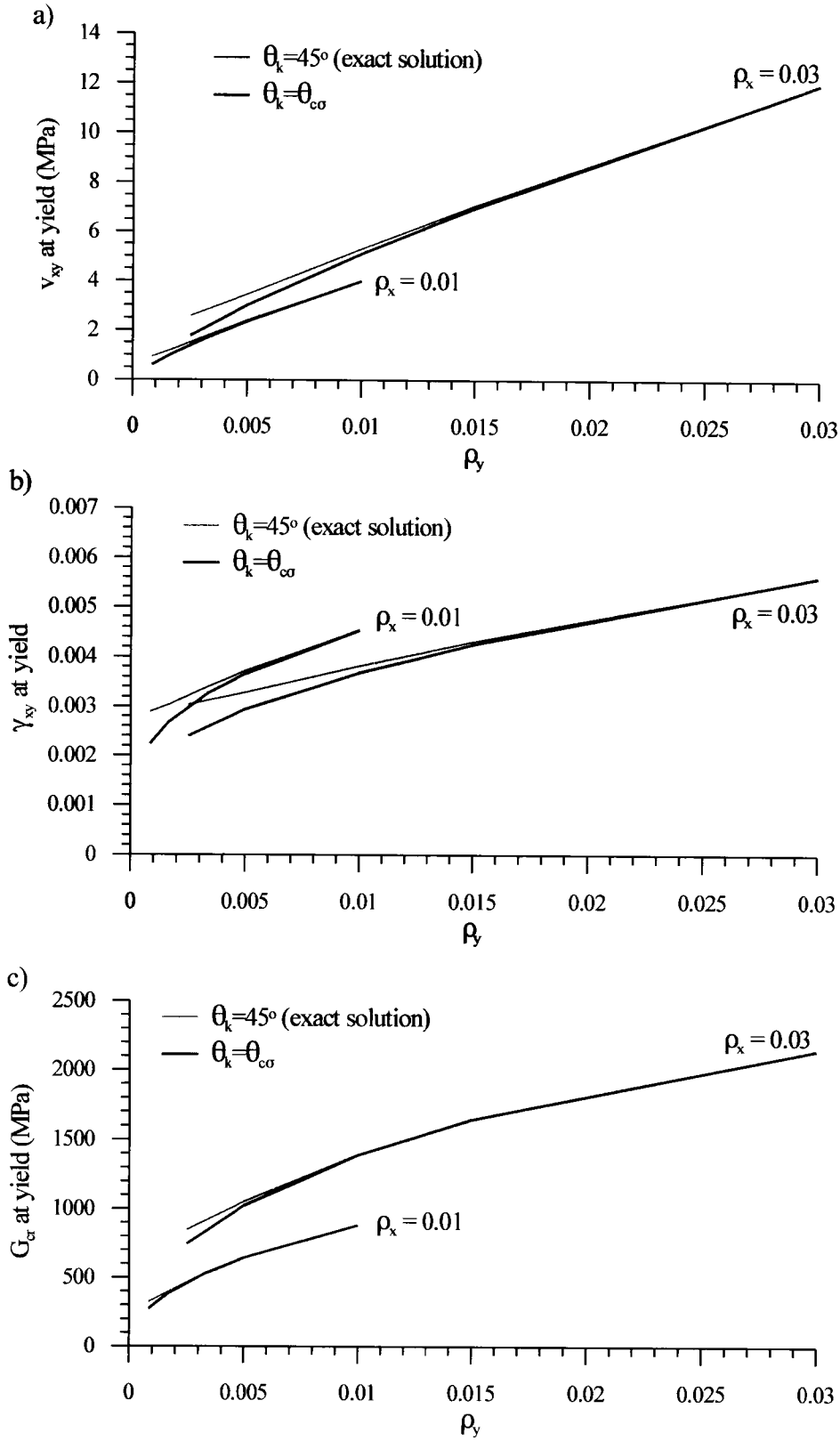

Figure 6.12 Influence of rotating cracks simplification, function of reinforcement ratios ($n_x = n_y = 0$): a) on shear stress at yield, b) on shear strain at yield, c) on cracked section shear stiffness

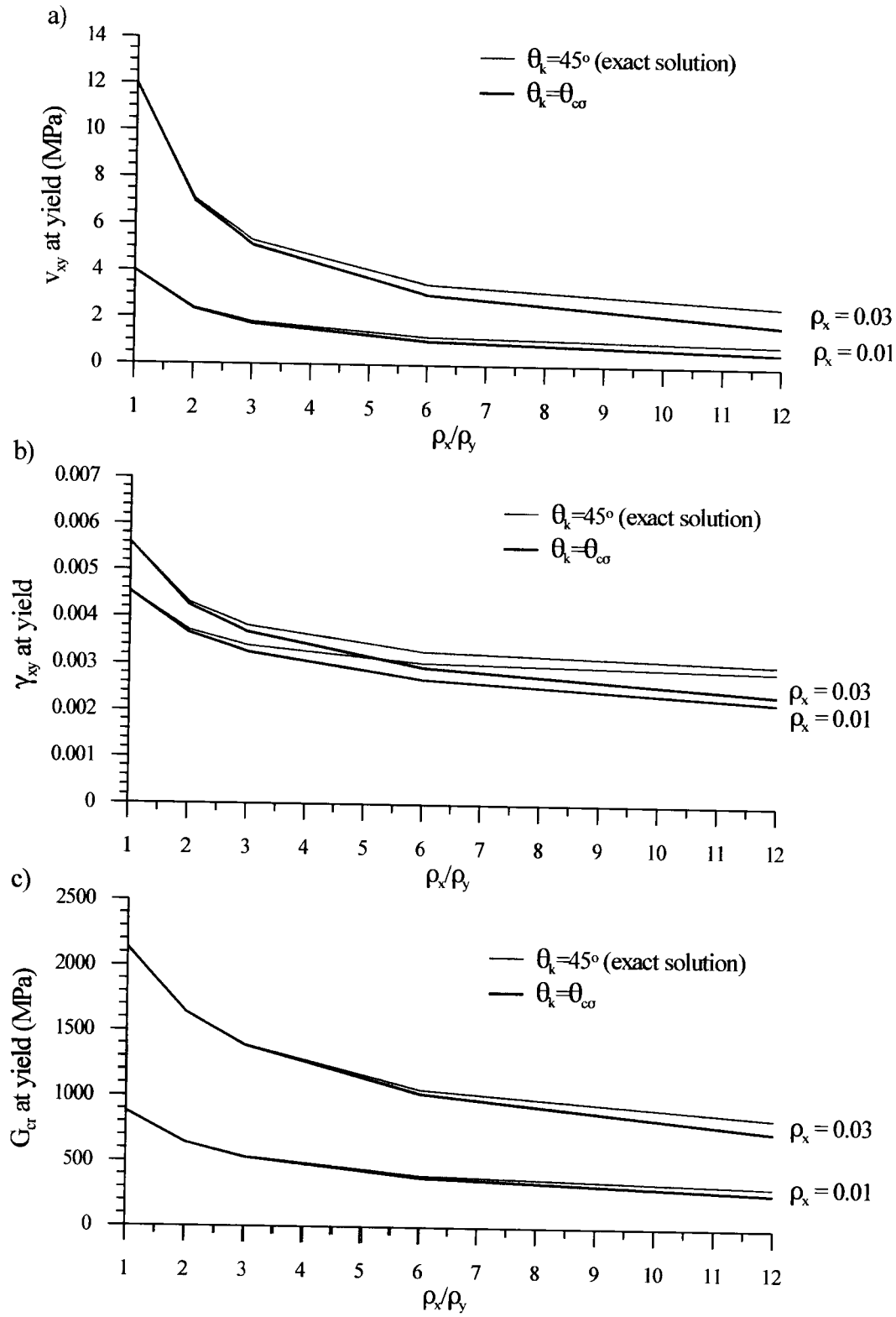

Figure 6.13 Influence of rotating cracks simplification, function of relative reinforcement ratios ($n_x = n_y = 0$): a) on shear stress at yield, b) on shear strain at yield, c) on cracked section shear stiffness

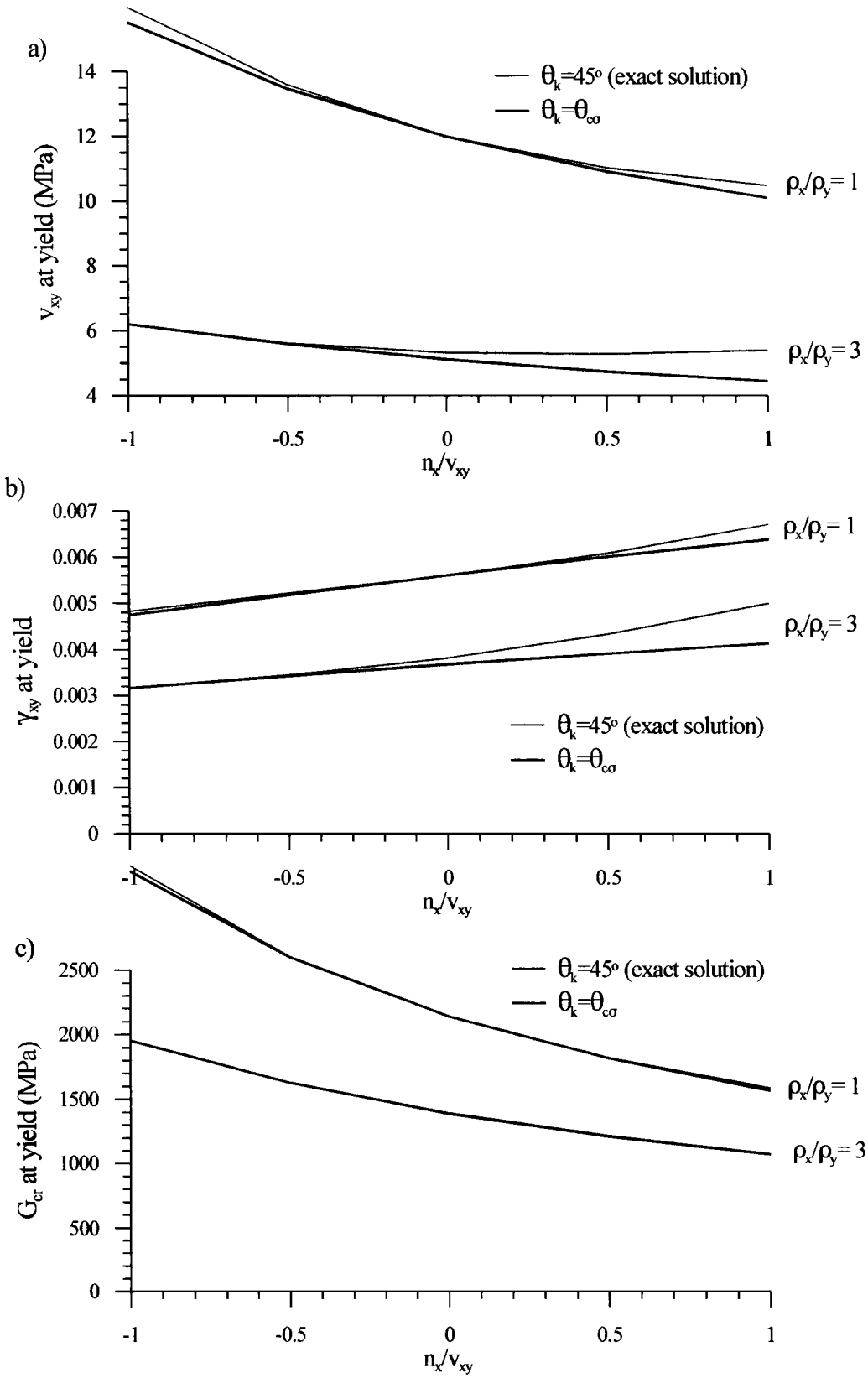

Figure 6.14 Influence of rotating cracks simplification, with varying n_x axial load (n_y = 0, ρ_x=0.03): a) on shear stress at yield, b) on shear strain at yield, c) on cracked section shear stiffness

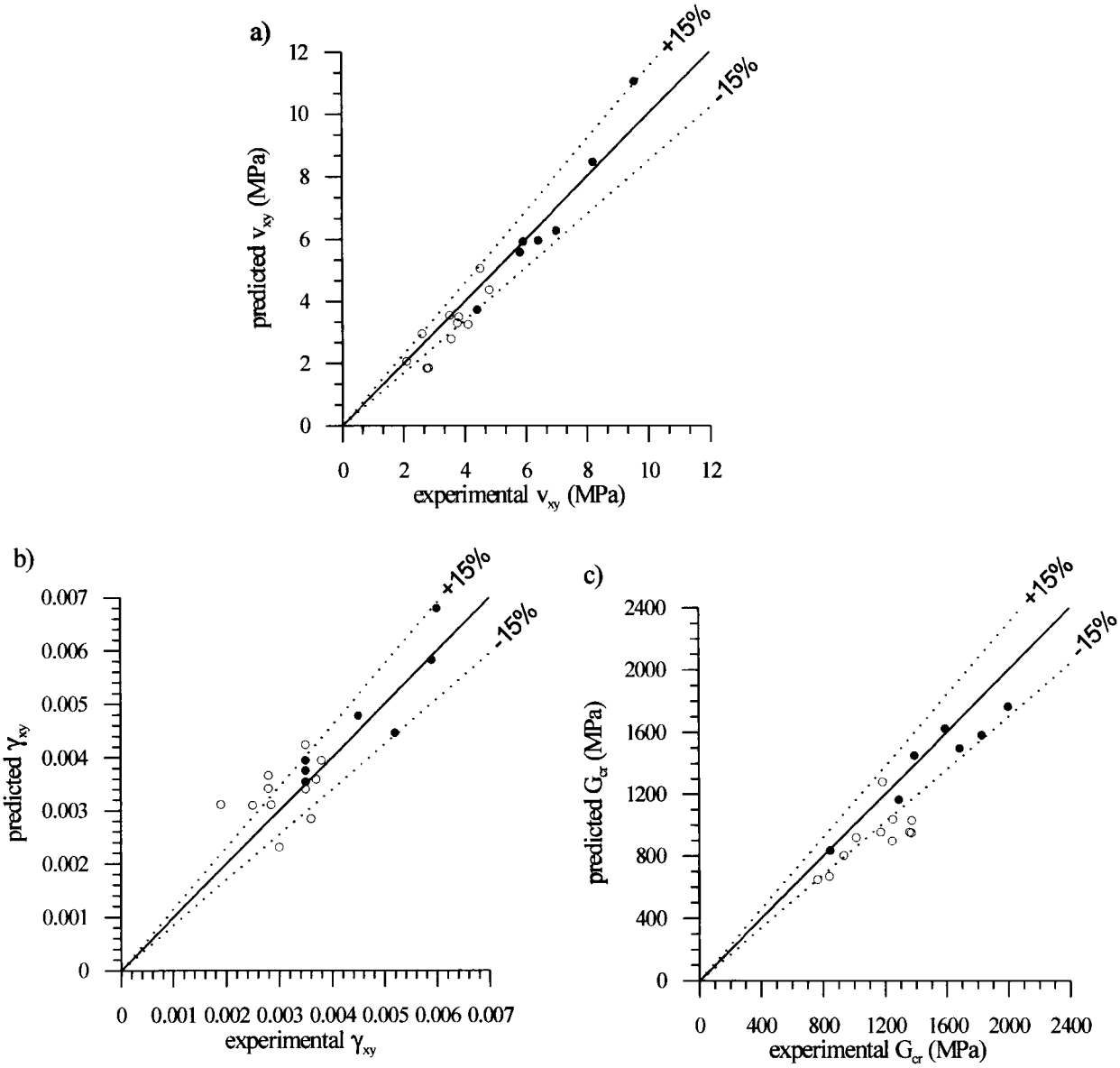

Figure 6.15 Simplified model vs experimental: a) shear stress at yield, b) shear strain at yield, c) cracked section shear stiffness (solid = LVDT data, hollow = Vecchio-Collins, 1982 data)

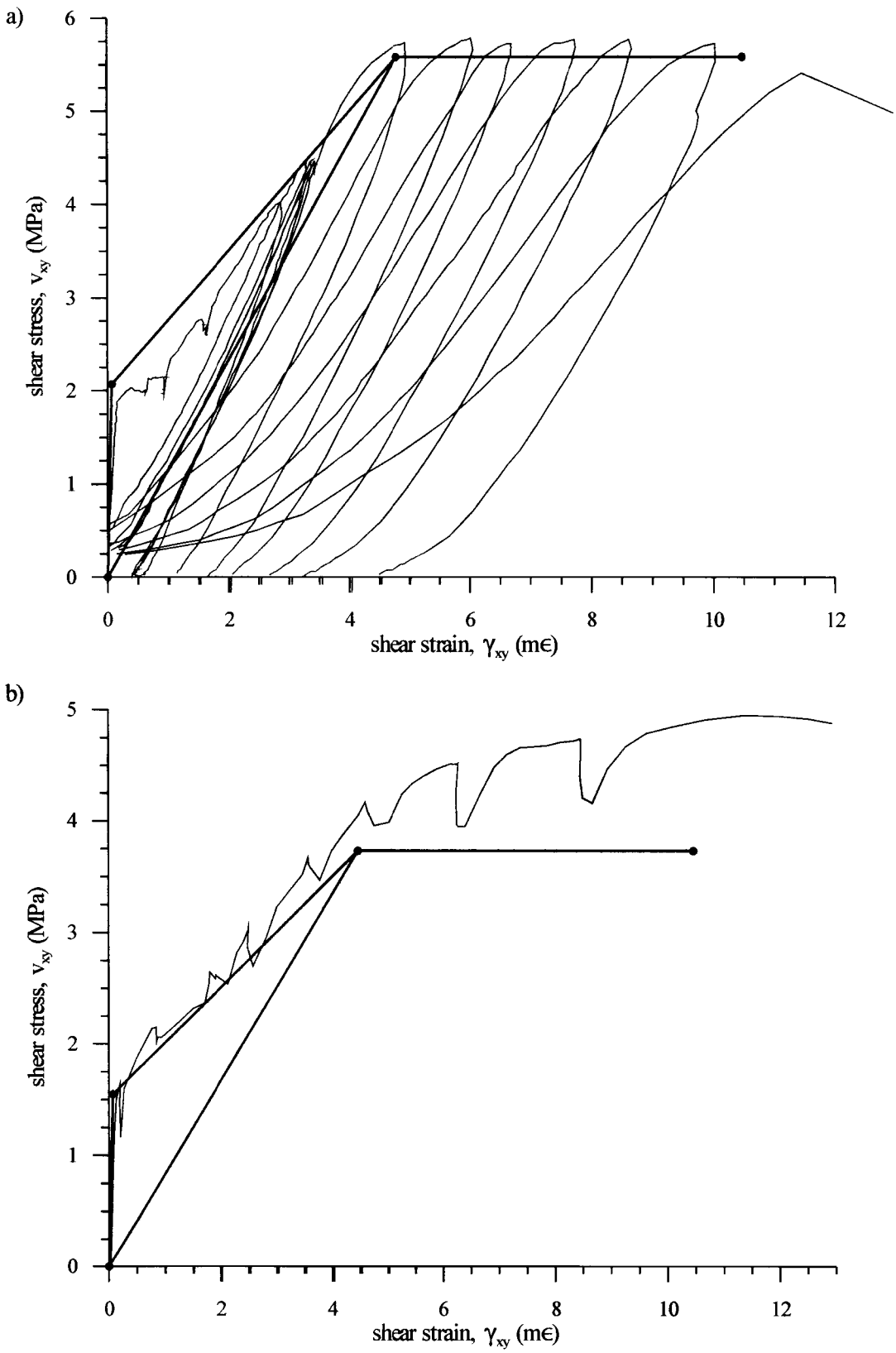

Figure 6.16 Simplified predicted response, bi-linear and tri-linear envelopes: a) SE8, b) PP1

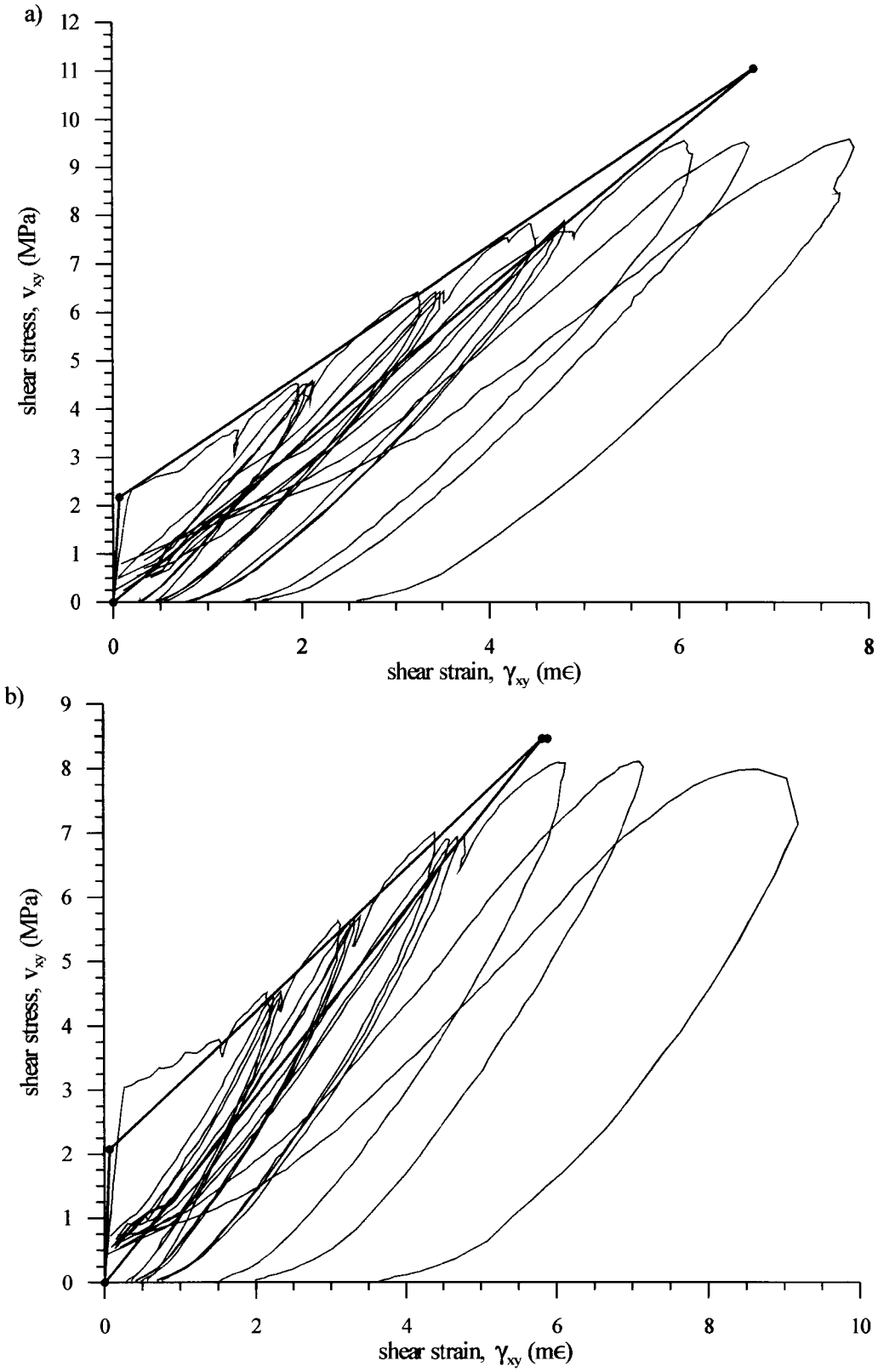

Figure 6.17 Simplified predicted response, bi-linear and tri-linear envelopes: a) SE9, b) SE10

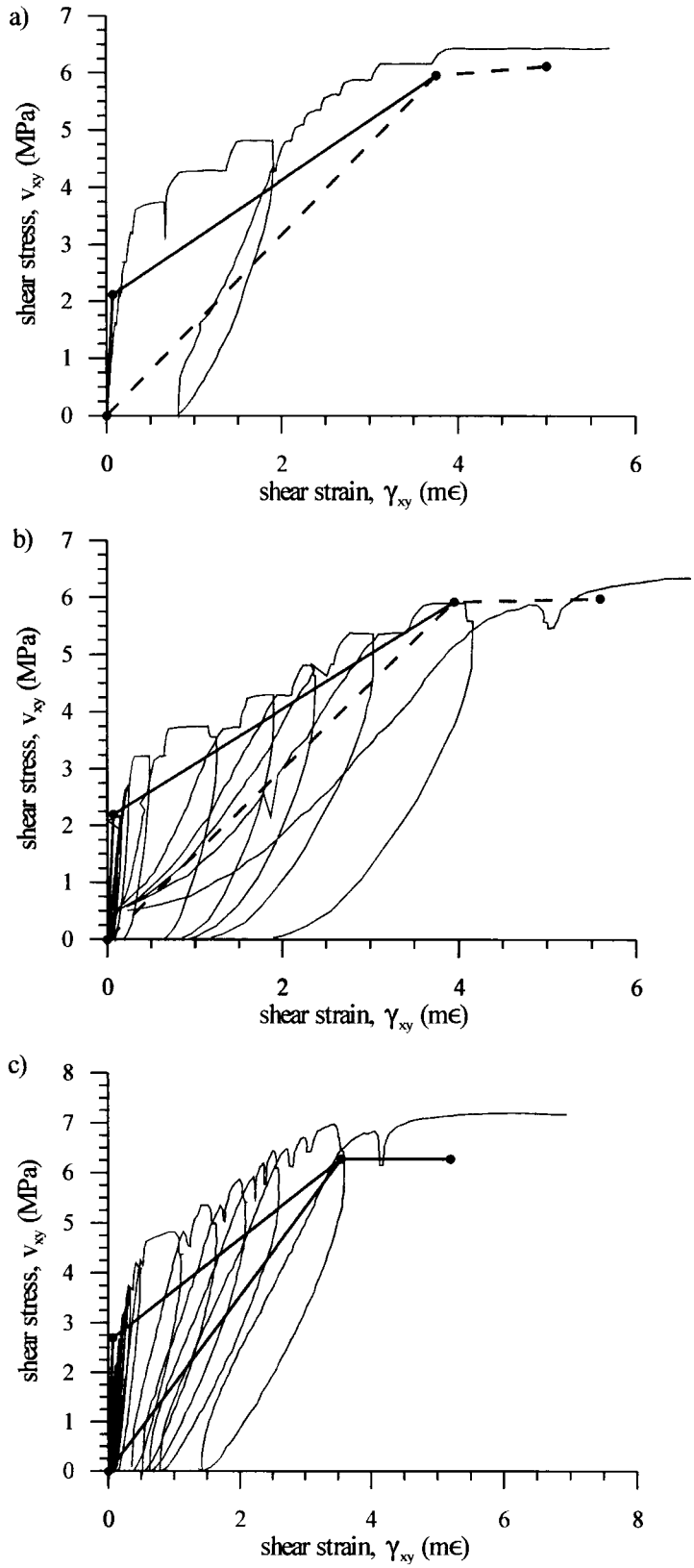

Figure 6.18 Simplified predicted response, bi-linear and tri-linear envelopes: a) PDV1, b) PDV2, c) PDV3

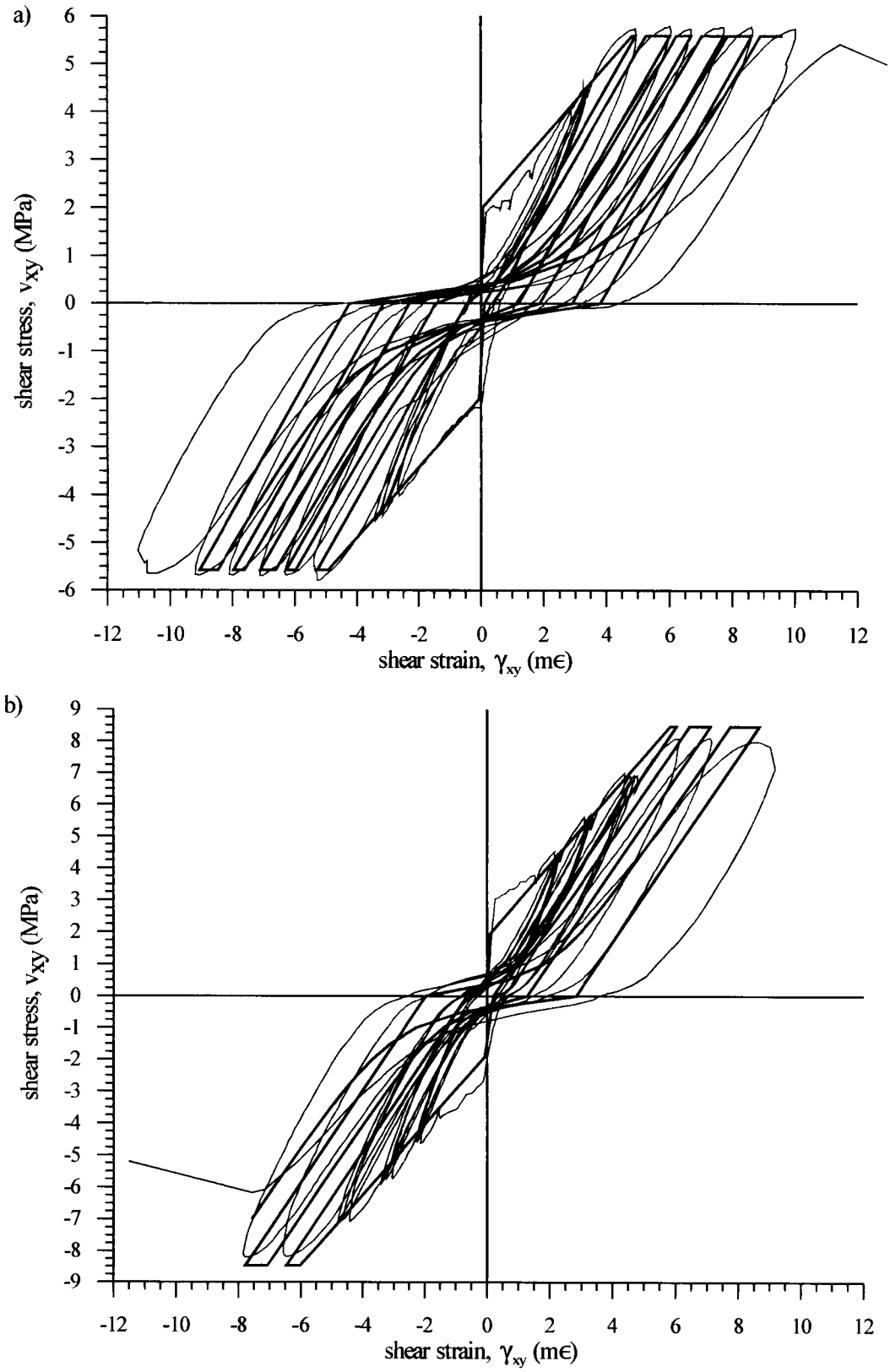

Figure 6.19 Simplified predicted response, reverse-cyclic model: a) SE8, b) SE10

References

ACI Committee 318. 2002. *Building code requirements for reinforced concrete (ACI 318-02)*. Detroit: American Concrete Institute.

Adebar, P. 1989. "Shear design of concrete offshore structures." PhD thesis, University of Toronto.

American Association of State Highway and Transportation Officials (AASHTO). 1998. *LRFD bridge design specifications*. Washington, D.C.

ASCE. 2000. *FEMA 356 Prestandard and commentary for the seismic rehabilitation of buildings*. Washington, D.C.: Federal Emergency Management Agency (FEMA).

ASCE-ACI Committee 445 on shear and torsion. 1998. Recent approaches to shear design of structural concrete. *Journal of Structural Engineering, ASCE* 124, no. 12: 1375-1417.

Baumann, T. 1972. Zur Frage der Netzbewehrung von Flächentragwerken (On the Problem of Net Reinforcement of Surface Structures). *Bauingenieur* 47, no. 10: 367-377.

Belarbi, A., and T. T. C. Hsu. 1994. Constitutive laws of concrete in tension and reinforcing bars stiffened by concrete. *ACI Structural Journal* 91, no. 4: 465-474.

Belarbi, A., and T. T. C. Hsu. 1995. Constitutive laws of softened concrete in biaxial tension-compression. *ACI Structural Journal* 92, no. 5: 562-573.

Canadian Standards Association (CSA). 1994. *A23.3-94 Design of concrete structures*. Rexdale, Ontario: CSA.

CEB-FIP. 1978. *Model code for concrete structures: CEB-FIP International Recommendations*. 3rd ed. Paris: Comité Euro-International du Béton.

Collins, M. P. 1978. Towards a rational theory for RC members in shear. *Journal of the Structural Division, ASCE* 104, no. ST4: 649-666.

Collins, M. P. 1979. Investigating the stress-strain characteristics of diagonally cracked concrete. *IABSE Colloquium on the Plasticity in Reinforced Concrete*, 27-34.

Collins, M. P., and D. Mitchell. 1991. *Prestressed concrete structures*. New Jersey: Prentice Hall.

Collins, M. P., D. Mitchell, P. Adebar, and F. J. Vecchio. 1996. A general shear design method. *ACI Structural Journal* 93, no. 1: 36-45.

Duthinh, D. 1999. Sensitivity of shear strength of reinforced concrete and prestressed concrete beams to shear friction and concrete softening according to modified compression field theory. *ACI Structural Journal* 96, no. 4: 495-508.

Fronteddu, L. F. 1993. " Response of reinforced concrete to reverse cyclic loading." MASc thesis, Department of Civil Engineering, The University of British Columbia.

Gopalaratnam, V. S., and S. P. Shah. 1985. Softening response of plain concrete in direct tension. *ACI Journal* 82, no. 3: 310-323.

Hsu, T. T. C. 1998. Stresses and crack angles in concrete membrane elements. *Journal of Structural Engineering, ASCE* 124, no. 12 : 1476-1484.

Hsu, T. T. C., A. Belarbi, and X.-B. D. Pang. 1991. *Universal panel tester*, Research Report No. UHCEE 91-1. Department of Civil and Environmental Engineering, University of Houston.

Hsu, T. T. C., and L.-X. Zhang. 1996. Tension stiffening in reinforced concrete membrane elements. *ACI Structural Journal* 93, no. 1: 108-115.

Hsu, T. T. C., and L.-X. Zhang. 1997. Nonlinear analysis of membrane elements by fixed-angle softened-truss model. *ACI Structural Journal* 94, no. 5: 493-492.

Hsu, T. T. C., and R. R. H. Zhu. 2002. Softened membrane model for reinforced concrete elements in shear. *ACI Structural Journal* 99, no. 4: 460-469.

International Conference of Building Officials (ICBO). 1997. *Uniform Building Code (UBC-97)*. Whittier, California: ICBO.

Kaufmann, W., and P. Marti. 1998. Structural concrete: cracked membrane model. *Journal of Structural Engineering, ASCE* 124, no. 12: 1467-1475.

Kent, D. C., and R. Park. 1973. Cyclic load behaviour of reinforcing steel. *Strain (Journal of the British Society for Strain Measurement)* 9, no. 3: 98-103.

Kirschner, U., and M. P. Collins. 1986. *Investigating the behaviour of reinforced concrete shell elements*, 86-09. Department of Civil Engineering, University of Toronto.

Kollegger, J., and G. Mehlhorn. 1987. Material model for cracked reinforced concrete. *IABSE Colloqium on Computational Mechanics of Concrete Structures: Advances and Applications*, 63-74.

Kupfer, H. 1964. "Erweiterung der Morsch schen Fachwerkanalogie mit Hilfe des Prinzips vom Minimum der Formanderungsarbeit (Generalization of Mörsch's truss analogy using the principle of minimum strain energy)." *Comité Euro-International du Béton, Bulletin d'Information*, Comité Euro-International du Béton. No. 40. CEB, Paris.

Mansour, M. Y., T. T. C. Hsu, and J. Y. Lee. 2000. Pinching effect in hysteretic loops of R/C shear elements. *ACI Fall Convention.*

Matsuzaki, Y., H. Fukuyama, T. Iizuka, and H. Noguchi. 1989. Behavior of a crack under reversed cyclic loading. *Structural Design, Analysis, and Testing: Proceedings of Structures Congress '89*ASCE.

Meyboom, J. 1987. "An experimental investigation of partially prestressed, orthogonally reinforced concrete elements subjected to membrane shear." Department of Civil Engineering, University of Toronto.

Mitchell, D., and M. P. Collins. 1974. Diagonal compression field theory - a rational model for structural concrete in pure torsion. *ACI Journal* 71: 396-408.

Miyahara, T., T. Kawakami, and K. Maekawa. 1988. Nonlinear behavior of cracked reinforced concrete plate element under uniaxial compression. *Proceedings, Japan Society of Civil Engineers* 11, no. June: 131-144.

Ohmori, N., H. Tsubota, N. Inoue, S. Watanabe, and K. Kurihara. 1987. Reinforced concrete membrane elements subjected to reversed cyclic in-plane shear stress. *Structural Mechanics in Reactor Technology: Transactions ofthe 9th International Conference on Structural Mechanics in Reactor Technology*, 513-24 Rotterdam: Wittmann, Folker H.

Pang, X.-B. D., and T. T. C. Hsu. 1995. Behavior of reinforced concrete membrane elements in shear. *ACI Structural Journal* 92, no. 6: 665-677.

Pang, X.-B. D., and T. T. C. Hsu. 1996. Fixed angle softened truss model for reinforced concrete. *ACI Structural Journal* 93, no. 2: 197-207.

Park, R., and T. Paulay. 1975. *Reinforced concrete structures*. New York: John Wiley & Sons.

Paulay, T., and M. J. N. Priestley. 1992. Seismic design of reinforced concrete and masonry buildings. New York: John Wiley & Sons, Inc.

Pincheira, J. A., F. S. Dotiwala, and J. T. D'Souza. 1999. Seismic analysis of older reinforced concrete columns. *Earthquake Spectra, EERI* 15, no. 2: 245-272.

Popov, Egor P. 1968. *Introduction to mechanics of solids*. Englewood Cliffs, New Jersey: Prentice-Hall, Inc.

Rose, B., P. B. Shing, E. Spacone, and K. Willam. 2002. Modeling of the shear behavior of RC members. *Seventh U.S. National Conference on Earthquake Engineering (7NCEE)* EERI.

Roux, S. 1998. "Seismic shear response of rc members with varying ductility." MASc Thesis, Department of Civil Engineering, The University of British Columbia.

Saatcioglu, M. 1991. "Modeling hysteretic force-deformation relationships for reinforced concrete elements." *Earthquake-Resistant Concrete Structures: Inelastic Response and Design*, SP-127. American Concrete Institute.

Shirai, S., and H. Noguchi. 1989. Compressive deterioration of cracked concrete. *Structural Design, Analysis , and Testing: Proceedings of Structures Congress '89*ASCE.

Stevens, N. J., M. P. Collins, and S. M. Uzumeri . 1991. Reinforced concrete subjected to reversed-cyclic shear - experiments and constitutive model. *ACI Journal* 88, no. 2: 135-146.

Stevens, N. J., S. M. Uzumeri, and M. P. Collins . 1987. *Analytical modelling of reinforced concrete subjected to monotonic and reversed loadings*, 87-1. Department of Civil Engineering, University of Toronto.

Vecchio, F. J. 2000. Disturbed stress field model for reinforced concrete: Formulation . *Journal of Structural Engineering, ASCE* 126, no. 9: 1070-1077.

Vecchio, F. J. 1999. Towards cyclic load modelling of reinforced concrete. *ACI Structural Journal* 96, no. 2.

Vecchio, F. J., and M. P. Collins. 1982. *The response of reinforced concrete to in-plane shear and normal stresses*, 82-03. Department of Civil Engineering, University of Toronto.

Vecchio, F. J., and M. P. Collins. 1986. The modified compression-field theory for reinforced concrete elements subjected to shear. *ACI Journal* 83, no. 2: 219-231.

Vecchio, F. J., and M. P. Collins. 1993. Compression response of cracked reinforced concrete. *Journal of Structural Engineering, ASCE* 119, no. 12: 3590-3611.

Villani, D. R. 1995. "Reinforced concrete subjected to cyclic loads: a pilot study." BASc thesis, Department of Civil Engineering, University of Toronto.

Wagner, H. 1929. Ebene Blechwandtrager mit sehr dunnem Steglech. *Zeitschrift Für Flugtechnik Und Motorluftschiffahrt, Berlin, Germany* 20, no. 8-12.

Walraven, J. C. 1981. Fundamental analysis of aggregate interlock. *Journal of Structural Engineering, ASCE* 107, no. 11: 2245-2270.

Zararis, P. D. 1986. State of stress in RC plates under service conditions. *Journal of Structural Engineering, ASCE* 112, no. 8: 1908-1927.

Zararis, P. D. 1988. Failure mechanisms in R/C plates carrying in-plane forces. *Journal of Structural Engineering, ASCE* 114, no. 3: 553-573.

Zararis, P. D. 1996. Concrete shear failure in reinforced-concrete elements. *Journal of Structural Engineering, ASCE* 122, no. 9: 1006-1015.

Zhu, R. R. H., and T. T. C. Hsu. 2002. Poisson effect in reinforced concrete membrane elements. *ACI Structural Journal* 99, no. 5: 631-640.

Zhu, R. R. H., T. T. C. Hsu, and J.-Y. Lee. 2001. Rational shear modulus for smeared-crack analysis of reinforced concrete. *ACI Structural Journal* 98, no. 4: 443-450.

APPENDIX A

Additional Equations and Derivations

A.1 AVERAGING STRAINS MEASURED IN FOUR DIRECTIONS

The data for specimens SE8, SE9 and SE10 (Stevens, Uzumeri, and Collins 1987) was obtained as strain data corresponding to each LVDT. Averaging the data from the two faces, in each direction, results in average strains at four orientations: 0°, 90°, +45°, and −45° (clockwise positive from the x axis). The four average strains can then be combined to define a compatible average strain state. This is done by calculating average principal strains and an average shear strain.

From the strains in 4 directions, four sets of minimum and maximum principal strains are obtained:

$$\varepsilon_{1,2} = \frac{\varepsilon_a + \varepsilon_c}{2} \pm \frac{1}{2}\sqrt{(\varepsilon_a - \varepsilon_c)^2 + (2\varepsilon_b - \varepsilon_a - \varepsilon_c)^2} \tag{A.1}$$

where ε_1 is the maximum principal strain, ε_2 is the minimum principal strain, ε_a and ε_c are strains in two orthogonal directions, e.g., 0° and 90° or +45° and −45°, and ε_b is one of the two remaining strains.

Averaging the four equations represented by Eq. A.1 yields

$$\varepsilon_{1,2} = \frac{\varepsilon_y + \varepsilon_{-45} + \varepsilon_x + \varepsilon_{+45}}{4} \pm \frac{1}{2}\sqrt{(\varepsilon_y - \varepsilon_x)^2 + (\varepsilon_{-45} - \varepsilon_{+45})^2} \tag{A.2}$$

For the shear strain with respect to the x and y axes, two equations are available from the strains in four directions:

$$\gamma_{xy} = 2\varepsilon_{-45} - (\varepsilon_x + \varepsilon_y) \tag{A.3}$$

$$\gamma_{xy} = (\varepsilon_x + \varepsilon_y) - 2\varepsilon_{+45} \tag{A.4}$$

Averaging Eqs. A.3 and A.4 gives

$$\gamma_{xy} = \varepsilon_{-45} - \varepsilon_{+45} \tag{A.5}$$

Equations A.2 and A.5 define a compatible average strain state. The orientation of the principal strains is defined by

$$\theta_\varepsilon = \begin{cases} \frac{1}{2}\tan^{-1}\left(\dfrac{\gamma_{xy}}{\varepsilon_y - \varepsilon_x}\right); \varepsilon_y \neq \varepsilon_x \\ 45^\circ; \varepsilon_y = \varepsilon_x \end{cases} \tag{A.6}$$

where the angle defines the orientation of the minimum principal strain, ε_2, relative to the x axis (clockwise positive).

Figures A.1 to A.3 compare the compatible average strain state (Eqs. A.2 and A.5) to the average LVDT data in each direction. The small difference between the two confirms the validity of assuming the average strains are compatible.

A.2 EQUATIONS FOR PRINCIPAL CONCRETE STRESS ANGLE

A2.1 General equation with concrete tension

From Mohr's circle of concrete stress,

$$\sigma_{cy} = \sigma_{c1} - v_{cxy} \tan\theta_{c\sigma} \tag{A.7}$$

$$\sigma_{cx} = \sigma_{c1} - \frac{v_{cxy}}{\tan\theta_{c\sigma}} \tag{A.8}$$

$$v_{xy} = (\sigma_{c1} - \sigma_{c2}) \sin\theta_{c\sigma} \cos\theta_{c\sigma} \tag{A.9}$$

where σ_{cx} and σ_{cy} are the concrete stresses in the reinforcement directions, σ_{c1} and σ_{c2} are the maximum and minimum principal concrete stresses, v_{cxy} is the concrete shear stress, and $\theta_{c\sigma}$ is the principal concrete stress angle (clockwise positive from the x direction to the minimum principal direction).

Defining $\mu_1 = \sigma_{c1}/v_{cxy}$, Eqs A.7 and A.8 can be written

$$\sigma_{cy} = v_{cxy}(\mu_1 - \tan\theta_{c\sigma}) \tag{A.10}$$

$$\sigma_{cx} = v_{cxy}(\mu_1 - \frac{1}{\tan\theta_{c\sigma}}) \tag{A.11}$$

and Eq. A.9 can be rearranged to

$$\sigma_{c2} = v_{cxy}\left(\mu_1 - \frac{1}{\sin\theta_{c\sigma} \cos\theta_{c\sigma}}\right) \tag{A.12}$$

From Mohr's circle of strain,

$$\varepsilon_2 = (\varepsilon_x - \varepsilon_y \tan^2\theta_{c\sigma})\frac{1}{1 - \tan^2\theta_{c\sigma}} \tag{A.13}$$

where ε_2 is the minimum principal strain, and ε_x and ε_y are the total strains in each reinforcement direction.

The total strains in each reinforcement direction, ε_x and ε_y, can be expressed as a function of the shear stress. As discussed in Chapter 2, the total strains are assumed equal to the reinforcement strains, ε_{sx} and ε_{sy}. The reinforcement strains are related to the reinforcement stresses by the linear relationship $\varepsilon_s = \sigma_s/E_s$. Then the equilibrium equations (of the form: $\rho_s\sigma_s + \sigma_c = n$) can be used to replace the reinforcement stresses with concrete stresses in the

reinforcement directions, σ_{cx} and σ_{cy}. Finally, substituting for σ_{cy} and σ_{cx} with Eqs A.10 and A.11, the strains in the x and y directions are:

$$\varepsilon_x = \frac{v_{cxy}}{E_s \rho_x}\left(\mu_x - \mu_1 + \frac{1}{\tan\theta_{c\sigma}}\right)$$
$$\varepsilon_y = \frac{v_{cxy}}{E_s \rho_y}\left(\mu_y - \mu_1 + \tan\theta_{c\sigma}\right) \tag{A.14}$$

where $\mu_x = n_x/v_{cxy}$ and $\mu_y = n_y/v_{cxy}$.

Substituting for ε_x and ε_y in Eq. A.13, assuming the linear relationship $\sigma_{c2} = E_c\varepsilon_2$ for the concrete in compression, and replacing E_s/E_c by the modular ratio n, Eq. A.13 can be written in terms of stresses:

$$\sigma_{c2} = v_{cxy}\left[\frac{1}{n\rho_x}\left(\mu_x - \mu_1 + \frac{1}{\tan\theta_{c\sigma}}\right) - \frac{1}{n\rho_y}(\mu_y - \mu_1 + \tan\theta_{c\sigma})\tan^2\theta_{c\sigma}\right]\frac{1}{1-\tan^2\theta_{c\sigma}} \tag{A.15}$$

Equating Eqs. A.12 and A.15, replacing $1/\sin\theta_{c\sigma}\cos\theta_{c\sigma}$ by $(\tan\theta_{c\sigma} + 1/\tan\theta_{c\sigma})$, and grouping like terms yields the identity:

$$\left(1+\frac{1}{n\rho_x}\right) = \left(1+\frac{1}{n\rho_y}\right)\tan^4\theta_{c\sigma} - \mu_1\left(1+\frac{1}{n\rho_y}\right)\tan^3\theta_{c\sigma}$$
$$+\frac{\mu_y}{n\rho_y}\tan^3\theta_{c\sigma} + \mu_1\left(1+\frac{1}{n\rho_x}\right)\tan\theta_{c\sigma} - \frac{\mu_x}{n\rho_x}\tan\theta_{c\sigma} \tag{A.16}$$

Defining

$$\alpha = \frac{\left(1+\frac{1}{n\rho_x}\right)}{\left(1+\frac{1}{n\rho_y}\right)} \tag{A.17}$$

Eq. A.16 can be written

$$\tan^4\theta_{c\sigma} - \alpha + \mu_1(\alpha\tan\theta_{c\sigma} - \tan^3\theta_{c\sigma}) + \frac{\mu_y}{1+n\rho_y}\tan^3\theta_{c\sigma} - \mu_x\frac{\rho_y}{\rho_x}\left(\frac{1}{1+n\rho_y}\right)\tan\theta_{c\sigma} = 0 \quad \text{(A.18)}$$

which is Eq. 4.6 presented in Chapter 4.

A2.2 Baumann's equation (no concrete tension)

Assuming no concrete tension ($\mu_1 = 0$), Eq. A.16 reduces to Baumann's equation (Baumann 1972), presented as Eq. 4.4 in Chapter 4.

A2.3 Collins' equation (no concrete tension, no axial loads)

Assuming no concrete tension and no axial loads ($\mu_1 = \mu_x = \mu_y = 0$), Eq. A.18 reduces to $\tan^4\theta_{c\sigma} = \alpha$, or

$$\tan^4\theta_{c\sigma} = \frac{\left(1+\frac{1}{n\rho_x}\right)}{\left(1+\frac{1}{n\rho_y}\right)} \quad \text{(A.19)}$$

which is the form presented by Collins (1978), and presented as Eq. 4.5 in Chapter 4.

A2.4 Influence of crack angle, modular ratio, and axial load

Influence of axial load

Figure A.4 plots the stress angle from Eq. A.18 (with no concrete tension) for various axial load ratios (μ_x and μ_y). As the figure indicates, axial loads can significantly change the predicted stress angle and should be included when they are present. Note that as the axial loads increase, the response becomes less shear dominated.

Influence of crack angle

In the derivation of the angle equations, the concrete tension has either been defined in the principal direction or assumed to be zero. This results in equations which are independent of

the crack angle. In the proposed model (described in Chapter 3), concrete tension is defined in the direction normal to the cracks instead of in the principal direction. Assuming no axial loads, the principal tension stress is

$$\sigma_{c1} = \sigma_{c2} + 2\left(\frac{\sigma_{cn} - \sigma_{c2}}{1 + \cos(2\theta_k - 2\theta_{c\sigma})}\right) \tag{A.20}$$

where σ_{cn} is the concrete stress normal to the cracks, σ_{c1} and σ_{c2} are the maximum and minimum principal concrete stresses, $\theta_{c\sigma}$ is the principal concrete stress angle and θ_k is the crack angle (both angles are clockwise positive from the x axis).

For the compression-only concrete stress state (defined in Chapter 3, Sec. 3.6), the tension normal to the cracks is zero and Eq. A.20 reduces to

$$\sigma_{c1} = -\sigma_{c2} \tan^2(\theta_k - \theta_{c\sigma}) \tag{A.21}$$

Using Eq. A.21 in the definition of μ_1 and re-deriving Eq. A.18 (with $\mu_x = \mu_y = 0$), the principal stress angle is defined by the identity:

$$\frac{1}{\left(\cos 2(\theta_k - \theta_{c\sigma}) + 1\right)\left(1 - \tan^2\theta_{c\sigma}\right)} \begin{bmatrix} \dfrac{\left(\cos 2(\theta_k - \theta_{c\sigma}) - \cos 2\theta_{c\sigma}\right)\tan^2\theta_{c\sigma}}{n\rho_y} \\ -\dfrac{\cos 2(\theta_k - \theta_{c\sigma}) + \cos 2\theta_{c\sigma}}{n\rho_x} \end{bmatrix} = 1 \tag{A.22}$$

Equation A.22 defines the principal stress angle, zero concrete tension normal to the cracks and no axial load.

Equation A.22 is plotted in Fig. A.5 with $\theta_k = \theta_\sigma$ and with $\theta_k = 45°$. As the figure shows, the crack angle has little influence on the predicted stress angle. This can be seen directly from Eq. A.22: the crack angle only appears in cosine terms which are close to 1 when the difference between the crack angle and the concrete stress angle is less than 15°.

Influence of modular ratio

Equation A.19 is plotted in Fig. A.6 for modular ratios ranging from 5 to 14. As the figure shows, the predicted angle is essentially independent of the modular ratio, i.e., essentially independent of the concrete strength.

A.3 ESTIMATING THE STRAIN NORMAL TO THE CRACKS AT YIELD

In the general model, the concrete residual tension stress is a function of the total strain normal to the cracks, ε_n. In the rigorous solution, this strain is determined iteratively at each load increment. For the simplified model, a simple equation to approximate the strain at yield can be used. The approximate equation presented in Chapter 6 (Eq. 6.11) is derived below.

From Mohr's circle of strain,

$$\varepsilon_n = \varepsilon_x + \varepsilon_y - \varepsilon_p \tag{A.23}$$

where ε_n is the strain normal to the cracks, ε_p is the strain parallel to the cracks, and ε_x and ε_y are the strain in the reinforcement directions.

At yield,

$$\varepsilon_y = \frac{f_{yy}}{E_s} \tag{A.24}$$

$$\varepsilon_x = \frac{1}{E_s \rho_x}\left(n_x - n_y + \rho_y f_{yy} + \frac{2v_{xy}}{\tan 2\theta_{c\sigma}}\right) \tag{A.25}$$

$$\varepsilon_p = \varepsilon_{cp} = \frac{1}{E_c}\left(\sigma_{cn} - 2v_{xy}\frac{\cos(2\theta_k - 2\theta_{c\sigma})}{\sin 2\theta_{c\sigma}}\right) \tag{A.26}$$

Assuming the concrete tension stress at yield is negligible ($\sigma_{cn} = 0$), substituting Eqs. A.24 to A.26 into Eq. A.23, and using Eq. 6.9 for v_{xy} at yield,

$$\varepsilon_{n,yield} = \frac{f_{yy}}{E_s}\left(1 + \frac{\rho_y}{\rho_x}\frac{(1+2n\rho_x)\cos(2\theta_k - 2\theta_{c\sigma}) + \cos 2\theta_{c\sigma}}{\cos(2\theta_k - 2\theta_{c\sigma}) - \cos 2\theta_{c\sigma}}\right) + \frac{n_x}{E_s\rho_x} - \frac{n_y}{E_s\rho_x}\left(\frac{(1+2n\rho_x)\cos(2\theta_k - 2\theta_{c\sigma}) + \cos 2\theta_{c\sigma}}{\cos(2\theta_k - 2\theta_{c\sigma}) - \cos 2\theta_{c\sigma}}\right) \tag{A.27}$$

Applying the approximation $\theta_k = \theta_{c\sigma}$, Eq. A.27 simplifies to

$$\varepsilon_{n,yield} = \frac{f_{yy}}{E_s}\left[1 + \frac{\rho_y}{\rho_x}\frac{1}{\tan^2\theta_{c\sigma}} + \frac{\rho_y n}{\sin^2\theta_{c\sigma}}\right] + \frac{N_x}{E_s\rho_x} - \frac{N_y}{E_s}\left(\frac{1}{\rho_x\tan^2\theta_{c\sigma}} + \frac{n}{\sin^2\theta_{c\sigma}}\right) \tag{A.28}$$

With no or negligible axial loads ($n_x = n_y = 0$), the principal stress angle varies from 45° for $\rho_x/\rho_y = 1$ to approximately 30° for $\rho_x/\rho_y = 12$. Correspondingly, $1/\sin^2\theta_{c\sigma}$ varies from 2.0 to 4.0 and can be approximated by $2(\rho_x/\rho_y)^{0.3}$. Similarly, $1/\tan^2\theta_{c\sigma}$ varies from 1.0 to 3.0 and can be approximated by $(\rho_x/\rho_y)^{0.44}$. Substituting into Eq. A.28 gives the approximate equation (Eq. 6.11):

$$\varepsilon_{n,yield} = \frac{f_{yy}}{E_s}\left[1 + \left(\frac{\rho_x}{\rho_y}\right)^{-0.56} + n\rho_y\left(\frac{\rho_x}{\rho_y}\right)^{0.3}\right] \tag{A.29}$$

A.4 SHEAR STRAIN AS A FUNCTION OF STRESSES

In Chapter 6, the shear strain at yield is expressed as a function of stresses (Eq. 6.13). This is done as follows:

From the Mohr's circle of strains, the shear strain is related to the strain in each reinforcement direction and the strain parallel to the open cracks by

$$\gamma_{xy} = \frac{\varepsilon_x}{\tan\theta_k} + \varepsilon_y\tan\theta_k - \varepsilon_p\left(\tan\theta_k + \frac{1}{\tan\theta_k}\right) \tag{A.30}$$

where γ_{xy} is the shear strain, ε_x and ε_y are the strains in the reinforcement directions, ε_p is the strain parallel to the cracks, and θ_k is the crack angle.

The strain in each reinforcement direction is related to the reinforcement stress by the linear stress-strain relationship ($\varepsilon_s = \sigma_s/E_s$). It is also related to the concrete stresses via the equilibrium equations. Thus,

$$\varepsilon_y = \frac{f_{sy}}{E_s} = \frac{n_y - \sigma_{cy}}{E_s \rho_y} \tag{A.31}$$

where f_{sy} is the y-reinforcement yield stress, n_y is the y-direction applied stress, σ_{cy} is the y-direction concrete stress, ρ_y is the y-reinforcement ratio and E_s is the steel modulus.

From Mohr's circle of concrete stress,

$$\sigma_{cy} = \sigma_{cn} + v_{cxy}\left(\frac{1}{\tan 2\theta_{c\sigma}} - \frac{\cos(2\theta_k - 2\theta_{c\sigma})}{\sin 2\theta_{c\sigma}}\right) \tag{A.32}$$

where σ_{cy} is the concrete stress in the y direction, σ_{cn} is the concrete stress normal to the cracks, v_{cxy} is the concrete shear stress, $\theta_{c\sigma}$ is the principal concrete stress angle and θ_k is the crack angle.

Substituting Eq. A.32 into Eq. A.31,

$$\varepsilon_y = \frac{1}{E_s \rho_y}\left[n_y - \sigma_{cn} - v_{cxy}\left(\frac{1}{\tan 2\theta_{c\sigma}} - \frac{\cos(2\theta_k - 2\theta_{c\sigma})}{\sin 2\theta_{c\sigma}}\right)\right] \tag{A.33}$$

Similarly in the x direction,

$$\varepsilon_x = \frac{1}{E_s \rho_x}\left[n_x - \sigma_{cn} + v_{cxy}\left(\frac{1}{\tan 2\theta_{c\sigma}} + \frac{\cos(2\theta_k - 2\theta_{c\sigma})}{\sin 2\theta_{c\sigma}}\right)\right] \tag{A.34}$$

At yield, the previous-direction cracks are assumed fully closed, thus the strain parallel

to the cracks is equal to the concrete strain parallel to the cracks, i.e., $\varepsilon_p = \varepsilon_{cp}$. From Mohr's circle of concrete strains,

$$\varepsilon_{cp} = \left(\varepsilon_{cn} - (\varepsilon_{cn} - 2\varepsilon_{c2})\cos(2\theta_k - 2\theta_{c\sigma})\right)\frac{1}{1+\cos(2\theta_k - 2\theta_{c\sigma})} \tag{A.35}$$

where ε_{cp} is the concrete strain parallel to the cracks, ε_{cn} is the concrete strain normal to the cracks, ε_{c2} is the minimum principal concrete strain, and $\theta_{c\sigma}$ is used for $\theta_{c\varepsilon}$ (since they are assumed equal).

Assuming linear stress-strain relationships for the concrete in compression and in tension (normal to the cracks), i.e., $\varepsilon_{c2} = \sigma_{c2} / E_c$ and $\varepsilon_{cn} = \sigma_{cn} / E_c$, and using, from Mohr's circle of concrete stress,

$$\sigma_{c2} = \sigma_{cn} - v_{cxy}\frac{1+\cos(2\theta_k - 2\theta_{c\sigma})}{\sin 2\theta_{c\sigma}} \tag{A.36}$$

Eq. A.35 can be written as

$$\varepsilon_p = \frac{1}{E_c}\left(\sigma_{cn} - 2v_{cxy}\frac{\cos(2\theta_k - 2\theta_{c\sigma})}{\sin 2\theta_{c\sigma}}\right) \tag{A.37}$$

Substituting Eqs A.33, A.34 and A.37 into A.30, the shear strain can be expressed as a function of the stresses:

$$\gamma_{xy} = \frac{v_{cxy}}{\sin 2\theta_{c\sigma}}\left[\begin{array}{l} \dfrac{\cos(2\theta_k - 2\theta_{c\sigma}) + \cos 2\theta_{c\sigma}}{E_s\rho_x \tan\theta_k} \\ + \dfrac{\tan\theta_k\left(\cos(2\theta_k - 2\theta_{c\sigma}) - \cos 2\theta_{c\sigma}\right)}{E_s\rho_y} \\ + \dfrac{2\cos(2\theta_k - 2\theta_{c\sigma})}{E_c}\left(\tan\theta_k + \dfrac{1}{\tan\theta_k}\right) \end{array}\right] \tag{A.38}$$

$$-\sigma_{cn}\left[\frac{1}{E_s\rho_x \tan\theta_k} + \frac{\tan\theta_k}{E_s\rho_y} + \frac{1}{E_c}\left(\tan\theta_k + \frac{1}{\tan\theta_k}\right)\right] + \frac{n_x}{E_s\rho_x \tan\theta_k} + \frac{n_y \tan\theta_k}{E_s\rho_y}$$

Concrete strain normal to the cracks, ε_{cn}

The derivation of Eq. A.38 assumes the linear relationship

$$\varepsilon_{cn} = \sigma_{cn} / E_c \tag{A.39}$$

however, stress–strain relationships for concrete are usually defined in terms of the principal stresses, σ_{c1} and σ_{c2} (which have no associated shear stress). To use the relationship $\varepsilon_{c1} = \sigma_{c1} / E_c$ would require determining σ_{c1} from σ_{cn}, v_{xy}, θ_σ and θ_k; calculating ε_{c1} from σ_{c1}; and determining ε_{cn} from ε_{c1}, ε_{c2}, $\theta_{c\varepsilon}=\theta_\sigma$, and θ_k. The concrete strain normal to the cracks would then be defined as

$$\varepsilon_{cn} = \frac{\sigma_{cn}}{E_c} + \frac{1}{2}\left(\frac{\sigma_{c2}}{E_c} + F(\sigma_{c2})\right)\left(1 - \cos(2\theta_k - 2\theta_{c\sigma})\right) \tag{A.40}$$

where $F(\sigma_{c2})$ represents the parabolic stress–strain function used for concrete in compression.

While Eq. A.40 can be used in a detailed model, it is not practical for a simplified model. Assuming $\cos(2\theta_k - 2\theta_{c\sigma}) \approx 1$, which is reasonable for stress angles within 15° of the crack angle, the second term of Eq. A.40 vanishes and Eq. A.40 reduces to Eq. A.39.

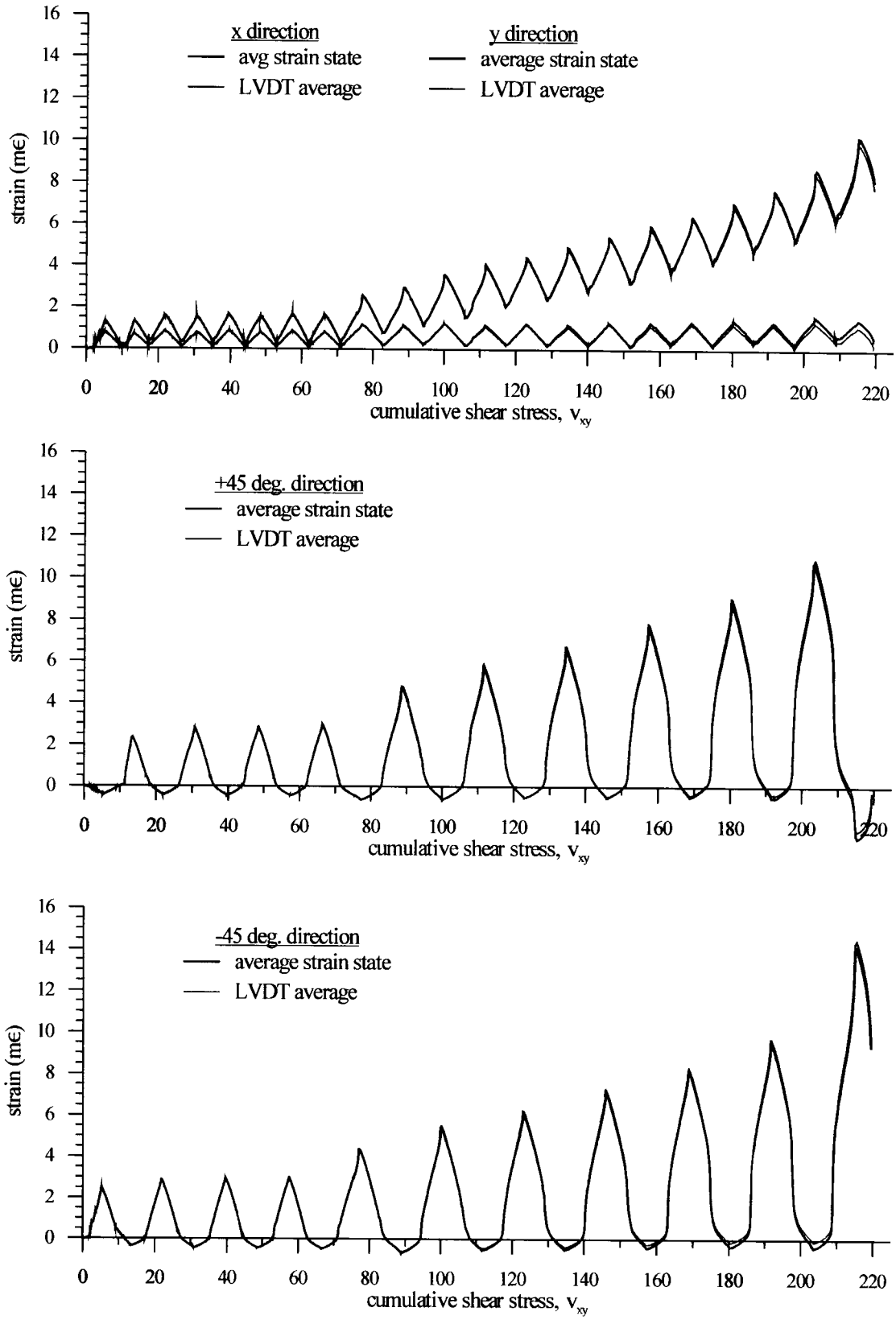

Figure A.1 Average (compatible) strain state compared to LVDT data (averaged in each direction): SE8

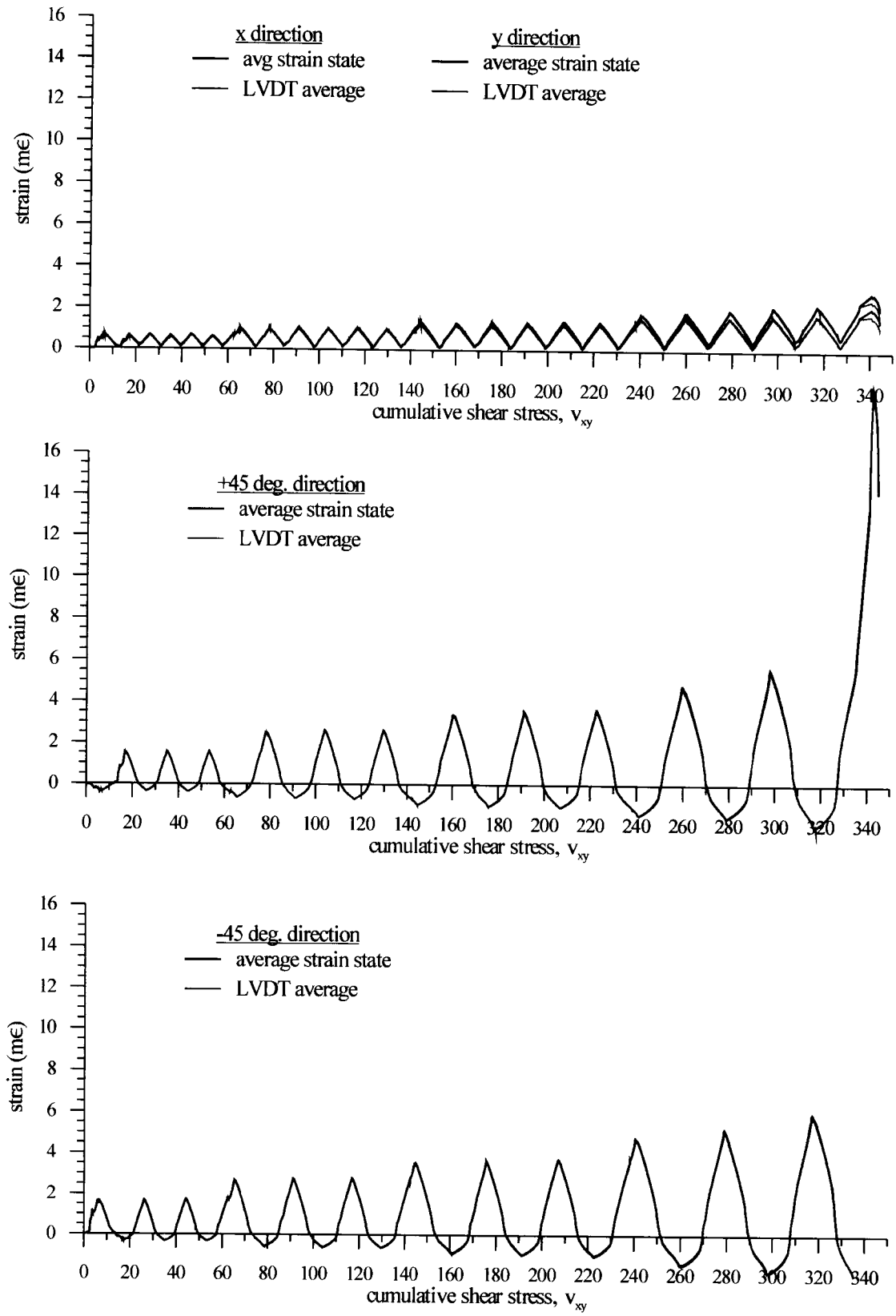

Figure A.2 Average (compatible) strain state compared to LVDT data (averaged in each direction): SE9

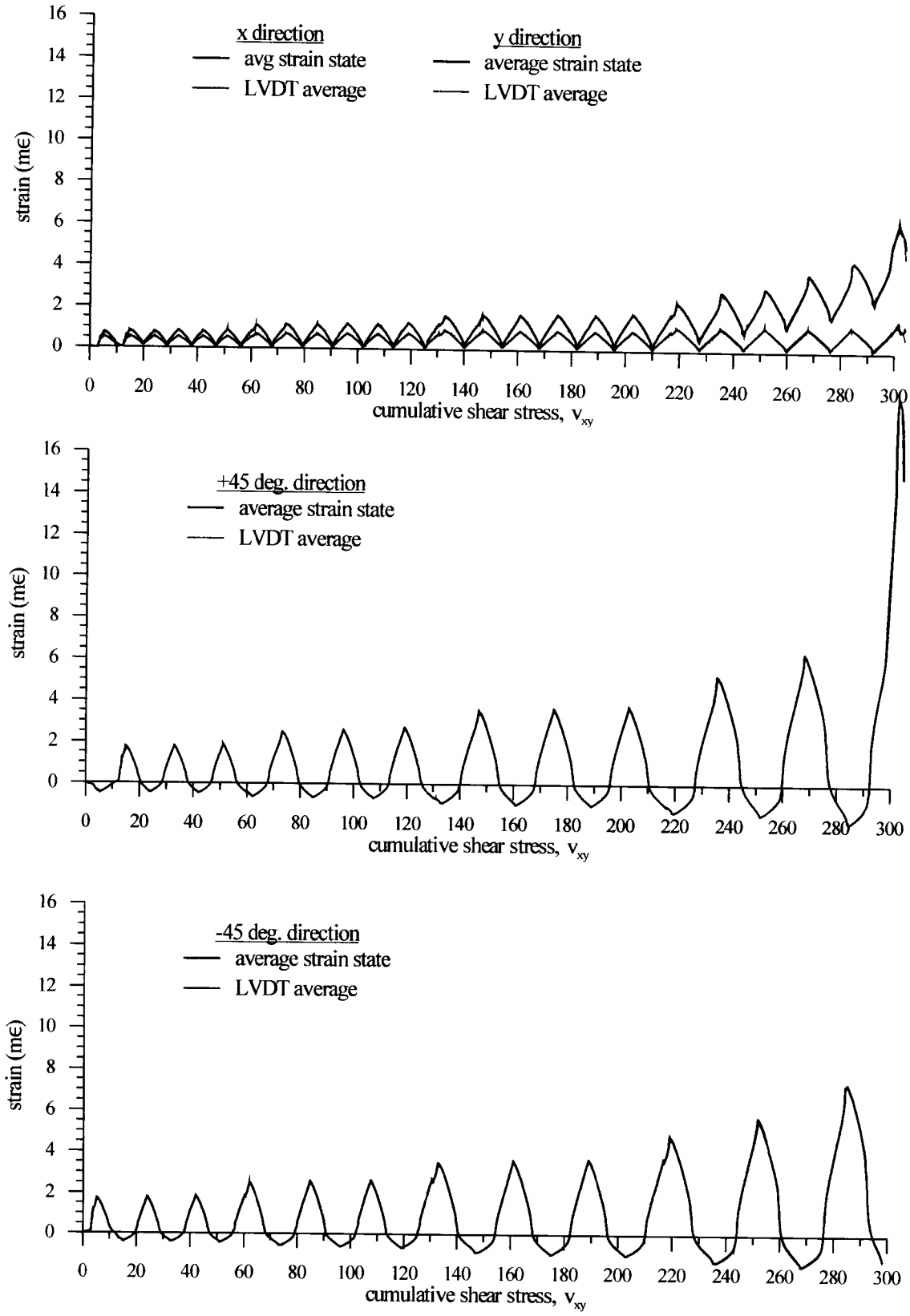

Figure A.3 Average (compatible) strain state compared to LVDT data (averaged in each direction): SE10

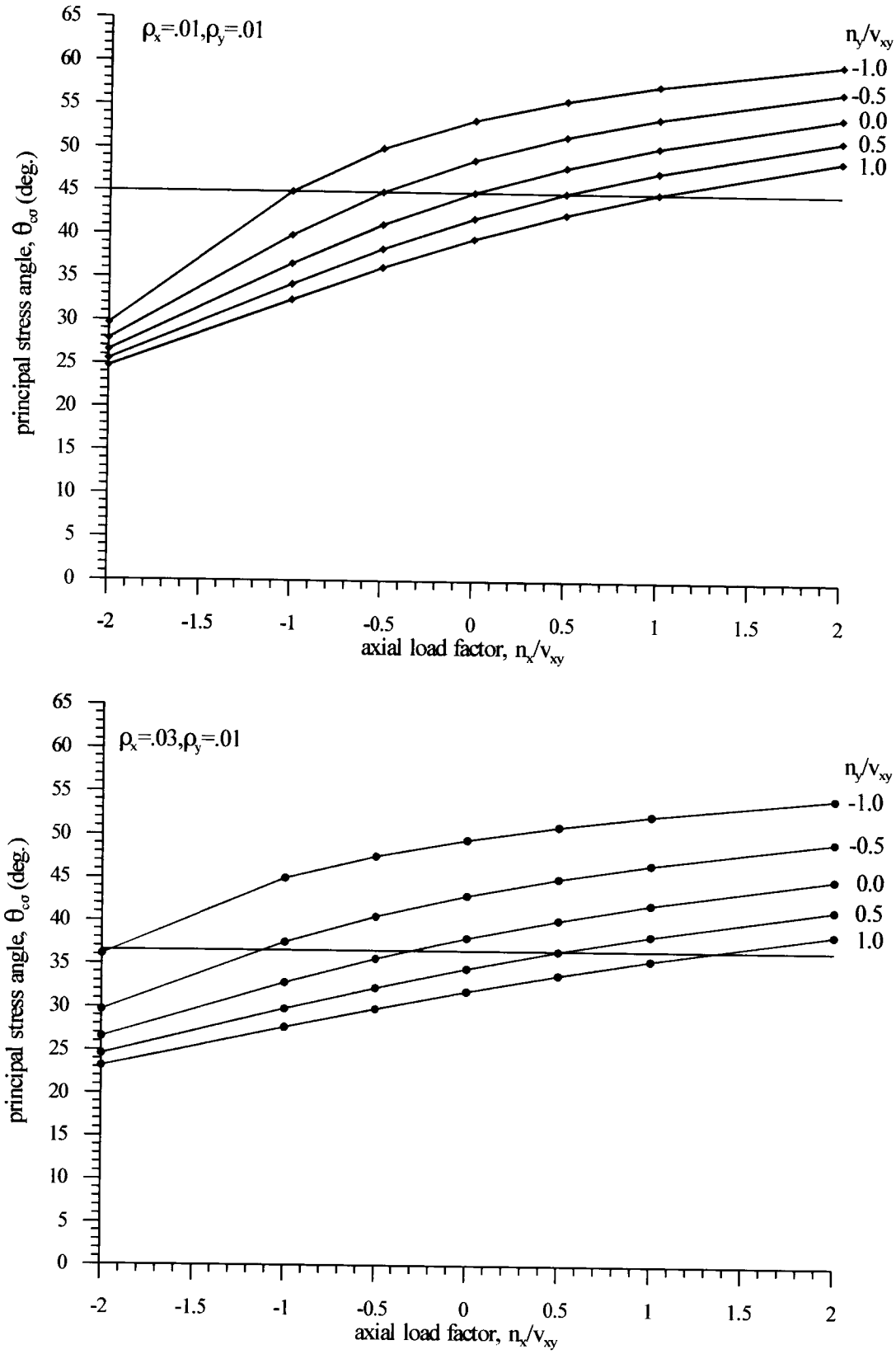

Figure A.4 Influence of axial loads on calculated principal stress angle

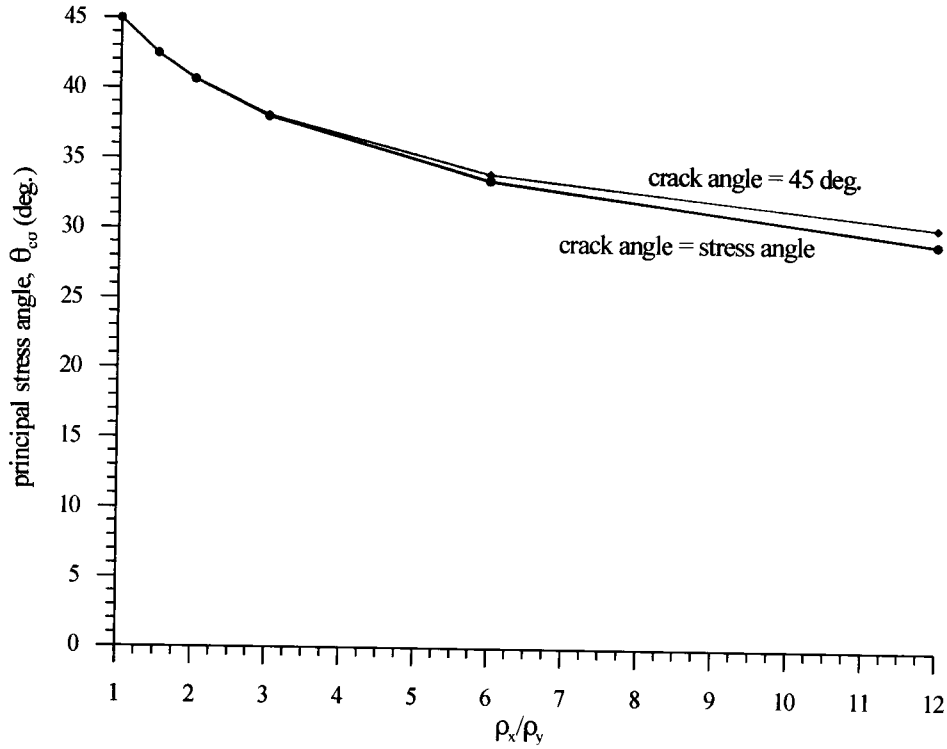

Figure A.5 Influence of crack angle on calculated principal stress angle ($n_x = n_y = 0$, concrete tension = 0)

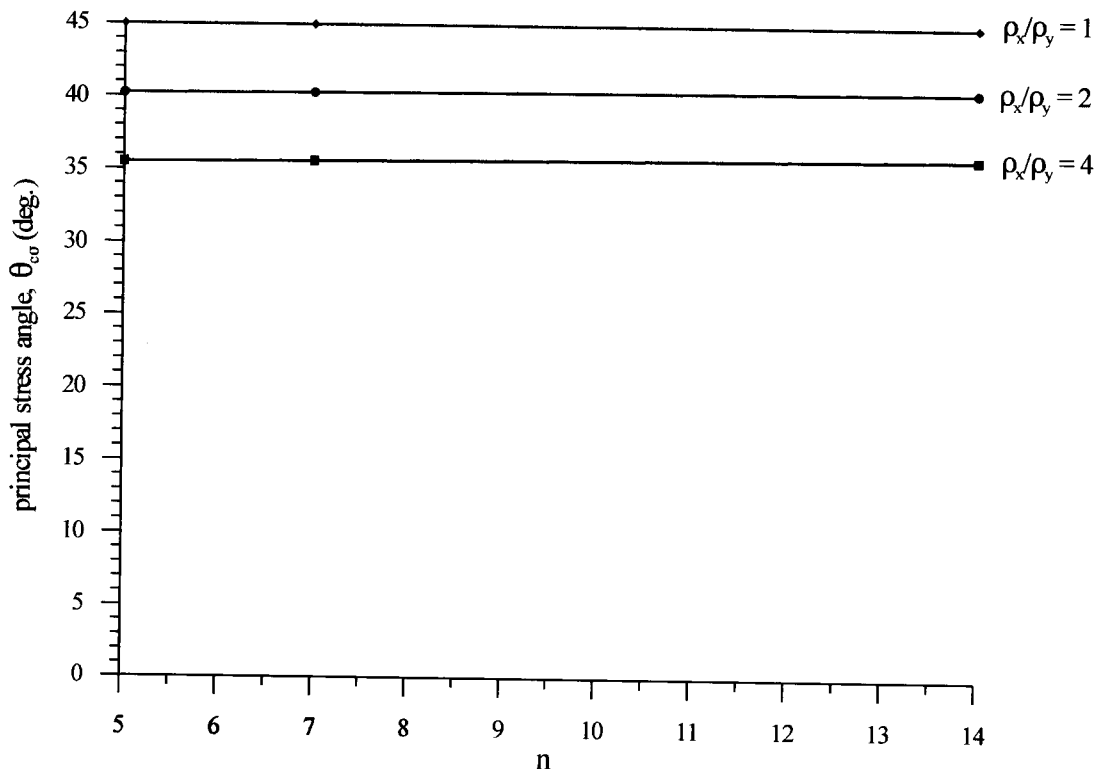

Figure A.6 Influence of modular ratio on calculated principal stress angle ($\rho_x = 0.01$, $n_x = n_y = 0$, concrete tension = 0)

APPENDIX B

Selected Experimental Data

B.1 PV SERIES PANELS

Complete details of the PV panels are presented in Vecchio and Collins (1982). Details for the 15 panels used in this thesis are listed in Table B.1; only the panels subjected to pure shear and which did not fail prematurely due to edge failures or poor casting were selected.

B.2 CRACKING POINTS

The cracking point for each of the seven LVDT instrumented specimens is listed in Table B.2. The concrete cracking stress is assumed to be the peak principal concrete tension stress and the cracking strain is the corresponding principal tension strain.

B.3 YIELD POINTS

Table B.3 lists the experimental data corresponding to first yielding of the weak reinforcement, for the seven LVDT instrumented specimens.

B.4 GRAPHICALLY DETERMINED YIELD POINTS

The graphically determined yield points are listed in Table B.4, and shown in Figs. B.1 to B.12.

B.5 FAILURE POINTS

The experimental failure points are listed in Table B.5. The failure modes and the ratio $\varepsilon_{c2}/\varepsilon_2$ are discussed in Chapter 3, Sec. 3.7.

B.6 AVERAGE CRACK SPACING

Tables B.6 and B.7 list the data used in estimating the average crack spacing (using Eqs. 3.43, 3.44).

Table B.1 Characteristics of selected PV panels

Panel	ρ_x	f_{yx} (MPa)	ρ_y	f_{yy} (MPa)	f_c' (MPa)	ε_c'
PV4	0.0106	242	0.0106	242	26.6	0.0025
PV6	0.0179	266	0.0179	266	29.8	0.0025
PV9	0.0179	455	0.0179	455	11.6	0.0028
PV10	0.0179	276	0.0100	276	14.5	0.0027
PV11	0.0179	235	0.0131	135	15.6	0.0026
PV12	0.0179	469	0.0045	269	16.0	0.0025
PV16	0.0074	255	0.0074	255	21.7	0.0020
PV19	0.0179	458	0.0071	299	19.0	0.0022
PV20	0.0179	460	0.0089	297	19.6	0.0018
PV21	0.0179	458	0.0130	302	19.5	0.0018
PV22	0.0179	458	0.0152	420	19.6	0.0020
PV26[1]	0.0179	456	0.0101	463	21.3	0.0019
PV27	0.0179	442	0.0179	442	20.5	0.0019
PV29	0.0179	441	0.0089	324	21.7	0.0018
PV30[2]	0.0179	437	0.0101	472	19.1	0.0019

[1] pre-cracked in biaxial tension
[2] subjected to reverse-cyclic shear

Table B.2 Principal tensile stress and strain at cracking

Specimen	Cracking Stress f_{cr} (MPa)	Cracking Strain ε_{cr} (x 10^{-3})
SE8	2.07	0.065
SE9	2.18	0.116
SE10	2.08	0.114
PP1	1.55	0.395
PDV1	2.12	0.205
PDV2	2.20	0.375
PDV3	2.70	0.350

Table B.3 Experimental data at first yielding of weak reinforcement

Specimen	v_{xy} (MPa)	γ_{xy} (x10^{-3})	ε_x (x10^{-3})	ε_y (x10^{-3})	θ_ε (deg.)	$\theta_{c\sigma}$ (deg.)	σ_{c2} (MPa)	σ_{c1} (MPa)	$\mu_1 = \sigma_{c1}/v_{xy}$
SE8	5.71	4.769	1.169	2.435	37.6	39.6	-11.61	0.01	0.00
SE9	-9.45	-7.27	1.686	2.116	-43.3	-48.8	-20.83	-1.76	0.19
SE10	-7.70	-5.62	1.064	2.39	-38.4	-42.1	-15.80	-0.32	0.04
PP1	4.05	4.47	1.09	2.48	36.4	41.0	-7.77	0.40	0.10
PDV1	6.16	3.129	0.907	1.408	40.5	43.3	-11.51	0.83	0.13
PDV2	5.90	3.714	0.931	1.43	41.2	43.0	-11.20	0.63	0.11
PDV3	6.70	2.998	0.696	1.409	38.3	45.1	-11.87	1.53	0.23

Table B.4 Graphically Determined Yield Points

Specimen	$v_{xy,yld}$	$\gamma_{xy,yld}$
SE8	5.80	0.0045
SE9	9.55	0.0060
SE10	8.20	0.0059
PP1	4.40	0.0052
PDV1	6.40	0.0035
PDV2	5.90	0.0035
PDV3	7.00	0.0035
PV4	2.60	0.0019
PV6	4.50	0.0038
PV10	3.75	0.0037
PV11	3.50	0.0028
PV12	2.80	0.0030
PV16	2.10	0.0025
PV19	3.55	0.00285
PV20	4.10	0.0035

Table B.5 Failure Points

Failure mode	Specimen	v_{cxy} (MPa)	γ_{xy} (x 10^{-3})	ε_2 (MPa)	ε_1 (MPa)	$\varepsilon_{c2}/\varepsilon_2$
concrete compression	PV9	3.76	8.06	-2.94	5.12	1.00
	PV22	3.72	5.27	-1.07	4.23	0.99
	PV26	5.41	5.88	-1.00	5.03	0.92
	PV27	6.24	4.54	-1.12	3.42	1.00
	PV30	3.71	4.99	-1.13	3.96	0.96
	SE5	8.09	7.50	-2.40	5.10	1.00
	SE9	9.05	8.49	-2.20	6.31	0.87
concrete shear	PV10	3.97	7.31	-1.46	6.37	0.82
	PV12	3.13	7.39	-1.03	7.84	0.29
	PV19	3.96	10.51	-1.58	11.32	0.25
	PV20	4.19	11.51	-1.91	11.75	0.44
	PV21	5.03	8.66	-1.46	8.10	0.69
	PV29	5.57	6.12	-1.27	5.19	0.86
	PP1	4.95	11.39	-1.63	11.52	0.47
	SE1	6.11	5.33	-0.70	4.94	0.79
	SE8	5.41	11.48	-1.76	12.06	0.34
	SE10	6.18	7.57	-1.56	6.69	0.92
reinforcement	PV4	2.84	10.06	-0.37	9.71	0.98
	PV6	4.47	4.15	-0.48	3.68	0.99
	PV11	3.56	5.32	-1.02	4.39	0.96
	PV16	2.14	5.55	-0.28	5.28	0.99
	PDV1	7.06	4.70	-0.49	4.32	0.92
	PDV2	6.11	5.75	-0.96	4.88	0.96
	PDV3	8.09	4.66	-0.49	4.26	0.92

Table B.6 Average crack spacing: seven LVDT specimens

Specimen	k_1	d_{bx} (mm)	ρ_x	s_x (mm)	c_x (mm)	d_{by} (mm)	ρ_y	s_y (mm)	c_y (mm)	θ (deg.)	s_{mx} (mm)	s_{my} (mm)	$s_{m\theta}$ (mm)
SE8	0.4	20	0.0294	72	111	10	0.0098	31	94	45	304	296	212
SE9	0.4	20	0.0294	72	111	20	0.0294	31	89	45	304	252	195
SE10	0.4	20	0.0294	72	111	10	0.0098	31	94	45	304	296	212
PP1	0.4	20	0.0195	108	111	10	0.0065	31	94	45	346	348	245
PDV1	0.4	6	0.0182	44	23	6	0.0091	88	17	45	88	118	71
PDV2	0.4	6	0.0182	44	23	6	0.0091	88	17	45	88	118	71
PDV3	0.4	6	0.0182	44	23	6	0.0091	88	17	45	88	118	71

Table B.7 Average crack spacing: PV specimens

Specimen	k_1	d_{bx} (mm)	ρ_x	s_x (mm)	c_x (mm)	d_{by} (mm)	ρ_y	s_y (mm)	c_y (mm)	θ (deg.)	s_{mx} (mm)	s_{my} (mm)	$s_{m\theta}$ (mm)
PV4	0.8	3.45	0.01056	50	23	3.45	0.01056	50	17	45	121	109	81
PV6	0.8	6.35	0.01785	50	23	6.35	0.01785	50	17	45	127	115	85
PV9	0.8	6.35	0.01785	50	23	6.35	0.01785	50	17	45	127	115	85
PV10	0.8	6.35	0.01785	50	23	4.7	0.00999	50	17	45	127	138	94
PV11	0.8	6.35	0.01785	50	23	5.44	0.01306	50	17	45	127	127	90
PV12	0.8	6.35	0.01785	50	23	3.18	0.00446	50	17	45	127	187	107
PV16	0.8	4.09	0.00700	50	23	4.09	0.00700	50	17	45	167	155	113
PV19	0.8	6.35	0.01785	50	23	4.01	0.00713	50	17	45	127	156	99
PV20	0.8	6.35	0.01785	50	23	4.47	0.00885	50	17	45	127	145	96
PV21	0.8	6.35	0.01785	50	23	5.41	0.01296	50	17	45	127	127	90
PV22	0.8	6.35	0.01785	50	23	5.87	0.01524	50	17	45	127	121	88
PV26	0.8	6.35	0.01785	50	23	4.78	0.01009	50	17	45	127	139	94
PV27	0.8	6.35	0.01785	50	23	6.35	0.01785	50	17	45	127	115	85
PV29	0.8	6.35	0.01785	50	23	4.47	0.00885	50	17	45	127	145	96

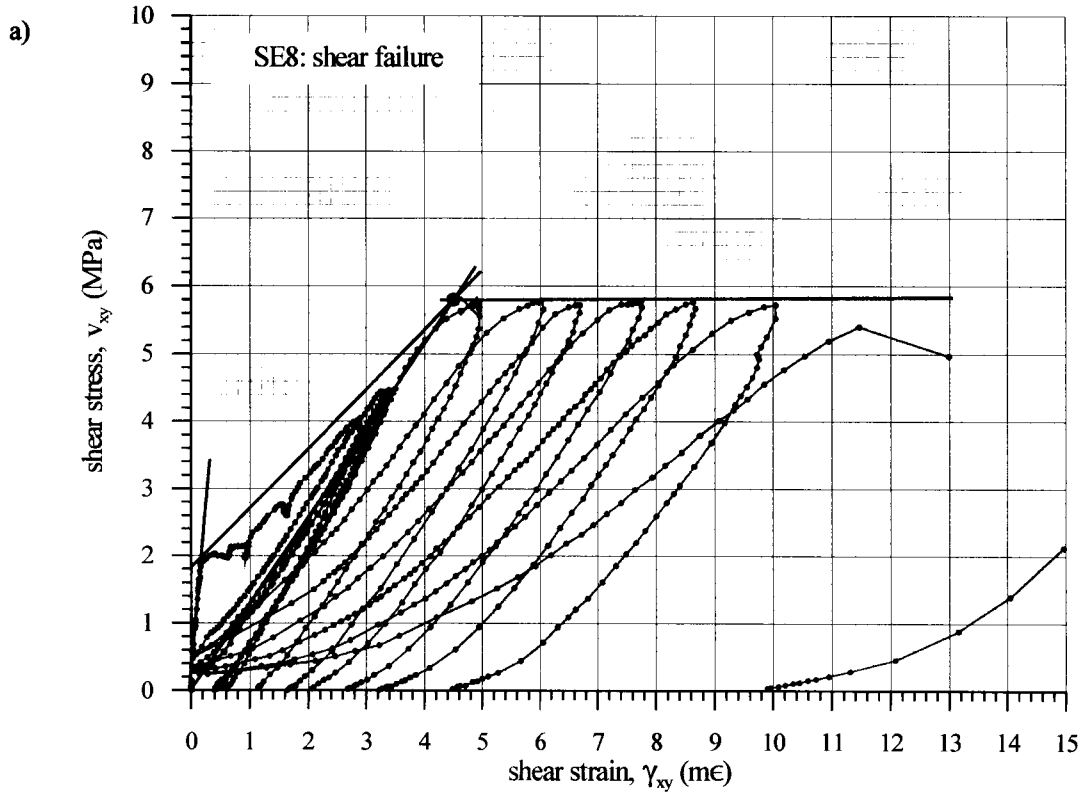

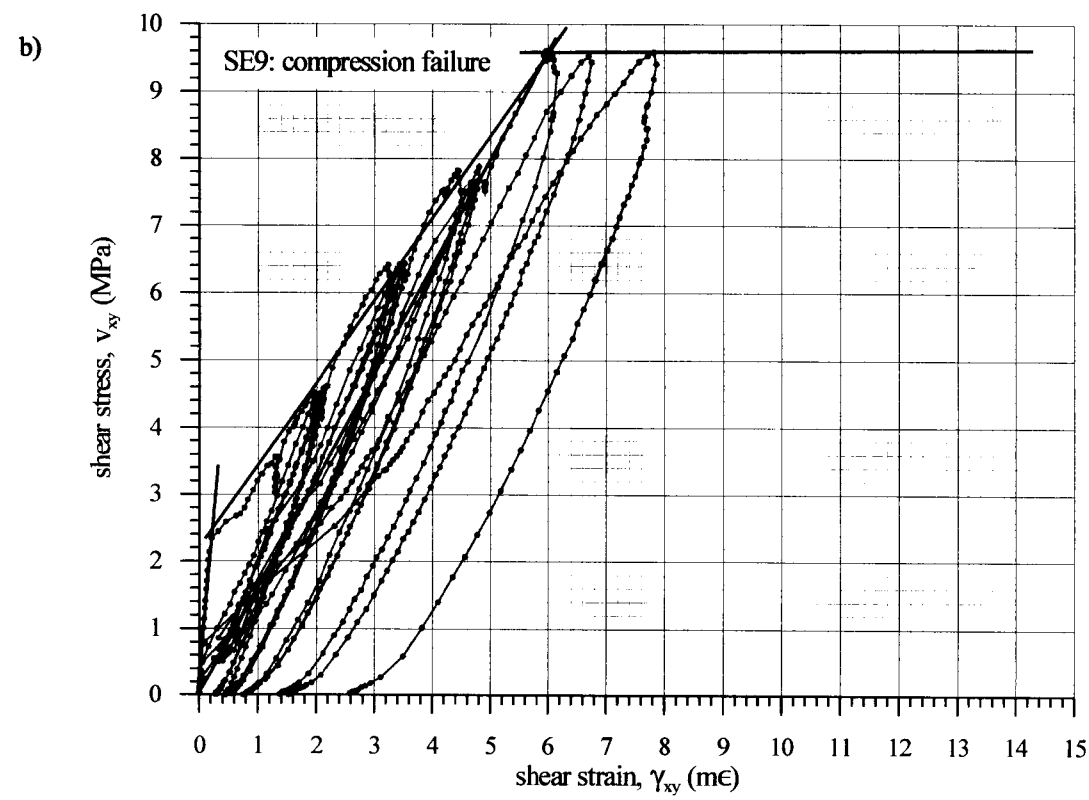

Figure B.1 Graphically determined yield point: a) SE8, b) SE9

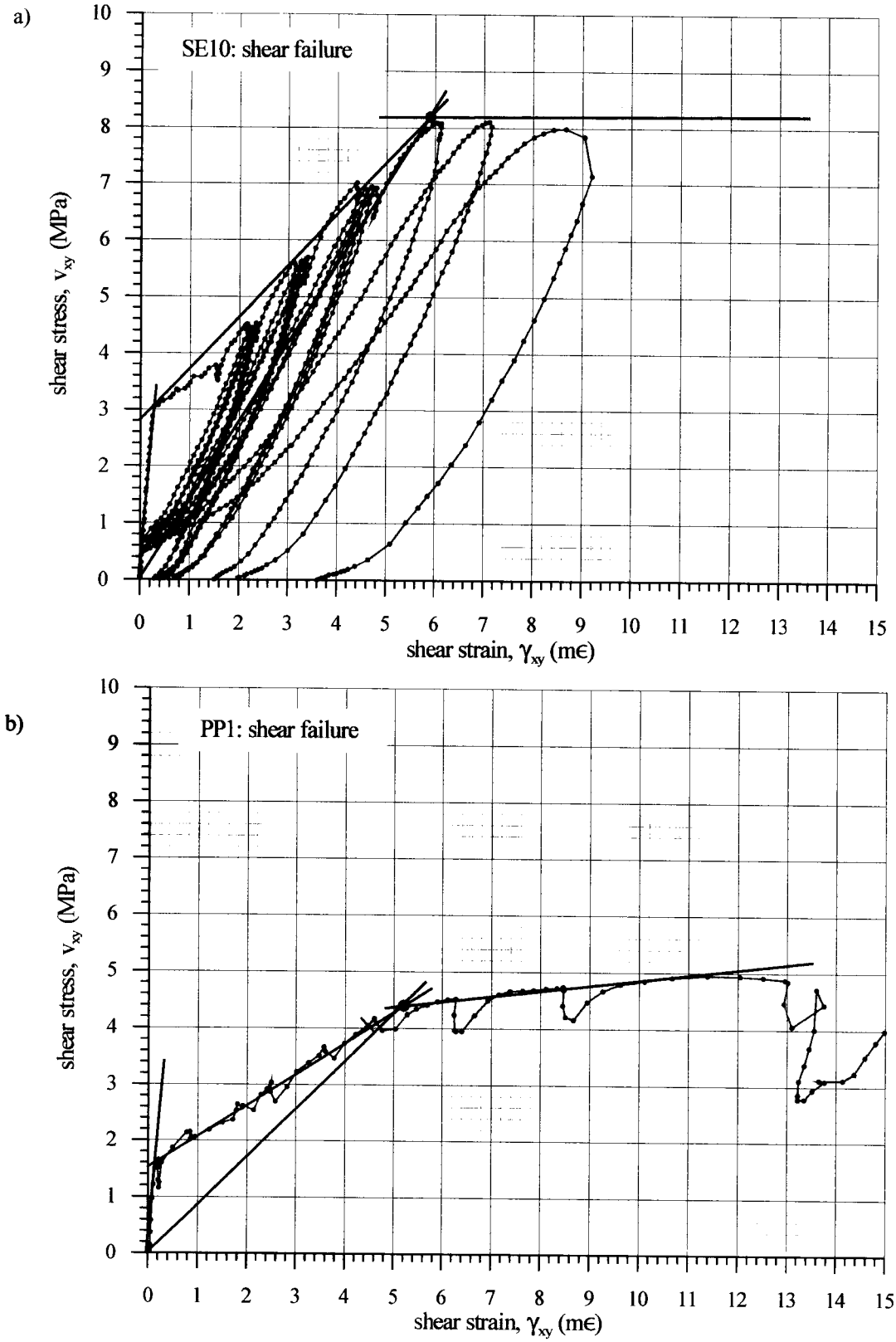

Figure B.2 Graphically determined yield point: a) SE10, b) PP1

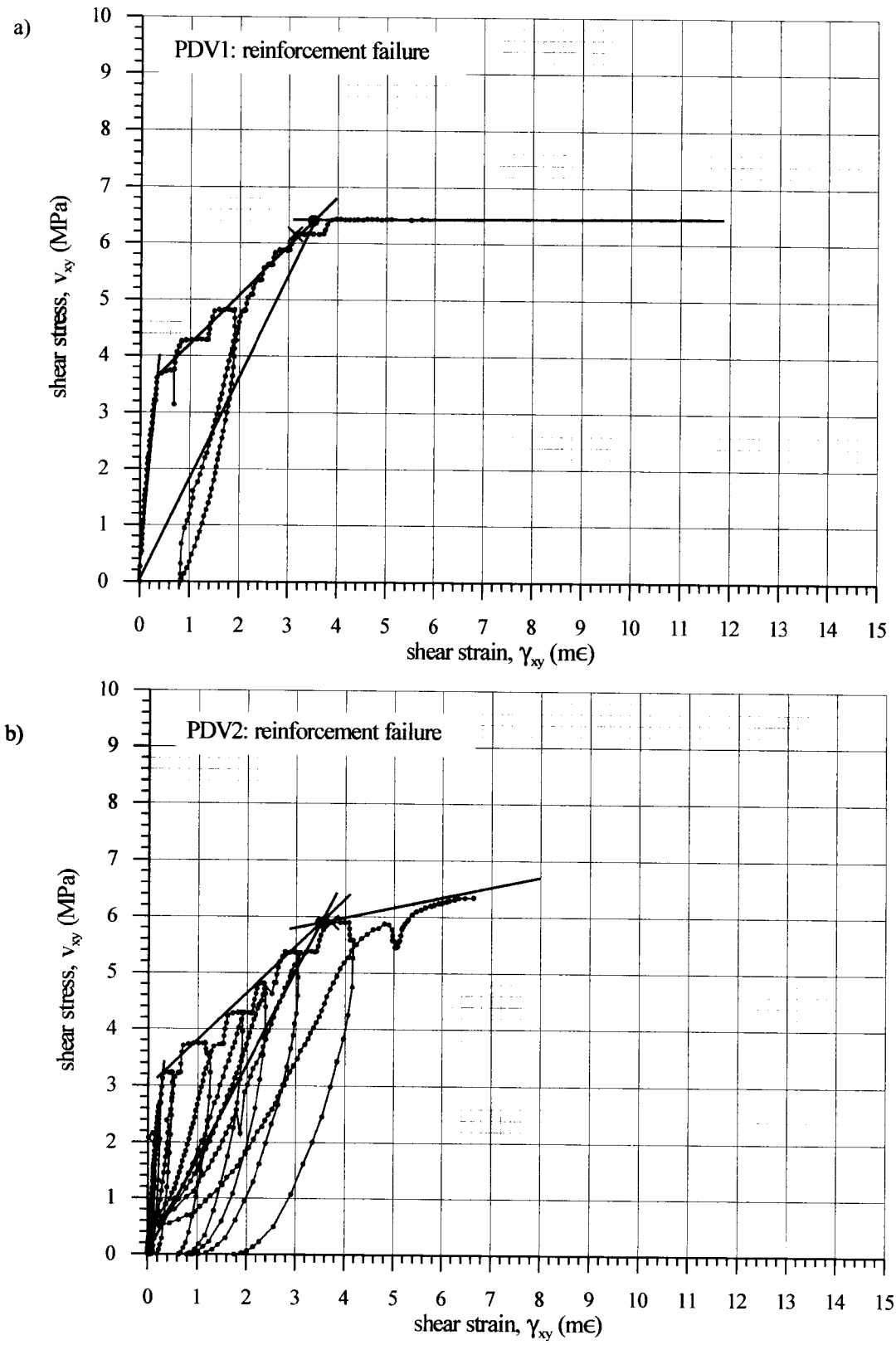

Figure B.3 Graphically determined yield point: a) PDV1, b) PDV2

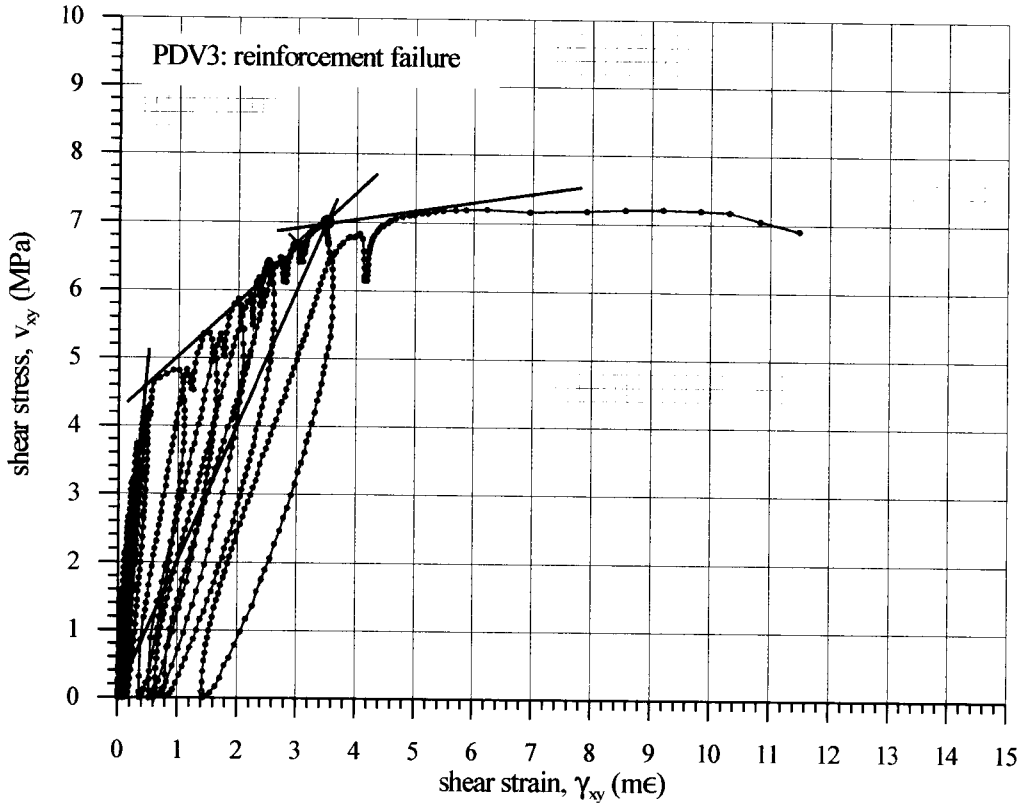

Figure B.4 Graphically determined yield point: PDV3

a)

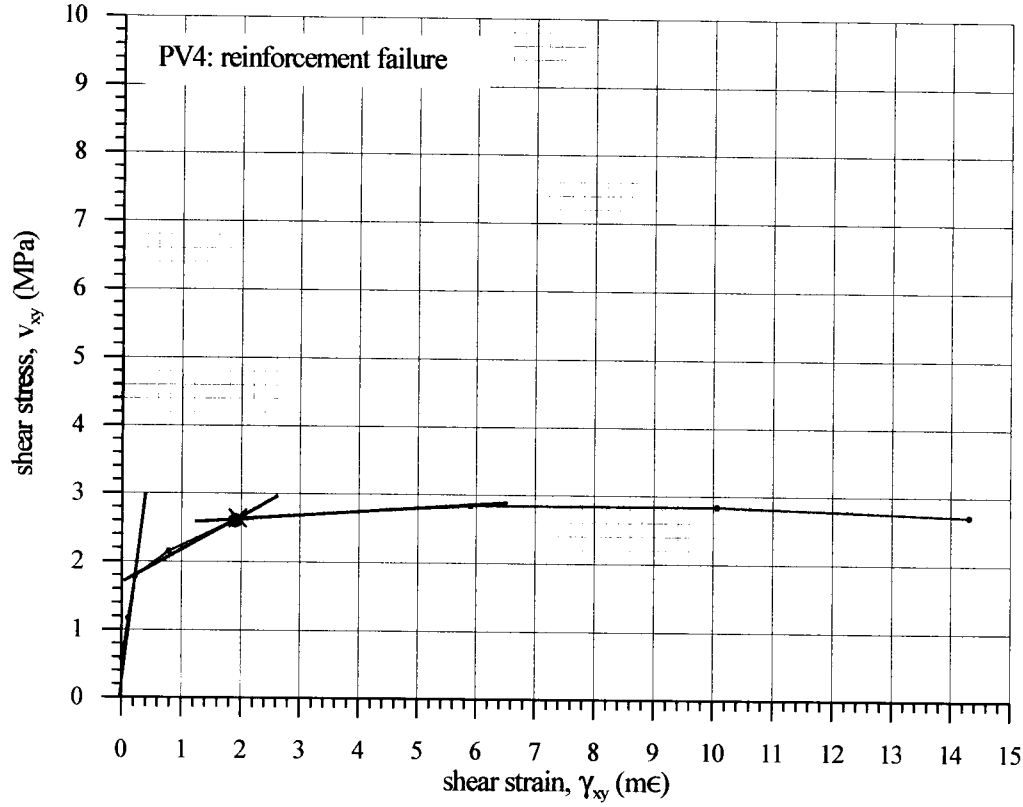

b)

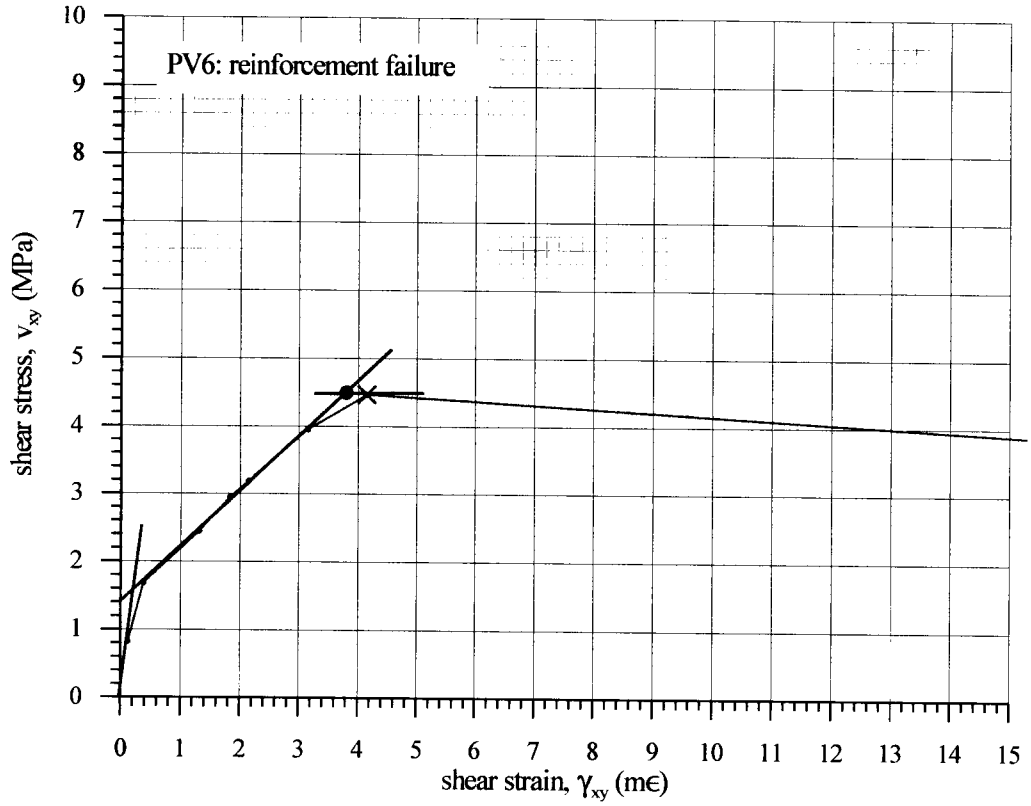

Figure B.5 Graphically determined yield point: a) PV4, b) PV6

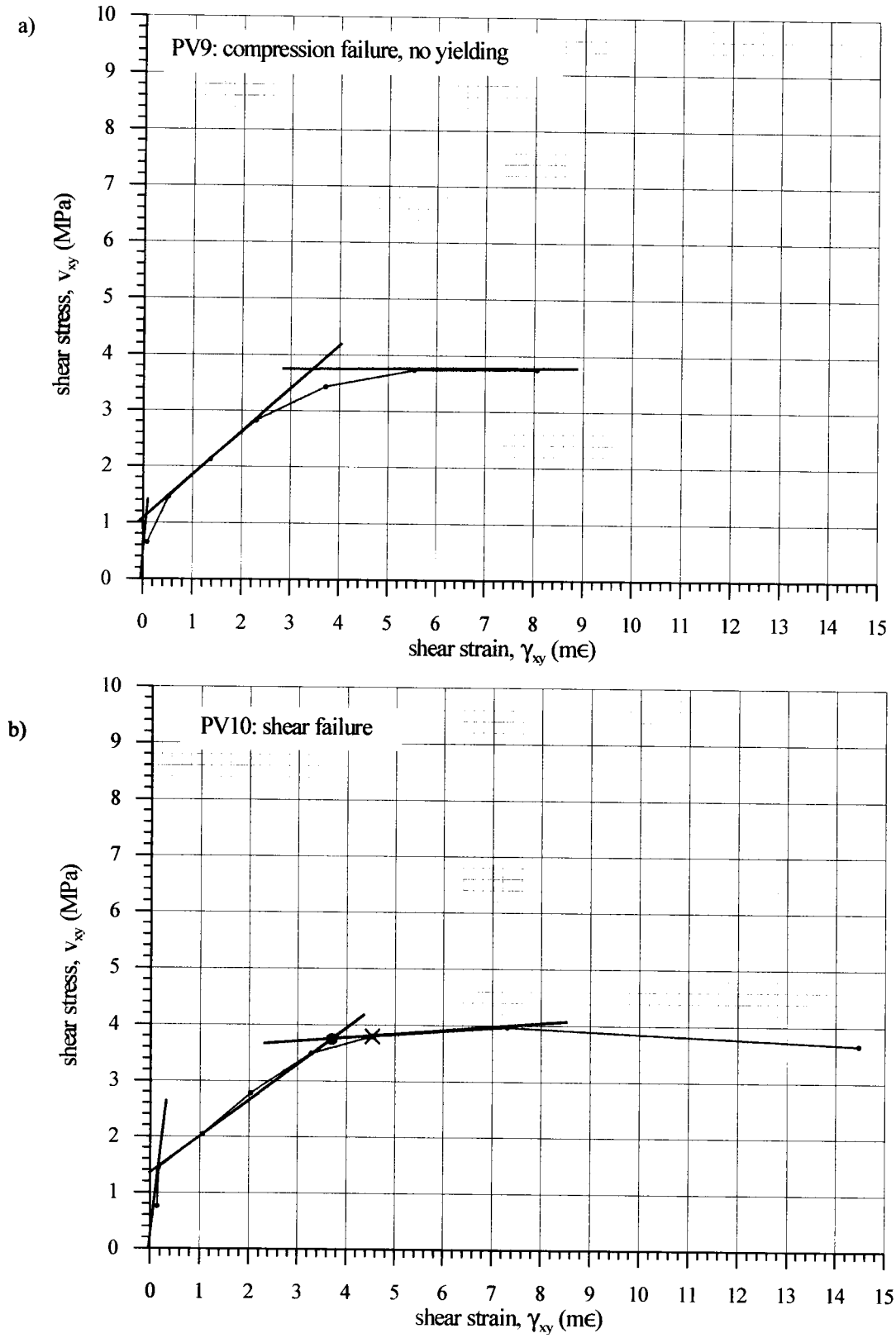

Figure B.6 Graphically determined yield point: a) PV9, b) PV10

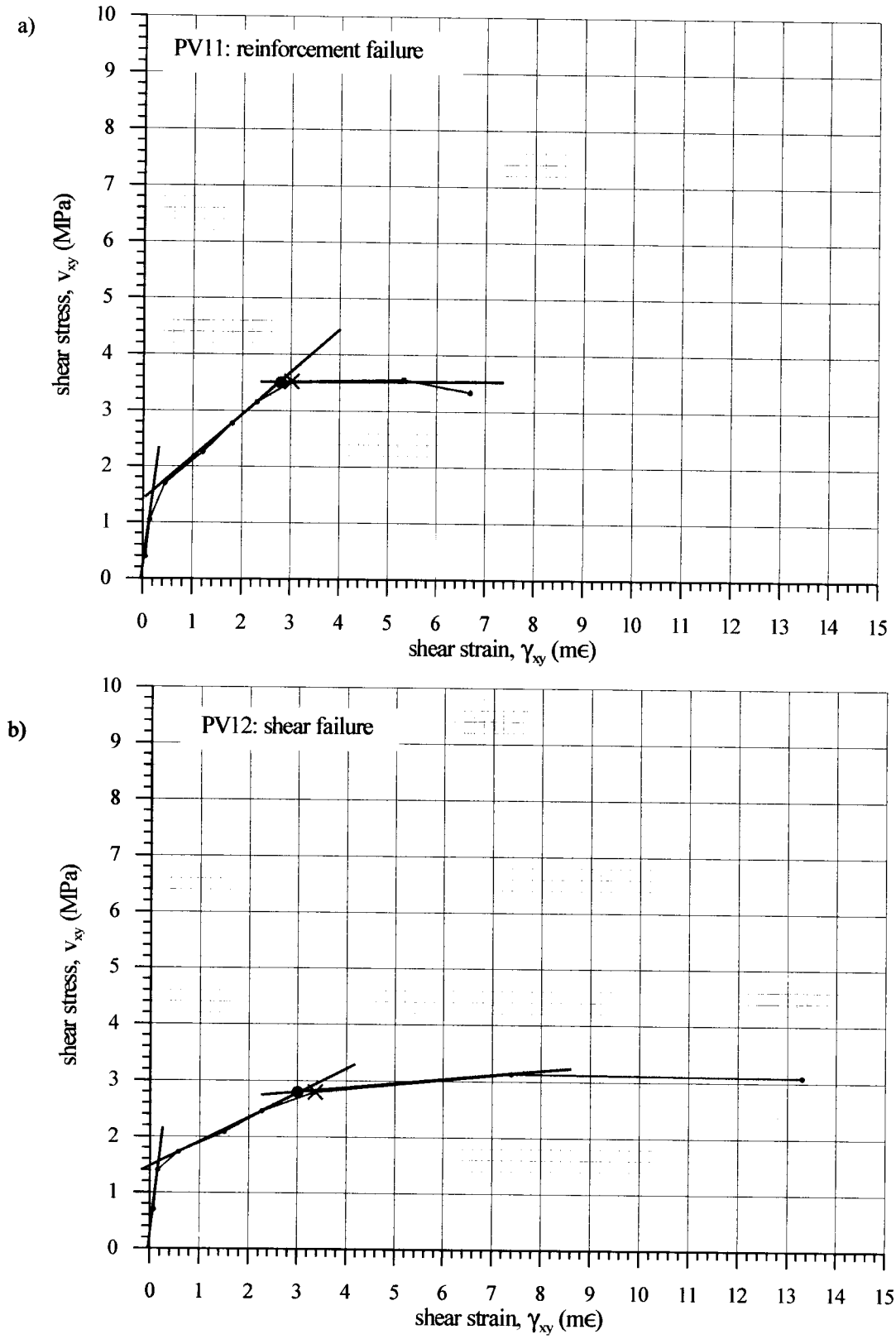

Figure B.7 Graphically determined yield point: a) PV11, b) PV12

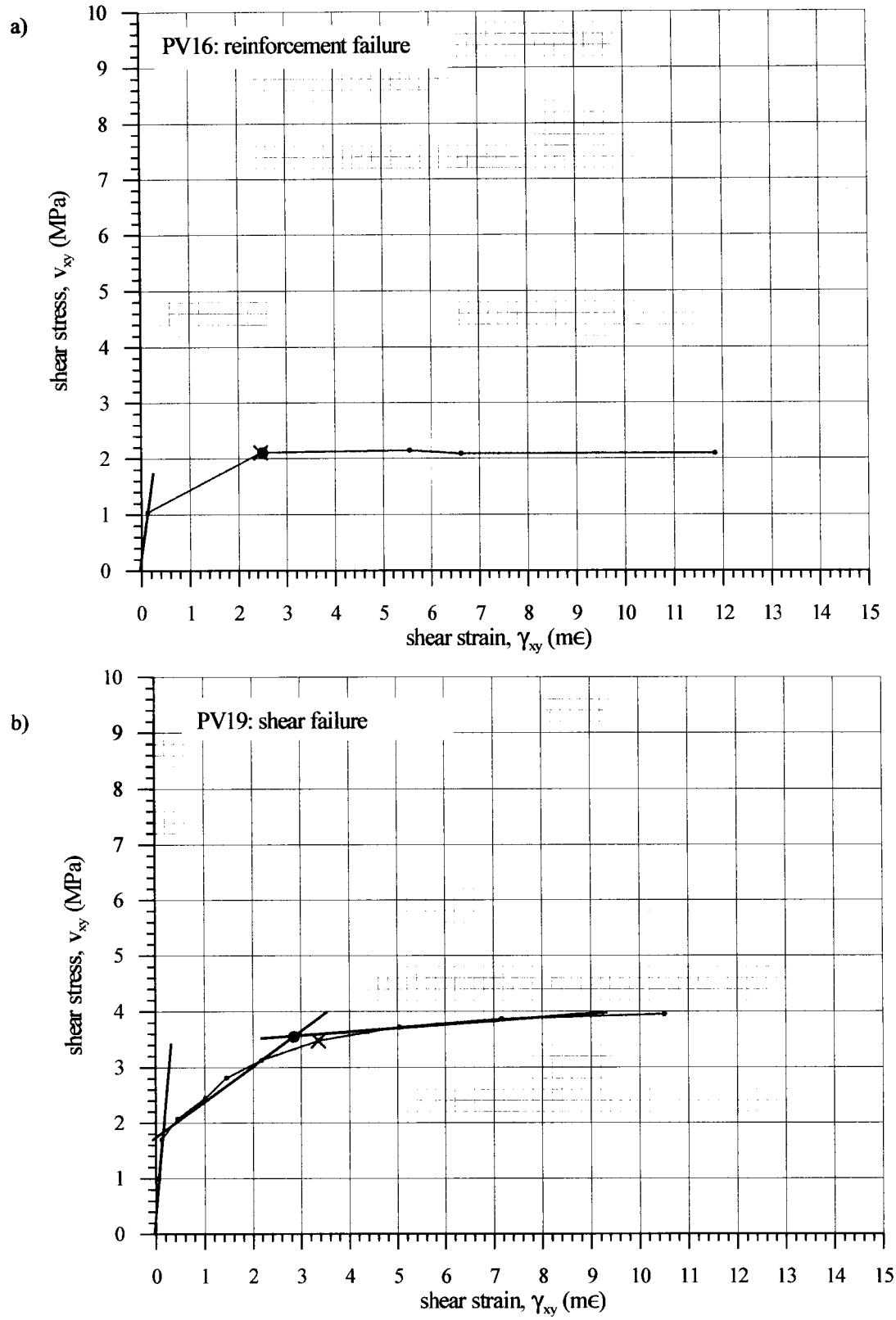

Figure B.8 Graphically determined yield point: a) PV16, b) PV19

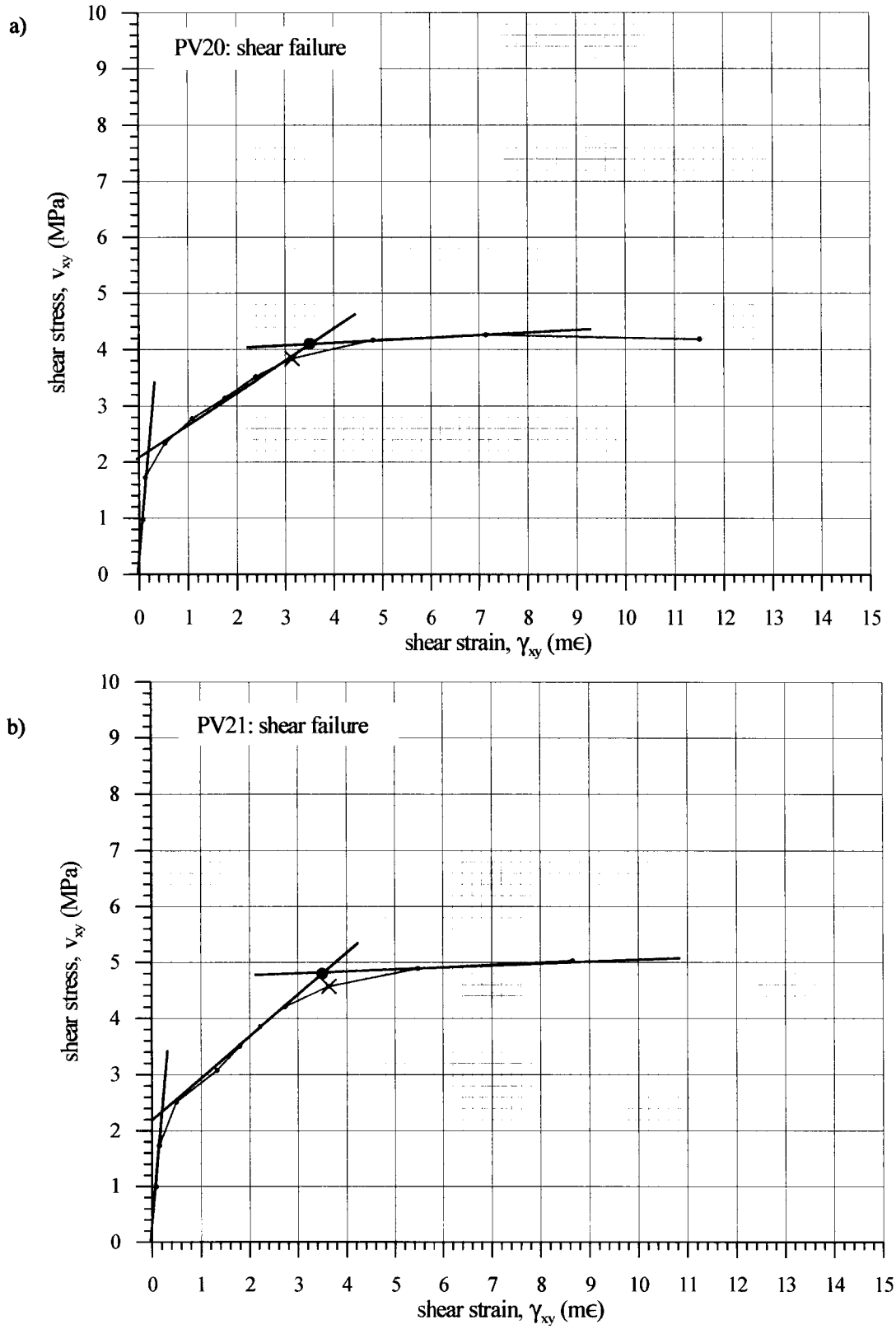

Figure B.9 Graphically determined yield point: a) PV20, b) PV21

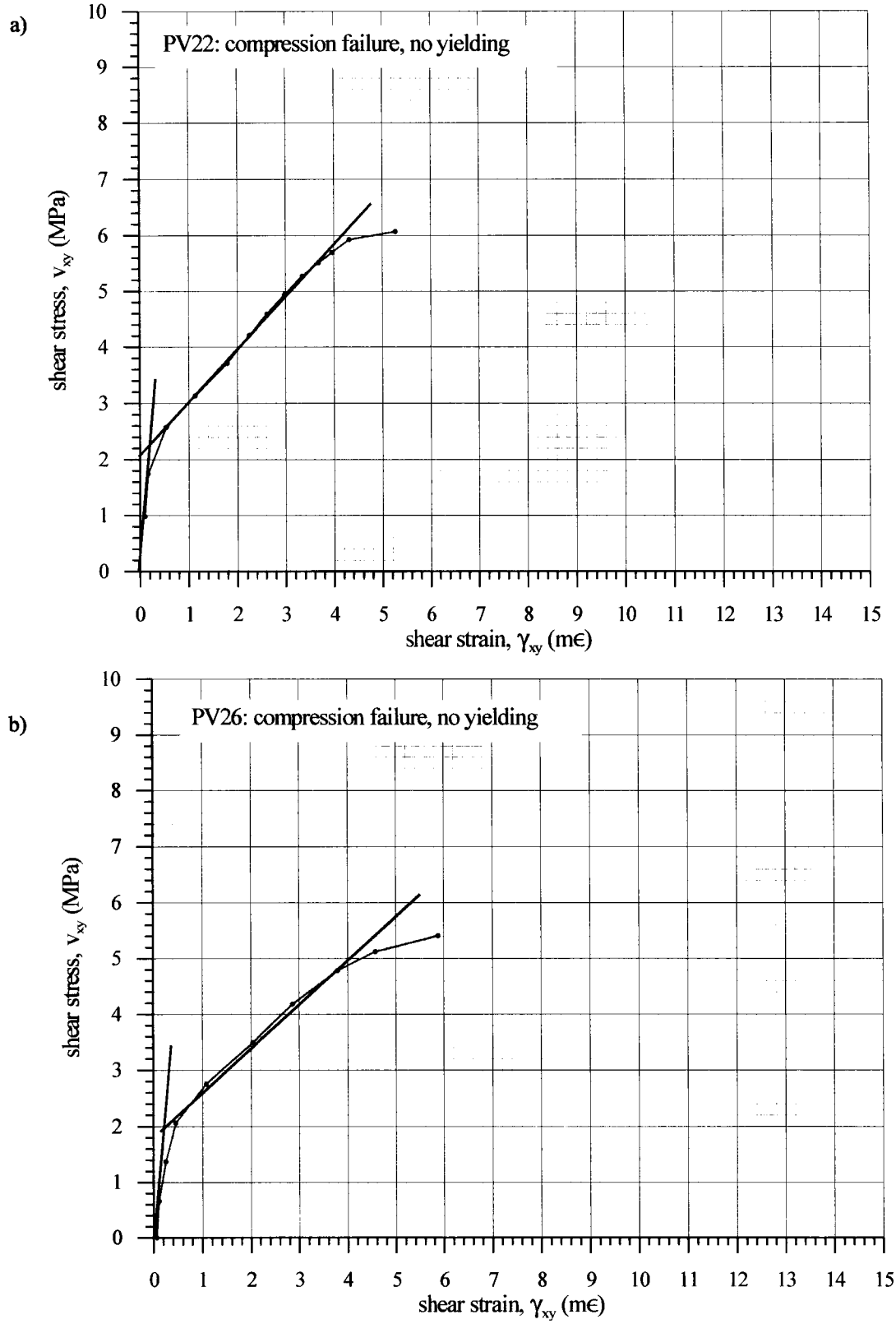

Figure B.10 Graphically determined yield point: a) PV22, b) PV26

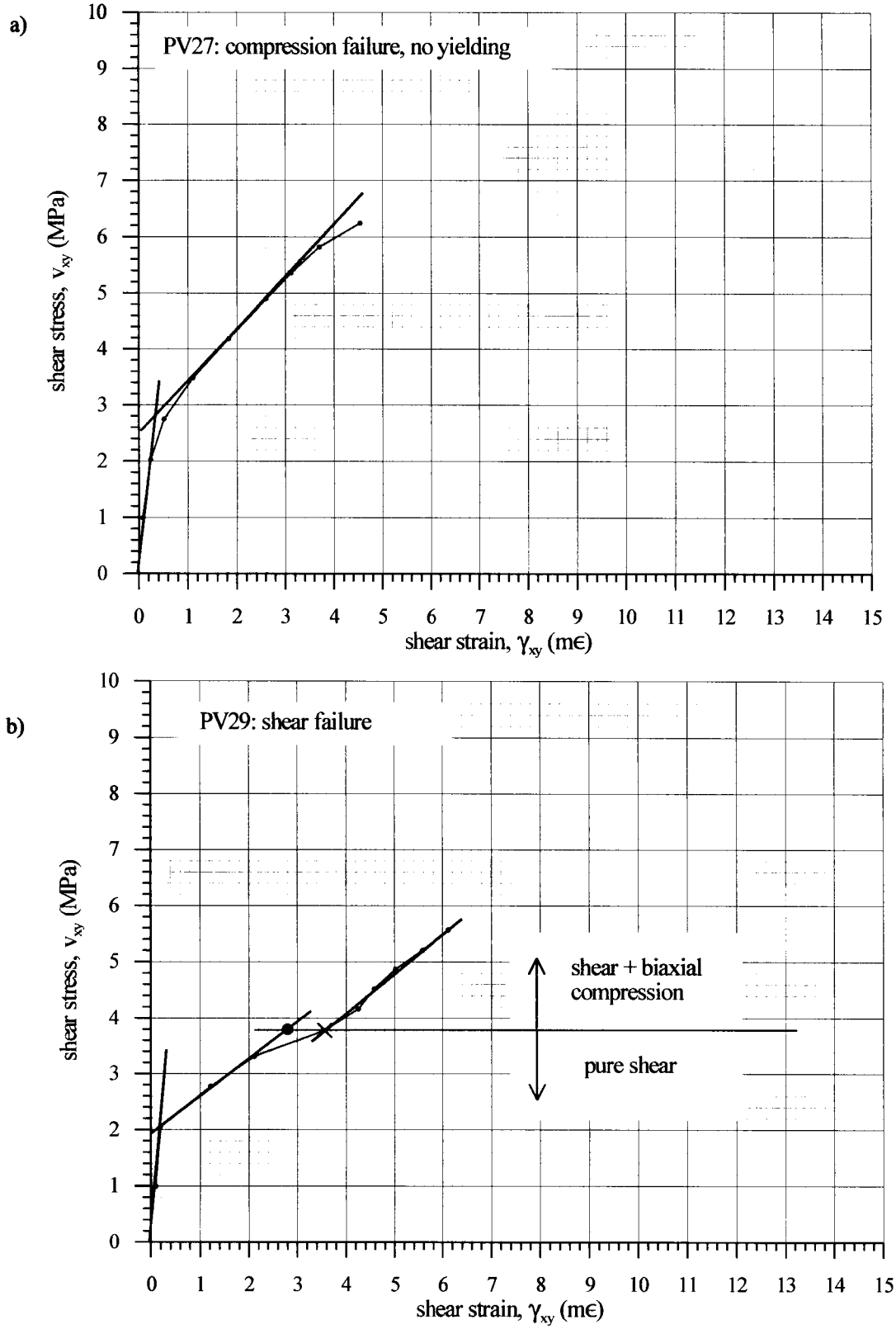

Figure B.11 Graphically determined yield point: a) PV27, b) PV29

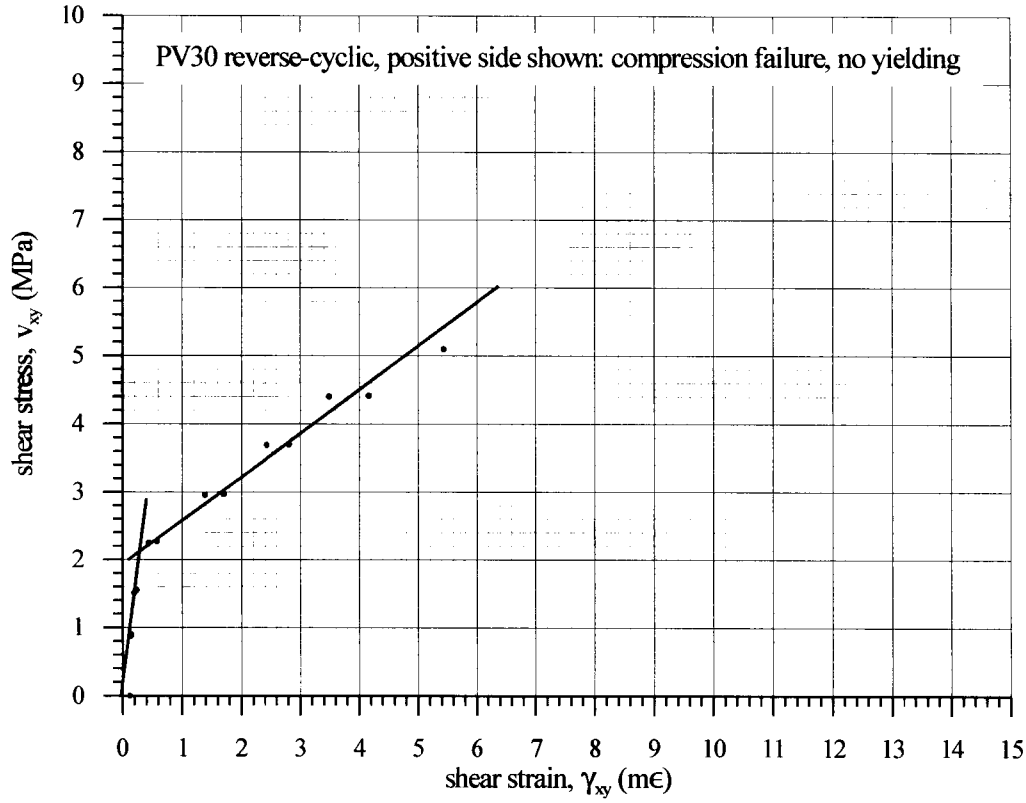

Figure B.12 Graphically determined yield point: PV30

APPENDIX C

Notation

SUBSCRIPTS

c	concrete
k	cracks
n	direction normal to opening cracks
p	direction parallel to opening cracks
s	steel reinforcement
t	tension; total
x	stronger reinforcement direction
y	weaker reinforcement direction
ε	strain
σ	stress
1	maximum principal direction
2	minimum principal direction
+45	direction 45° clockwise from x direction
−45	direction 45° counter-clockwise from x direction

SYMBOLS

A	area
c	clear cover

d_b bar diameter

E modulus of elasticity

f_{cr} concrete cracking stress

f_c' concrete compression strength

f_t concrete tensile strength

f_y reinforcement yield stress

G_{gross} gross section shear modulus

G_{cr} cracked section shear modulus

k ratio of applied principal tension to tensile strength

k_1, k_2 coefficients for crack spacing equation

l gauge length

N applied normal force

n applied normal stress

n modulus ratio

s maximum spacing between bars

$s_{m\theta}$ average crack spacing

V applied shear force

v average shear stress

w average crack width

α softening coefficient for concrete modulus

β compression softening coefficient related to ϵ_2

β_c compression softening coefficient related to ϵ_{c2}

γ average shear strain

ε average normal strain

ε_c' strain at peak concrete compression stress

θ angle, clockwise-positive from x direction

μ ratio of shear stress to normal stress

ν Poisson's ratio

ρ reinforcement ratio

σ average normal stress